GEOLOGICA ULTRAIECTINA

Mededelingen van het
Instituut voor Aardwetenschappen der
Rijksuniversiteit te Utrecht

No. 43

GEOLOGICAL ANALYSIS OF PALEOZOIC LARGE-SCALE FAULTING IN THE SOUTH-CENTRAL PYRENEES

ARIE SPEKSNIJDER

GEOLOGICA ULTRAIECTINA

Mededelingen van het
Instituut voor Aardwetenschappen der
Rijksuniversiteit te Utrecht

No. 43

GEOLOGICAL ANALYSIS OF PALEOZOIC LARGE-SCALE FAULTING IN THE SOUTH-CENTRAL PYRENEES

GEOLOGICAL ANALYSIS OF PALEOZOIC LARGE-SCALE FAULTING IN THE SOUTH-CENTRAL PYRENEES

GEOLOGISCHE ANALYSE VAN PALEOZOISCHE GROOTSCHALIGE BREUKBEWEGINGEN IN DE ZUIDELIJKE CENTRALE PYRENEEËN

(met een samenvatting in het Nederlands)

PROEFSCHRIFT

TER VERKRIJGING VAN DE GRAAD VAN DOCTOR IN
DE WISKUNDE EN NATUURWETENSCHAPPEN AAN
DE RIJKSUNIVERSITEIT TE UTRECHT, OP GEZAG VAN
DE RECTOR MAGNIFICUS PROF. DR. O.J. DE JONG,
VOLGENS BESLUIT VAN HET COLLEGE VAN DEKANEN
IN HET OPENBAAR TE VERDEDIGEN OP MAANDAG
21 APRIL 1985 DES NAMIDDAGS TE 4.15 UUR

DOOR

ARIE SPEKSNIJDER

GEBOREN OP 15 FEBRUARI 1951 TE GOUDA

1986
OFFSETDRUKKERIJ KANTERS B.V., ALBLASSERDAM

PROMOTOR : PROF. DR. H.J. ZWART
CO-PROMOTOR: DR. P.J.C. NAGTEGAAL

ISBN 90-71577-01-5

CONTENTS

SAMENVATTING

Het voorkomen van een oost-west strekkende fundamentele breukzone in de zuidelijke centrale Pyreneeën is aangetoond met behulp van gedetailleerd struktureel en sedimentologisch onderzoek. Deze breukzone is met tussenpozen aktief geweest vanaf het Devoon of wellicht eerder. Bijzondere aandacht is besteed aan de bestudering van breuk-begrensde, post-Varistische (Stephano-Permische) sedimentaire bekkens en de invloed van laat-Paleozoische breukvorming op het onderliggend Varistisch grondgebergte. De huidige struktuur van het grondgebergte is tamelijk gekompliceerd ten gevolge van het optreden van opeenvolgende Varistische en jongere vervormingen. De aard en de uitgebreidheid van de post-Varistische breukvorming kan om die reden slechts duidelijk worden gemaakt met behulp van een uitgebreide analyse van oudere strukturen.

De oudst bewaarde aanwijzingen voor Paleozoische deformatie in de Pyreneeën houden verband met Devonische bekkenontwikkeling in een rechts-laterale, divergente zijschuivingszone. Tijdens de eerste aanzet van de Varistische orogenese werden open, makroskopische noord-zuid en oost-west plooien gevormd, die later herplooid werden door twee opeenvolgende generaties oost-west plooien. Deze laatste plooien zijn vrij dicht en gaan vergezeld van een druksplijting. Het einde van de Varistische orogene cyclus wordt gemarkeerd door het voorkomen van kleinschalige noord-zuid plooien en knikplooien ontstaan door verkorting in het horizontale vlak.

De in het grondgebergte optredende post-Varistische rechts-laterale schuif langs bestaande oost-west druksplijtingsvlakken wordt onder andere tot uitdrukking gebracht door het systematisch oostwaards afbuigen (gaande van zuid naar noord) van laat-Varistische noord-zuid strekkende assenvlakken. Deze schuif, die op een geschatte diepte van 4 tot 5 km onder het Varistisch diskordantievlak plaats vond, is van dezelfde ouderdom als post-Varistisch bros breukgedrag en bekkenvorming aan het aardoppervlak. Aldus kan de konklusie getrokken worden dat het optreden van verschillende deformatie-typen een uitdrukking is van de verandering in deformatie-mechanismen met de diepte; alle deformatie heeft niettemin plaatsgevonden onder invloed van hetzelfde regional krachtenveld.

Alluviale sedimenten van Stephaan en Perm ouderdom zijn afgezet in een langgerekt bekken dat begrensd werd door breuken waarlangs rechts-laterale zijschuiving plaatsvond. Deze gevolgtrekking is gebaseerd op de verdeling van sedimentaire facies, de vertikale opeenvolging van gesteente-typen en tenslotte paleo-stroomrichtingen. De breuken waren aktief tot aan het einde van het Paleozoicum.

In het bestudeerde gebied zijn geen aanwijzingen gevonden voor deformatie van Mesozoische ouderdom. In het Paleogeen daarentegen vond sterke noord-zuid gerichte Alpiene verkorting plaats, hetgeen zowel in het grondgebergte als in de sedimentaire bedekking tot verplaatsing van grootschalige dekbladen aanleiding gaf. De fundamentele breukzone in de zuidelijke centrale Pyreneeën werd in het Neogeen gereaktiveerd als een links-laterale schuifzone.

SUMMARY

Detailed structural and sedimentological analysis reveals the existence of an east-west directed fundamental fault zone in the south-central Pyrenees, which has been intermittently active from (at least) the Devonian on. Emphasis is laid on the study of fault-bounded post-Variscan (Stephano-Permian) sedimentary basins, and the influence of Late Paleozoic faulting on the underlying Variscan basement. The present structure of the basement is rather complex as it results from multiple Variscan and younger deformation. The nature and extent of post-Variscan basement faulting can therefore only be appreciated with the aid of a comprehensive analysis of older structures.

The oldest preserved record of Paleozoic deformation in the Pyrenees is related to Devonian basin development in an east-west divergent oblique-slip zone of right-lateral sense. At the onset of the Variscan orogeny, open macroscopic north-south and east-west folds were formed, later to be overprinted by two generations of tight east-west cleavage folds. The end of the Variscan orogenic cycle is marked by the occurrence of minor north-south folds and compressive kinkbands.

Post-Variscan right-lateral shearing in the basement along pre-existing east-west cleavage (anisotropy) planes is reflected by the consistent eastward bending (from south to north) of Late Variscan north-south axial planes. This shearing, which took place at an estimated depth of 4-5 km below the Variscan unconformity, is of the same age as post-Variscan brittle faulting and basin development at the surface. It must be concluded that the occurrence of two different types of faulting reflects a change in deformation mechanism with depth within the same regional stress-field.

Stephanian and Permian alluvial sediments were deposited in an elongated fault-bounded basin in an overall right-lateral setting, as witnessed by the distribution of sedimentary facies, sequential arrangement of lithotypes, and paleocurrent directions. Fault movements ceased at the end of the Paleozoic.

No evidence for Mesozoic deformation has been found in the studied area. In the Paleogene, north-south shortening in the Alpine mobile belt caused the emplacement of large nappes, both in the Variscan basement and the cover. In the Neogene, the fundamental fault zone in the south-central Pyrenees was reactivated as a left-lateral shear zone.

CHAPTER I

INTRODUCTION

INTRODUCTION

Fundamental faults (de Sitter, 1964) extend deep into the crust and have a long history of movement. Sibson (1977, 1983) describes the change in deformational mechanism with depth along continental faults: from an upper seismogenetic frictional slip regime to a deeper quasi-plastic shearing regime, in which mylonites prevail. This change occurs at a depth of 8-15 km in the crust (Sibson, 1983) in the brittle-ductile transition zone. The persistency of movement on faults that extend downwards below the brittle-ductile transition, suggests that these faults may be easily reactivated at depth as a function of their material properties.

Most fundamental faults show considerable horizontal offset (10's to 100's of km). Some of these are transform faults, related to plate boundaries, like the San Andreas Fault and the Alpine Fault of New Zealand (Reading, 1980). Others are true continental strike-slip faults, classical examples being the Great Glen Fault and the North Anatolian Fault (Reading, 1980).

Direct evidence for the fundamental character of exposed faultzones is often lacking. The occurrence of fault-related rocktypes (gouges, breccias, pseudotachylytes and mylonites; Gibson, 1983) does not necessarily imply large offsets. The width of a shear zone may be more or less related to its total offset, although there is by no means a direct positive correlation between these parameters (Sorensen, 1983). Work on western Greenland has established that shear zones can widen with depth (Bak et al., 1975; Grocott, 1977), while on the other hand a strong upward widening of fault zones towards the surface is observed in the case of basement-induced strike-slip faulting (Naylor et al., 1986). Large strike-slip faults show a complicated anastomosing surface pattern of splaying and rejoining subsidiary faults or shearzones, along which rocks of different age and sedimentary/ metamorphic facies may be juxtaposed.

The most important criteria for the recognition of fundamental faults are, therefore, not directly related to the structure itself, but are instead of stratigraphical, sedimentological and regional geological nature. An example of the latter is the correlation of the Strontian and Foyers granites at both sides of the Great Glen Fault, indicating a possible 65 mile sinistral offset (Kennedy, 1946).

In the next four chapters of this thesis, an account will be given of properties and geological history of a fundamental faultzone in the Spanish Pyrenees. Also in this case, most of the evidence put forward to characterise the faultzone is of indirect nature.

Before discussing this fault zone in detail, however, a short introduction to the geology of the Pyrenees will be presented below, with special reference to major faults.

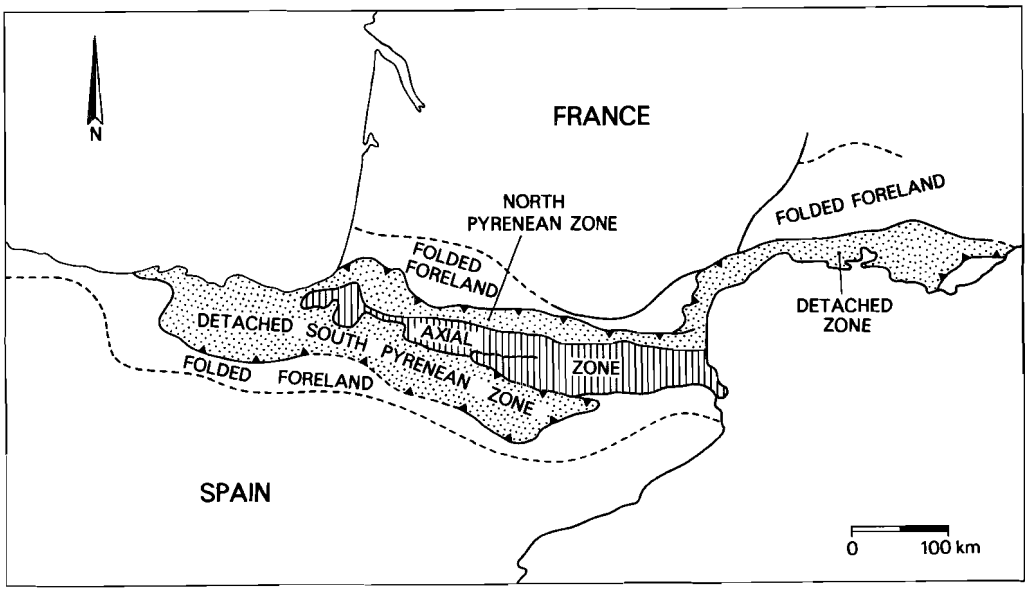

Fig. I.1. Tectonic setting of the Alpine Pyrenean orogenic belt.

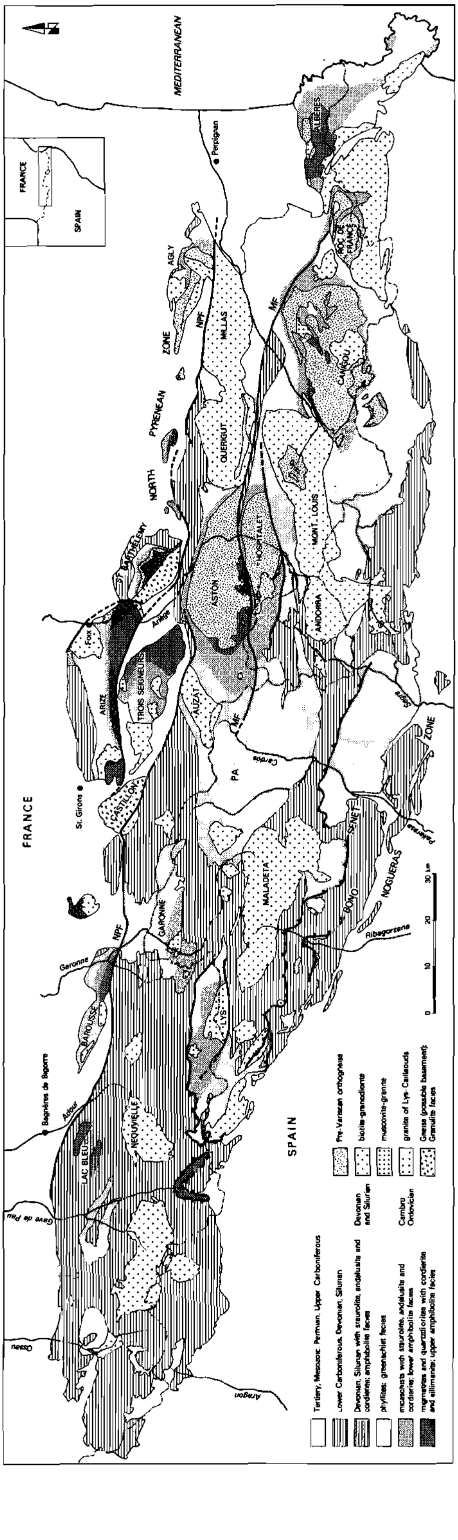

MEDITERRANEAN
FRANCE
SPAIN
Perpignan
ALBÈRES
ROC DE FRANCE
AGLY
MILLAS
CANIGOU
NORTH PYRENEAN ZONE
NPF
MF
QUERIGUT
MONT. LOUIS
HOSPITALET
ASTON
ANDORRA
ST BARTHÉLEMY
Foix
Ariège
ARIZE
TROIS SEIGNEURS
AULUS
PA
St. Girons
CASTILLON
SENET
ZONE
MALADETA
BONO
NOGUERAS
Ribagorzana
GARONNE
Garonne
BAROUSSE
LYS
Bagnères de Bigorre
Adour
NEOUVIELLE
LAC BLEU
Gave de Pau
Ossau
Aragon
0 10 20 30 km
Tertiary, Mesozoic, Permian, Upper Carboniferous
Lower Carboniferous, Devonian, Silurian
Devonian, Silurian with staurolite, andalusite and cordierite; amphibolite facies
Devonian and Silurian
phyllites; greenschist facies
micaschists with staurolite, andalusite and cordierite; lower amphibolite facies
Cambro Ordovician
migmatites and quartzdiorites with cordierite and sillimanite; upper amphibolite facies
Pre-Variscan orthogneiss
biotite-granodiorite
muscovite-granite
granite of Lys-Caillaouas
Gneiss (possible basement); Granulite facies

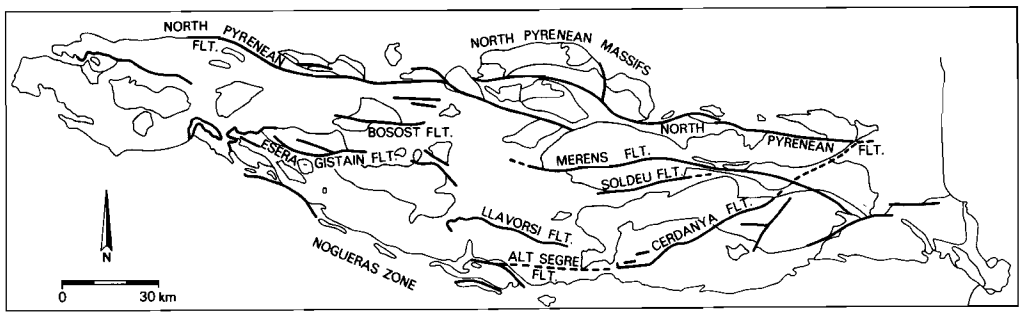

Fig. I.2. a.(left) Geological map, and b.(above) structural sketch map of the Axial Zone of the Pyrenees.

The Pyrenees are an elongated, roughly east-west trending collision belt between the Iberian microplate and the European plate (Fig. I.1). Broad deformed basins filled with Mesozoic and Tertiary sediments characterise both the southern and northern part of the chain. The central part of the present outcrop of the Pyrenees is occupied by the sedimentary and crystalline Variscan rocks of the Axial Zone (Figs. I.1 and I.2; Zwart, 1979). This zone forms the "backbone" of the Pyrenees and is cut-off in the north by the North Pyrenean Fault (de Sitter, 1954, 1965), which runs parallel to the strike of the (Variscan and Alpine) orogenic belt (Fig. I.2b). The North Pyrenean Zone, north of the North Pyrenean Fault, contains a complicated mosaic of isolated "satellite massifs" (de Sitter and Zwart, 1959), surrounded by deformed and metamorphosed Mesozoic rocks. These massifs are not only built of Variscan rocks, but also contain their Precambrian basement. Differences in metamorphic grade on both sides of the North Pyrenean Fault led Zwart (1954) to postulate a throw of 5 km or more on the fault, with a downthrown southern block. The same author postulated a reverse sense of movement (towards the south) on the east-west Merens Fault (Zwart, 1958), transsecting the Aston and Hospitalet Massifs in the Axial Zone (Fig. I.2).

South of the Axial Zone, Variscan rocks crop out in the Nogueras Zone (Fig. I.2), which further comprises deformed post-Variscan rocks (Misch, 1934). This author, followed by many others (e.g. de Sitter, 1965), considered the Variscan outcrops to be autochthonous structural units,

comparable to the North Pyrenean satellite massifs. A steep major fault would then separate the Nogueras Zone from the Axial Zone. Already Dalloni (1913), however, envisaged a allochthonous origin of the Nogueras Zone. This interpretation was further substantiated by the work of Séguret (1970), and it is now widely accepted that extensive Alpine nappe complexes, including the Nogueras Zone, have developed south of, and probably also within, the Axial Zone (Williams, 1985). Still it seems that the boundary between Axial Zone and Nogueras Zone is underlain by a major post-Variscan (and probably older) shear zone, as will be shown in the following chapters.

The structure and history of the North Pyrenean Fault and the North Pyrenean Zone have also been subject to re-interpretation. In addition to the vertical offset recorded by Zwart (1954), Le Pichon et al. (1971) proposed Mesozoic left-lateral movements up to hundreds of km. This proposal was basically supported by Choukroune (1974). Arthaud and Matte (1977), on the other hand, suggested large-scale Late Paleozoic movements of right-lateral sense. There is still much debate in literature about the role of the North Pyrenean Fault in the Tertiary and earlier history of the Pyrenees. Paleomagnetic data indicates that it marks the boundary between the Iberian and European plates (Van der Voo & Boessenkool, 1973), and the occurrence of ultrabasic rocks (lherzolites) confirms its deep-seated nature (Avé-Lallemant, 1969). Geophysical methods reveal a sudden change in depth of the Moho beneath the present trace of the North Pyrenean Fault, from 45 km on the southern side to 30 km on the northern side (Daignières et al., 1982). This leads Séguret et al. (1985) to propose a thick-skinned thrust model, in which the North Pyrenean Fault is the direct surface expression of the suture between the two plates (Fig. I.3a), whereas Williams and Fischer (1984) claim an allochtonous position of almost the entire Pyrenees in their thin-skinned interpretation, including the surface trace of the North Pyrenean Fault (Fig. I.3b). In both models, however, it is assumed that the North Pyrenean Fault is of pre-Late Cretaceous age, but it is probably much older than that.

The same holds for several large faults within the Axial Zone, such as the Merens Fault, on which both Alpine and Variscan movement did occur (Lamouroux et al., 1981; Soula, 1982).

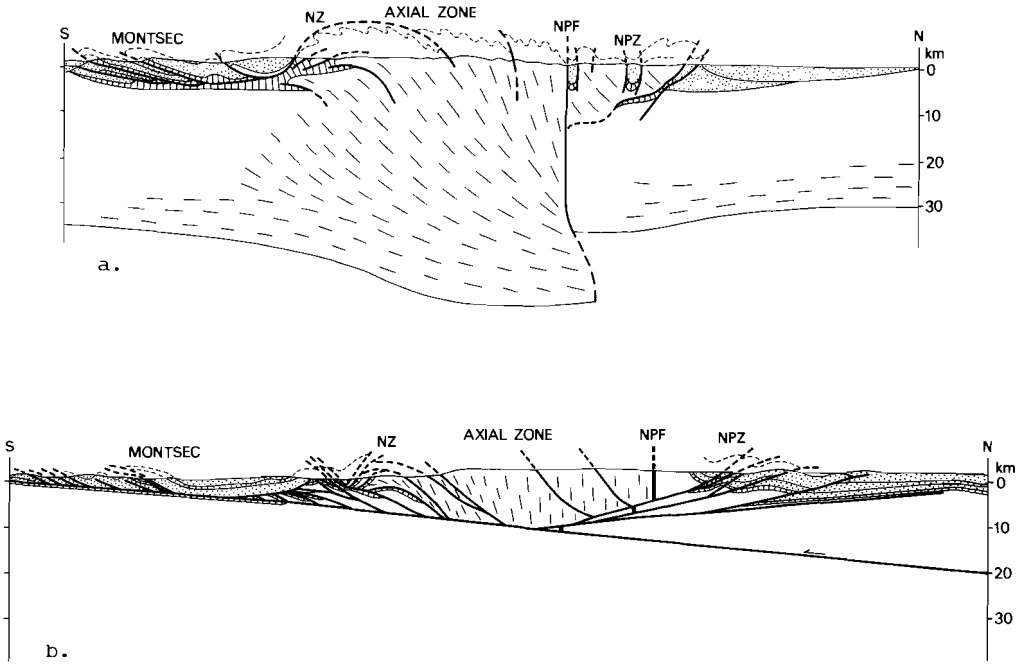

Fig. I.3. (a) Thick-skinned (after Séguret et al., 1985), and (b) thin-skinned (after Williams and Fischer, 1984) thrust models for the Pyrenees. The N-S profiles run close to each other through the central Pyrenees. Scales are identical; no vertical exaggeration. Pre-Triassic rocks are unornamented except for thin lines indicating foliation attitude, Triassic rocks are striped, and post-Triassic sediments are shown stippled. NZ= Nogueras Zone; NPF= North Pyrenean Fault; NPZ= North Pyrenean Zone.

The importance of faults with other than east-west direction, such as the Catalunya Fault, has been stressed by Peybèrnes and Souquet (1984) and Souquet et al. (1977). These faults may have been active as secondary shears during left-lateral movement within the Pyrenean mobile belt in the Mesozoic and Tertiary.

As can be noticed from the above review, most of the knowledge on large-scale faulting in the Pyrenees is restricted to Mesozoic and younger

deformation. Furthermore, little is known about major faults in the southern Axial Zone.

The next chapters of this thesis deal with an east-west fundamental fault zone that corresponds with the Alt Segre-Gerri de la Sal lineament system (Fig. 1.2b) observed on satellite images by Sole-Sugrañes (1978). Its present expression along the southern Axial Zone and the northern Nogueras Zone is mainly of Tertiary age, when left-lateral movements took place. In post-Variscan (Stephano-Permian) times, however, the movement direction was right-lateral (c.f. Arthaud & Matte, 1977).

Chapter II describes facies development and sequential arrangement of lithotypes in post-Variscan, fault-induced sedimentary basins overlying the Axial Zone. Sedimentary analysis indicates that these basins must have generated in an elongated oblique-slip zone in which frequent alternations of divergent and convergent wrenching took place. Total lateral offset is estimated to be in the order of 10 km, whereas fault throw amounts to 1.5 km. The latter value emphasises the superficial brittle nature of the faulting within the basins.

The next two chapters deal with deformation in the basement underlying the Stephano-Permian sedimentary basins. In chapter III, pre-Variscan and Early Variscan deformation is discussed, represented by major faults and open macroscopic folds respectively. Chapter IV deals in some detail with Variscan and later deformation in the Orri dome, which forms part of the basement in the southern Axial Zone.

The contents of the previous three chapters are summarised and discussed in a final chapter.

Chapter II of this thesis has been published in identical form in Sedimentary Geology, 44 (1985), pp. 179-223. Chapters III-V have been submitted as individual articles to scientific geological journals.

ACKNOWLEDGEMENTS

I thank Antonia and Joan Marsá, Paco Santamaria and many other inhabitants of La Seu d'Urgell for their hospitality.

I am indebted to the Koninklijke/Shell Exploratie en Produktie Laboratorium for permission to make use of word-processing facilities.

REFERENCES

Arthaud, F. & Matte, P. (1977). Late Paleozoic strike-slip faulting in southern Europe and northern Africa: Result of right-lateral shear zone between the Appalachians and the Urals.
Geol.Soc.Am.Bull., 88, pp. 1305-1320.

Avé-Lallemant, H.G. (1969). Structural and petrofabric analysis of an "Alpine-type" peridote: the lherzolite of the French Pyrenees.
Leidse Geol.Meded., 42, pp. 1-57.

Bak, J., Grocott, J., Korstgard, J.A., Sorensen, K., Nash, D.F. & Watterson, J. (1975). Tectonic implications of Precambrian shear belts in western Greenland.
Nature, 254, pp. 566-569.

Choukroune, P. (1974). Structure et évolution tectonique de la zone nordpyrénéenne.
Ph.D. thesis, Montpellier, 276 pp.

Daignières, M., Gallart, J., Banda, E. & Hirn, A. (1982). Implications of the seismic structure for the orogenic evolution of the Pyrenean range.
Earth Plan.Sci.Lett., 57, pp. 88-100.

Grocott, J. (1977). The relationship between Precambrian shear belts and modern fault systems.
Jl.geol.Soc.London, 133, pp. 257-262.

Kennedy, W.Q. (1946). The Great Glen Fault.
Quart.J.Geol.Soc.London, 102, pp. 41-76.

Lamouroux, C., Soula, J.-C. & Roddaz, B. (1981). Les zones mylonitiques des massifs du Bessiès et de l'Aston (Haute Ariège).
Bull. B.R.G.M., I, 2, pp. 103-111.

Le Pichon, X., Bonnin, J., Francheteau, J. & Sibuet, J.C. (1971). Une hypothese d'évolution tectonique du Golfe de Gascogne. In: Histoire structurale du Golfe de Gascogne, pp. VI-II, 1-44. Ed. Technip, Paris.

Misch, P. (1934; translation 1948). La estructura tectonica de la region central de los Pirineos meridionales.
Publ.extranjeras Geol.Esp., 4, pp. 5-178.

Naylor, M.A., Mandl, G. and Sijpesteyn, C.H.K. (1986). Fault geometries in basement-induced wrench faulting under different initial stress states.
J.Struct.Geol., in press.

Peybèrnes, B. & Souquet, P. (1984). Basement blocks and tectono-sedimentary evolution in the Pyrenees during Mesozoic times.
Geol.Mag., 121, pp. 397-405.

Reading, H.G. (1980). Characteristics and recognition of strike-slip fault systems. In: P.F. Ballance and H.G. Reading (Editors), Sedimentation in Oblique-slip Mobile Zones. Spec.Publ.Int.Assoc.Sedimentol., 4, pp. 7-26.

Séguret, M. (1970). Etude tectonique des nappes et séries décollées de la partie centrale du versant sud des Pyrénées.
Ph.D. thesis, Montpellier, 155 pp.

Séguret, M., Daignières, M. et al. (1985). Coupes balancées d'échelle crustale des Pyrénées.
C.R.Acad.Sc.Paris, 30, pp. 341-346.

Sibson, R.H. (1977). Fault rocks and fault mechanisms.
Jl.geol.Soc.London, 133, pp. 191-214.

Sibson, R.H. (1983). Continental fault structure and the shallow earthquake source.
Jl.geol.Soc.London, 140, pp. 741-767.

Sitter, L.U. de (1954). La faille Nord-Pyrénéenne dans l'Ariège et la Haute-Garonne.
Leidse Geol.Meded., 18, pp. 287-291.

Sitter, L.U. de (1964). Structural Geology.
2nd edn., McGraw-Hill, New York, 551 pp.

Sitter, L.U. de (1965). Hercynian and Alpine orogenies in northern Spain.
Geol.Mijnbouw, 44, pp. 373-383.

Sitter, L.U. de & Zwart, H.J. (1959). Geological map of the Paleozoic of the Central Pyrenees, sheet 3, Ariege, France, 1:50.000.
Leidse Geol.Meded., 22, pp. 351-418.

Sole-Sugrañes, L. (1978). Alineaciones y fracturas en el sistema Catalan a segun las imagenes Landsat-1.
Tecniterrae, 22, pp. 1-11.

Sorensen, K. (1983). Growth and dynamics of the Nordre Stromfjord shear zone.
J.geophys.Res., 88, pp. 3419-3437.

Soula, J.-C. (1982). Characteristics and mode of emplacement of gneiss domes and plutonic domes in the central-eastern Pyrenees.
J.Struct.Geol., 3, pp. 313-342.

Souquet, P., Peybèrnes, B., Bilotte, M. & Debroas, E.-J. (1977). La chaîne alpine des Pyrénées.
Géologie Alpine, 53, pp. 193-216.

Voo, R. van der & Boessenkool, A. (1973). Permian paleomagnetic results from the western Pyrenees delineating the plate boundary between the Iberian peninsula and stable Europe.
J.Geophys.Res., 78, pp. 5118-5127.

Williams, G.D. (1985). Thrust tectonics in the south central Pyrenees.
J.Struct.Geol., 7, pp. 11-17.

Williams, G.D. & Fischer, M.W. (1984). A balanced section across the Pyrenean orogenic belt.
Tectonics, 3, pp. 773-780.

Zwart, H.J. (1954). La géologie du massif du Saint-Barthélémy, Pyrénées, France.
Leidse Geol.Meded., 18, pp. 1-228.

Zwart, H.J. (1958). La faille de Merens dans les Pyrénées ariègoises.
Bull.Soc.geol.Fr., 8, pp. 793-796.

Zwart, H.J. (1979). The geology of the central Pyrenees.
Leidse Geol.Meded., 50, pp. 1-74.

CHAPTER II

ANATOMY OF A STRIKE-SLIP FAULT CONTROLLED SEDIMENTARY BASIN, PERMIAN OF THE SOUTHERN PYRENEES, SPAIN

(Published in identical form in Sedimentary Geology, 44 (1985), pp. 179-223)

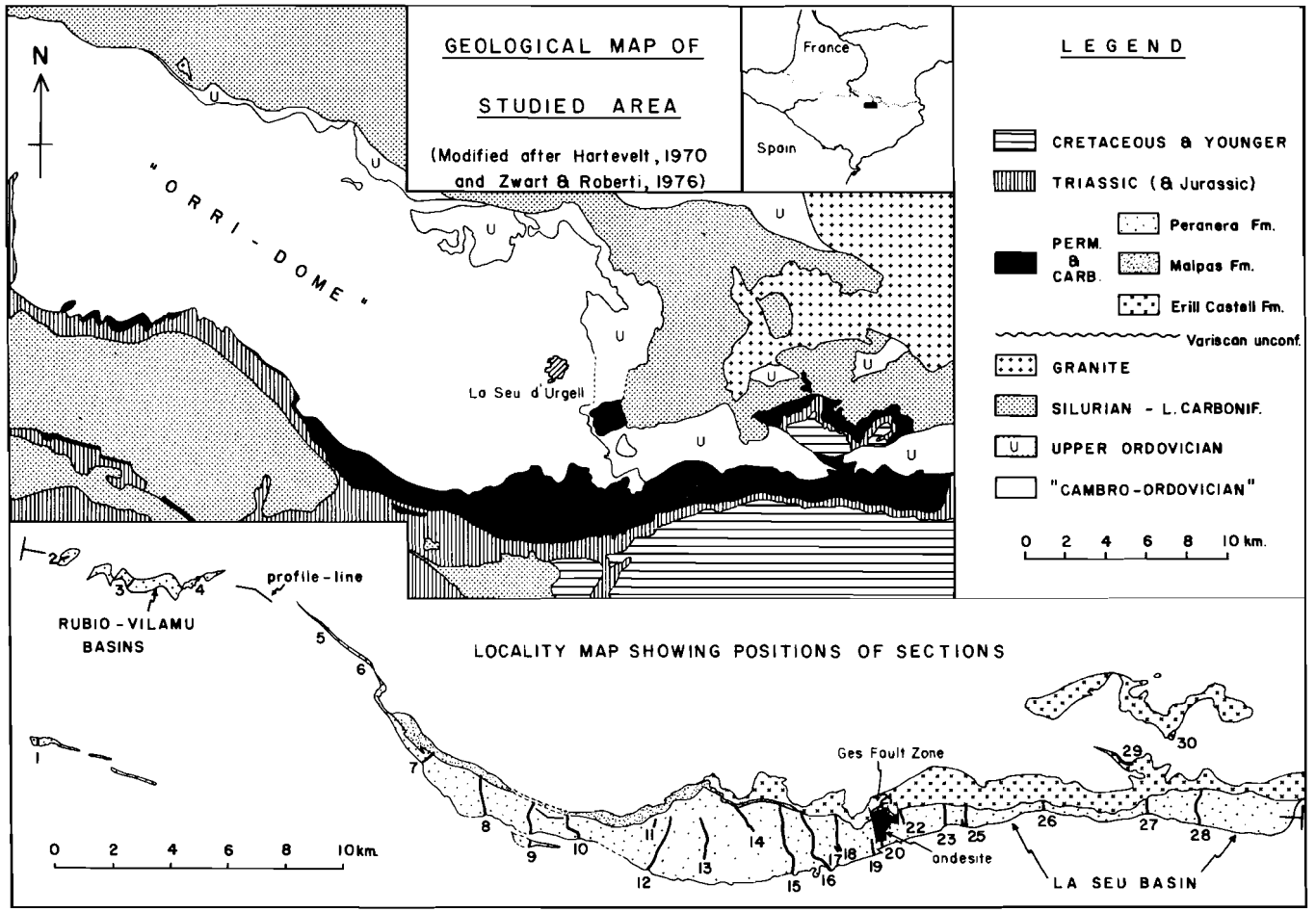
GEOLOGICAL MAP OF
STUDIED AREA
(Modified after Hartevelt, 1970
and Zwart & Roberti, 1976)
France
Spain
N
"ORRI-DOME"
La Seu d'Urgell
U
LEGEND
CRETACEOUS & YOUNGER
TRIASSIC (& Jurassic)
PERM. & CARB.
Peranera Fm.
Malpas Fm.
Erill Castell Fm.
Variscan unconf.
GRANITE
SILURIAN - L.CARBONIF.
UPPER ORDOVICIAN
"CAMBRO-ORDOVICIAN"
0 2 4 6 8 10 km.
RUBIO - VILAMU
BASINS
profile - line
LOCALITY MAP SHOWING POSITIONS OF SECTIONS
Ges Fault Zone
andesite
LA SEU BASIN
0 2 4 6 8 10km.

INTRODUCTION

This paper forms part of a series in which the relationship between structural and depositional history of a number of dominantly strike-slip sedimentary basins is investigated using both structural and sedimentological data.

The present article mainly deals with a detailed sedimentological description and interpretation of a sequence of terrestrial redbeds of probable Permian age known as the Peranera Formation (Nagtegaal, 1969), which accumulated in a number of elongated fault-bounded basins in the Spanish southern Pyrenees. In addition, it analyses the geometry and evolution of these basins, partly with the aid of structural data from the underlying basement.

Figure II.1 shows the geographical distribution of the studied basins: to the east the large La Seu basin, called after the town of La Seu d'Urgell, some 5 km north of the present-day outcrop area of the basin. The associated small Rubio-Vilamu basins to the west have been named after the villages of the same names.

Careful sedimentological study involving interpretation of depositional environment for the various lithotypes recognised, the grouping of these lithotypes into facies, facies associations and sequences, and finally the study of paleocurrent data turned out to be a powerful tool in the analysis of the structural organisation and the evolution of the sedimentary basins where structural analysis alone would have been inadequate.

Fig. II.1. (left) Geological and situation map of the studied area.

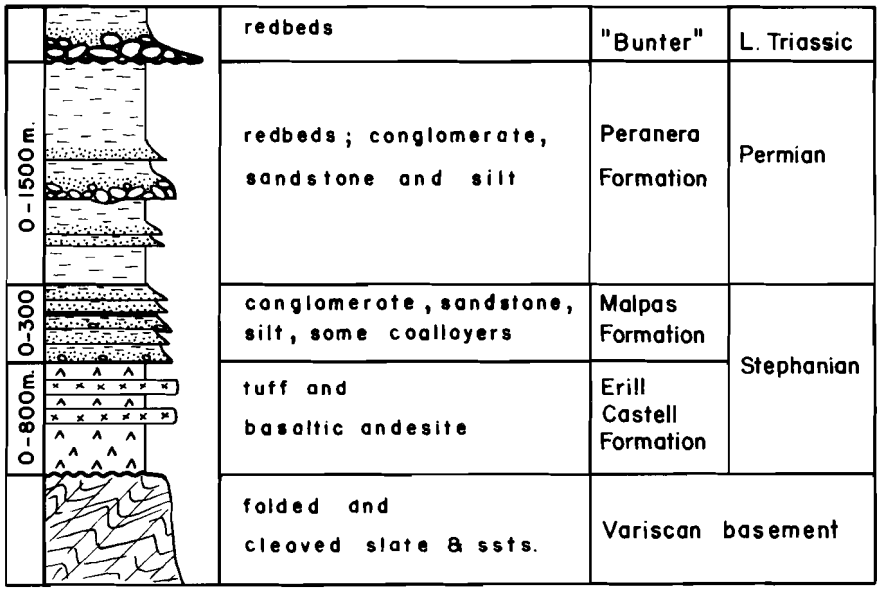

Fig. II.2. Generalised stratigraphical section of post-Variscan rocks in the south-central Pyrenees. No scale implied. Thicknesses refer to present study area.

Geological setting and structural geology of the basement

The La Seu and Rubio-Vilamu basins crop out with dominant east-west strike over a length of 55 km along the southern border of the so-called Axial Zone of the Pyrenees. The Axial Zone consists of rocks folded, metamorphosed and intruded during the Variscan orogeny (Zwart, 1979), while the basins contain unmetamorphosed sediments of Westphalian D and younger Paleozoic age which unconformably overlie the Variscan basement. The stratigraphy of these basinfills, which is summarised in Fig. II.2, has been set up by Mey (1968), Mey et al. (1968) and Nagtegaal (1969). The latter author carried out a detailed study of similar post-Variscan rocks in an area to the west of the La Seu basin.

The redbeds of the Peranera Formation form the main subject of the present paper. Although their precise age is not known, they are generally

regarded to be of Permian age, as they occur between sediments of proven Stephanian and Lower Triassic age (Hartevelt, 1970).

As a result of strong Tertiary uplift of the Axial Zone, the beds of the Peranera Formation, as well as the Variscan unconformity plane, now dip approximately 45° towards the south. Consequently, the directly underlying Variscan rocks must also have been influenced by this tilting. This implies that Paleozoic rocks now cropping out just north of the inclined Variscan unconformity, once formed part of the basement more or less underlying the La Seu and Rubio-Vilamu basins. Therefore, a structural study of the Variscan basement north of the present outcrop of the Peranera Formation will provide useful information on the deformation of the rocks that once lay below the La Seu basin, and may thus help clarify the structural setting of the basin.

A structural analysis of the so-called Orri-dome (Hartevelt, 1970; see Fig. II.1) revealed the occurrence of five or six separate Variscan deformation generations, one of post-Variscan Paleozoic (probably Stephano-Permian) age and at least two of Alpine age (see chapter III).

The Stephano-Permian deformation is thought to have been of primary importance to the development of the La Seu basin. It was of the simple shear type and caused dextral east-west shear movements along various anisotropy planes of Variscan age such as cleavages, steep faults and thrusts. Dextral east-west simple shear in the basement and development of an east-west aligned strike-slip basin at the surface are proposed to be different expressions of the same regional stress field at different levels in the crust.

Previous work

Apart from Nagtegaal's (1969) work west of the present study area, the Peranera Formation was briefly described by Hartevelt (1970), who made the first detailed map of the outcrop area of the La Seu basin. The map by Zwart and Roberti (1976) includes the Rubio-Vilamu basins, while Hartevelt & Roger (1968) present a brief description of one of these basins. Sopeña et al. (1977) give a review of the occurrence of Permian rocks in the Spanish Pyrenees. References to earlier work are given by the authors mentioned above. More recently, Gisbert (1981) published an abstract of his thesis

covering the sedimentology of Stephanian, Permian and Lower Triassic rocks in the same area with emphasis on diagenesis and paleoclimatology. His conclusions regarding the environment of deposition of the sedimentary sequence fully agree with mine.

Bixel and Lucas (1983) describe the magmatism, tectonics and sedimentation in Stephano-Permian basins in the western Pyrenees. These authors attribute the opening of the sedimentary basins to E-W directed "late Hercynian transcurrent shearing" which partly reactivated older Variscan structures. The concept of basin formation by reactivation of basement structures in the western Pyrenees was already forwarded by Soula et al. (1979).

Methods of study

In order to analyse the geometry and sedimentary history of the La Seu and Rubio-Vilamu basins, a great part of this study was taken up by fieldwork. Some 30 sections were measured on a 1:500 scale, in total representing more than 10 km of (stratigraphic) sediment thickness (Fig. II.1).

Special attention was paid to sedimentary structures and the paleocurrent directions they reveal, although in most sections sedimentary structures were hard to recognise due to poor outcrop conditions. The properties of some conglomerate beds, including maximum pebble size, sorting, bed thickness/ maximum pebble size ratio and pebble composition were determined in order to throw some light upon mode of transportation and deposition. Maximum pebble size was defined as the mean of the longest axes of the three largest pebbles in a conglomerate bed that occur in a zone approximately 1-5 m wide on both sides of the section line (Bluck, 1967).

Correlations between adjacent sections are based on similarities of distribution of very coarse- and very fine-grained intervals, fining upward (FU) and coarsening upward (CU) patterns, pebble composition, study of aerial photographs and direct tracing of beds in the field.

SEDIMENTARY FACIES

In the Permian rocks of the La Seu- and the Rubio-Vilamu basins the following sedimentary facies have been distinguished: (1) breccia facies; (2) conglomerate facies; (3) pebbly sandstone and coarse cross-bedded sandstone facies; (4) fine-grained sandstone facies; and (5) silt and clay facies.

As will be shown in the next chapter, these facies can be grouped into three facies associations.

Breccia facies

Description. The breccia facies only occurs in the lowest levels of the Rubio-Vilamu basins (sections 2-5) and in the top of section 9 (see Fig. II.1 for positions of sections). In the former case they are composed of angular to very angular cobbles and pebbles, and are without exception derived from the Ordovician slates and sandstones on which they rest unconformably. A profile typical of the transition zone from Variscan to post-Variscan rocks shows from bottom to top: Unaltered folded and cleaved sandstones and slates; weathered to strongly weathered rocks, often with faint pink staining; loose but in-situ fragments, often dragged apart, with some infill of red sandstone and mud between them; and, finally, breccia consisting of red-stained coarse debris in a red sandstone and/or silt matrix (Fig. II.3).

Higher in the breccia units the fragments usually float in the matrix which largely consists of silt. The units show no internal structure, pebbles have no preferred orientation and are very badly sorted. Complete sequences show, nevertheless, marked fining-upward tendencies. Breccia units are separated from each other by thin layers of silt, pebbly siltstone or (pebbly) fine sandstone.

Although individual breccia units have maximum thicknesses of 10-12 m, they occur to a height of 30 m above the Variscan unconformity and form wedge-shaped bodies on the downthrown sides of steep normal faults bordering the Rubio-Vilamu basins. Breccias grade into finer deposits in a vertical as

Fig. II.3. Breccia at the base of section 3, just above the Variscan unconformity plane. For position see Fig. II.10. The hammershaft lies approximately parallel to the unconformity plane; the sequence becomes younger towards the left.

well as a lateral sense, in directions at large angles to the approximately north-south striking bounding faults.

The breccia in the top part of section 9 shows many features similar to the ones described above. It is usually matrix-supported (silt-grade) and occurs in units a few meters thick which are interbedded with mudstone and

pebbly mudstone. Pebble composition, rounding and sorting are the same as in the Rubio-Vilamu basins and in nearly all cases the beds also lack internal structures. The lower contacts of individual sedimentation units are non-erosional. The base of this breccia interval is not exposed and its three-dimensional shape is not well known. To the east and the west, however, sediments from the same part of Basinfill Sequence F (Figs. II.9 and II.19) are very fine-grained and field observations suggest that the breccias are bounded, as in the Rubio-Vilamu basins, by north-south striking high-angle faults.

Interpretation. The described contact between Variscan basement and breccia, showing almost in situ, dragged-apart cobbles and pebbles, strongly suggests that the base of the breccia unit is a fossil slope breccia. As for the remainder of the deposits, the pebble composition, the very poor rounding and sorting, the absence of any preferred orientation of the clasts, the occurrence of both framework- and matrix support, the lack of internal sedimentary structures and the non-erosive lower bedcontacts, point to short-distance mass flow transport.

The wedge-shaped geometry of the breccia bodies and their association with steep faults bounding the basin (only occurring immediately next to the faults on their downthrown sides) imply that transportation and subsequent sedimentation of scree breccia and debris flows were triggered by tectonic activity. Breccias form the lower part of the infill of rapidly subsiding grabens and are incorporated in the grabenfill facies association. The breccia and mudflows of section 9 differ little from the previously described ones and are also classified with this association.

Throughout the breccia units the occurrence of FU sequences is interpreted as a result of waning energy conditions (Bluck, 1967; Steel, 1974).

Conglomerate facies

Field data. Conglomerate beds usually show great lateral extent, from some hundreds of meters to some tens of kilometers, with only minor changes of their properties. They always form the lower part of well-defined FU

Fig. II.4. Unstratified conglomerate in the lower part of Basinfill Sequence F in section 15. See Fig. II.12 for location. Bedding plane just visible in upper left-hand corner.

cycles, thus overlain by sandstones and silt. On the scale of an outcrop, scouring might occur at the base, but on a larger scale the beds are flat-based and indications for significant erosion are lacking. In a few cases there is a thin (10-20 cm) sandstone layer beneath the conglomerate bed.

Maximum bed thickness is a few meters (the only exception being the lower beds of the youngest basin-infill, see Fig. II.12). Often the deposits are framework conglomerates, but in some cases the pebbles, which may have a diameter up to a few dm, are suspended in a matrix of usually coarse sand showing pink to red colours. Sorting of the clasts ranges from poorly to well-sorted and is often in the range of moderately to moderately well-sorted. Rounding is in general poor but moderately well rounded pebbles do occur. Whenever limestone pebbles are present, the matrix of the conglomerate beds and all underlying rocks may be strongly calcified.

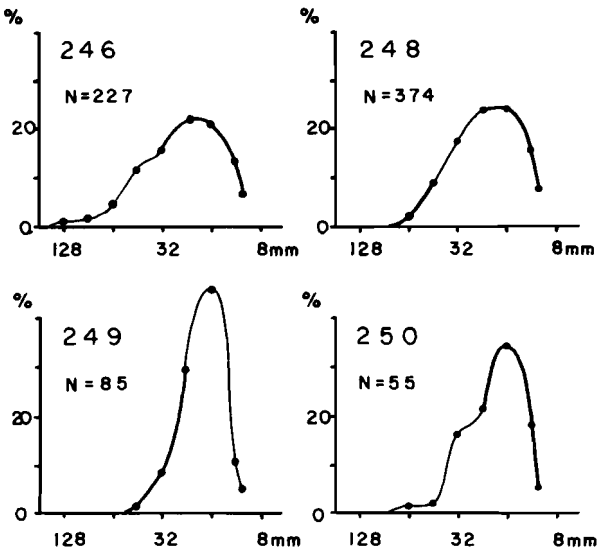

Fig. II.5. Clast-size distribution of four conglomerate beds in section 15. Horizontal scale shows clast size, vertical scale gives percentages per clast size class (each class covers 1/2 ϕ unit). Thick lines indicate normal distributions of clast sizes as tested on log-normal graph paper. N is number of measurements, numbers 246-250 are bed numbers in section 15 (see Fig. II.12). (Note: as only clasts larger than 1 cm have been measured, the distributions have been cut-off at their fine tail which introduces some skewness towards the coarse tail. However, this effect is not large enough to explain the strong skewnesses shown in this figure.)

Although the above description holds for all conglomerates, they can be subdivided into two types: stratified and unstratified conglomerates. Unstratified conglomerates lack internal structure (Fig. II.4). Usually there is no obvious internal grading but CU, FU and stacked CU-FU tendencies have been observed. Stratified conglomerates only occur within Basinfill Sequence F (Fig. II.16) and are well exposed in section 15. Bed thicknesses vary between 0.5 and 3 m. Structures frequently are large-scale, high-angle tabular cross-bedding, organised in sets of a few dm to one meter in height.

Lower bed contacts can be erosive but conglomerates are not noticeably restricted to channels.

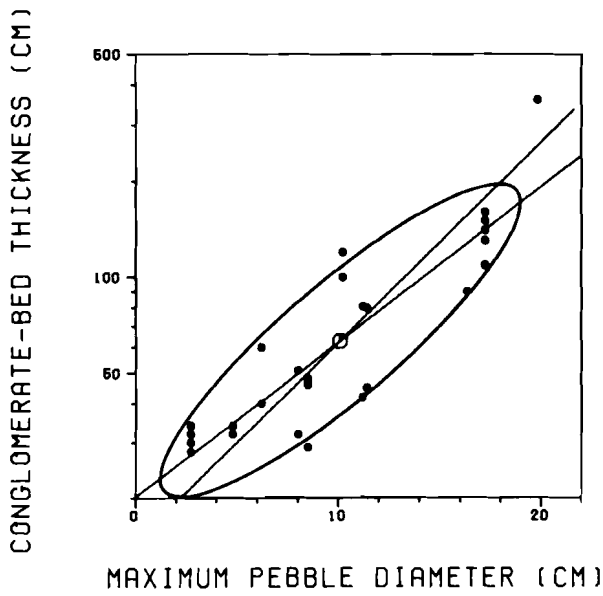

Fig. II.6. Relation between maximum pebble diameter and conglomerate bed thickness for unstratified conglomerate beds in section 15. Number of readings: 26; correlation coefficient: 0.88. Regression lines x-on-y and y-on-x, and 75% confidence ellipse are shown.

Clast-size distribution. Figure II.5 shows four representative clast-size distribution diagrams for conglomerate beds in section 15. The distributions are markedly skewed towards their coarse tails, indicating that some lagging process was operative, producing an enrichment in coarse clasts. Such lagging may be the result of two different processes: winnowing out or bypassing of fines (Bluck, 1967).

Relation bed thickness/maximum pebble diameter. Figure II.6 shows the relation between maximum pebble diameter and unstratified conglomerate bed thickness in section 15. Two important conclusions can be drawn from the good correlation between these two properties (see Bluck, 1967, and Steel, 1974):

(1) As is discussed by Blatt et al. (1972, p. 91), the Shield criterion relates the critical bottom stress of a water stream to the size of (quartz-)particles in transport. Following the criterion, a linear relationship between grain size and competence of the stream can be expected for the conglomerates of the Peranera Formation. As, on the other hand, Fig. II.6 shows a linear relationship between pebble diameter and conglomerate bed thickness, it follows that conglomerate bed thickness and stream competence are also linearly related. If we consequently take bed thickness to be a measure of the total volume of debris laid down in one depositional event, a relation is established between competence of the stream and total volume of sediment deposited from it. This, together with the observation that there is little or no evidence for erosion in the conglomerates, suggests deposition from "single-event" debris flows (Bluck, 1967).

(2) In alluvial systems pebble size decreases in directions away from the source (c.f. Heward, 1978a). Because maximum pebble-size is proportional to conglomerate bed thickness, bed thickness should also decrease in directions away from the source, with the consequence that the beds will be wedge-shaped. This property is not restricted only to conglomerate beds, as is illustrated in Fig. II.7.

Relationship of percentage limestone pebbles to maximum pebble-size. The lower part of Basinfill Sequence F within the La Seu basin mainly consists of thick (up to 10 m) stratified and unstratified conglomerate beds usually containing high quantities of limestone pebbles, together with quartz-, quartzite- and sandstone pebbles (Fig. II.12). To find an explanation for the strongly varying limestone pebble content, the ratio limestone pebble percentage /maximum pebble diameter has been determined in six sections. Figure II.8 offers a representative selection of the results and there clearly is a positive correlation between the two properties. As clast size decreases with length of transport path and/or reworking, this relation will also hold for limestone pebble percentage. The conclusion is, of course, not a surprising one: limestone pebbles are known to be relatively sensitive to mechanical as well as chemical weathering.

The lowest units of Basinfill Sequence F invariably show the largest pebbles and the highest limestone pebble content. Both properties, however, decline with height above the base of the basinfill sequence (Fig. II.12).

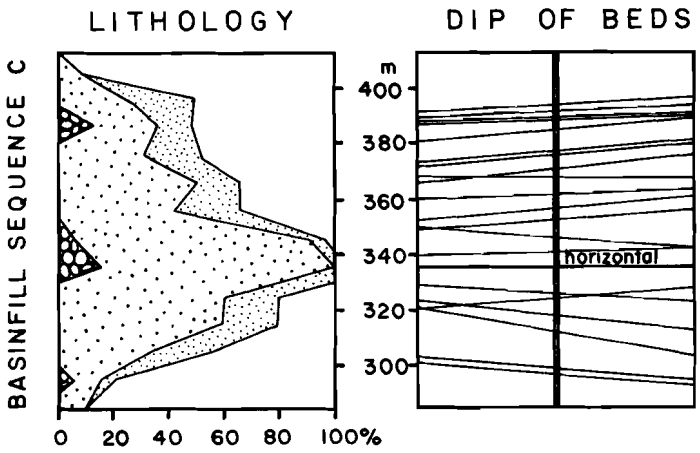

Fig. II.7. Wedge-shaped arrangement of conglomerate- and sandstone beds in a major CU-FU megasequence of Basinfill Sequence C. Vertical scale represents height above base of section 15. The left part of the figure shows distribution of lithotypes (conglomerate, coarse sandstone, fine sandstone and silt, respectively). In the right part of the figure, lines show dips of individual beds after rotation of the thickest conglomerate bed in the megasequence (at 336 m) to a horizontal position.

Consequently, the high limestone pebble percentages and large pebbles from the base of the basinfill sequence reflect mass-flow transportation over only short distances, without significant reworking, where stratified conglomerates in higher stratigraphic levels originate from reworking of older (unstratified) conglomerates and have been transported over relatively larger distances.

Interpretation. The unstratified conglomerate beds at the base of Basinfill Sequence F have greater thickness and lateral extent than all other conglomerates in the La Seu basin. This property, together with the sharp, non-erosive bases, absence of internal structures such as imbrication, the clast/matrix relation, lack of sorting, the average clast size and presence of faint normal and inverted grading are all typical field

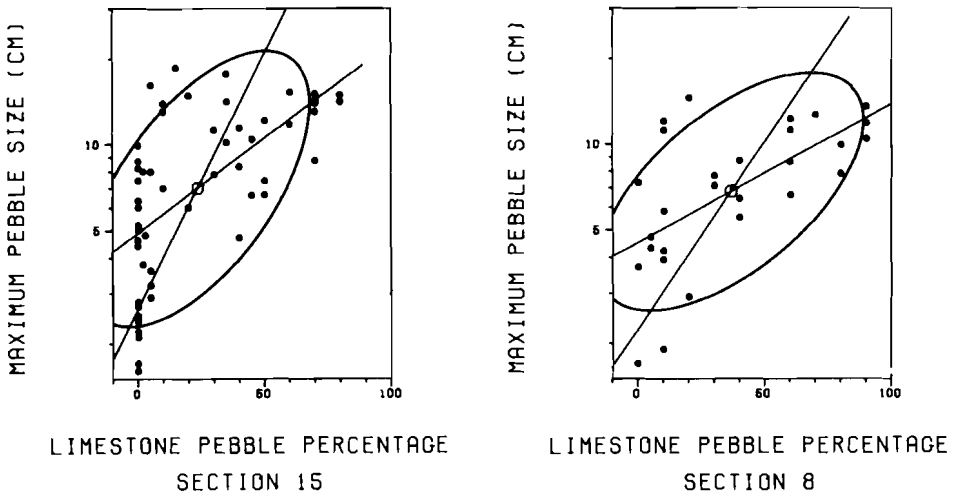

Fig. II.8. Relation between limestone pebble percentage and maximum pebble size in sections 8 and 15. Number of readings: 28 and 54, respectively; correlation coefficients 0.62 and 0.61, respectively; 75% confidence ellipses and regressions x-on-y and y-on-x shown in both cases.

aspects of a debris flow deposit. The relationship between maximum pebble size and bed thickness confirms this origin. Due to their mode of deposition and wedged shape, the conglomerates of the lower part of Basinfill Sequence F are considered to be proximal alluvial fan deposits.

The other unstratified conglomerates of the La Seu basin are basically of the same type but are thinner and laterally less extensive compared to the ones interpreted above. Furthermore, their bases may be erosive, sorting is usually better and they contain fewer limestone pebbles. This type of sediment shows many resemblances to the "A type" conglomerates of Allen (1981), who interpreted them as fossil longitudinal bar deposits, i.e. thick gravel sheets with little topographic relief. In the Peranera Formation, the vertical as well as lateral grading of conglomerate into sandstone further supports their interpretation as longitudinal bars.

The erosive bases, lateral extent, FU sequences, often large clast size and the occurrence of large-scale cross-bedding within the stratified conglomerates point to deposition from competent, turbulent streams of low

viscosity, spreading out over considerably large, flat areas. According to Heward (1978b) this type of stratified conglomerate must be situated in the mid-fan area.

Skewness of clast size distribution and the maximum pebble size/limestone pebble content relationships (Figs. II.5 and II.8) are indicative of considerable reworking of earlier deposited sediments. This reworking must in this case be the result of scarp retreat and lowering of relief (Heward, 1978a, p. 685).

In conclusion, unstratified as well as stratified conglomerates form part of the "alluvial fan and ephemeral stream facies association", in which debris flows occupy a relatively proximal fan position, where other conglomerate types are the products of reworking of older sediment and occur on relatively low reaches of alluvial fans and, further basinward, in the ephemeral stream environment.

Pebbly sandstone and coarse cross-bedded sandstone facies

Description. Pebbly sandstone and coarse cross-bedded sandstone beds are usually continuous for hundreds of meters but can grade laterally into conglomerates or fine sandstones and eventually silt. They make up the greater part of the coarse-grained basinfill. The bases of the beds are almost exclusively erosive, scouring and channelling (with associated lag deposits) occur on a meter scale. Nevertheless, it has not been possible to recognise larger channels. Individual beds have thicknesses between 0.5 and 5 m, and typically show red, pink and grey colours. Because of strong weathering of the beds, sedimentary structures are often hard to identify, but high angle trough cross-stratification seems to be abundant. The trough sets have heights between some dm and 2 m. In thick sandstone units it is often difficult to recognise the principal surface of accumulation, especially if cross-stratification is well developed.

In the pebbly sandstones, clasts can occur in a lag deposit and in strings along foresets or they appear to be randomly distributed. In the latter case pebbles have a maximum diameter of a few cm only. Clast composition shows little variation and comprises quartz, quartzite, sandstone and rare limestone pebbles. In some sandstones mudclasts have been found which were clearly derived from the underlying silts. The matrix is

usually made up of fine and coarse sandstone. Sorting is moderate to moderately good, but pebbles are poorly rounded.

On top of cross-bedded units, even-laminated coarse sandstone layers may be found, generally lacking pebbles. The transition between the two is gradual, but takes place within a few cm. Even-laminated, coarse sandstone may also alternate with silt levels. Within Basinfill Sequence F (Fig. II.16) a special type of sandstone has been found showing well-developed lag deposits consisting of mudclasts, well-rounded pebbles and plant remains. The lag is overlain by cross-bedded coarse sandstone with distinct lateral accretion surfaces. The bases of the beds are erosive and a complete sequence is always fining upward. In all observed cases, paleocurrent directions are roughly perpendicular to the accretion surfaces.

Interpretation. The pebbly sandstone and cross-bedded sandstone facies represents "braided stream deposits" (Steel & Wilson, 1975) occurring below the intersection point of alluvial fans (Brookfield, 1980). The thin even-laminated sandstone units are interpreted as sheetflood deposits, which may develop downstream from braided stream deposits, but might also be laid down during overbank flooding of streamflood channels. In both cases deposition is from shallow waterflows.

The pebbly sandstones and coarse cross-bedded sandstones make up the bulk of the alluvial fan and ephemeral stream facies association, but sheet-flood deposits belong to the basin floor association.

The special type of sandstones of Basinfill Sequence F, showing discrete accretion surfaces and lags, are part of point bar deposits of the basin floor association.

Fine-grained sandstone facies

Description. Fine-grained sandstones are volumetrically insignificant in the La Seu basin. Very often they form part of FU sequences, overlying coarse-grained sandstone and overlain by silts. Transitions in grain size are gradual, but may occur within a few cm or dm. Maximum bed thickness is a few metres and sedimentary structures include (trough) cross-bedding, even-lamination or small-scale structures (ripples and cross-lamination). Sorting

is usually moderate to good and rounding ranges from bad to moderate. Sometimes fine-grained sandstones do not form part of FU sequences and are then intercalated in silts. In this case they may be divided into two groups: Firstly, units less than 1 m thick, laterally grading into silts and/or coarser-grained sediments. In the latter case bed thickness may increase rapidly over short distances. The lower boundary is often slightly erosive, whereas the upward transition to silts is always gradual. Due to moderate to good sorting and poor outcrop conditions it is generally hard to detect any sedimentary structures, though even-lamination and (trough-?) cross-bedding have been found.

The second group consists of thin to very thin sandstones, occurring between thick (more than 5-10 m) siltstone units. They show no obvious relationship with coarser-grained sediments and possess sharp upper and lower boundaries. They may reach considerable lateral extent. Sorting and rounding are good. Sedimentary structures have seldom been recognised.

Interpretation. Fine sandstones that form part of FU sequences are thought to have been deposited during the waning current stage of a sedimentary event in an alluvial fan or braided stream environment. In this respect they are the fine-grained equivalent of coarse cross-bedded sandstones found on top of thick conglomerate beds. This type of fine sandstone belongs to the alluvial fan and ephemeral stream association.

The first type of fine-grained sandstone intercalated in silt, showing a relationship with coarser grained sediments, is interpreted as the lateral equivalent of braided streams. The second type, not showing such a relation, represents a lateral or downcurrent equivalent of sheetfloods or possibly a crevasse-type of intrafan or basinfloor deposit. Most of the fine sandstones embedded in silts are attributed to the basin floor association, especially the type embedded in siltstone units.

Silt and Clay Facies

Description. Silt is the most widespread lithofacies in the La Seu basin. In section 15 (Fig. II.1), for example, 52% of the total rock volume is silt and in Basinfill Sequence F in this section there is no less than

79% silt. Clay occurs in only very limited amounts, at the very top of FU sequences. A hard red to purple colour is very characteristic of both lithotypes. Silts are usually massive, but sometimes vague even lamination and/or (trough-) cross-lamination is developed. At some levels rootlets are present, but well-preserved mottling has never been found. Hartevelt (1970) mentions the occurrence of badly preserved plant imprints in the upper part of Basinfill Sequence F. Mudcracks are often encountered, especially in the top of the Peranera Formation. Rain imprints are less frequent but they may be found at any level throughout the formation. Much the same holds for "puddle deposits", first described by Nagtegaal (1969).

A remarkable feature is the occurrence of caliches and calcretes in the fine-grained intervals. The first type of concretions is defined as isolated nodules of $CaCO_3$, while calcretes occur in more or less continuous layers, often exhibiting wavy lamination. Sometimes it can be proved that the latter type, which is of very limited occurrence, developed from $CaCO_3$ enrichment in fine sandstone, but in all other cases the original sediment was silt. Caliche-bearing profiles range in thickness from a few dm up to 40 m (c.f. Fig. II.12). Rocks from the top of Basinfill Sequence F may comprise very thin (less than 5 cm) limestone layers which show great lateral persistency (Fig. II.9). Eastwards, towards the Ges Fault Zone (Figs. II.1 and II.16), the limestones are gradually replaced by fine-grained sandstones.

Interpretation. The silts of the La Seu basin have been deposited as intrachannel and/or intrafan- as well as basin floor deposits. The few sedimentary structures that could be found do not exclude this kind of genesis. It was already pointed out by Nagtegaal (1969), however, that very thick silt intervals might in fact be thick accumulations of wind-blown dust. Unfortunately, no evidence has been found for an aeolian origin and sand dunes are apparently absent in the La Seu basin. Collinson (1978a) suggests a possible aeolian genesis of Old Red Sandstone silts and discusses the difficulties in establishing criteria to identify fossil loess deposits: "Few ancient loess deposits older than the Pleistocene have been recognised. This is probably due to the rather featureless nature of such deposits and the consequent lack of positive criteria for their recognition". Whatever

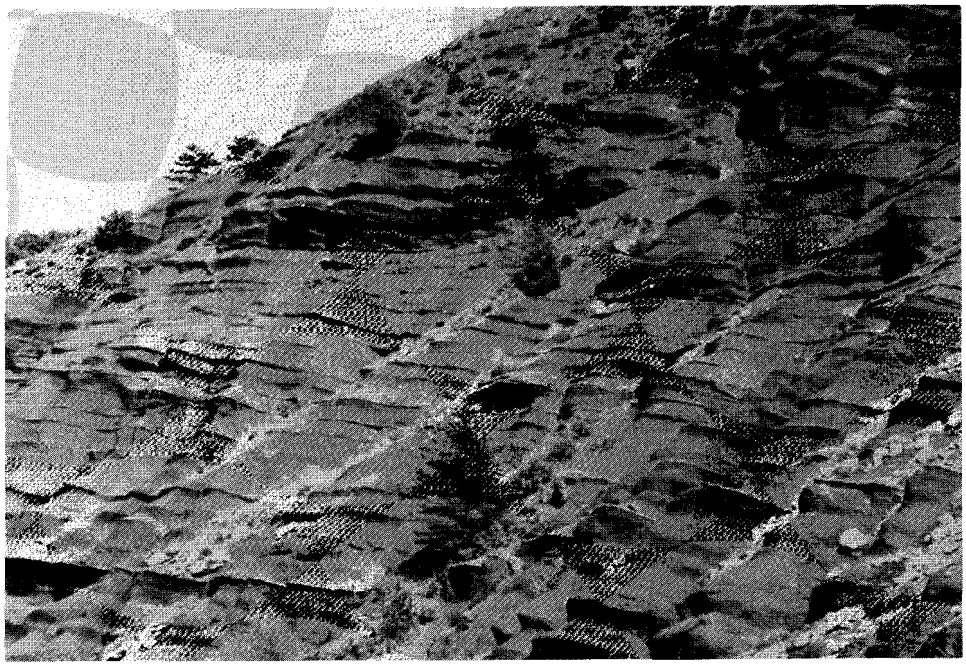

Fig. II.9. Upper part of section 15 showing silts with intercalated very thin limestone layers of sabkha origin.

the nature of the silts, the occurrence of rootlets and sporadic plant remains, as well as the development of caliche profiles indicate soil formation. However, the preservation of rain imprints, mud-cracks, sedimentary structures, absence of mottling and bioturbation demonstrate there was no permanent vegetational cover in Permian times. The undisturbed nature of the puddle deposits, originated in dried-up pools, also points in this direction.

Semi-arid climatic conditions during deposition can be inferred from the strong red colouring of the sediments and the occurrence of caliche and calcrete (as well as some other of the criteria mentioned above). Both Nagtegaal (1969) and Gisbert (1981) propose environments of deposition which are climatologically and morphologically comparable to the present-day savannahs and steppes.

The thin limestone layers in Basinfill Sequence F probably form part of fossil sabkha deposits, developed by evaporation of intrabasinal ephemeral

lakes occupying topographical depressions. The sandstones by which they are replaced towards the Ges Fault Zone are deposits of currents flowing from the both structurally and topographically high Ges Zone towards the sabkha lake.

Despite their uncertain mode of transportation and deposition, all sediments of the silt and clay facies are grouped with the basin floor facies association.

FACIES ASSOCIATIONS

The sedimentary facies described in the previous chapter are grouped into three facies associations: (1) the grabenfill facies association; (2) the alluvial fan and ephemeral stream facies association; and (3) the basin floor facies association.

The occurrence of the first of these associations is basically restricted to the Rubio-Vilamu basins, whereas the second and third associations are typical for the La Seu basin. As their names suggest, the latter two represent the more coarse-grained and fine-grained part of the basinfill, respectively.

Grabenfill facies association

The typical grabenfill association shows a FU sequence, some hundreds of meters thick, comprising (from bottom to top): fossil scree deposits, debris-flow deposits (breccia and conglomerate), alluvial fan and ephemeralstream deposits (mainly sandstones) and finally a top of thick silts which may comprise as much as half the thickness of the whole fill (Fig. II.10).

The development of this association is directly related to dip-slip movement on normal faults bordering the basins. An overall decrease of net displacement during sedimentation resulted in the remarkably well-defined FU sequences of the type described above.

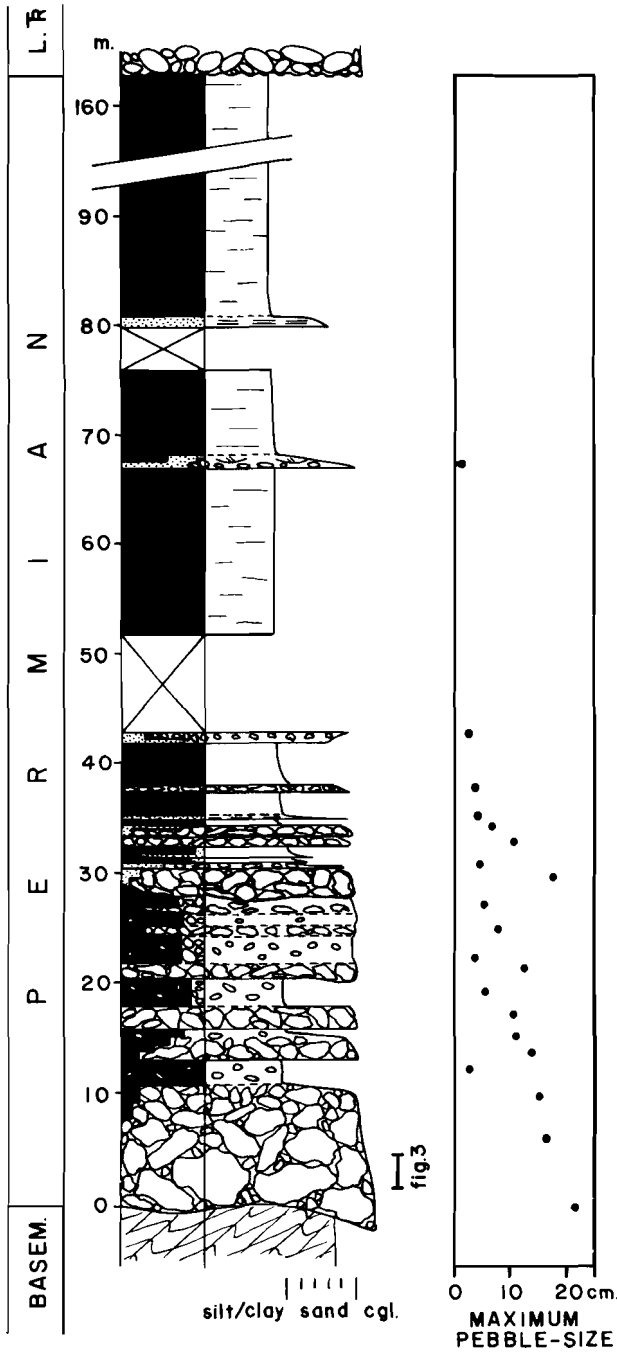
L.P.
PERMIAN
BASEM.
m.
160
90
80
70
60
50
40
30
20
10
0
fig.3
silt/clay sand cgl.
0 10 20cm.
MAXIMUM
PEBBLE-SIZE

Alluvial fan and ephemeral stream facies association

The alluvial fan and ephemeral stream facies association in principle comprises all sedimentary facies of the La Seu basin, arranged in stacked FU sequences, usually on scale of 10's of m. In view of this stacking and the reconstructed depositional environments and -mechanisms of the facies, deposition on alluvial fans and their downstream ephemeral stream and silty equivalents seems very likely. In a broad sense, grain size (and therefore the dominantly occurring facies) will be a function of "proximality" on the fan body, although the semi-arid climate with occasional catastrophic rainstorms, abundant debris in the source area and rapidly decreasing depositional energy during floods certainly had a strong impact on the differences in grain size observed today.

Nevertheless, it is believed that thick, unstratified conglomerates, deposited by mass-flow processes hold a proximal position relative to the source area, whilst unstratified conglomerates deposited in longitudinal bars, stratified conglomerates and pebbly sandstones are transitional to (distal) coarse and fine sandstones and silts, thus resembling the threefold fan division of McGowen & Groat (1971). Gisbert (1981) arrives at a similar conclusion.

Upstream the alluvial fan and ephemeral stream facies association may grade into the grabenfill association and downstream it may pass into the basin floor association.

Fig. II.10. (left) Sedimentary log of section 3 situated in the centre of the Rubio-Vilamu basins. The section is composed of one large fining-upward megasequence classified with the grabenfill facies association. The lower 30-35 m of the section is occupied by deposits of the breccia facies with some associated pebbly mudstone, whereas the upper 130 m is dominated by silt (silt and clay facies). The photograph of Fig. II.3 covers part of the lowest breccia unit just above the Variscan basement.

Basin floor facies association

The silt and clay facies is the main constituent of this association, but fine- and coarse-grained sandstones occur as well. The latter lithotype forms part of well-developed point-bar sequences that originated from lateral migration of high-sinuosity rivers, occupying the basin floor between a period of violent basin-fill by alluvial fans and ephemeral streams, and the final fill of the La Seu basin by very thick silts (Basinfill Sequence F).

The sparsely occurring fine-grained sandstones are lateral or downstream equivalents of coarser grained sediments of alluvial fan or ephemeral stream origin.

The term "basinfloor" as used here might be somewhat misleading: it is not defined as restricted to the lowest central part of the basin but must be attributed to any part of the basin exhibiting low gradients and receiving relatively fine-grained sediments. This usage of the term can be justified as follows: immediately after periods of strong tectonic activity, there was no, or only a narrow strip of basin floor left between coarse-grained deposits building out from fault scarps towards the basin centre from at least two sides (see section on paleogeography). When tectonic activity had ceased and only very low gradients existed in the La Seu basin, silts and some associated sands were deposited all over the basin so that the "basin floor" almost completely covered the whole basin.

SEQUENTIAL ARRANGEMENT

In a discussion about the origin of sedimentary sequences as a function of sedimentary and tectonic processes, Heward (1978a) suggested a threefold subdivision of sequences which is also applicable to the La Seu basin: (1) "sequences" in a specific sense, 1-10's of m thick, consisting of a single bed or a series of related beds; (2) "megasequences", 10's -100's of m thick, consisting of arrangements of related beds and sequences; and (3) "basinfill sequences", consisting of arrangements of sequences and

megasequences. In the case of the La Seu basin, basinfill sequences are often separated by unconformity planes.

Sequences

Sequences almost without exception show an organisation of lithotypes in FU patterns. They are very well suited for investigation by the Transition Probability or Markov-analysis, in order to establish the relations between lithotypes in a vertical sense. An account of the method is given by Miall (1973), Harbaugh & Bonham-Carter (1970) and Reading (1978).

In the sections 13,14 and 15, which are well-exposed over 570, 620 and 1490 m, respectively, a total of 1604 transitions have been counted between the following lithofacies: (1) breccia and conglomerate; (2) pebbly sandstone; (3) coarse sandstone; (4) fine sandstone; (5) silt; and (6) silt with $CaCO_3$ concretions. Figure II.11 shows a schematic representation of the facies interrelations in the three sections. A significance test confirms the non-random nature of the Markov criterion (X^2=404,3 with 19 degrees of freedom, limiting value X^2=30,21 at 95% confidence level. For formulas and discussion see Miall, 1973 and Jones & Dixon, 1976). Similar transition probability tests were performed for all separate basinfill sequences of the three sections mentioned above, as well as combinations of those. They all show the same basic pattern of Fig. II.11, although slight differences exist between the 19 tests done.

The following conclusions can be drawn from the Markov analysis: (1) there is no marked cyclicity as transitions from fine-grained to coarse-grained lithotypes are ill-defined; (2) sequences are fining upward and stacked upon each other; (3) the "complete" sequence 1-6 seldom occurs, usually it is truncated at its top or base or both; (4) there is no preference for a transition from fine-grained sandstone to silts with- or without caliche concretions; and (5) facies 1 and 2 may form a "closed set" (Harbaugh & Bonham-Carter, 1970).

Sequences are thought to be the products of single depositional events, their marked FU tendency resulting from waning current conditions. According to a hypothesis by Schumm (1973), such a depositional event may start off as a mass-flow caused by the failure of large debris masses in geomorphic

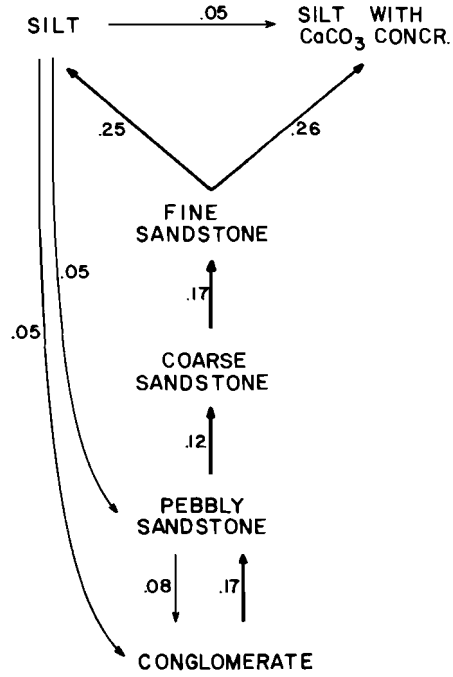

Fig. II.11. Transition probability diagram for three sections (13, 14 and 15) in the La Seu basin. Transitions with expected probabilities between 0 and 0.05 are not shown.

thresholds, but may also have been caused by a single rainstorm giving rise to erosion and subsequent redeposition of (unstable masses of) older deposits.

Megasequences

Whereas sequences always show a fining-upward trend, this is not exclusively the case with the megasequences, of which four types can be distinguished:

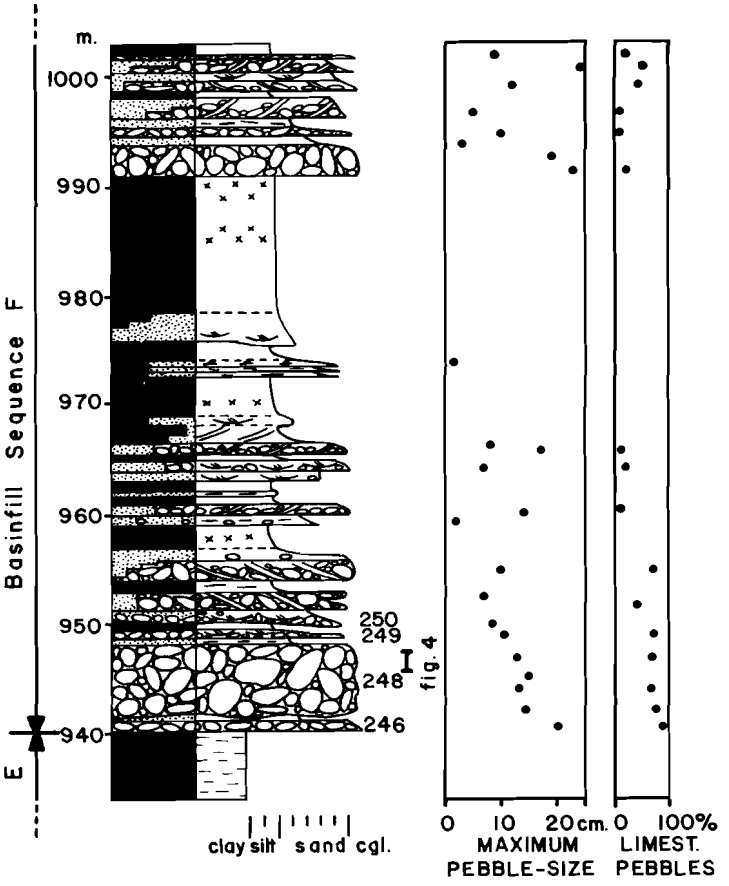

Fig. II.12. Fining-upward magasequences in section 15. The lower magasequence is developed between 940 and 990 m while of the overlying one only the basal part between 990 and 1003 m is shown. Small crosses in silt/clay intervals indicate calcite concretions (caliches). Beds between 940 and 950 m are labelled; Fig. II.5 shows clast size distributions of these beds.

(1) Fining-upward megasequences. The lower part of Basinfill Sequence F, especially in section 15, shows a good example of this type (Fig. II.12). Two megasequences are developed which grade from unstratified conglomerates

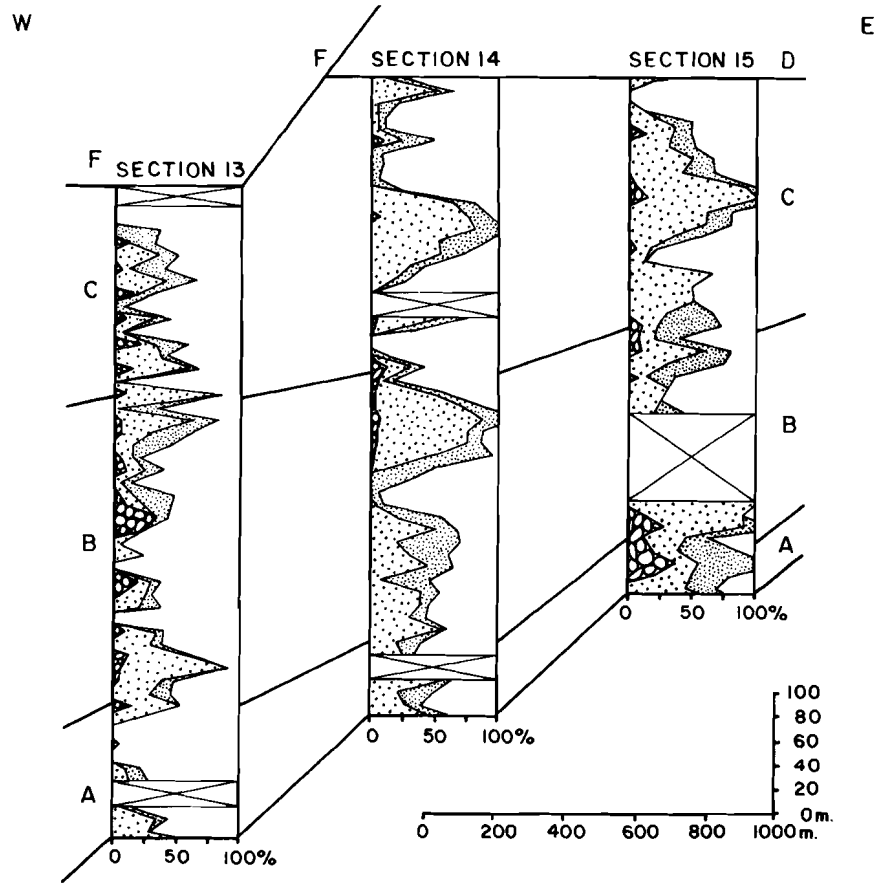

Fig. II.13. Symmetrical CU-FU megasequences and their relations in sections 13, 14 and 15. Ornamentation as in Fig. II.7. Capitals refer to basinfill sequences.

through sandstones into silts. The lower megasequence is 50 m thick, and the upper one 500 m, including more than 300 m of massive silt. Other examples are the FU megasequences of the graben-fill facies association of the Rubio-Vilamu grabens (Fig. II.10).

(2) Coarsening-upward megasequences. There are few CU megasequences in the La Seu basin which are not overlain by FU sequences (see next type of

megasequence). Their occurrence is almost completely restricted to Basinfill Sequences A and C which form the lowest parts of the basin infill west and east of the Ges Fault Zone, respectively (cf. lower parts of Fig. II.13).

(3) Combined CU-FU megasequences. These are characteristic for Basinfill Sequences B-D in the central parts of the La Seu basin. Figure II.13 shows that those megasequences are thick, well-developed and can easily be traced laterally.

(4) Megasequences without clear CU/FU trends. In some parts of the basin no clear megasequences are developed and basin-fill probably resulted from simple stacking of more or less identical sequences.

Fining-upward (mega-)sequences are thought to have been generated by vertical fault movements of waning intensity, resulting in decrease of the depositional gradient (partly as a result of scarp retreat) causing finer detritus to be supplied to the depositional basin (e.g. Deegan, 1973; Steel, 1974; Steel & Wilson, 1975; Heward, 1978a). Apart from scarp retreat, sourceward shift of the locus of faulting (that is, widening of the basin) may aid the generation of FU megasequences. On the other hand, gradual but increasing subsidence of the basin floor will lead to progradation of fans, thus creating CU sequences (see Heward, 1978a; his Table 1).

Combined CU-FU megasequences might simply result from a combination of the kinematics described above for the generation of CU- and FU sequences, i.e. a gradual but increasing subsidence of the basin floor up to a certain maximum rate, followed by a decrease of the vertical fault movement which eventually drops to zero.

Surprisingly, most CU-FU megasequences in the La Seu basin show a marked symmetrical character (Fig. II.13). This implies that a graph showing subsidence rate with time must be fairly symmetrical as well, because sedimentation is directly related to fault movement in semi-arid fault-controlled fans (maximum grain-size is more or less proportional to subsidence rate). Figure II.14 schematically pictures the variations in subsidence, subsidence rate, sediment thickness, sedimentation rate and maximum grain size with time.

In section 26 a small-scale CU-FU sequence has been studied as well as the fault to which it is related. A situation map and cartoons depicting the probable genesis of this sequence are combined in Fig. II.15.

The absence of any megasequence, caused by simple stacking of identical FU sequences, indicates that during sedimentation there was a delicate

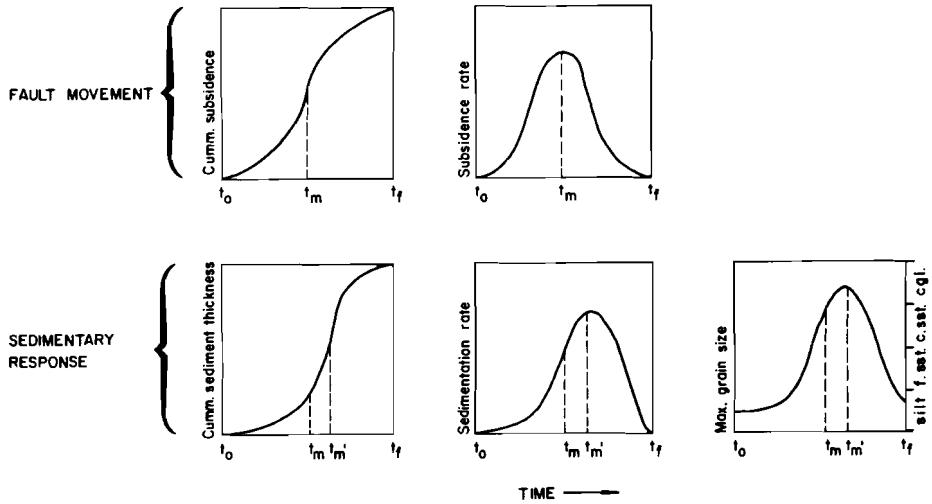

Fig. II.14. Time-dependent parameters important to megasequence development. Basin subsidence (vertical fault movement) starts on moment t_0 and reaches its maximum velocity at moment t_m. It is supposed that sedimentation can not completely keep up with subsidence around t_m, so thickest beds and maximum grain sizes are laid down at moment t'_m, slightly later than t_m. After t_m subsidence decreases and has dropped to zero at t_f. Subsequently thinner beds and smaller grain sizes will be deposited and after t_f no gradient will exist anymore. This marks the end of mega-sequence development, but if the basin continues to sink at very low subsidence rates, thick, fine-grained levels of detritus may still accumulate. This effect may be augmented by post-depositional compaction.

balance between basin subsidence, scarp retreat and depositional rate. This probably points to slow but constant lowering of the basin floor and the regular occurrence of spasmodic major flood events introducing sediment into the basin.

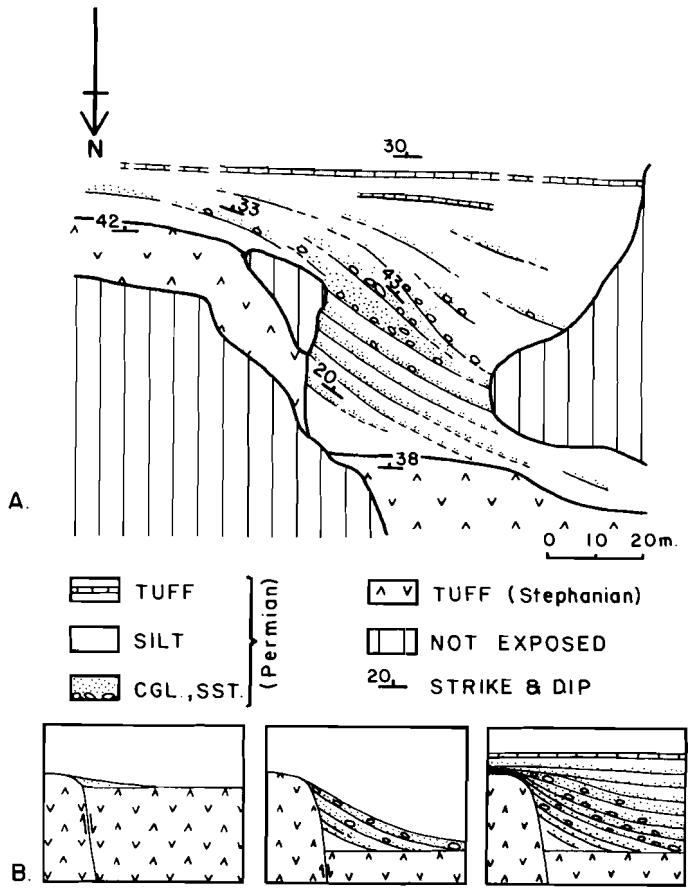

Fig. II.15. Small-scale CU-FU megasequence in section 26.
(A) Situation map showing distribution of lithologies, traces of individual (conglomeratic) sandstone beds and strike/dip data. As the regional structural dip amounts to 35°-45° towards the south, this map can also be read as an (oblique) profile. Fault throw is in the order of 30 m.
(B) Cartoons showing the probable genesis of the above structure. From left to right: situation just after fault initiation, last stage of fault development, and flattening of relief after fault movement ceased. For further discussion see text.

Fig. II.16. Schematic strike sections showing "backstripping" of the Rubio-Vilamu and the La Seu basins for the Stephanian and each of the basinfill sequences of the Peranera Formation, respectively. The top diagram shows the present-day situation (base of the unconformably overlying Bunter sediments supposed to be flat), while the diagram immediately beneath shows the same section with 10x vertical scale exaggeration. The same vertical scale exaggeration has been applied for all other sections. Within the Peranera Formation only the newly deposited sedimentary volume is indicated for each basinfill sequence (referred to in capitals). If, as in the case of the upper right-hand part of Basinfill Sequence B, recently added sediments are left blank, this is an expression of uncertainty about their relative age within the Peranera Formation.

RUBIO - VILAMU BASINS ← LA SEU BASIN →

GES FAULT ZONE

WEST EAST

0 km. 2 4

A-E A-E

0 4 8 12 16 20 km.

NO VERTICAL SCALE EXAGGERATION

F

andesite

E

D

C

B

A

MALPAS FM.

ERILL CASTELL FM.

0 m. 500 1000

0 4 8 12 16 20km.

PERMIAN → STEPHANIAN

Fig. II.17. Photograph showing the angular unconformity between Basinfill Sequences C and D in section 15 (compare with Fig. II.7). Picture taken from the crest of the andesitic rock mass in the Ges Fault Zone looking west along the strike of the section, see Fig. II.1.

Basinfill sequences

In the Rubio-Vilamu and the La Seu basins a total of six basinfill sequences has been recognised (labelled A-F in Fig. II.16). The basinfill sequences are separated from each other by angular unconformities at the edges of the basin (Fig. II.17), but in directions towards the center of the basin the unconformity planes may change character to (para-?) conformities. Basinfill Sequence A (only developed west of the Ges Fault Zone, Fig. II.1) is built up mainly of fine-grained sediments. Wherever megasequences can be recognised, they show a CU pattern. This also holds for Sequence C east of the Ges Fault Zone, forming the basal part of the basin infill in that

sector. Basinfill Sequences B-D are dominated by at least one symmetrical CU-FU megasequence, while within Basinfill Sequence E the CU-FU megasequences are asymmetrical and skewed towards their FU tail. Finally, Basinfill Sequence F exhibits one or more well-developed FU megasequences, as is also the case for the total grabenfill facies association of the Rubio-Vilamu basins (Fig. II.10).

In conclusion, the following movement pattern of the floor of the La Seu basin can be deduced from sedimentological sequentional observations: A phase of gentle, but increasing subsidence was followed by several individual phases of initially strongly accelerating but subsequently decelerating subsidence and most of these phases became separated by (sometimes major) unconformities. The last stage of basin development is characterised by a sudden and strong downward vertical movement of the basin floor (thick conglomerates at the base of Basinfill Sequence F), followed by lower subsidence rates and finally a very gentle downwarp of the whole basin which was partly due to (differential) compaction.

The conglomerates of Basinfill Sequence F show very high percentages of limestone-pebble content. In Sequences A-D hardly any limestone pebbles have been found, while in Sequence E the limestone-pebble content is usually low, though in some sections it may be up to 70%. This change in pebble composition suggests switching of available source area between deposition of Basinfill Sequences E and F, a view which is confirmed by paleocurrent analysis (see next section).

PALEOGEOGRAPHY

Figure II.18 shows a series of paleocurrent diagrams for each of the six basinfill sequences of the Permian the La Seu and Rubio-Vilamu basins, as well as the upper part of the Carboniferous Malpas Formation. The positions of sections 1-10 have been shifted somewhat to the south, thus correcting for the effects of postdepositional deformation. The traces of a number of faults which are believed to have been playing an important (synsedimentary) role in the La Seu basin have been added to these diagrams. Their possible existence has been mainly deduced from abrupt deviations in paleocurrent

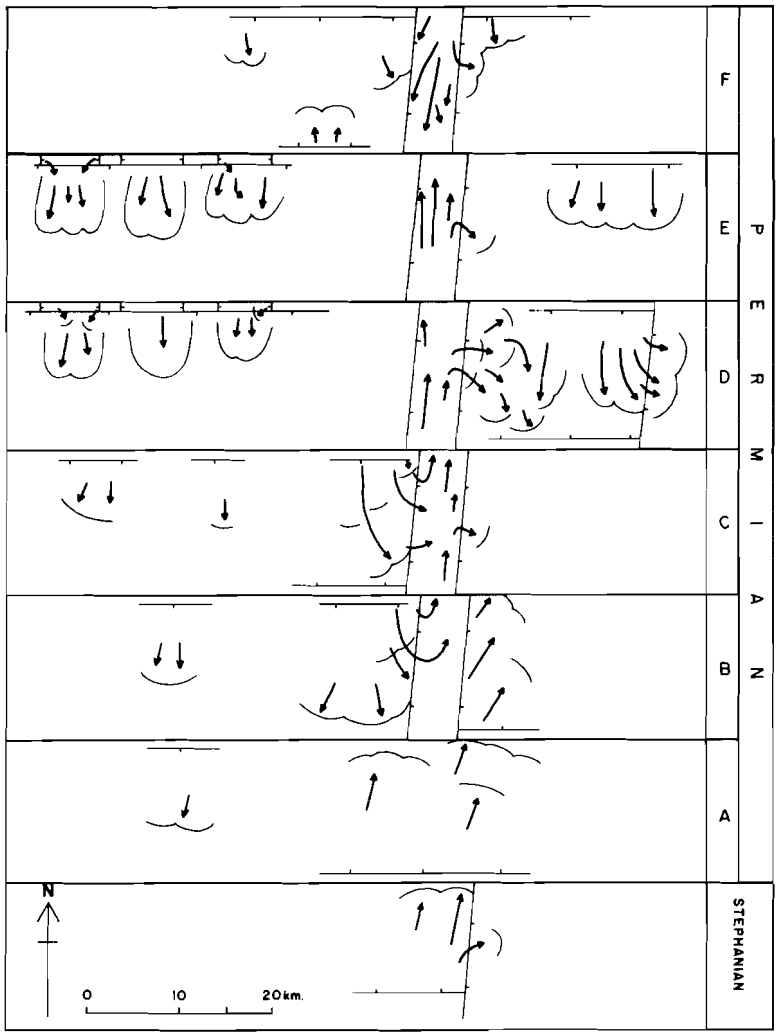

Fig. II.18. Semi-quantitative representation of measured paleocurrent directions in the Rubio-Vilamu and La Seu basins. Length and density of arrows are a measure for the number of readings; the whole diagram is based on 417 paleocurrent measurements in the Stephanian and Basinfill Sequences A-F of the Peranera Formation. The positions of normal faults, their sense of movement (equal to the dip direction of the fault planes indicated by barbs) and possible outline of alluvial fans are based on interpretation, mainly from paleocurrent directions and their sudden deviations, as well as some additional evidence (present-day positions of faults, geometry of alluvial wedges, etc.).

directions, other factors being observations on faults in the field, lined-up sudden changes in sedimentary facies, etc. The following conclusions can be drawn from Fig. II.18:

(1) Paleocurrent readings in the Rubio-Vilamu basins are, almost without exception, oriented towards the south. They represent longitudinal transport in N-S running, narrow grabens in which some coarse-grained lateral fills occur as well. The thin fine-grained sediments of section 1 (Fig. II.1), which are to be situated north of the Rubio-Vilamu basins in a palinspastic reconstruction (Séguret, 1970), also show paleocurrent directions towards the south. They are considered to be the upstream equivalents of the Rubio-Vilamu graben-fills. On a large scale, the Rubio-Vilamu basins obviously acted as lateral feeder channels to the main (La Seu) depositional basin.

(2) In the central part of the La Seu basin paleocurrents of Basinfill Sequences A-E consistently run north, concentrated in a narrow corridor. In Basinfill Sequence F paleocurrents run south. Outside of the central part, measurements indicate transport towards south and/or east. Sedimentation was apparently bounded by a N-S striking feature, possibly a (half-) graben, which will be called the La Bastida graben after the nearby small village of La Bastida de Ortons.

(3) Most observations on sedimentary structures outside the central part of the basin show transport towards the south, which proves the existence of a gradient from the north, the nature of the deposits pointing to a relief of tectonic origin. This suggests the presence of one or more long, individual, E-W striking faults towards the north, downthrowing to south. It is remarkable that the alluvial fans and ephemeral stream bundles which built out towards the south show very little dispersion of current directions. This effect can be easily explained by imagining coalescing fans forming a bajada (Collinson, 1978b) instead of half-cone shaped fan bodies building out from seperate fanhead canyons. Furthermore, the lack of dispersion of paleocurrent directions suggests straight, continuous fault traces at the surface.

(4) In some cases, paleocurrent directions suddenly change orientation towards the southeast, east or even northeast. As those changes in directions occur along more or less straight N-S striking lines (Fig. II.18), fault tectonics are held responsible for this feature. A satisfactory explanation would be the presence of normal faults with eastwards downthrown but westward tilted blocks.

STRUCTURAL ORGANISATION OF THE LA SEU AND RUBIO-VILAMU BASINS

Northern basin fault

As has been argued before, this limiting fault must be situated somewhere south of the Rubio-Vilamu basins and north of the present outcrop area of the La Seu basin. Towards the east, sections 29 and 30 show sediment thicknesses of only 10 m and 70 m respectively, while section 28, only 1.5 km further south (Fig. II.1), has a total thickness of 1100 m. This means that the bounding fault has to pass between those sections. Together with lineament patterns in the basement it leads us to postulate a rather

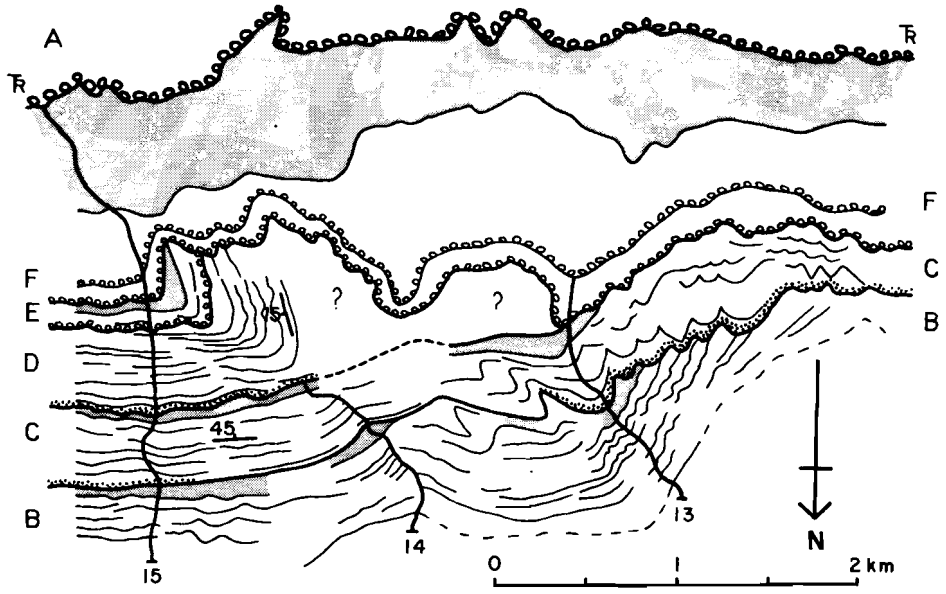

Fig. II.19. (A) Map (drawn from aerial photographs) of flapfold in the central part of the La Seu basin. This gravitational structure developed following detachment along the southern boundary fault of the basin and became deeply eroded before deposition of Basinfill Sequence F. For further discussion see text. Also note the angular unconformity west of section 13. Irregular bed traces in Basinfill Sequences B and C west of section 14 result from badland erosion.

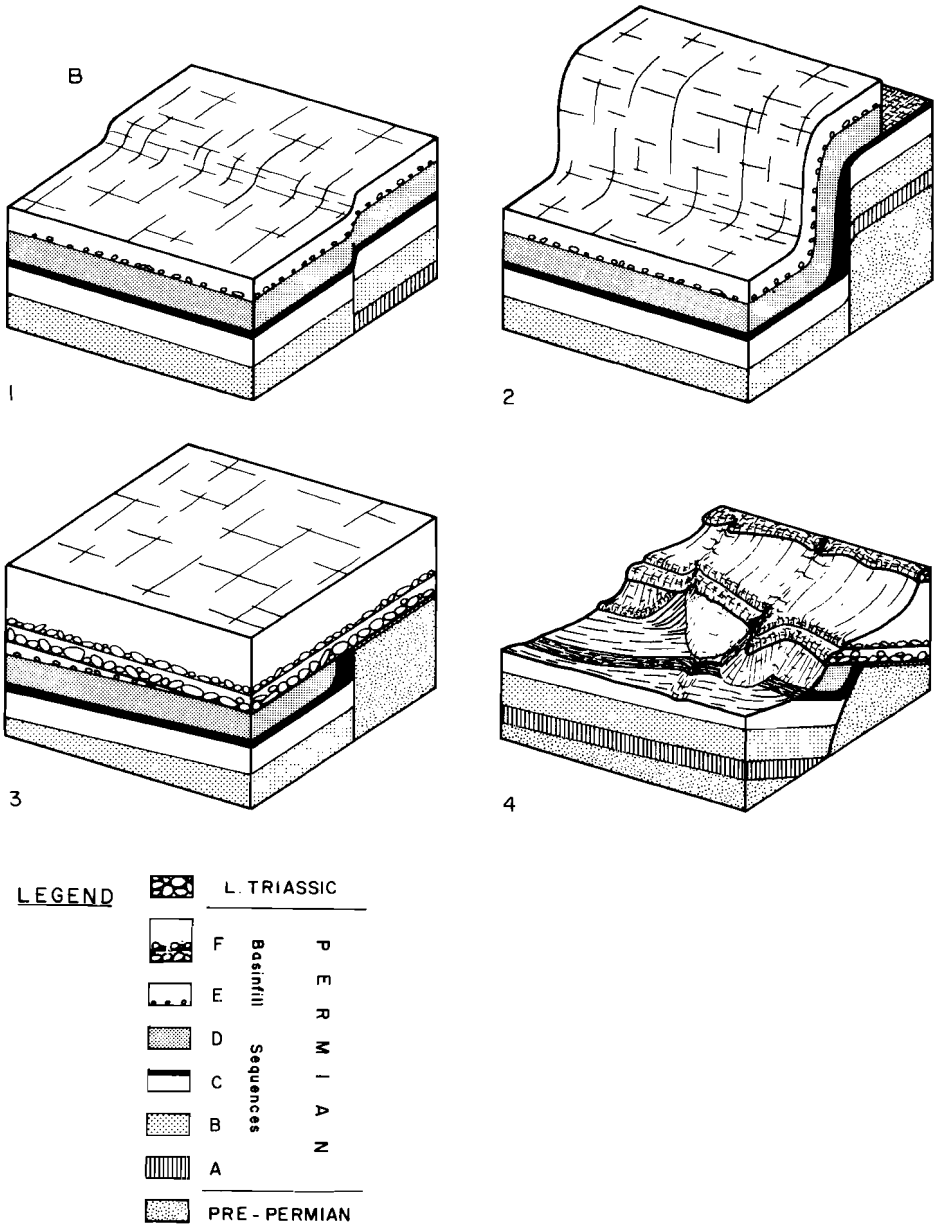

Fig. II.19. (B) Blockdiagrams showing the development of the flapfold shown in Fig. II.19A. Block 4 gives the recent situation.

straight, more or less E-W striking fault bounding the La Seu basin to the north.

Southern basin fault

The precise position of this fault is less clear. Towards the west it is assumed to be covered by a large allochthonous tectonic unit as described by Seguret (1970). To the east however, there are two important indications concerning its position. Firstly, the grabenfill sequence which forms part of Basinfill Sequence F in section 9 is composed of coarse-grained mass-flow breccia with paleocurrent directions towards the north (see section on breccia facies). The marginal fault must therefore have been situated close to the present position of the top of section 9.

A second, and more important indication, comes from a large-scale gravity-induced structure, developed below Basinfill Sequence F in sections 13, 14 and 15. Figure II.19 shows this structure on a map which has been oriented in such a way that it can also be regarded as an oblique profile through the fold due to the regional 45° southward dip. The base of Basinfill Sequence D rests conformably upon a thick silt level which here forms the top of Basinfill Sequence C. This level obviously acted as a décollement horizon enabling the sedimentary pile above it to slide down from the basin edge. No large-distance transport occurred, however, as in section 15 Basinfill Sequence D is still rooted to its "basement". The structure therefore must be a large flapfold, the upper foldhinge of which was removed by subsequent erosion as the base of Basinfill Sequence F cuts obliquely through the upright limb of the fold.

Reconstruction of the fold-axis shows that it was close to horizontal and had a 100°-280° direction before later deformation. Additionally, the asymmetry of the fold indicates a movement of its crest towards the north.

It is suggested, in conclusion, that the southern marginal fault of the La Seu basin lies directly south of the present-day outcrop of the Permian rocks, has a rather straight outline and strikes approximately east-west.

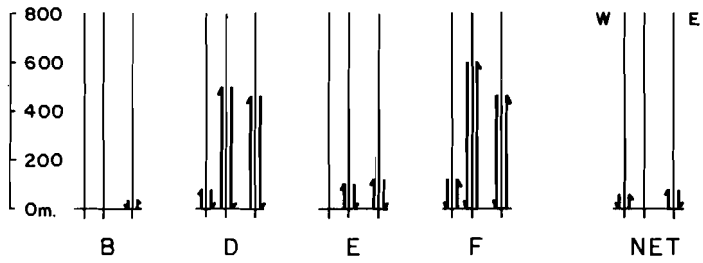

Fig. II.20. Dip-slip movement along the three main branches of the Ges Fault Zone during the Permian. Capitals refer to basinfill sequences; the right-hand part of the diagram shows the net vertical offset. Width of the fault zone is approximately 1 km.

Ges Fault Zone

At the present level of erosion this fault zone consists of three main and several subsidiary branches defining a total width of 1 km (Figs. II.1 and II.16). It has been named after the hamlet of Ges, southeast of La Seu d'Urgell. Figure II.16 clearly reveals the importance of the Ges Fault Zone in the development of the La Seu basin. It was already active in Upper Carboniferous times (but the structure may be much older; see Zwart, 1979; and Mey, 1968); had great impact on Permian sedimentation and was reactivated during the Eocene. It stands out as an obvious N-S lineament on Landsat- and Skylab images in which it can be traced over a distance of about 10 km. (The fault zone may nevertheless extend over a much larger distance as it is covered by allochtonous Devonian units in the north and by Mesozoic sediments in the south). Figure II.20 depicts the reconstructed net vertical offsets for individual basinfill sequences along the three main branches of the fault zone. During deposition of a single basinfill sequence, cumulative net offsets along the whole Ges Fault Zone may have been in the order of 1000 - 1200 m, but for the complete Permian section (right part of Fig. II.20) the net effect only consists of a minor uplift of the fault zone itself, the amount of which is probably close to the error limits involved in the reconstruction. So, in spite of the occurrence of

considerable movements at distinct time intervals, there was no net vertical offset during the Permian.

The maximum amounts of reconstructed offset suggest that the Ges Fault Zone must reach deep into the crust. This view is confirmed by the outpouring of lavas of mainly andesitic character after deposition and erosion of Basinfill Sequence D. They are of the same composition as tuffs and lavas from the Stephanian Erill Castell Formation described by Morre & Thiébaut (1964), occurring stratigraphically below the Permian deposits. Hartevelt (1970) incorrectly attributed the crystalline rocks of the Ges Fault Zone to the Stephanian too, but the intercalation of lavas between Permian sediments and the nature of the contacts prove that they must be younger.

In profile the Ges Fault Zone shows similarities to typical strike-slip fault systems (c.f. Miall, 1978), but, unfortunately, conclusive data on the horizontal movement along the Ges Zone are lacking, although a substantial dextral offset cannot be excluded. Therefore, it is tentatively proposed that due to negligible net vertical movements and resemblances with well-described strike-slip systems, the Ges Fault Zone acted as an oblique-slip zone with a large horizontal component.

Migration of depocentre

The profiles of Fig. II.16 show that the position of accumulation of maximum sediment thickness (after compaction, deformation and erosion) shifted through time in the La Seu basin. Figure II.21 demonstrates this feature in more detail. It is clear that the migration of the depocentre invariably occurred towards the east, but that the Ges Fault Zone acted as a barrier against this dynamic evolution. The main depocentre of the basin never crossed this barrier, but a newly nucleated depocentre jumped over during deposition of Basinfill Sequence D. The distances over which the depocentres migrated (4.5-12.5 km of proven minimum migration) are considerable compared to the maximum preserved thickness of sediment (1.5 km). If the ratio minimum translation distance/maximum preserved sediment thickness is taken to be a measure for the net strike-slip/net dip-slip ratio, it follows that the latter must be in the order of 3-8, or an average 5.5. This estimation must, however, certainly be a conservative one, because

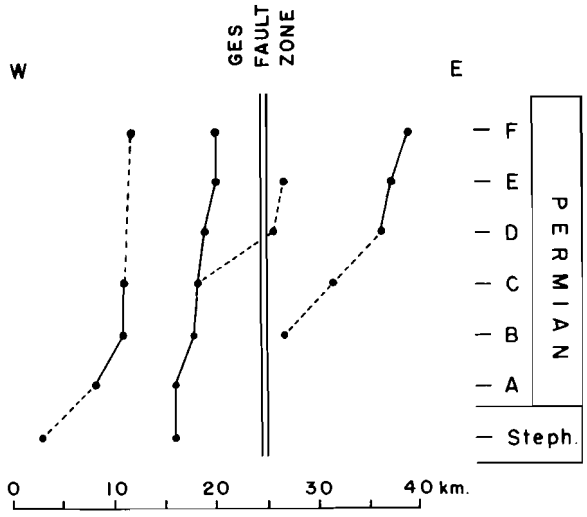

Fig. II.21. Migration of depocentre in the La Seu basin with time. Data mainly taken from Fig. II.16. Capitals refer to basinfill sequences.

the La Seu basin was bounded to the north as well as to the south by blocks which moved in opposite directions with respect to the basin. Therefore, the net movement along the whole strike-slip system may have been much larger than the recorded translation distance of the depocentre. Figure II.22 illustrates this principle.

A relatively large, unidirectional and uniform translation of the locus of maximum sediment accumulation in a sedimentary basin with time is considered to be indicative of a strike-slip dominated fault-bounded basin (Steel & Gloppen, 1980).

A similar shift of depocentre towards the east can be concluded from a reinterpretation of one of Nagtegaal's (1969) profiles through a sedimentary basin of Permian age some 50 km west of La Seu d'Urgell.

Relations between basinfill sequences

Basin development in a oblique-slip zone can only occur in a situation of transtension (strike-slip with superimposed extension; Harland, 1971),

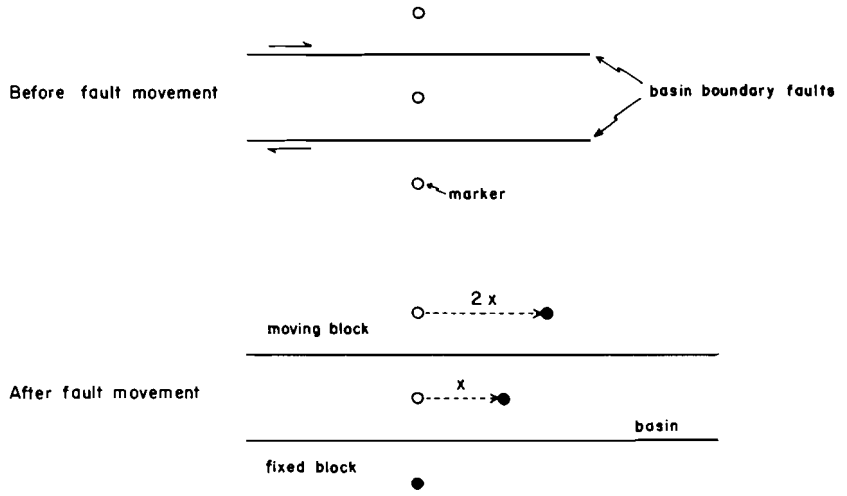

Fig. II.22. Diagram showing the theoretical relationship between migration of a marker (e.g. depocentre) within the La Seu basin and the net strike-slip movement along the boundary faults of the basin. If identical offset is assumed for both faults, the total offset will amount to a distance 2x while the marker within the basin only travelled over half that distance.

characterised by normal faulting, drape folding and volcanicity (Reading, 1980). On the other hand, folding, uplift and subsequent erosion points to transpression (strike-slip with superimposed compression; Harland, 1971). In the case of the La Seu basin, episodes of sedimentation with associated volcanicity and gravity folding have been followed by periods of deformation (involving uplift and folding) and erosion, thus separating six basinfill sequences by distinct unconformities. It follows that the combined depositional and structural histories of the La Seu basin show that a number of alternating transtensive and transpressive regimes were responsible for its development. It is felt that such alternations of different structural regimes result from continuous movement along locally slightly curved strike-slip faults (see Reading, 1980). In this respect it is significant that along the strike of the basin the unconformity planes may change character over short distances into conformable contacts, thus marking the transition from transpressive to non-transpressive regions.

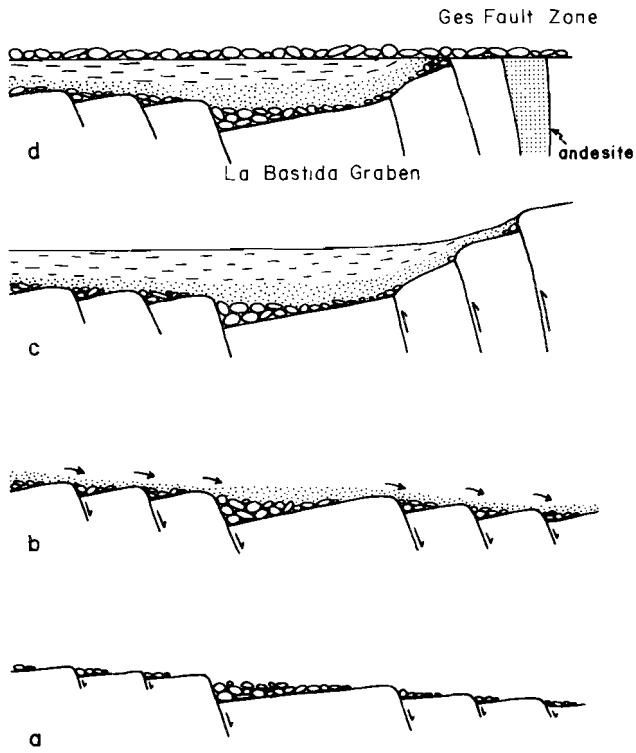

Fig. II.23. Schematic strike section through the central part of the La Seu basin depicting normal faults perpendicular to the basin axis and westward tilted fault blocks. (a) Sedimentation restricted to N-S striking half-grabens (e.g. the La Bastida Graben). Paleocurrent directions run perpendicular to the section; (b) eastward transport of fine-grained sediments (compare Fig. II.18); (c) during transpressional phases faults change character to reverse faults in the Ges Fault Zone; and (d) geometry after deformation and erosion.

Normal faults perpendicular to the basin axis

Numerous small- and medium-scale, north-south striking faults have been recognised in the field. Unfortunately there is often no control on the importance of possible strike-slip components. An example of a small-scale north-south striking fault from section 26 has been described in a previous section, see Fig. II.15. Analysis of paleocurrent directions has revealed

the existence of some major north-south striking normal faults separating westward tilted blocks (Fig. II.18), which also points to the existence of an extensional stress regime during deposition of each of the basinfill sequences. As these normal faults have not been recognised in the field, their positions in Fig. II.23 can only be tentative.

Soula et al. (1979) and Bixel and Lucas (1983) explain the formation of Stephano-Permian N-S directed (half-)grabens in the western Pyrenees by the wedging open of older N-S Variscan faults as a result of E-W left-lateral simple shear.

Strike-slip faults parallel to the basin axis

As discussed above, the traces of the east-west faults bounding the La Seu basin are well individualised and rather straight on a regional scale. This is a remarkable feature for a strike-slip zone in high crustal levels, as they often show a complicated anastomosing fault pattern dominated by Riedel shears (Harding, 1976; Tchalenko, 1970). Recent experiments have shown, however, that the development of fault configurations in a sedimentary cover as a response to faulting in a "basement" is dependent upon so-called pre-stress conditions. When the longest and shortest principal pre-stress axes are both horizontal, and parallel and perpendicular to the basement fault respectively, Riedel shears will only develop at low angles to this master-fault (G.Mandl & M.A.Naylor, pers.com., 1982). Furthermore, large displacements will cause the "breakthrough" of a master fault at the surface as Riedel shears and other associated structures become connected parallel to the basement fault (Tchalenko, 1970). With respect to the present study it is proposed that a tensile tectonic regime was responsible for graben development in Upper Carboniferous times, as witnessed by the outpouring of substantial amounts of tuff and lava. When the tectonic regime changed into one of oblique-slip faulting, tensile pre-stress conditions prevented Riedel shears from developing at high angles to the graben-axis direction. Subsequently, large displacements along the master fault straightened the basin boundary faults.

An additional speculation about the rather straight outline of the faults is to assume that they are reactivations of an older (Variscan or pre-Variscan?) fault system. Any stress field applied will cause slip along pre-existing planes of weakness as long as the angular relationships between principle stress axes and fault planes are favourable (Price, 1966; Jaeger, 1969).

SUMMARY AND CONCLUSIONS

(1) The La Seu basin is one of a series of east-west striking, narrow post-Variscan sedimentary basins, cropping out in a single, well-defined zone along the southern border of the Axial Zone of the Pyrenees (Mey et al., 1968; Brouwer, 1968; Bloemraad, 1969; Nagtegaal, 1969; Hartevelt, 1970; Gisbert, 1981). Some post-Variscan basins further to the west show an evolution comparable to that of the La Seu basin, including eastward migration of their depocentre.

(2) The strong correlation between sequences, megasequences and basinfill sequences throughout the basin, proves that tectonic control was of major importance for its development. The absence of any trace of regional metamorphism in the post-Variscan rocks indicates that the deformation must have been of the shallow-crustal type.

(3) The overall net strike-slip/net dip-slip ratio within the basin is at least five but probably more, whereas its length/width ratio is ten or more.

(4) Considerable shift of the depocentre occurred in space and time.

(5) Normal faulting, drape folding and outpouring of lavas point to (trans-) tensional tectonics, where the occurrence of erosional levels, angular unconformities and reverse faulting point to (trans-)pressional

Fig. II.24. Block-diagrams of the Rubio-Vilamu (left) and the La Seu basins. Arrows indicate relative sense of movement along the basin boundary faults.

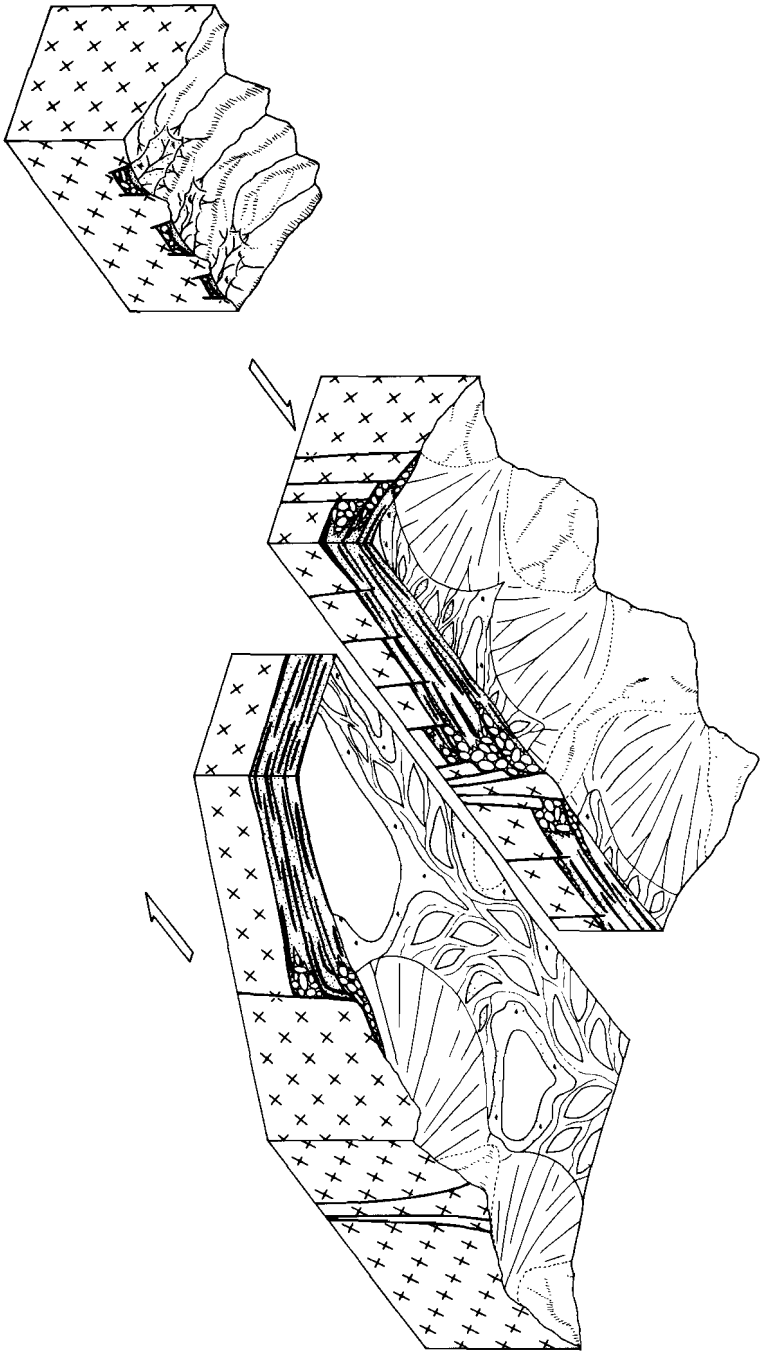

tectonics. Alternation of transtension and transpression is considered to be typical of strike-slip basins (Reading, 1980) and results from movement along non-planar fault-surfaces.

(6) Tensional pre-stress conditions and graben development as indicated by the presence of extrusive rocks in the Upper Carboniferous, gave rise to the development of a set of straight and well-defined bounding faults. Alternatively, reactivation of older structures can certainly not be excluded.

(7) Throughout the evolution of the La Seu basin cross-cutting faults like the Ges Fault Zone repetitively changed character from normal to reverse faults.

(8) Several relatively small north-south running grabens, such as the Rubio-Vilamu grabens, acted as lateral feeder channels to the La Seu basin, with basinward transport to the south as well as to the north. In the La Bastida Graben, paleocurrent directions can therefore be 180° opposed within the same sedimentary unit.

(9) Due to the shape of the basin, transport of coarse debris was mainly lateral with tectonically induced deflections towards the east (i.e. the direction of depocentre migration), especially in the lower and upper fine-grained parts of mega- and basinfill sequences.

(10) Alluvial fans and ephemeral streams coalesced to form bajadas, pointing to straight boundary faults, low gradients, smooth topography, and semi-arid climatic conditions.

(11) Important changes in pebble composition, types of megasequences and paleocurent directions between Basinfill Sequences A-E and F, are indicative of changes in tectonic regime: from a repetition of transtensile/ transpressive tectonics to a major transtensile phase, with associated large-scale vertical movements.

The structural setting and geometry of the sediment fill of the Rubio-Vilamu and the La Seu basins are conceptually depicted in Fig. II.24.

ACKNOWLEDGEMENTS

I am very much indebted to Dr. P.J.C. Nagtegaal who thoroughly reviewed several versions of this article, and to my former supervisors and colleagues at the Structural Geology Department of Utrecht State University where this work was initiated. In particular I thank Mr. W.Nijman for guidance in the field and his permanent assistance and enthusiasm. Bart van Hasselt and Eppo van Straten assisted during fieldwork.

Throughout every stage of this study Ineke Smeets was a continuous source of help and stimulation, for which I am very grateful.

REFERENCES

Allen, P.A. (1981). Sediments and processes on a small stream-flow dominated alluvial fan, Shetland Islands.
Sediment.Geol., 29, pp. 31-66.

Ballance, P.F. (1980). Models of sediment distribution in non-marine and shallow marine environments in oblique-slip fault zones. In: P.F. Ballance and H.G. Reading (Editors), Sedimentation in Oblique-slip Mobile Zones.
Spec.Publ.Int.Ass.Sediment., 4, pp. 229-236.

Bixel, F. and Lucas, C. (1983). Magmatisme, tectonique et sédimentation dans les fossés stéphano-permiens des Pyrénées occidentales.
Rev.Géogr.phys.Géol.dynam., 24, pp. 329-342.

Blatt, H., Middleton, G.V. and Murray, R.C. (1972). Origin of sedimentary rocks.
Prentice-Hall, New Jersey, 634 pp.

Bloemraad, J. (1969). Verslag van een geologische kartering tussen het Cerdaña bekken en Ribas de Freser.
Int. report Univ. Leiden, 44 pp.

Bluck, B.J. (1967). Deposition of some Upper Old Red Sandstone conglomerates in the Clyde area: A study in the significance of bedding.
Scott.J.Geol., 3, pp. 139-167.

Brookfield, M.E. (1980). Permian intermontane basin sedimentation in southern Scotland.
Sediment.Geol., 27, pp. 167-194.

Brouwer, Th.N. (1968). Verslag van een geologische kartering in de omgeving van de Cerdaña vallei, oostelijke Pyreneeën, Spanje.
Int. report Univ. Leiden, 34 pp.

Collinson, J.D. (1978a). Deserts. In: H.G. Reading (Editor), Sedimentary Environments and Facies.
Blackwell, Oxford, pp. 80-96.

Collinson, J.D. (1978b). Alluvial sediments. In: H.G. Reading (Editor), Sedimentary Environments and Facies. Blackwell, Oxford, pp. 15-60.

Deegan, C.E. (1973). Tectonic control of sedimentation at the margin of a Carboniferous depositional basin in Kirkudbrightshire. Scott.J.Geol., 9, pp. 1-28.

Folk, R.L. and Ward, W.C. (1957). Brazos River Bar: a study in the significance of grain size parameters. Journ.Sediment.Petr., 27, pp. 3-27.

Gisbert, J. (1981). Estudio geológico-petrológico del Estefaniense-Pérmico de la Sierra del Cadí (Pirineo de Lérida). Tesis Doctoral, Departamento de Petrología, Universidad de Zaragoza, 313 pp.

Harbaugh, J.W. and Bonham-Carter, G. (1970). Computer Simulation in Geology. Wiley-Interscience, New York, 575 pp.

Harding, T.P. (1976). Predicting productive trends related to wrench faults. World Oil, 182, pp. 64-69.

Harland, W.B. (1971). Tectonic transpression in Caledonian Spitzbergen. Geol.Mag., 108, pp. 27-42.

Hartevelt, J.J.A. (1970). Geology of the Upper Segre and Valira Valleys, Central Pyrenees, Andorra/Spain. Leidse Geol.Meded., 45, pp. 167-236.

Hartevelt, J.J.A. and Roger, Ph. (1968). Quelques aspects de la topographie permo-triassique dans le Haute-Sègre et de la Haute-Pallaresa (Lérida, Espagne). C.R.Somm.Séances Soc.géol.Fr., 6, pp. 182-184.

Heward, A.P. (1978a). Alluvial fan sequence and megasequence models: with examples from Westphalian D- Stephanian B coalfields, northern Spain. In: A.D. Miall (Editor), Fluvial Sedimentology. Mem.Can.Soc.Pet.Geol., 5, pp. 669-702.

Heward, A.P. (1978b). Alluvial fan and lacustrine sediments from the Stephanian A and B (La Magdalena, Ciñera-Matallana and Sabero) coalfields, northern Spain. Sedimentology, 25, pp. 451-488.

Jaeger, J.C. (1969). Elasticity, fracture and flow with engineering and geological applications. Methuen and Co., London, pp.268.

Jones, B. and Dixon, O.A. (1976). Storm deposits in the Read Bay Formation (Upper Silurian), Somerset Island, Artic Canada. (An application of Markov Chain Analysis).
Journ.Sed.Pet., 46, pp. 393-401.

McGowen, J.H. and Groat, C.G. (1971). VanHorn Sandstone, West Texas: an alluvial fan model for mineral exploration.
Bureau of Economic Geology, Univ. of Texas, Austin.

Mey, P.H.W. (1968). Geology of the Upper Ribagorzana and Tor valleys, Central Pyrenees, Spain.
Leidse Geol.Meded., 41, pp. 229-292.

Mey, P.H.W., Nagtegaal, P.J.C., Roberti, K.J. & Hartevelt, J.J.A. (1968). Lithostratigraphic subdivision of post-Hercynian deposits in the South-Central Pyrenees, Spain.
Leidse Geol.Meded., 41, pp. 221-228.

Miall, A.D. (1973). Markov chain analysis applied to an ancient alluvial plane succession.
Sedimentology, 20, pp. 347-364.

Miall, A.D. (1978). Tectonic setting and syndepositional deformation of molasse and other nonmarine-paralic sedimentary basins.
Can.J.Earth Sci., 15, pp. 1613-1632.

Morre, N. and Thiébaut, J. (1964). Constitution de quelques roches volcaniques permiennes de la Sierra del Cadí (Pyrénées catalanes).
Bull.Soc.géol.Fr., VI, pp. 389-396.

Nagtegaal, P.J.C. (1969). Sedimentology, paleoclimatology, and diagenesis of post-Hercynian continental deposits in the south-central Pyrenees, Spain.
Leidse Geol.Meded., 42, pp. 143-238.

Price, N.J. (1966). Fault and Joint Development in Brittle and Semi-Brittle Rock.
Pergamon Press, New York, 176 pp.

Reading, H.G. (1980). Characteristics and recognition of strike-slip fault systems. In: P.F. Ballance and H.G. Reading (Editors), Sedimentation in Oblique-Slip Mobile Zones.
Spec.Publ.Int.Assoc.Sedimentol., 4, pp. 7-26.

Reading, H.G. (1978). Sedimentary Environments and Facies.
Blackwell, Oxford, 557 pp.

Schumm,S.A. (1973). Geomorphic thresholds and complex response of drainage systems. In: M. Morisawa (Editor), Fluvial Geomorphology. (Publ. in Geomorphology).
State University of New York, Binghampton, N.Y., pp. 299-310.

Séguret, M. (1970). Etude tectonique des nappes et séries décollées de la partie centrale du versant sud des Pyrénées.
Ph.D. thesis, Montpellier, 155 pp.

Sopeña, A., Virgili, C., Hernando, S. and Ramos, A. (1977). Pérmico continental en España.
Cuad.Geol.Iber., 4, pp. 11-34

Soula, J.-C., Lucas, C. & Bessière, G. (1979). Genesis and evolution of Permian and Triassic basins in the Pyrenees by regional simple shear acting on older Variscan structures: field evidence and experimental models.
Tectonophysics, 58, pp. T1-T9.

Steel, R.J. (1974). New Red Sandstone floodplain and piedmont sedimentation in the Hebridean Province.
J.Sediment.Petrol., 44, pp. 336-357.

Steel, R.J. and Gloppen, T.G. (1980). Late Caledonian (Devonian) basin formation, western Norway: signs of strike-slip tectonics during infilling. In: P.F. Ballance and H.G. Reading (Editors), Sedimentation in Oblique-Slip Mobile Zones.
Spec.Publ.Int.Assoc.Sedimentol., 4, pp. 79-103.

Steel, R.J. and Wilson, A.C. (1975). Sedimentation and tectonism (?Permo-Triassic) on the margin of the North Minch Basin, LeWis.
J.Geol.Soc.Lond., 131, pp. 183-202.

Tchalenko, J.S. (1970). Similarities between shear zones of different magnitudes.
Bull.Geol.Soc.Am., 81, pp. 1625-1640.

Zwart, H.J. (1979). The geology of the central Pyrenees.
Leidse Geol.Meded., 50, pp. 1-74.

Zwart, H.J. and Roberti, K.F. (1976). Geological map of the central Pyrenees. Sheet 9: Flamisell-Pallaresa.
Geological Institute, Leiden.

CHAPTER III

THE DETECTION AND SIGNIFICANCE OF EARLY DEFORMATION IN THE SOUTHERN VARISCAN PYRENEES, SPAIN; IMPLICATIONS FOR REGIONAL PALEOZOIC STRUCTURAL EVOLUTION

(Submitted to Geologische Rundschau)

INTRODUCTION

In the central Variscan Pyrenees several generations of folding, which are usually associated with well developed axial plane cleavages, can be recognised. The most important and apparently oldest of these generations can be traced throughout the Paleozoic of the Pyrenees and is often referred to as the mainphase (F_1) folding (Zwart, 1979). It is characterised by (usually asymmetrical) cleavage-folds on a mm to km scale which dominate the present-day outcrop pattern of the central Variscan Pyrenees. It was first demonstrated by Boschma (1963), however, that mainphase folds are sometimes overprinting older structures which were therefore labelled pre-mainphase (F_0) or pre-cleavage folds (Zwart, 1979). Since their first discovery, pre-cleavage folds have been described by many Dutch and French authors (e.g. Mey, 1967b, 1968; Hartevelt, 1970; Muller & Roger, 1977; Laumonier & Guitard, 1978 and Lamouroux et al., 1979; for a review see Zwart, 1979).

Three classes of evidence have been used by these authors to prove the existence of pre-cleavage folds: interference patterns, overprinting relationships and statistical analysis of the distribution of intersection lineations. In this paper the last method will be applied to demonstrate the presence of two separate pre-cleavage folding generations in a small area in the Spanish Pyrenees south of Andorra. In addition, an analysis and reinterpretation of published data on pre-mainphase folding will be

Fig. III.1. (next page) Map of the Variscan Pyrenees, showing the Axial Zone and isolated massifs towards the north and south. Frame shows the outline of Fig. III.2.

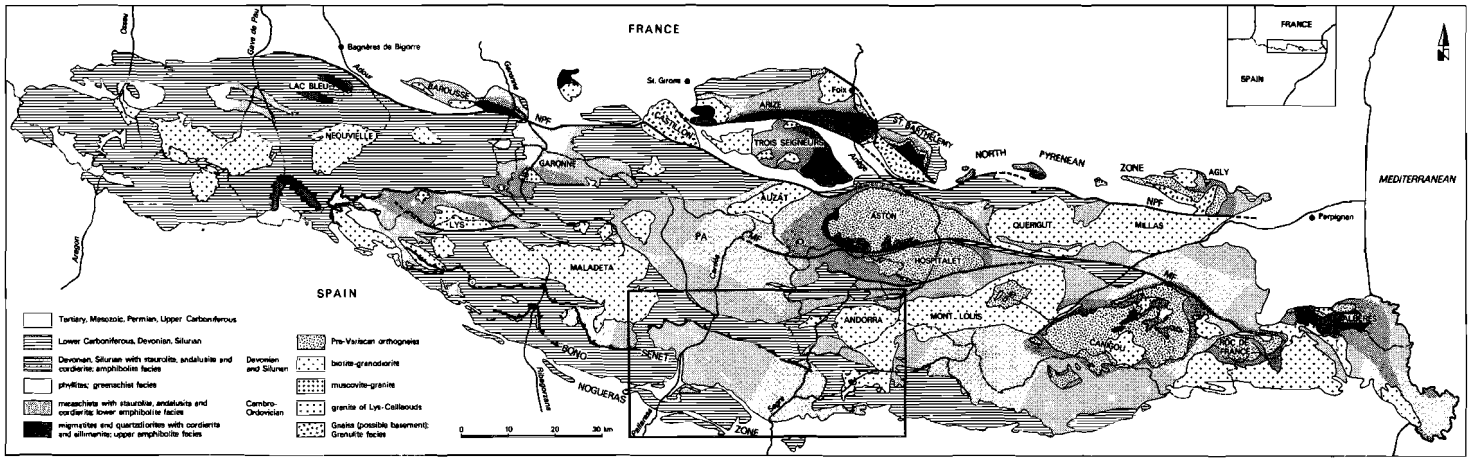
FRANCE
SPAIN
Bagnères de Bigorre
St. Girons
LAC BLEU
BAROUSSE
NIEOUVIELLE
CASTILLON
ARIZE
TROIS SEIGNEURS
Foix
ST BARTHELEMY
NORTH PYRENEAN ZONE
AGLY
AUZAT
ASTON
QUERIGUT
MILLAS
Perpignan
MEDITERRANEAN
ELYS
PA
MALADETA
MONTALET
ANDORRA
MONT LOUIS
CANIGOU
NOGUERAS
BOSSOST
SENET
ZONE
Tertiary, Mesozoic, Permian, Upper Carboniferous
Lower Carboniferous, Devonian, Silurian
Devonian, Silurian with staurolite, andalusite and cordierite; amphibolite facies
phyllites; greenschist facies
Devonian and Silurian
mesaschists with staurolite, andalusite and cordierite; lower amphibolite facies
migmatites and quartzdiorites with cordierite and sillimanite; upper amphibolite facies
Cambro-Ordovician
Pre-Variscan orthogneiss
biotite-granodiorite
muscovite-granite
granite of Lys-Caillaouas
Gneiss (possible basement); Granulite facies
0 10 20 30 km

presented, and finally an attempt will be made to bring out the significance of early folding in the overall structural evolution of the Variscan Pyrenees.

GEOLOGICAL SETTING OF THE STUDIED AREA

The Pyrenees are an essentially Alpine orogenic belt situated along the suture between the relatively stable European plate and the Iberian subplate. The latter underwent considerable rotation and translation during the Mesozoic (van der Voo, 1969; Le Pichon et al., 1971; Ries, 1978). As a result of strong Alpine uplift and subsequent erosion, the Variscan basement is now exposed in large areas along the strike of the Pyrenees, while towards the north and south progressively younger Mesozoic and Tertiary rocks can be found (Fig. III.1). The largest basement outcrop, usually referred to as the Axial Zone (Zwart, 1979), consists of Paleozoic rocks which were folded, metamorphosed and intruded during the Variscan orogeny in Late Carboniferous times. Towards the north the Axial Zone is cut-off by the North Pyrenean fault which is of Alpine age. There is good evidence for important Alpine thrusting within and south of the Axial Zone (e.g. Williams, 1985; Lamouroux et al., 1979; Parish, 1984). Nevertheless, in many areas the influence of Alpine overprinting seems to be negligible or can be easily distinguished from Variscan deformation.

As in many orogenic belts, lithology distribution had an important control on structural style in the Pyrenees. In the Axial Zone the following Paleozoic stratigraphic units have been recognised:

Fig. III.2. Geological map of the Orri dome and surroundings. Frames show the outlines of the studied area (Fig. III.7), and the Ges-Estana structural unit (Fig. III.12a).

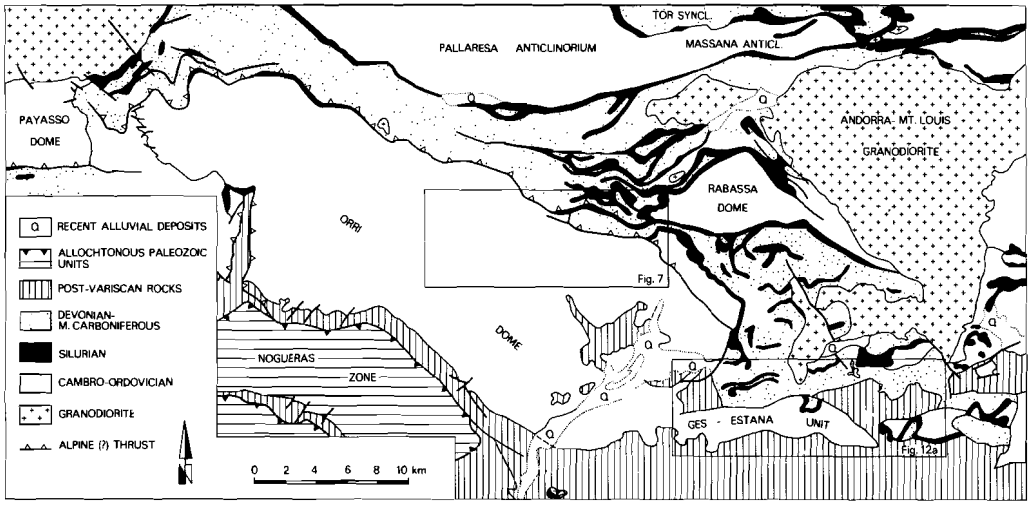
TOR SYNCL.
PALLARESA ANTICLINORIUM
MASSANA ANTICL.
PAYASSO DOME
ANDORRA MT. LOUIS GRANODIORITE
RABASSA DOME
ORRI
Fig. 7
DOME
NOGUERAS ZONE
GES - ESTANA UNIT
Fig. 12a
RECENT ALLUVIAL DEPOSITS
ALLOCHTONOUS PALEOZOIC UNITS
POST-VARISCAN ROCKS
DEVONIAN-M. CARBONIFEROUS
SILURIAN
CAMBRO-ORDOVICIAN
GRANODIORITE
ALPINE (?) THRUST
N
0 2 4 6 8 10 km

- Undated "Cambro-Ordovician", consisting of siliciclastic deposits (mainly sandy slates) of large but unknown thickness, called the Seo Formation by Hartevelt (1970). Asymmetrical folds on all scales are developed in these rocks. Small-scale sedimentary structures such as cross-lamination and burrows provide excellent criteria for determination of the polarity of the beds.

- A group of Upper Ordovician sediments, mainly coarse-grained siliciclastic in nature with the thick Rabassa Conglomerate Formation at its base (Hartevelt, 1970).

- The black shales of the Silurian, probably some 100's of metres thick (the exact thickness is difficult to estimate as the shales are often strongly tectonised).

- Carbonates of Devonian and Lower Carboniferous age, frequently thrown into narrow, upright folds.

- Locally developed siliciclastic Upper Carboniferous.

Several generations of Variscan deformation can be distinguished in the Axial Zone, of which the mainphase deformation is the most important. It must be pointed out, however, that exact correlation of deformational events is not always possible, not even over relatively small distances. Thus mainphase folding is not necessarily of the same age throughout the Axial Zone (Zwart, 1981).

On a large scale, a fundamental subdivision of the Variscan Pyrenees can be made into an "infrastructure", characterised by a penetrative, subhorizontal foliation, as well as a complex multiple deformational and metamorphic history; and a "suprastructure" usually built of unmetamorphosed or low-grade sediments in which cleavages have a relatively steep attitude (Zwart, 1963). The boundary between infra- and suprastructure may be expressed as a level of décollement within the Silurian black shales (Kleinsmiede, 1960), or it can be situated along the transition zone from low- to high grade metamorphic rocks as in the Aston massif (Verhoef et al., 1984).

The Axial Zone is dominated by the occurrence of large "domes" (Figs. III.1 and III.2), separated by narrow synclines. Where these domes have been deeply eroded, their metamorphic core (belonging to the infrastructure) is

Fig. III.3. Typical small-scale mainphase fold from the western part of the Orri dome. North is towards the right. Axial plane cleavage is poorly developed in this case.

often exposed; e.g. Aston and Hospitalet massifs. Alternatively, only low-grade or unmetamorphosed Cambro-Ordovician rocks crop out, like in the Massana and Orri domes.

The Orri dome (Fig. III.2) and adjacent areas were first mapped in great detail by Hartevelt (1970), who paid, however, little attention to the small-scale structures developed in the rocks of the Seo Formation. Therefore, a detailed structural analysis of the Orri dome was subsequently carried out by the present author. Structural analysis in the monotonous Cambro-Ordovician rocks is seriously hindered by an almost complete lack of marker horizons and the occurrence of several deformational overprints of Variscan age, whereas all Variscan structures have been overprinted by Late Paleozoic post-Variscan and Alpine deformation. Nevertheless, mainphase folding and three later Variscan deformation generations can be recognised (Speksnijder, 1986b; chapter IV).

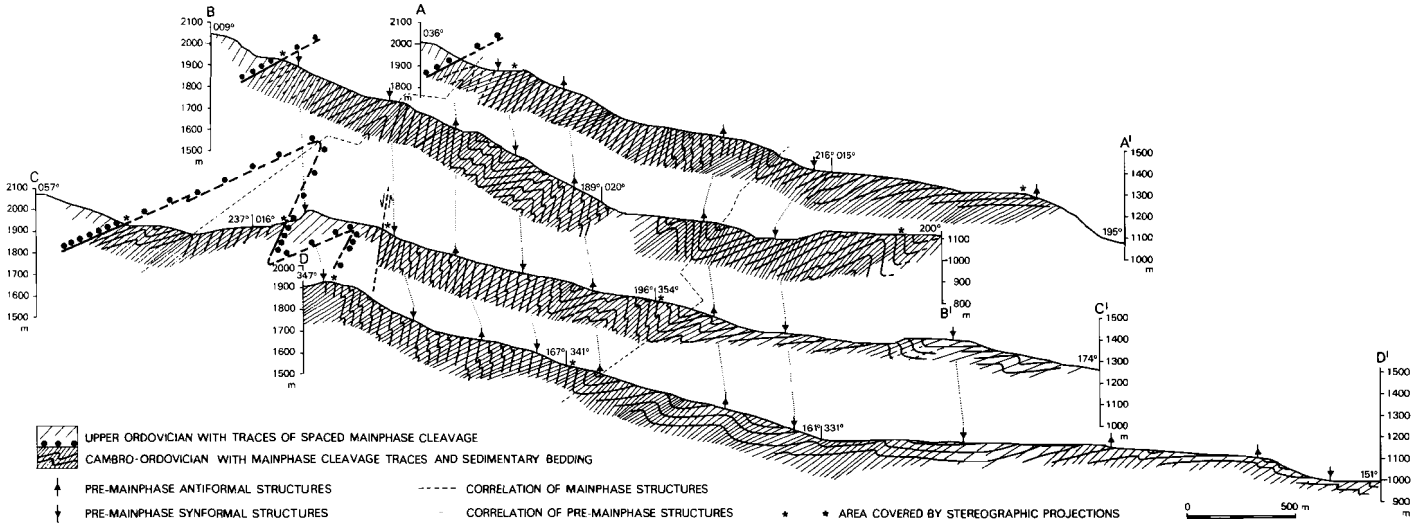
B
A
C
D
A'
B'
C'
D'
009°
036°
057°
237° 016°
347°
189° 020°
216° 015°
200°
196° 354°
167° 341°
161° 331°
195°
174°
151°
2100
2000
1900
1800
1700
1600
1500
1400
1300
1200
1100
1000
900
800
m
UPPER ORDOVICIAN WITH TRACES OF SPACED MAINPHASE CLEAVAGE
CAMBRO-ORDOVICIAN WITH MAINPHASE CLEAVAGE TRACES AND SEDIMENTARY BEDDING
PRE-MAINPHASE ANTIFORMAL STRUCTURES
PRE-MAINPHASE SYNFORMAL STRUCTURES
CORRELATION OF MAINPHASE STRUCTURES
CORRELATION OF PRE-MAINPHASE STRUCTURES
AREA COVERED BY STEREOGRAPHIC PROJECTIONS
0
500 m

In order to study the geometrical properties of mainphase folds and to investigate the possible occurrence of pre-mainphase structures, an area in the central northern part of the Orri dome was selected (Fig. III.2) in which mainphase structural elements are well developed, while there is no indication for significant overprinting by later deformation generations.

GEOMETRICAL ANALYSIS OF MAINPHASE FOLDS

The mainphase cleavage folds developed in the slates and sandstones of the Orri dome are similar and asymmetrical in profile with relatively long, gently north dipping limbs and relatively short, often overturned steep limbs (Fig. III.3). Their wavelength varies from a few mm to at least hundreds of metres. Axial planes dip 40°-60° towards the north. Cleavage is usually well developed although it may locally be absent on long, little deformed limbs. Field observations suggest that cleavage is essentially parallel to the axial planes of the folds and shows little fanning in the fold profile. The cleavage is frequently developed as a slaty cleavage in fine-grained rocks but it may take the form of a spaced cleavage in sandstones, or of a crenulation cleavage folding a finely laminated sedimentary fabric. In some cases differentiated layering parallel to the mainphase cleavage may occur in areas of large strain, e.g. in fold-hinge

Fig. III.4. Conceptual structural profiles through the north-central Orri dome. No marker horizons could be traced in the monotonous Cambro-Ordovician slates and sandstones. The fold geometry suggests that Upper Ordovician rocks could be expected to outcrop in the central part of the profiles; as this is not the case the contact between Upper Ordovician and older rocks can be a thrust (as indicated in Fig. III.2), or the Cambro-Ordovician is cut by (numerous) faults. The age (post-Variscan?) and significance of the observed normal fault in the northern part of profile CC' are unknown.
In areas of poor data control, no effort has been made to show the possible influence of pre-mainphase folds on the enveloping surface. Stippled and dashed lines show correlations of pre-mainphase and mainphase axial planes, respectively.
The positions of the profiles are indicated in Fig. III.7.

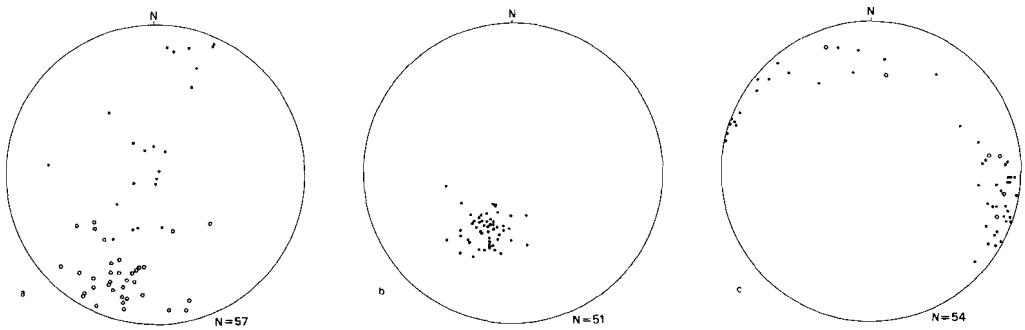

Fig. III.5. Examples of stereographic projections for structural elements in profile CC'.
(a) Poles to sedimentary bedding. Dots indicate normal polarity of the beds, open circles stand for reverse polarity (overturned short foldlimbs).
(b) Poles to mainphase cleavage. (c) Intersection lineations bedding/mainphase cleavage (dots), and small-scale mainphase foldaxes (open circles).

regions. Intersection lineations between sedimentary bedding and mainphase cleavage are generally well developed.

The geometrical properties of the mainphase folds were investigated along four approximately N-S running profiles in the north-central part of the Orri dome (Fig. III.4). For each of the profiles, which run at large angles to the general mainphase strike, directional data on sedimentary bedding (S_0), mainphase cleavage (S_1), intersection lineations bedding/mainphase cleavage (L_1) and small-scale mainphase foldaxes (B_1) were collected and plotted in stereographic projections (Fig. III.5). All directional data were subsequently processed in a computer program for directional statistics (Fig. III.6). For an outline of the background to the program and additional information the reader is referred to the Appendix.

The following results were obtained (cf. Fig. III.6 and Appendix):

- Poles to cleavage often concentrate in point-maxima, i.e. cleavage planes are co-planar. There is usually no (statistically significant)

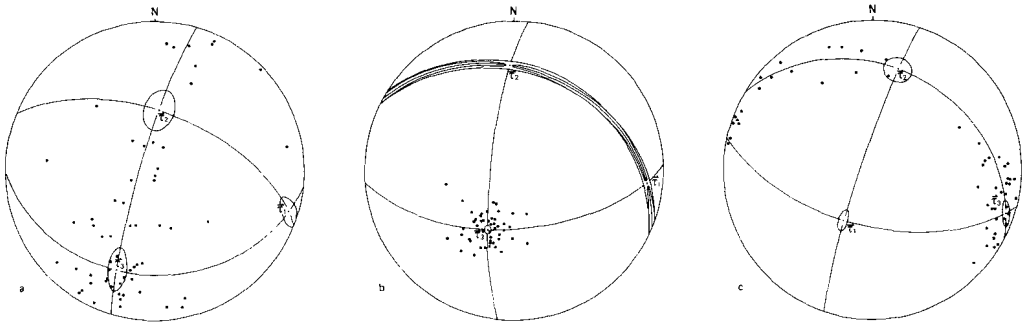

Fig. III.6. Stereographic projections showing eigenvector directions and their confidence ellipses for the orientation tensors of the data set of Fig. III.5a-c. The very large angle of the confidence ellipses in the $\vec{\tau}_1$ - $\vec{\tau}_2$ plane of Fig. III.6b reflects the ill-defined nature of the great circle through poles to mainphase cleavage.

fanning of cleavage in fold profiles. In addition, cleavages can be proved to be axial plane cleavages.

- Mainphase structures are non-cylindrical. The statistically significant difference in "curvature" of the beds per fold limb, in combination with the co-planarity of the cleavage, suggests that the bedding was not co-planar (i.e. had been folded) before mainphase folding took place.

- Intersection lineations and small-scale mainphase foldaxes spread on great circles, the poles of which coincide with the average orientation of poles to cleavage (i.e. all lineations lie, statistically, within the cleavage planes). The angle of spreading, however, is much larger than to be expected on the basis of our statistical analysis of the mainphase structures. Given the co-planarity of the cleavage and the observed lack of significant refolding in this part of the Orri dome, the spreading can again only be attributed to the initial non-planar nature of bedding before the onset of mainphase deformation. In other words, the sedimentary bedding probably was already folded before mainphase folding took place.

INDICATIONS FOR THE PRESENCE OF PRE-MAINPHASE FOLDS

There are four indications (of different kinds and relative importances) that pre-mainphase folds might occur in the northern part of the Orri dome:

1. A very limited number of small-scale (cm-dm), irregular recumbent folds were found in the sandstones of the Seo Formation, both limbs of which are cut by mainphase cleavage at the same angle. These asymmetrical folds occur within discrete layers and their upper limbs are often eroded, while undisturbed sedimentary layers are overlying the folds. There can be no doubt that these structures are of synsedimentary nature and bear no relation to any (regional) deformation generation.

2. It could be argued that the remarkable differences in sedimentary properties between the Cambro-Ordovician Seo Formation (shallow marine, low-energy deposits) and the overlying Upper Ordovician Rabassa Conglomerate Formation (Hartevelt, 1970) might be an indication of the unconformable nature of the contact between these formations. The Rabassa Formation is a thick (up to 100 m) and coarse-grained (maximum pebble size up to 25 cm) immature conglomerate sequence of possible continental origin, which according to Santanach-Prat (1972) and earlier workers was deposited unconformably upon folded Seo slates in areas north and east of the Orri dome. The existence of a pre-Caradoc regional unconformity, which would imply Caledonian orogenic movements in the Pyrenees, was nevertheless disputed by some authors (cf. Hartevelt, 1970; Zwart, 1979). The present writer agrees that in the Orri dome no convincing evidence for a regional angular unconformity can be found.

3. Interference structures involving mainphase and earlier folds were mapped by Hartevelt (1970) in the southern part of the Llavorsi syncline, just north of the Orri dome. These interference structures (type 1 of Ramsay, 1967; p.531), however, occur in the Devonian rocks of the "suprastructure", and an Alpine fault of unknown but probably large (reverse?) throw is separating the Llavorsi syncline from the Orri dome.

4. As stated previously, intersection lineations (L_1) between sedimentary bedding and mainphase cleavage show considerable spreading in a stereographic projection, which can only be satisfactorily explained under the assumption that pre-mainphase folding took place in the Orri dome.

As is shown in Fig. III.7, it has been possible to delineate areas of more or less constant L_1 orientation in the present study area. The chequerboard pattern of Fig. III.7 suggests that two structural trends control the distribution of intersection lineations in the area, one striking approximately 170°-350° and another striking roughly 80°-260°. These directions are taken to represent the axial surface directions of pre-cleavage folds, since areas of constant L_1 orientation must represent the (more or less flat) limbs of the pre-mainphase structures which were later cut by mainphase cleavage. The same method has been applied by Laumonier & Guitard (1978) to identify pre-mainphase folds in rocks of similar age east of the Orri dome. It should be stressed that most of the area boundaries in Fig. III.7 are by no means uniquely defined, especially not in parts with poor data control. Furthermore, most data were collected along approximately north-south running profiles in which the location of the 170°-350° striking boundaries is difficult.

Although it will not be possible, in practice, to map all individual fold hinges of both pre-mainphase systems, the axial surface directions can nevertheless reasonably well be established from the existing data. In the ideal case one should be able to distinguish between synformal and antiformal pre-cleavage foldaxes on the basis of L_1 attitudes with respect to the trace of the axial surfaces: if L_1 lineations plunge away at both sides from an axial surface trace, then pre-cleavage foldlimbs should dip away from the hinge, i.e. the axial surface is related to an antiformal fold. Conversely, L_1 lineations around synformal hinge lines should plunge towards that hinge.

Application of the above principle to our L_1 data sometimes turned out to be unsuccessful as lineations do not always systematically change their plunge direction over an axial surface trace. In addition, some hinge zones interpreted to be antiformal at one place appear to be synformal when traced laterally. This apparent discrepancy can be explained by the low "direction stability" (Ramsay, 1967) of the L_1 and B_1 lineations: intersection lineation directions are very sensitive to relatively small changes in dip of the sedimentary layering, which is illustrated in Fig. III.8. It can be easily read off the diagrams that in the case of folding around a N-S axis

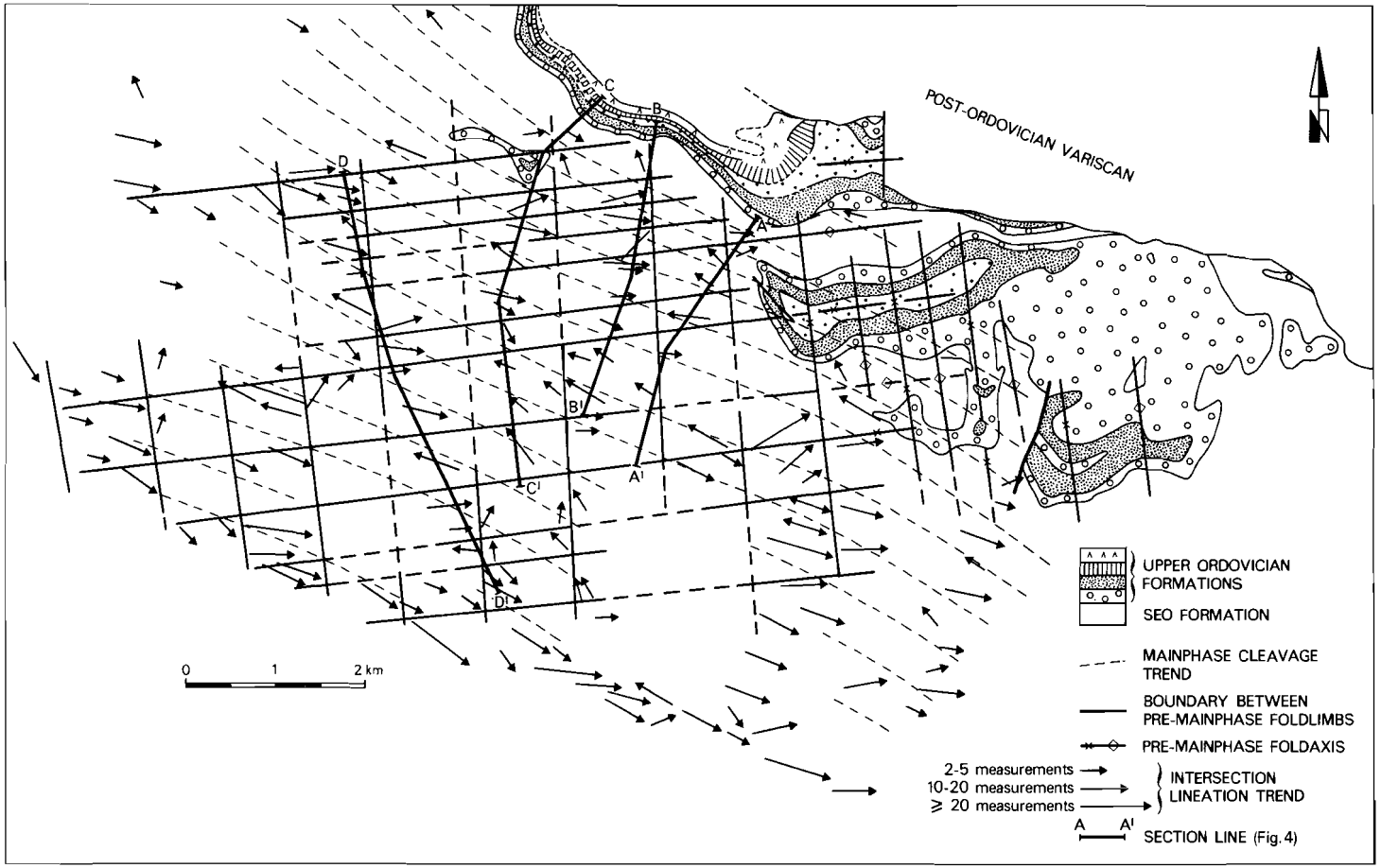
POST-ORDOVICIAN VARISCAN
N
A
A'
B
B'
C
C'
D
D'
0 1 2 km
UPPER ORDOVICIAN FORMATIONS
SEO FORMATION
MAINPHASE CLEAVAGE TREND
BOUNDARY BETWEEN PRE-MAINPHASE FOLDLIMBS
PRE-MAINPHASE FOLDAXIS
2-5 measurements
10-20 measurements
≥ 20 measurements
INTERSECTION LINEATION TREND
A A' SECTION LINE (Fig. 4)

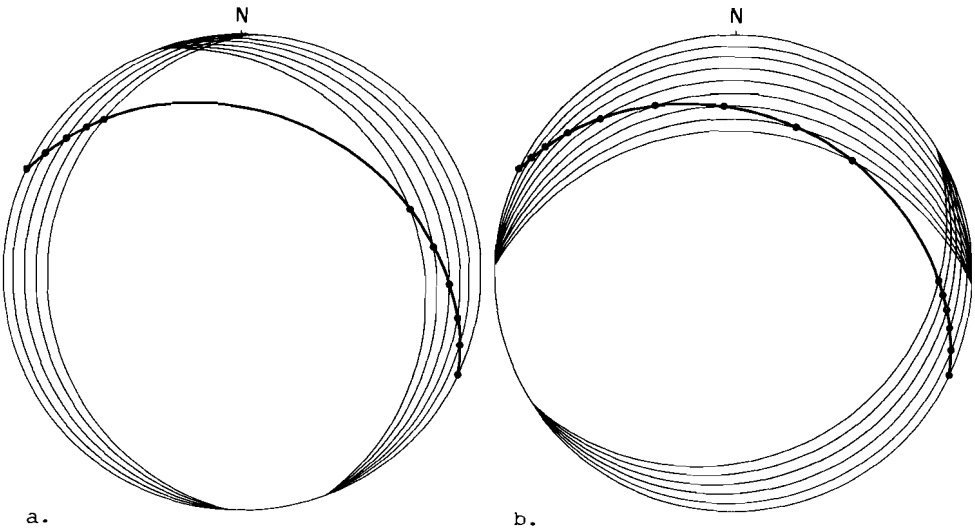

Fig. III.8. Direction instability of intersection lineations (shown by dots) between average mainphase cleavage plane (heavy lines) and sedimentary bedding on shallow dipping flanks of pre-mainphase structures. Diagrams show configurations for N-S (Fig. III.8a) and E-W (Fig. III.8b) directed pre-mainphase foldaxes. The range of possible bedding attitudes is shown by great circles, each representing 5° dip increment from horizontal up to the reconstructed maximum dip angle for the pre-mainphase flanks (Fig. III.10).

large spreading occurs in east-plunging L_1 lineations as a result of only minor changes in bedding attitude. Similarly, north-plunging L_1 lineations will show considerable spreading in pre-cleavage folds with axis 080/00. The combined direction instabilities on the two interfering pre-cleavage

Fig. III.7. Conceptual structural map, showing pre-mainphase foldaxes in Upper Ordovician sediments and boundaries between areas of constant mainphase intersection lineation directions in the Cambro-Ordovician Seo Formation. For explanation see text. The map area is indicated in Fig. III.2.

structures will lead to irregular lineation distributions. Possible non-cylindricity of one or both early fold systems would further enhance the spreading of intersection lineations.

In spite of the difficulty to identify antiformal and synformal structures in the slates of the Seo Formation with much certainty, the distribution of Upper Ordovician rocks mapped by Hartevelt (1970) along the northern edge of the Orri dome clearly reveals the existence of mainphase/pre-mainphase interference patterns (Fig. III.7).

THE GEOMETRY AND ORIENTATION OF PRE-MAINPHASE FOLDS

The distributions of poles to bedding, poles to mainphase cleavage and intersection lineations of the area under study are shown in stereographic projection in Fig. III.9. The influence of refolding in this area is negligible as shown by the point maximum distribution of poles to cleavage. The basis for an analysis of the geometry and orientation of pre-cleavage folds can be summarised as follows:

1. The boundaries between areas of constant L_1 orientation represent axial surface traces of pre-cleavage folds (i.e. they strike 80°-260° and 170°-350°).

2. Since no pre-mainphase structures have been recognised in outcrop and as L_1 lineations only rarely plunge steeper than 45°, it is assumed that pre-cleavage folds were macroscopic open folds with maximum dips of 45° on the foldlimbs.

3. The semi-regional distribution of lithologies suggests that there is no significant axial plunge of the Variscan fold system. Therefore, pre-mainphase foldaxes are supposed to be subhorizontal.

With the aid of the above, the original orientations of pre-mainphase foldlimbs can be reconstructed using a trial-and-error method. The great circles drawn in Fig. III.10 represent the (average) steepest foldlimbs of the pre-mainphase structures. Less steeply inclined fold limbs most probably occur in both pre-cleavage systems, but unfortunately the distribution of

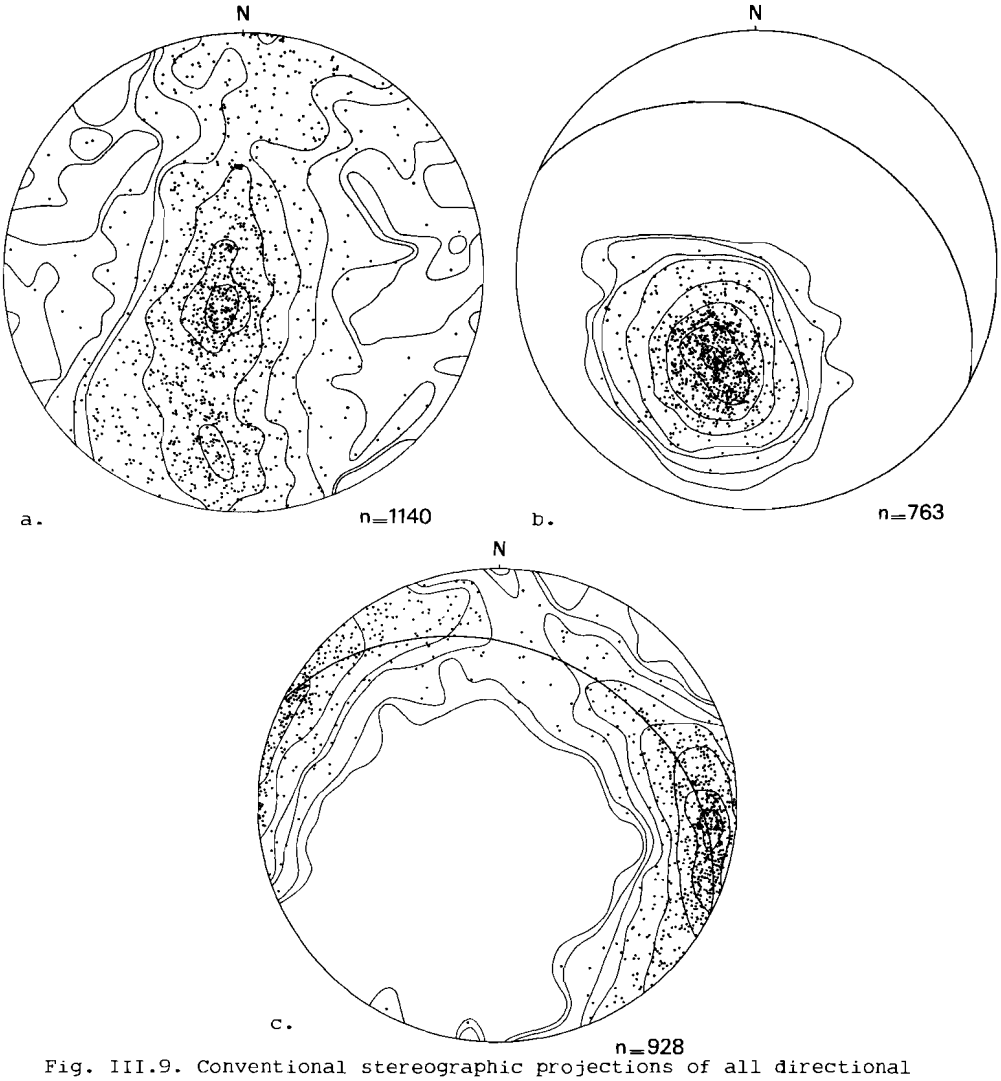

Fig. III.9. Conventional stereographic projections of all directional data from the area covered by profiles AA'-DD', shown in Fig. III.7. (a) Poles to sedimentary bedding. Contours represent 0.09, 0.18, 0.44, 0.88, 2.19, 4.39 and 6.58% per 1% area; maximum 8.25% per 1% area. (b) Poles to mainphase cleavage. Contours represent 0.1, 0.3, 0.7, 1.3, 3.2, 6.6 and 13.1% per 1% area; maximum 19.7% per 1% area. (c) Intersection lineations and small-scale mainphase foldaxes. Contours represent 0.1, 0.2, 0.5, 1.1, 2.7, 5.4, 8.1 and 10.8% per 1% area; maximum 12.0% per 1% area.
dipping flanks (Fig. III.7), it is tentatively concluded that E-W striking pre-mainphase folds are upright, subhorizontal and symmetrical.
lineations in Fig. III.9 does not allow discrimination between separate low-angle dipping foldlimbs.

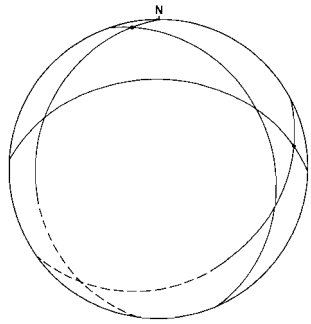

Fig. III.10. Reconstruction of (average) steepest foldlimbs of pre-mainphase structures in the studied area, and orientation of pre-mainphase foldaxes (dots). Based on data shown in Fig. III.9, for further explanation see text.

The following geometry of pre-cleavage folds can be deduced (see Figs. III.9 and III.10): North-south folds are very open folds with an interlimb angle of at least 135°, but probably more. The foldaxes plunge gently north and axial planes are subvertical. From the map pattern (Fig. III.7), a minimum detectable wavelength of 1 km for large folds can be inferred.

East-west folds are open folds (interlimb angle at least 115°). Maximum dips on fold limbs seem to be up to 40° towards north and only 25° towards ESE. A possible asymmetry of these folds is nevertheless difficult to establish. The observation that L_1 readings on the N dipping flank are abundant compared to those on the ESE dipping flanks is misleading, as the spreading of L_1 is not only governed by the attitude of pre-mainphase foldlimbs but also by the orientation of S_1 planes (Fig. III.5), which excludes the presence of S plunging lineations. For the same reason, it is not impossible that ESE flanks are steeper than suggested by the distribution of intersection lineations. As the map pattern shows no systematic differences in length between reconstructed north- and south The fact that intersection lineations show fairly constant orientations on the limbs of pre-mainphase structures, suggests that both early systems are characterised by chevron-type folds.

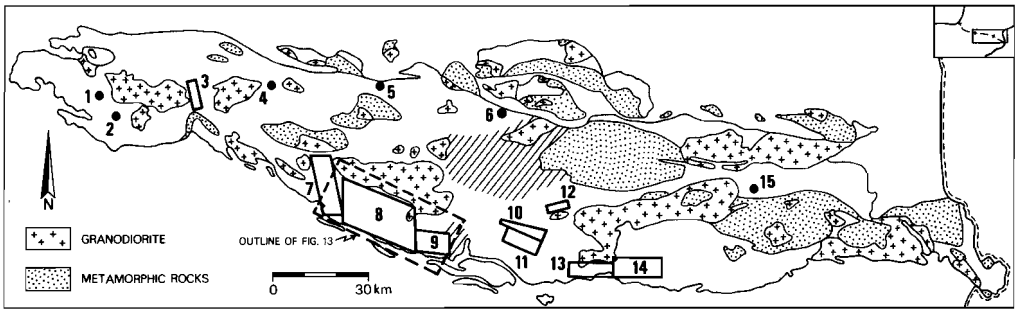

Fig. III.11. Location of areas in the Axial Zone in which pre-mainphase folds have been proved to occur. Numbers refer to listing in Table III.I. Diagonal striping indicates regions in which no pre-mainphase folding seems to have taken place. The area covered by this map equal to that on Fig. III.1.

COMPARISON WITH OTHER AREAS

Most locations or areas in the Axial Zone for which the existence of pre-mainphase folding has been postulated or proven are indicated on Fig. III.11, while orientations and geometrical properties are summarised in Table III.I. Data from metamorphic areas have not been included as they often underwent intense deformation compared to non-metamorphic areas (including transposition of older structures and fabrics); therefore, correlation of deformation generations between metamorphic- and non-metamorphic terranes is usually of very speculative nature, if possible at all (cf. Zwart, 1981).

Table III.I. (next two pages) Locations, orientations, and geometry of pre-mainphase folds in the Axial Zone of the Pyrenees, compiled from existing literature. Location numbers are indicated in Fig. III.11.

LOCATION	AUTHOR(S)	STRATIGRAPHIC LEVEL
1. Upper Gave de Brousset	Muller & Roger (1977)	Devono-Carboniferous
2. Pasino	Muller & Roger (1977)	Devono-Carboniferous
3. Gave de Pau	Lamouroux et al. (1979)	Devono-Carboniferous
4. Upper Aure valley	Muller & Roger (1977)	Upper Devonian, Lower Carboniferous
5. Northern rim Garonne Dome	Boschma (1963)	Carboniferous
6. Estours	de Sitter & Zwart (1962)	Upper Devonian, Carboniferous
7. Upper Esera and Isabena valleys	Wennekers (1968), Zwart (1979)	Devono-Carboniferous
8. Upper Ribagorzana, Baliera and Tor valleys - Northern part - Southern part	Mey (1967b, 1968), Boschma (1963)	 Lower and Middle Devonian Ordovician U. Devonian - Carboniferous Lower and Middle Devonian
9. Flamisell/Mañanet	Zwart (1979)	Devonian
10. Llavorsi syncline	Hartevelt (1970)	Devonian
11. Northern Orri Dome	Present paper	Cambro-Ordovician
12. Massana anticline/ Llavorsi syncline	Hartevelt (1970)	Cambro-Ordovician
13. Ges-Estana unit	Hartevelt (1970)	Cambro-Ordovician
14. Cerdanya	Brouwer (1968)	Upper Paleozoic
15. Villefranche de Conflent	Laumonier & Guitard (1978)	Ordovician

ORIENTATION AXIAL PLANE	FOLDAXIS	GEOMETRY	SCALE
Strike 30^0-210^0 to 50^0-230^0		Overturned towards NW	KM
Strike 30^0-210^0 to 50^0-230^0		Overturned towards NW	KM
	N-S	Recumbent	
NE-SW strike		Overturned towards NW	KM
"Oblique to strike of orogene"		Concentric	M-KM
NE-SW strike			
From N to S: N-S, NE-SW, and E-W striking		"Gentle"	
Steep E-W to WNW-ESE striking Steep NE-SW striking NW-SW striking, subvertical NE-SW striking, inclined to SE		Concentric Isoclinal (?) Tight Gentle-isoclinal	HM-KM M-KM KM
Steep N-S striking			
Steep N-S		Very flat domes	HM-KM
Strike 170^0-350^0, near vertical Strike 080^0-260^0, near vertical	Slightly N plunging Slightly E plunging	Very open, symm. Open, symmetrical	KM KM
Steep E-W striking	Subhorizontal		
NNW-SSE, steep	Subhorizontal	Very open	KM
Steep N-S (?)	Subhorizontal (?)		KM
Subhorizontal Subvertical WNW-ESE to E-W	E-W 20^0-40^0 to W	Tight recumbent Open cylindrical	KM HM-KM

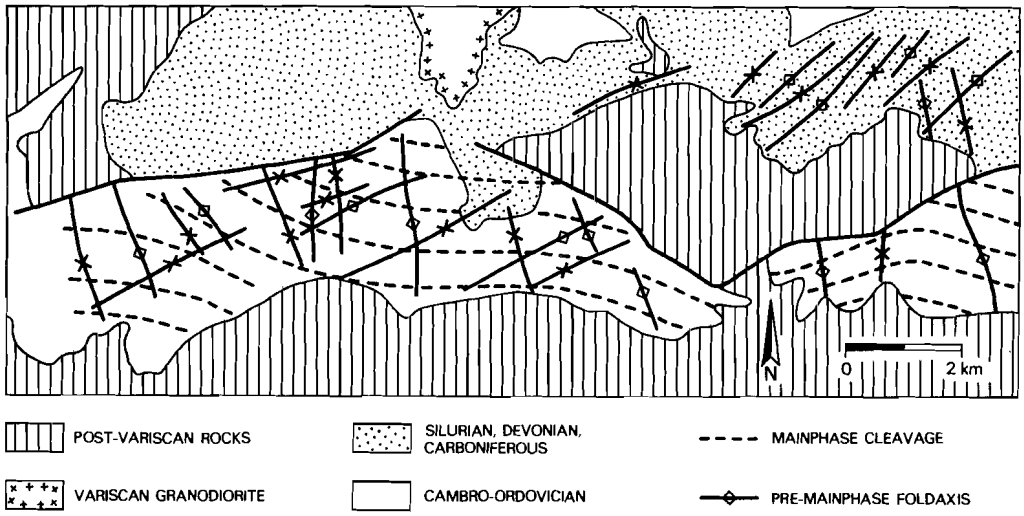

a.

Fig. III.12a. Pre-mainphase folds in the Ges-Estana area (map simplified after Hartevelt, 1970). For location see Figs. III.2 and III.11.

Table III.I shows that directions of pre-mainphase folds or strikes of axial planes seem to vary between NNW-SSE and ESE-WNW but dominantly lie within the first and third quadrants. Apart from the present paper, only one case has been published in which more than one pre-mainphase folding generation could be detected (Laumonier & Guitard, 1978). Reinterpretation of interference patterns on published maps, however, suggests that the occurrence of two early folding generations is rule rather than exception in the central Axial Zone:

Fig. III.12b. E-W cross-section through the Ges-Estana unit (after Hartevelt, 1970).

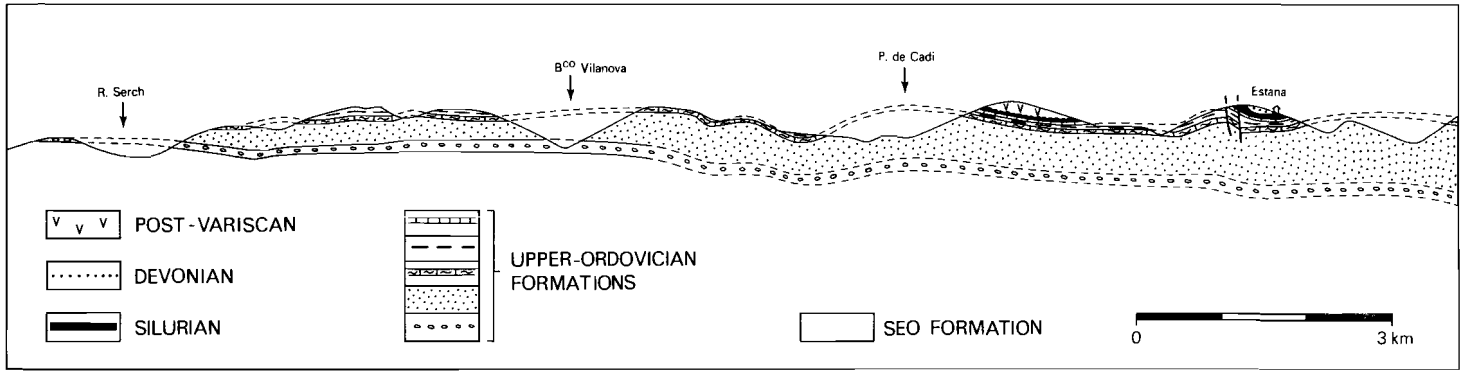
R. Serch
B^CO Vilanova
P. de Cadi
Estana
POST-VARISCAN
DEVONIAN
SILURIAN
UPPER-ORDOVICIAN FORMATIONS
SEO FORMATION
0
3 km

b.

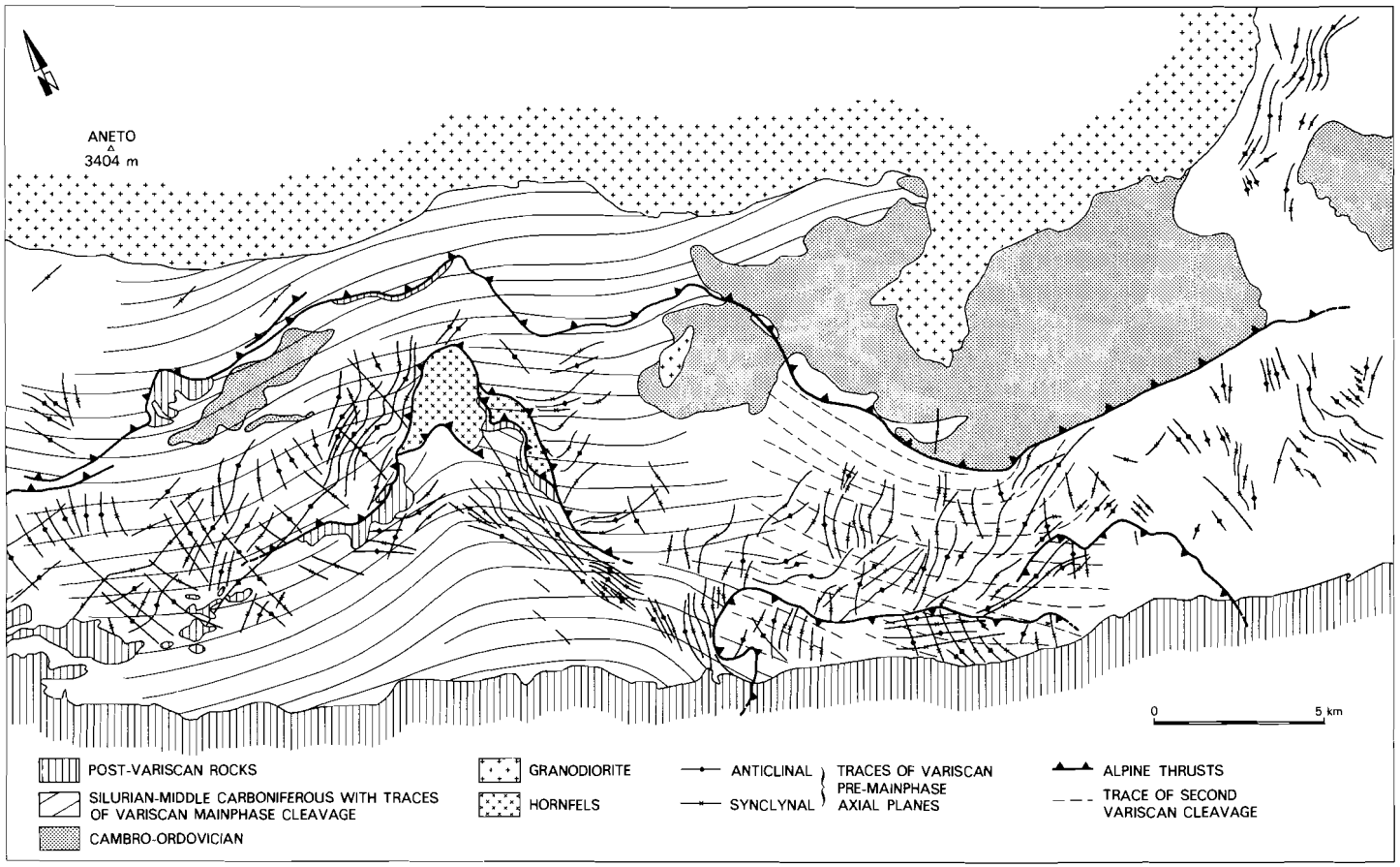
ANETO
3404 m
0
5 km
POST-VARISCAN ROCKS
SILURIAN-MIDDLE CARBONIFEROUS WITH TRACES OF VARISCAN MAINPHASE CLEAVAGE
CAMBRO-ORDOVICIAN
GRANODIORITE
HORNFELS
ANTICLINAL
SYNCLYNAL
TRACES OF VARISCAN PRE-MAINPHASE AXIAL PLANES
ALPINE THRUSTS
TRACE OF SECOND VARISCAN CLEAVAGE

1. Gentle undulations in the Upper Ordovician beds of the Ges-Estana structural unit were reported by Hartevelt (1970), Fig. III.12a & b. The relationship between fold interference pattern and mainphase cleavage traces mapped by this author suggests that two directions of pre-mainphase folding must be present in this unit (Fig. III.12a). In both cases folds appear to be open, upright and to have subhorizontal axes.

2. Along the southern border of the Axial Zone, between the rivers Esera and Noguera Pallaresa, numerous pre-mainphase folds have been mapped by previous workers (Fig. III.13 and Table III.I). Also in this case, reinterpretation of interference patterns leads us to propose that the (mainly Devonian) rocks in this area have been folded during two separate pre-mainphase deformational events. Axial surface traces make fairly large angles with one another, and their directions vary from NW-SE via N-S to NE-SW while some E-W traces are developed occasionaly. It is rather dubious, however, if the trends of the axial traces as observed at present still represent the original pre-mainphase directions in this area. Reorientation may have taken place as a result of the strong overprint by mainphase folds and a locally developed later Variscan refolding (cleavage traces shown in Fig. III.13). Furthermore, the area is cut by a number of thrusts displacing Variscan and post-Variscan rocks alike, while remnants of marly rocks of Middle to Late Triassic age crop out along the bases of the thrust units, even if these are built-up of Variscan rocks only. Hence, there can be no doubt about the Alpine age of thrust movement (cf. Williams, 1985). In many cases there is a striking difference in axial trace orientation between thrust units, and in addition Variscan mainphase cleavage seems to have been reoriented by Alpine thrusting, too (cf. thrust unit south of hornfels outcrop, Fig. III.13).

In conclusion, it turns out that most of the areas from which pre-mainphase folding has been described have been subject to two phases of

Fig. III.13. Trends of pre-mainphase folds in the Esera-Pallaresa area. For location see Fig. III.11. Map simplified after Mey (1967b, 1968), Wennekers (1968) and Zwart & Roberti (1976); cleavage traces after Mey (1967b, 1968).

early folding. Structural elements belonging to these phases tend to make large angles with each other. In areas where little or no reorientation of pre-mainphase structural elements seems to have taken place, foldaxes and traces of axial surfaces have NNW-SSE and ENE-WSW directions. It is assumed that these directions give a fair representation of original pre-mainphase trends.

TIMING OF PRE-MAINPHASE FOLDING

As can be read from Table III.I, most pre-cleavage folds have been detected in Devonian and Carboniferous sediments and, as they are overprinted by mainphase folds, there can be no doubt about the Variscan age of pre-mainphase folding. On the other hand, there are no good indications regarding the relative ages of NNW-SSE and ENE-WSW folds in the Orri dome or other areas. The superposition of two open fold systems at right angles to each other led to a simple dome and basin pattern in the northern part of the Orri dome, as witnessed by the chequer-board pattern of Fig. III.7. Hence, the relative timing of the pre-mainphase folding can not be established in this case. Much the same holds for the Ges-Estana unit (Fig. III.12). In the area between the rivers Esera and Noguera Pallaresa (Fig. III.13), the apparent bending of some early foldaxes is certainly due to mainphase folding, but again conclusive overprinting relationships between pre-cleavage folds are lacking. In addition, the (possibly strong) Alpine reorientation of structural elements in this area seriously complicates the interpretation of the pre-mainphase structural configuration.

It will be shown in the next paragraph that a dynamic/kinematic analysis of the evolution the north-Iberian Variscan mobile belt suggests that NNW-SSE pre-mainphase folds predate the ENE-WSW folds.

REGIONAL TECTONIC CONSIDERATIONS

Arthaud and Matte (1977) propose late Variscan right-lateral strike-slip faulting in southern Europe and northern Africa as a result of large-scale E-W directed shear. Within this plate-scale shear zone, the suture between stable Europe and the Iberian microplate could have played the role of a secondary shear fault in view of its orientation with respect to the shear zone proper (Arthaud and Matte, 1977; their Fig. 9). A fundamental contribution from transcurrent movements to Variscan orogenic development has been suggested by Heward and Reading (1980) for northern Spain, and by several authors for the entire European Variscan Belt (e.g. Edel et al., 1984; Wong and Degens, 1983). Others favour a subduction/collision process to explain (Central European) Variscan orogenesis, although the occurrence of late Variscan strike-slip faulting is certainly not excluded (Behr et al., 1984; Lorenz and Nicholls, 1984).

As will be demonstrated in the following, there are several reasons to assume that lateral movements played an important role in the evolution of the Variscan Pyrenean mobile belt. Therefore, an attempt will be made to explain Late Paleozoic basin development and orogeny in the Pyrenees as results of dextral strike-slip faulting along the northern boundary of the Iberian microplate. In the proposed dynamic/kinematic model the regional large-scale deformation within the Pyrenean mobile zone is ascribed to regionally averaged stress fields induced by the relative motions of the European and Iberian plates (cf. Arthaud and Matte, 1977). Large-scale superficial deformation under the influence of more or less uniform stress fields can be reasonably interpreted by means of the Coulomb criterion, which predicts the angular relationship between principal stress directions and fault orientation, as well as the sense of movement on the faults Stearns et al., 1981). Local deviations of stress orientation within the fault zone may occur on any scale smaller than the scale of consideration; nevertheless the regionally averaged stress field will be directly related to relative plate movement. Similarly, the trends of large-scale fold systems at shallow crustal levels (i.e. in the suprastructure of the

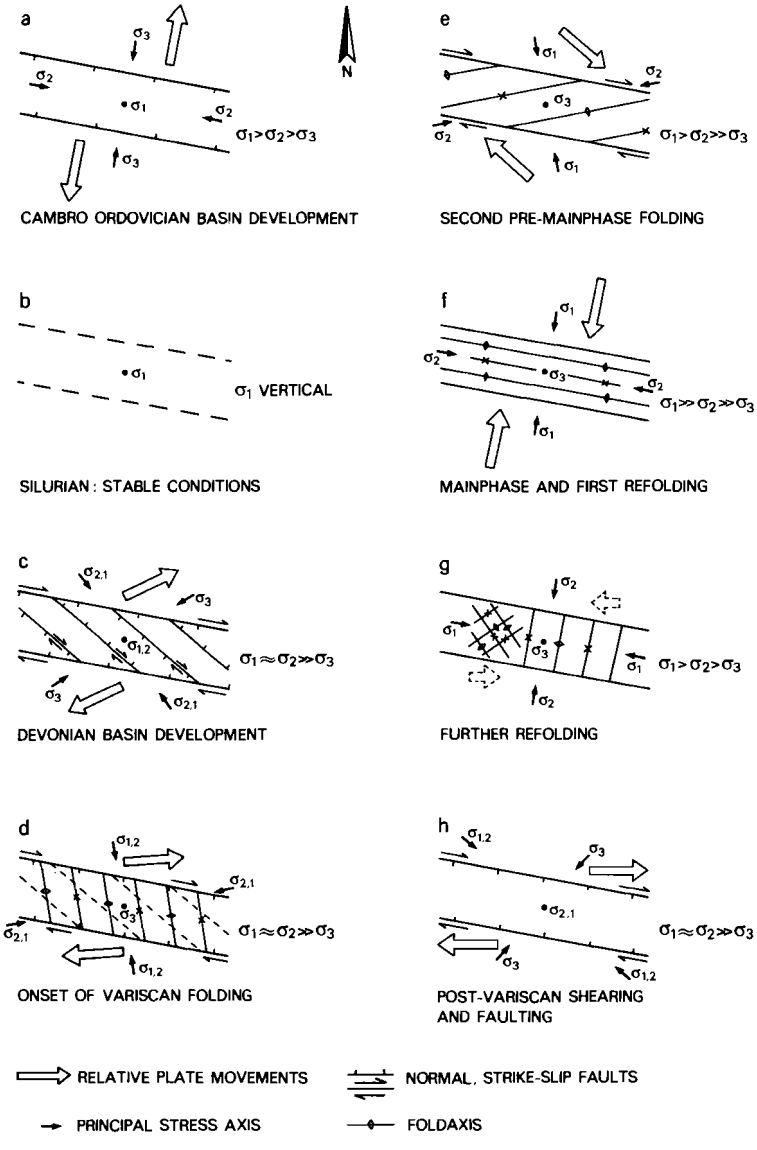
a
σ3
σ2
σ1
σ2
σ1>σ2>σ3
σ3
N
CAMBRO ORDOVICIAN BASIN DEVELOPMENT
b
σ1
σ1 VERTICAL
SILURIAN: STABLE CONDITIONS
c
σ2,1
σ3
σ1,2
σ1≈σ2≫σ3
σ3
σ2,1
DEVONIAN BASIN DEVELOPMENT
d
σ1,2
σ2,1
σ3
σ2,1
σ1≈σ2≫σ3
σ1,2
ONSET OF VARISCAN FOLDING
e
σ1
σ2
σ3
σ2
σ1>σ2≫σ3
σ1
SECOND PRE-MAINPHASE FOLDING
f
σ1
σ2
σ3
σ2
σ1≫σ2≫σ3
σ1
MAINPHASE AND FIRST REFOLDING
g
σ2
σ1
σ3
σ1
σ1>σ2>σ3
σ2
FURTHER REFOLDING
h
σ1,2
σ3
σ2,1
σ1≈σ2≫σ3
σ3
σ1,2
POST-VARISCAN SHEARING
AND FAULTING
RELATIVE PLATE MOVEMENTS
NORMAL, STRIKE-SLIP FAULTS
PRINCIPAL STRESS AXIS
FOLDAXIS

Variscan Pyrenees) will reflect the direction of plate convergence and therefore give an indication of induced stress directions.

Figure III.14 shows conceptual structural configurations, inferred relative plate motions and associated regional principal stress directions for a number of stages in the evolution of the Variscan mobile belt. It must be emphasised that the reconstructions serve as an illustration of possible relations between plate movements, stresses and large-scale structural trends at a certain time; they are definitely not intended to suggest a direct relation between stress and (finite) strain, as factors such as strain-rate, variation of mechanical properties within the suprastructure, and duration of deformational events have not been taken into account. In spite of this, an overall dynamic/kinematic model is preferred above a purely kinematic model as the former translates the essentially two-dimensional (horizontal) movement of the plates into three-dimensional stress-distribution in the fault zone between them. The proposed sequence of events does not always follow unequivocally from the available data, but is considered to be the most simple internally consistent one.

The following evolution of the Pyrenean mobile zone is envisaged (Fig. III.14):

a. Indications for major Cambro-Ordovician plate movements and basin differentiation are lacking as sediments are rather uniform in nature (Hartevelt, 1970; Laumonier and Guitard, 1978). Sedimentary facies patterns and thickness distributions suggest basin initiation along a WNW-ESE strike (Zandvliet, 1960), implying vertical maximum principal stress and least principal stress at large angles to the basin.

b. Stable conditions prevailed during the Silurian, because the black shales deposited in this period exhibit constant thickness and identical facies over the whole area of the present-day Variscan Pyrenees.

Fig. III.14. Cartoons showing the proposed dynamic/kinematic evolution of the north-east Iberian Paleozoic mobile belt. For discussion see text.

c. Basin differentiation, caused by significant extension, commences in the Early Devonian and governs structural patterns and facies development throughout the Devonian up to Middle Carboniferous times. Boersma (1973) presents a series of qualitative lithofacies maps of the Axial Zone covering the time-span lowermost Gedinnian-Visean. In view of the complexity of Pyrenean tectonics, Boersma (1973) does not attempt to palinspastically restore his lithofacies maps, and some of the stratigraphic correlations are based on poor paleontological data (see comments in Buchroithner and Milan, 1977; Mirouse et al., 1983; and Engel, 1984). Facies distributions and the outline of areas of little or no deposition in the Upper Paleozoic reveal E-W, ESE-WNW and SE-NW trends. The types of sedimentary facies, their differentiation across the Axial Zone and the occurrence of land areas within the sedimentary trough suggest that facies distribution was controlled by synsedimentary normal faulting along one or more of the trends mentioned above. The E-W trends on Boersma's (1973) maps can largely be ignored in this context as they are of Alpine age, e.g. the apparent facies transitions along the North Pyrenean fault and the trace of the Gavarnie nappe. Some apparent ESE-WNW facies boundaries are of Alpine age as well (e.g. along the Nogueras Zone; Williams, 1985), but in other cases they may represent original depositional breaks. Boersma (1973) and Mirouse et al. (1983) suggest that the central part of the Variscan basin, aligned ESE-WNW, was a deep trough in an otherwise rather shallow basin throughout most of the Devonian and the Carboniferous.

It is suggested that basin differentiation was controlled by intrabasinal SE-NW synsedimentary faulting (cf. Habermehl, 1970), as well as ESE-WNW faulting on a larger scale. This type of configuration and the overall depositional history of the Variscan basin would arise in the case of a divergent strike-slip induced grabenlike structure, internally dominated by SE-NW en-echelon Riedel shears (Tchalenko, 1970), as shown in the figure. The Iberian plate moved towards the southwest with respect to Europe (present day north for reference) to generate this structural configuration. The maximum and intermediate principal stresses must have been of comparable magnitude to allow for simultaneous subsidence and right-lateral movements. The angle between the largest horizontal principal stress and the fault zone is prescibed by the Coulomb criterion.

d. Flysch sedimentation, induced by increasing subsidence rates, starts in the late Visean and eventually covered the whole Pyrenean depositional

realm. Sediments laid down in the northern part of the flysch basin were derived from the north (Engel, 1984), whereas paleocurrent directions towards NNE and NE were reported by Buchroithner and Milan (1977) for turbidites in the southern Axial Zone. The general younging of the base of the flysch deposits and the migration of compressional deformation from E to W (Mirouse et al., 1983; Engel, 1984), indicates the transition from rapid downwarping of the depositional basin (transtension) in the W to compression and uplift (transpression) in the E along the north-Iberian plate margin. The transition point between transtension and transpression travelled westward in time as well. These observations are taken to indicate that the boundaries of the Iberian and European plates did not approach each other perfectly parallel, but that a rotational component of movement was involved as well. From our data it is not possible to deduce if this movement was caused by a slight "misfit" between the edges of the plates or that it resulted from finite rotation of the Iberian plate with respect to Europe. Overall relative plate movements were, however, approximately east-west.

A σ_1-σ_2-σ_3 permutation and a rotation of principal stresses in the horizontal plane may explain the occurrence of folds with N-S trend, particularly between offsets of pre-existing but still active Riedel shears (Rodgers, 1980). Further conditions for the generation of these folds will be presented in the next section.

e. The relative movement direction of the Iberian plate became northwest, i.e. the plates were approaching each other obliquely. With the increase of the differential stress (σ_1-σ_3), Riedels shears became locked and early open folding took place along an E-W strike.

f. Mainphase folding and subsequent refolding, in both cases involving relatively large strains and development of steep axial plane cleavages in the suprastructure, are caused by rapid plate convergence and increased heat flow. In this case, the strike of the folds is ESE-WNW. During this stage plate movement was at right angles to the Pyrenean mobile zone.

g. At the end of the Variscan orogeny, the magnitude of (differential) stresses and strain-rates dropped considerably, and eventually minor stresses caused further refolding of mainphase folds and older structures in the suprastructure (Speksnijder, 1986b; chapter IV). Folds developed in various orientations and are not constant in size. In metamorphic areas, late folds with varying orientation have been described as well (cf. Zwart,

1979). The regional kinematic significance of the occurrence of these folds is considered to be low, for the following reasons: some of the fold generations seem to be restricted to small metamorphic areas only; high temperature and large strain in the infrastructure could have caused reorientation of older structures; and finally, at least some of the late folds and cleavages in the metamorphic infrastructure may well be of Alpine age (Verhoef et al., 1984).

h. In the post-orogenic stage, considerable E-W shearing took place along pre-existing Variscan anisotropy planes, causing the formation of superficial strike-slip controlled sedimentary basins in Permian times. Within these basins there is good evidence for relatively small-scale alternations of transpressive and transtensive stress conditions (Speksnijder, 1985; chapter II).

Most of the Triassic rocks of the Pyrenees were deposited with uniform thickness and uniform facies as a blanket over a peneplain on top of the Variscan folded belt. Only in the western Pyrenees, minor shear movements reactivated pre-existing faults and small-scale sedimentary basins were formed (Soula et al., 1979). The fading of these movements marks the end of the Variscan orogenic cycle in the Pyrenees.

DISCUSSION; SIGNIFICANCE OF PRE-MAINPHASE FOLDING

The occurrence of pre-mainphase folds in the Paleozoic rocks of the Pyrenees can be explained in the context of an overall right-lateral strike-slip induced origin of the northeast-Iberian Variscan mobile belt.

Our model is readily summarised by a consideration of the history of principal stress orientation: in the initial stage of the Variscan orogeny, basin development within the elongated WNW-ESE fundamental strike-slip zone occurred in a stressfield in which $\sigma_1=\sigma_v$ (vertical stress, equal to the effective overburden weight), and σ_2 (of comparable magnitude to σ_v) was at a favourable angle to the strike of the fault zone to allow for lateral movement (Fig. III.14c,d). As σ_1 and σ_2 were of comparable magnitude, permutations between the two may have occurred. At the onset of Variscan

folding the magnitudes of σ_1 and σ_2 grew considerably, leaving σ_v as the least principal stress (Fig. III.14d). As a result, buckles were generated at right angles to σ_2.

Second pre-mainphase folding, mainphase folding and early refolding took place in stress fields in which σ_v continued to be equal to σ_3, while σ_1 rotated clockwise in the horizontal plane to become orthogonal to the mobile zone. As a result, strike-slip movements ceased completely (Fig. III.14e,f).

The transition from superficial brittle behaviour during the Devonian and Early Carboniferous to ductile flow expressed by buckling and foliation development in the Late Carboniferous can be attributed to an increased convergence rate and the well-documented anomalously high heat flow during the Variscan orogeny in the Pyrenees (Zwart, 1979).

In a kinematic sense, the inferred clockwise rotation of the maximum principal stress in the early stage of the Variscan orogeny reflects the changing relative movement of the Iberian microplate: from oblique divergence (and associated right-lateral strike-slip faulting) to oblique convergence (again with associated right-lateral strike-slip faulting). The oblique convergence closed the previously existing strike-slip sedimentary basin in a scissor-like movement from east to west, as demonstrated by Mirouse et al. (1983) and Engel (1984). During the mainphase stage of Variscan folding (and the first refolding stage), the north-eastern margin of Iberia collided with the European plate. Subsequent Variscan deformation is characterised by an irregular distribution of structures of variable size and orientation (Fig. III.14g), which are not to be related to the relative movements of the Iberian and European plates. This particularly holds for the development of some fold systems in metamorphic areas, e.g. recumbent N-S directed folds in the western Aston massif, which are related to local thermally induced gravity collapse of older structures (Verhoef et al., 1984). These folds, therefore, do not reflect on the relative plate movements.

Post-orogenic plate movements were basically parallel to the mobile zone and of dextral sense. We may assume that, like during Devonian basin development, the regionally averaged σ_3 direction was horizontal NE-SW (Fig. III.14h).

The first major conclusion drawn from this study is that a simple model involving alternating convergent and divergent right-lateral strike-slip movements can explain the generalities of the entire Variscan structural evolution of the Pyrenees, including the occurrence of early pre-mainphase folds, notwithstanding the strong variations in structural styles and orientations observed in detail.

The second major conclusion is that the occurrence of open folds at large angles to the general Variscan trend in the Pyrenees (both the first pre-mainphase folds and the late refolding) is related to the transition from divergent to convergent relative plate movements, and vice-versa.

ACKNOWLEDGEMENTS

I am indebted to Henk Zwart and Ide van der Molen for critically reading the text; to John Savage for introducing me to directional statistics, and for help in the processing and interpretation of many data; to Rob Smeets and Bruno Caline for translation of the French abstract; to Christian Hoecker for translation of the German abstract; to Eppo van Straten for assistence in the field; and to Ineke Smeets for supplying all possible help.

REFERENCES

Arthaud, F. and Matte, P. (1977). Late Paleozoic strike-slip faulting in southern Europe and northern Africa: Result of a right-lateral shear zone between the Appalachians and the Urals.
Geol.Soc.America Bull., 88, pp. 1305-1320.

Behr, H.-J., Engel, W., Franke, W., Giese, P. & Weber, K. (1984). The Variscan Belt in Central Europe: main structures, geodynamic implications, open questions. In: H.J. Zwart, H.-J. Behr & J.E. Oliver (Editors), Appalachian and Hercynian Fold Belts.
Tectonophysics, 109, pp. 15-40.

Bingham, C. (1964). Distributions on the Sphere and on the Projective Plane.
Ph.D. thesis, Yale University.

Boersma, K.Th. (1973). Devonian and Carboniferous Conodont stratigraphy, Central Spanish Pyrenees.
Leidse Geol.Meded., 49, pp. 303-377.

Boschma, D. (1963). Successive Hercynian structures in some areas of the Central Pyrenees.
Leidse Geol.Meded., 28, pp. 103-176.

Brouwer, Th.N. (1968). Verslag van een geologische kartering in de omgeving van de Cerdaña vallei, oostelijke Pyreneeën, Spanje.
Internal report Leiden University, 34 pp.

Buchroithner, M.F. and Milan, G. (1977). Spätvariszische Geosynklinal-entwicklung in den Ostpyrenäen.
N.Jb.Geol.Paläont.Abh., 155, pp. 1-17.

Charlesworth, H.A.K., Langenberg, C.W. & Ramsden, J. (1976). Determining axes, axial planes, and sections of macroscopic folds using computerbased methods.
Can.J.Earth Sci., 13, pp. 54-65.

Edel, J.-B., Coulon, M. & Hernot, M.-P. (1984). Mise en évidence par le paléomagnetisme d'une importante rotation antihoraire des Vosges meridionales entre le Viséen terminal et le Westphalien supérieur. Tectonophysics, 106, pp. 239-257.

Engel, W. (1984). Migration of folding and flysch sedimentation on the southern flank of the Variscan Belt (Montagne Noire, Mouthoumet Massif, Pyrenees).
Z.dt.geol.Ges., 135, pp. 279-292.

Habermehl, M.A. (1970). Depositional history and diagenesis of quartz-sand bars and lime-mud environments in the Devonian Basibe Formation (Central Pyrenees, Spain).
Leidse Geol.Meded., 46, pp. 1-55.

Hartevelt, J.J.A. (1970). Geology of the Upper Segre and Valira valleys, Central Pyrenees, Andorra/Spain.
Leidse Geol.Meded., 45, pp. 167-236.

Kleinsmiede, W.F.J. (1960). Geology of the Vall d'Aran (Central Pyrenees).
Leidse Geol.Meded., 25, pp. 129-245.

Langenberg, C.W., Rondeel, H.E. & Charlesworth, H.A.K. (1977). A structural study in the Belgian Ardennes with sections constructed using computer-based methods.
Geol.Mijnbouw, 56, pp. 145-154.

Laumonier, B. and Guitard, G. (1978). Contribution a l'étude de la tectonique superposée hercynienne des Pyrénées orientales: le problème des plissements précoces dans le Paléozoïque inférieur épizonal (série de Jujols) du synclinal de Villefranche de Conflent.
Rev.Géogr.phys.Géol.dyn., XX, pp. 177-212.

Lamouroux, C., Debat, P., Déramond, J. & Majesté-Menjoulas, C. (1979). Influence de massifs plutoniques hercyniens dans l'évolution des structures pyrénéennes: exemple du massif du Néouvielle.
Bull.Soc.géol.France, XXI, pp. 213-220.

Le Pichon, X., Bonnin, J., Francheteau, J. & Sibuet, J.-C. (1971). Une hypothese d'évolution tectonique du Golfe de Gascogne.
In: Histoire structurale du Golfe de Gascogne, VI.11, pp. 1-44. Ed. Technip, Paris.

Lorentz, V. and Nicholls, I.A. (1984). Plate and intraplate processes of Hercynian Europe during the Late Paleozoic.
Tectonophysics, 107, pp. 25-56.

Mardia, K.V. (1972). Statistics of directional data.
Academic Press, London, 357 pp.

Mardia, K.V. and Zemroch, P.J. (1977). Table of maximum likelihood estimates for the Bingham distribution.
J.Statist.Comput.Simul., 6, pp. 29-34.

Mey, P.H.W. (1967b). The geology of the Upper Ribagorzana and Baliera valleys, Central Pyrenees, Spain.
Leidse Geol.Meded., 41, pp. 153-220.

Mey, P.H.W. (1968). Geology of the Upper Ribagorzana and Tor valleys, Central Pyrenees, Spain.
Leidse Geol.Meded., 41, pp. 229-292.

Mirouse, R., Barrouquere, G., Bessière, G., Delvolve, J.-J. & Perret, M.-F., (1983). Amorce de la sédimentation synorogenique dans les Pyrénées Varisque. Données chronologiques; implications paléogéographiques.
Geol.Rundschau, 72, pp. 253-281.

Muller, J. & Roger, Ph. (1977). L'évolution structurale des Pyrénées (domaine central et occidental). Le segment hercynien, la chaîne de fond alpine.
Géologie alpine, 3, pp. 149-191.

Parish, M. (1984). A structural interpretation of a section of the Gavarnie nappe and its implications for Pyrenean geology.
J.Struct.Geol., 6, pp. 247-255.

Ramsay, J.G. (1967). Folding and fracturing of rocks.
McGraw-Hill, New York, 568 pp.

Ries, A.C. (1978). The opening of the Bay of Biscay, a review.
Earth-Science Reviews, 14, pp. 35-63.

Rodgers, D.A. (1980). Analysis of pull-apart basin development produced by en echelon strike-slip faults. In: P.F. Ballance and H.G. Reading (Editors), Sedimentation in Oblique-Slip Mobile Zones.
Spec.Publ.int.Ass.Sediment., 4, pp. 27-41.

Santanach-Prat, P.F. (1972). Sobra una discordancia en el Paleozoico inferior de los Pirineos orientales.
Acta Geol.Hisp., VII, pp. 129-132.

Sitter, L.U. de & Zwart, H.J. (1962). Geological map of the Paleozoic of the Central Pyrenees, sheet 1 Garonne and sheet 2 Salat, France.
Leidse Geol.Meded., 27, pp. 191-236.

Soula, J.-C., Lucas, C. & Bessière, G. (1979). Genesis and evolution of Permian and Triassic basins in the Pyrenees by regional simple shear acting on older Variscan structures: field evidence and experimental models.
Tectonophysics, 58, pp. T1-T9.

Speksnijder, A. (1985). Anatomy of a strike-slip fault controlled sedimentary basin, Permian of the Southern Pyrenees, Spain.
Sediment.Geol., 44, pp. 179-223 (Chapter II of this thesis).

Speksnijder, A. (1986b). The structural development of the Orri-dome, southern Variscan Pyrenees, Spain.
Eclogae geol.Helv. (Chapter IV of this thesis).

Stearns, D.W., Couples, G.D., Jamison, W.R. & Morse, J.D. (1981). Understanding faulting in the shallow crust: contributions to selected experimental and theoretical studies. In: N.L. Carter et al. (Editors), Mechanical behaviour of crustal rocks.
Geophysical monograph 24, American Geophysical Union, Washington, pp. 215-229.

Tchalenko, J.S. (1970). Similarities between shear zones of different magnitudes.
Bull.Geol.Soc.Am., 81, pp. 1625-1640.

Verhoef, P.N.W., Vissers, R.L.M. & Zwart, H.J. (1984). A new interpretation of the structural and metamorphic history of the western Aston massif (Central Pyrenees, France).
Geol. Mijnbouw, 63, pp. 399-410.

Voo, R. van der (1969). Paleomagnetic evidence for the rotation of the Iberian peninsula.
Tectonophysics, 7, pp. 5-56.

Watson, G.S. (1965). Equatorial distributions on a sphere.
Biometrika, 52, pp. 193-203.

Wennekers, J.H.N. (1968). The geology of the Esera valley and the Lys-Caillaouas massif, Central Pyrenees, Spain, France.
Unpublished Ph.D. thesis, Leiden, 46 pp.

Williams, G.D. (1985). Thrust tectonics in the south central Pyrenees.
J.Struct.Geol., 7, pp. 11-17.

Wong, H.K. and Degens, E.F. (1983). Effects of CO_2-H_2O and oblique collision on orogenesis- the European Hercynides as an example.
Tectonophysics, 95, pp. 191-220.

Zandvliet, J. (1960). The geology of the Upper Salat and Pallaresa valleys, Central Pyrenees, France/Spain.
Leidse Geol.Meded., 25, pp. 1-127.

Zwart, H.J. (1963). The structural evolution of the Paleozoic of the Pyrenees.
Geol.Rundschau, 53, pp. 170-205.

Zwart, H.J. (1979). The geology of the central Pyrenees.
Leidse Geol.Meded., 50, pp. 1-74.

Zwart, H.J. (1981). Three profiles through the Central Pyrenees.
Geol.Mijnbouw, 60, pp. 97-104.

Zwart, H.J. and Roberti, K.F. (1976). Geological map of the Central Pyrenees, sheet 9: Flamisell-Pallaresa.
Geological Institute Leiden.

APPENDIX

Directional statistics of structural elements

In order to gain insight into the geometrical properties of mainphase folds and the possible occurrence of pre-mainphase folds, a statistical analysis was carried out on directional data from profiles AA'-DD', shown in Fig. III.4. The data sets comprise the orientations of sedimentary bedding (S_0), mainphase cleavage (S_1), intersection lineations bedding/cleavage (L_1), and small-scale mainphase foldaxes (B_1). Care was taken that only data from areas where no refolding of mainphase structures was visible in the field were considered; the boundaries of these areas are indicated by asterixes in Fig. III.4. For each structural element discrimination was made between data collected from long limbs, short limbs and fold-hinge areas of the mainphase folds.

Apart from plotting in conventional stereographic projections, all data were processed in a computerprogram for directional statistics designed by dr.J.F.Savage (State University of Utrecht), based on the principles outlined by Bingham (1964), Watson (1965), Mardia (1972), Charlesworth et al. (1976), Mardia and Zemroch (1977) and Langenberg et al. (1977).

For each population, the directions of the axes of the orientation tensor and its normalised eigenvalues ($\vec{\tau}_1 \leq \vec{\tau}_2 \leq \vec{\tau}_3$) were computed. The maximum likelihood estimates of the concentration parameters ($\hat{\kappa}_1 \leq \hat{\kappa}_2 \leq \hat{\kappa}_3 = 0$) for the Bingham distribution, which can describe populations of geological directional data in three dimensions, were found from the tables published by Mardia and Zemroch (1977). Subsequently, the angles δ_{ij} of the confidence ellipses around the eigenvectors of the distributions were calculated using:

$$\delta_{ij(0.95)} = \frac{1}{n} \times \frac{1.96 \times 180}{\pi} \{2(\hat{\kappa}_i - \hat{\kappa}_j)(\vec{\tau}_i - \vec{\tau}_j)\}^{-1/2},$$

in which n= total number of measurements.

The numerical values of $\vec{\tau}_i$, $\hat{\kappa}_i$ and δ_{ij} are given in Table III.A.I. The stereographic projections of Fig. III.A.1 show some examples of eigenvector directions and their confidence ellipses.

Fig. III.A.1. Directional data of some structural elements from profiles AA'-DD'. The stereographic projections show eigenvector directions and their confidence ellipses for a number of distributions involving lineations and poles to planar surfaces. S_0 = sedimentary bedding, S_1 = mainphase cleavage, L_1 = intersection lineation bedding/mainphase cleavage, and B_1 = small-scale mainphase foldaxis.

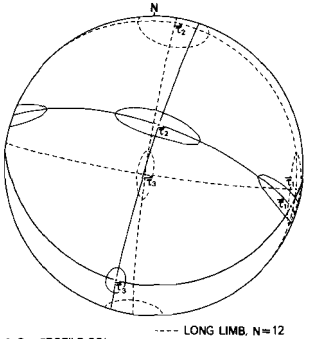

1. S_0, PROFILE DD'

---- LONG LIMB, N=12

—— SHORT LIMB, N=40

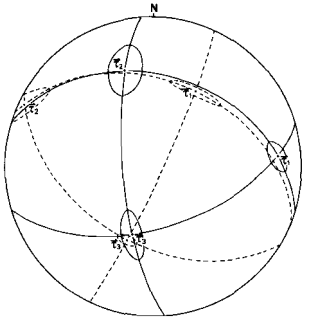

2. S_0/S_1, PROFILE BB'

---- S_0, N=51

—— S_1, N=37

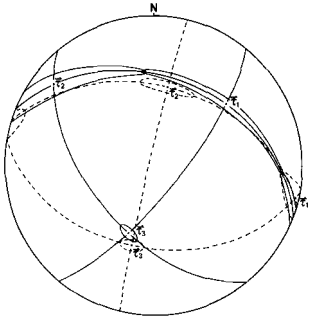

3. S_1, PROFILE BB'

---- LONG LIMB, N=18

—— SHORT LIMB, N=18

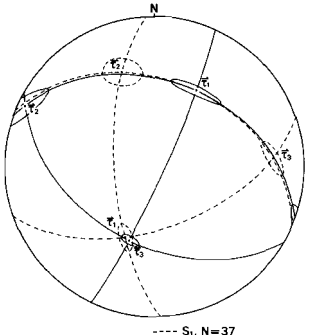

4. S_1/δ_1 & B_1, PROFILE BB'

---- S_1, N=37

—— δ_1 & B_1, N=38

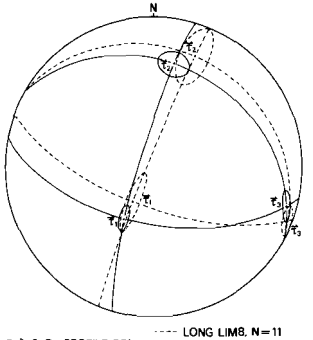

5. δ_1 & B_1, PROFILE DD'

---- LONG LIMB, N=11

—— SHORT LIMB, N=35

S E D I M E N T A R Y B E D D I N G			
PROFILE	TOTAL	LONG	SHORT
AA'	$\vec{\tau}_1$=.0565 $\hat{\kappa}_1$= -9.50 $\vec{\tau}_2$=.1901 $\hat{\kappa}_2$= -3.18 $\vec{\tau}_3$=.7534 $\hat{\kappa}_3$= 0 δ_{12}= 16.33^0 δ_{23}= 11.21^0 N=28 δ_{31}= 5.83^0	$\vec{\tau}_1$=.0318 $\hat{\kappa}_1$=-15.72 $\vec{\tau}_2$=.0878 $\hat{\kappa}_2$= -6.50 $\vec{\tau}_3$=.8804 $\hat{\kappa}_3$= 0 δ_{12}= 33.32^0 δ_{23}= 10.55^0 N=11 δ_{31}= 6.55^0	$\vec{\tau}_1$=.0284 $\hat{\kappa}_1$=-17.61 $\vec{\tau}_2$=.1005 $\hat{\kappa}_2$= -5.77 $\vec{\tau}_3$=.8711 $\hat{\kappa}_3$= 0 δ_{12}= 22.19^0 δ_{23}= 9.72^0 N=15 δ_{31}= 5.32^0
BB'	$\vec{\tau}_1$=.0600 $\hat{\kappa}_1$= -8.97 $\vec{\tau}_2$=.2602 $\hat{\kappa}_2$= -2.12 $\vec{\tau}_3$=.6796 $\hat{\kappa}_3$= 0 δ_{12}= 9.50^0 δ_{23}= 11.80^0 N=51 δ_{31}= 4.72^0	$\vec{\tau}_1$=.0335 $\hat{\kappa}_1$=-14.93 $\vec{\tau}_2$=.0508 $\hat{\kappa}_2$= -9.84 $\vec{\tau}_3$=.9162 $\hat{\kappa}_3$= 0 δ_{12}= 52.48^0 δ_{23}= 5.34^0 N=26 δ_{31}= 4.29^0	$\vec{\tau}_1$=.0519 $\hat{\kappa}_1$= -9.63 $\vec{\tau}_2$=.1163 $\hat{\kappa}_2$= -5.00 $\vec{\tau}_3$=.8319 $\hat{\kappa}_3$= 0 δ_{12}= 30.32^0 δ_{23}= 8.75^0 N=23 δ_{31}= 6.04^0
CC'	$\vec{\tau}_1$=.0398 $\hat{\kappa}_1$=-13.20 $\vec{\tau}_2$=.1359 $\hat{\kappa}_2$= -4.40 $\vec{\tau}_3$=.8243 $\hat{\kappa}_3$= 0 δ_{12}= 15.26^0 δ_{23}= 8.07^0 N=36 δ_{31}= 4.36^0	$\vec{\tau}_1$=.0149 $\hat{\kappa}_1$=-33.56 $\vec{\tau}_2$=.0213 $\hat{\kappa}_2$=-23.47 $\vec{\tau}_3$=.9638 $\hat{\kappa}_3$= 0 δ_{12}=156.25^0 δ_{23}= 9.20^0 N=4 δ_{31}= 7.04^0	$\vec{\tau}_1$=.0391 $\hat{\kappa}_1$=-13.18 $\vec{\tau}_2$=.1053 $\hat{\kappa}_2$= -5.60 $\vec{\tau}_3$=.8556 $\hat{\kappa}_3$= 0 δ_{12}= 21.57^0 δ_{23}= 7.46^0 N=27 δ_{31}= 4.66^0
DD'	$\vec{\tau}_1$=.0595 $\hat{\kappa}_1$= -8.97 $\vec{\tau}_2$=.2594 $\hat{\kappa}_2$= -2.12 $\vec{\tau}_3$=.6811 $\hat{\kappa}_3$= 0 δ_{12}= 9.07^0 δ_{23}= 11.22^0 N=56 δ_{31}= 4.49^0	$\vec{\tau}_1$=.0150 $\hat{\kappa}_1$=-33.33 $\vec{\tau}_2$=.0822 $\hat{\kappa}_2$= -6.97 $\vec{\tau}_3$=.9028 $\hat{\kappa}_3$= 0 δ_{12}= 17.22^0 δ_{23}= 9.58^0 N=12 δ_{31}= 4.21^0	$\vec{\tau}_1$=.0565 $\hat{\kappa}_1$= -9.50 $\vec{\tau}_2$=.1139 $\hat{\kappa}_2$= -5.00 $\vec{\tau}_3$=.8297 $\hat{\kappa}_3$= 0 δ_{12}= 24.70^0 δ_{23}= 6.64^0 N=40 δ_{31}= 4.63^0

Table III.A.I. Nummerical values of $\vec{\tau}_i$= normalised eigenvalues of the orientation tensor, $\hat{\kappa}_i$= the concentration parameters of the Bingham distribution, δ_{ij}= the angles of the eigenvector confidence ellipses, and N= total number of measurements for the orientation distributions of structural elements in profiles AA' - DD'.

M A I N P H A S E C L E A V A G E			
PROFILE	TOTAL	LONG	SHORT
AA'	$\vec{\tau}_1$=.0204 $\hat{K}_1$=-24.51 $\vec{\tau}_2$=.0505 $\hat{K}_2$= -9.90 $\vec{\tau}_3$=.9291 $\hat{K}_3$= 0 δ_{12}= 24.97° δ_{23}= 5.61° N=23 δ_{31}= 3.51°	$\vec{\tau}_1$=.0182 $\hat{K}_1$=-27.47 $\vec{\tau}_2$=.0312 $\hat{K}_2$=-16.03 $\vec{\tau}_3$=.9506 $\hat{K}_3$= 0 δ_{12}= 84.06° δ_{23}= 8.44° N=6 δ_{31}= 6.41°	$\vec{\tau}_1$=.0180 $\hat{K}_1$=-27.78 $\vec{\tau}_2$=.0479 $\hat{K}_2$=-10.44 $\vec{\tau}_3$=.9341 $\hat{K}_3$= 0 δ_{12}= 29.47° δ_{23}= 6.98° N=14 δ_{31}= 4.21°
BB'	$\vec{\tau}_1$=.0174 $\hat{K}_1$=-28.74 $\vec{\tau}_2$=.0571 $\hat{K}_2$= -8.76 $\vec{\tau}_3$=.9259 $\hat{K}_3$= 0 δ_{12}= 14.66° δ_{23}= 4.73° N=37 δ_{31}= 2.55°	$\vec{\tau}_1$=.0122 $\hat{K}_1$=-40.98 $\vec{\tau}_2$=.0639 $\hat{K}_2$= -8.90 $\vec{\tau}_3$=.9239 $\hat{K}_3$= 0 δ_{12}= 14.53° δ_{23}= 6.76° N=18 δ_{31}= 3.06°	$\vec{\tau}_1$=.0223 $\hat{K}_1$=-22.42 $\vec{\tau}_2$=.0392 $\hat{K}_2$=-12.76 $\vec{\tau}_3$=.9385 $\hat{K}_3$= .0 δ_{12}= 46.32° δ_{23}= 5.52° N=18 δ_{31}= 2.92°
CC'	$\vec{\tau}_1$=.0151 $\hat{K}_1$=-33.11 $\vec{\tau}_2$=.0249 $\hat{K}_2$=-20.08 $\vec{\tau}_3$=.9600 $\hat{K}_3$= 0 δ_{12}= 39.28° δ_{23}= 3.24° N=32 δ_{31}= 2.51°	Insufficient data (N=3)	Similar to total cleavage (N=27)
DD'	$\vec{\tau}_1$=.0192 $\hat{K}_1$=-26.04 $\vec{\tau}_2$=.0230 $\hat{K}_2$=-21.74 $\vec{\tau}_3$=.9578 $\hat{K}_3$= 0 δ_{12}= 88.74° δ_{23}= 2.52° N=49 δ_{31}= 2.29°	$\vec{\tau}_1$=.0053 $\hat{K}_1$=-94.34 $\vec{\tau}_2$=.0336 $\hat{K}_2$=-14.88 $\vec{\tau}_3$=.9611 $\hat{K}_3$= 0 δ_{12}= 16.74° δ_{23}= 6.76° N=10 δ_{31}= 2.64°	$\vec{\tau}_1$=.0149 $\hat{K}_1$=-33.56 $\vec{\tau}_2$=.0205 $\hat{K}_2$=-24.39 $\vec{\tau}_3$=.9646 $\hat{K}_3$= 0 δ_{12}= 58.40° δ_{23}= 2.76° N=36 δ_{31}= 2.35°

Table III.A.I (continued)

I N T E R S E C T I O N L I N E A T I O N S			
PROFILE	TOTAL	LONG	SHORT
AA'	$\vec{\tau}_1$=.0236 $\hat{K}_1$=-23.60 $\vec{\tau}_2$=.2290 $\hat{K}_2$= -2.55 $\vec{\tau}_3$=.7473 $\hat{K}_3$= 0 δ_{12}= 7.22° δ_{23}= 13.05° N=28 δ_{31}= 3.63°	$\vec{\tau}_1$=.0120 $\hat{K}_1$=-41.67 $\vec{\tau}_2$=.2570 $\hat{K}_2$= -2.20 $\vec{\tau}_3$=.7310 $\hat{K}_3$= 0 δ_{12}= 7.70° δ_{23}= 23.44° N=11 δ_{31}= 4.37°	$\vec{\tau}_1$=.0300 $\hat{K}_1$=-16.67 $\vec{\tau}_2$=.2307 $\hat{K}_2$= -2.56 $\vec{\tau}_3$=.7417 $\hat{K}_3$= 0 δ_{12}= 12.18° δ_{23}= 17.93° N=15 δ_{31}= 5.95°
BB'	$\vec{\tau}_1$=.0292 $\hat{K}_1$=-17.12 $\vec{\tau}_2$=.2084 $\hat{K}_2$= -2.95 $\vec{\tau}_3$=.7624 $\hat{K}_3$= 0 δ_{12}= 8.08° δ_{23}= 10.08° N=38 δ_{31}= 3.64°	$\vec{\tau}_1$=.0320 $\hat{K}_1$=-15.63 $\vec{\tau}_2$=.2280 $\hat{K}_2$= -2.55 $\vec{\tau}_3$=.7395 $\hat{K}_3$= 0 δ_{12}= 11.09° δ_{23}= 15.55° N=20 δ_{31}= 5.34°	$\vec{\tau}_1$=.0262 $\hat{K}_1$=-19.08 $\vec{\tau}_2$=.2223 $\hat{K}_2$= -2.70 $\vec{\tau}_3$=.7515 $\hat{K}_3$= 0 δ_{12}= 10.44° δ_{23}= 15.66° N=18 δ_{31}= 5.03°
CC'	$\vec{\tau}_1$=.0163 $\hat{K}_1$=-30.74 $\vec{\tau}_2$=.2659 $\hat{K}_2$= -2.18 $\vec{\tau}_3$=.7174 $\hat{K}_3$= 0 δ_{12}= 5.26° δ_{23}= 14.15° N=32 δ_{31} 3.02°	Insufficient data (N=4)	Similar to total cleavage (N=27)
DD'	$\vec{\tau}_1$=.0125 $\hat{K}_1$=-40.00 $\vec{\tau}_2$=.1702 $\hat{K}_2$= -3.50 $\vec{\tau}_3$=.8173 $\hat{K}_3$= 0 δ_{12}= 4.88° δ_{23}= 7.78° N=46 δ_{31}= 2.06°	$\vec{\tau}_1$=.0099 $\hat{K}_1$=-50.51 $\vec{\tau}_2$=.0797 $\hat{K}_2$= -6.96 $\vec{\tau}_3$=.9104 $\hat{K}_3$= 0 δ_{12}= 13.73° δ_{23}= 9.96° N=11 δ_{31}= 3.55°	$\vec{\tau}_1$=.0127 $\hat{K}_1$=-39.37 $\vec{\tau}_2$=.1962 $\hat{K}_2$= -3.03 $\vec{\tau}_3$=.7910 $\hat{K}_3$= 0 δ_{12}= 5.20° δ_{23}= 10.00° N=35 δ_{31}= 2.43°

Table III.A.I (continued)

PROFILE	SEDIMENTARY BEDDING			MAINPHASE CLEAVAGE			INTERSECTION LIN.		
	TOTAL	LONG	SHORT	TOTAL	LONG	SHORT	TOTAL	LONG	SHORT
AA'	G	G	P	P	G	P	G	G	G
BB'	G	P	P	P	-	-	G	-	-
CC'	G	P	P	G	G	P	G	G	G
DD'	G	P	P	G	P	P	G	G	G

Table III.A.II. Types of distributions of (poles to) structural elements for all profiles. G=(partial) girdle: $\vec{r}_1 < \vec{r}_2$; P=point maximum: $\vec{r}_1 \simeq \vec{r}_2$. "Long" and "short" refer to mainphase foldlimbs.

Unimodal distributions of structural data can be usefully typified by their orientation tensor and include point maxima as well as partial- or complete symmetrical girdles. Significance tests compiled by Savage (unpublished data), indicate distributions as shown in Table III.A.II.

As regards to the mainphase folding, a cylindricity test was done for all profiles. The null hypothesis of this test is that coaxiality of foldlimbs has to be rejected with confidence $(1-\alpha)$ if:

$$\frac{\vec{r}_1 - (\vec{r}_{11} + \vec{r}_{12})}{(\vec{r}_{11} + \vec{r}_{12})} \times \frac{(n_1 + n_2 - 4)}{2} > F_{(2,n_1+n_2-4)\alpha}$$ (Langenberg et al., 1977)

In the present case, this formula was used to test the differences in distribution of poles to sedimentary bedding on long and short foldlimbs of mainphase folds with respect to the whole fold. In all investigated profiles this leads to the rejection of coaxiality, i.e. folds are non-cylindrical (Table III.A.III).

Comparison of eigenvector directions (and their ellipses of confidence) for each structural element in each profile reveals the following relationships (numbers refer to examples in Fig. III.A.1):

1. Sedimentary bedding (S_0). Except for profile AA', confidence ellipses of the eigenvectors $\vec{r}_1$ for the short and long limbs of the mainphase folds overlap one another. This suggests that they have been folded around the same foldaxis (i.e. they are co-axial). A cylindricity test (Table III.A.III), however, rejects cylindricity for all profiles, so that computed $\vec{r}_1$ directions must represent apparent foldaxes. This might indicate that

Profile	$\frac{\vec{\tau}_1 - (\vec{\tau}_{11}+\vec{\tau}_{12})}{\vec{\tau}_{11}+\vec{\tau}_{12}} \times \frac{n_1+n_2-4}{2}$	$F_{0.95}$	cylindricity (co-axiality)
AA'	11.44	$F_{2,22} = 3.44$	rejected
BB'	16.41	$F_{2,45} = 3.22$	rejected
CC'	3.66	$F_{2,27} = 3.36$	rejected
DD'	8.82	$F_{2,48} = 3.21$	rejected

Table III.A.III. Results of cylindricity tests for profiles AA' - DD'. The test compares orientations of (poles to) sedimentary bedding in mainphase folds, using $\vec{\tau}_1$ = eigenvector for the total distribution, and $\vec{\tau}_{11}$ & $\vec{\tau}_{12}$ = eigenvectors for long and short foldlimbs respectively. For formulation of the null hypothesis see text.

sedimentary bedding has been folded during at least two non-coaxial deformational events.

It is demonstrated in the main text of this article that two pre-mainphase deformation generations can be distinguished in the investigated area, which are both characterised by very open folds. The tight mainphase folding caused strong redistribution of the bedding, so that the calculated $\vec{\tau}_1$ directions are more or less similar but not identical to the direction of the local mainphase foldaxis). The cylindricity test proves, indeed, that some kind of inhomogeneity must have been present that could have resulted from earlier deformation.

2. Bedding/cleavage (S_0/S_1). The centres of point maxima of poles to cleavage distributions ($\vec{\tau}_3^{S_1}$) always fall on the $\vec{\tau}_2^{SS} - \vec{\tau}_3^{SS}$ great circle of poles to sedimentary bedding. With the exception of profile BB', $\vec{\tau}_3^{S_1}$ is symmetrical with respect to $\vec{\tau}_3^{SS_{long}}$ and $\vec{\tau}_3^{SS_{short}}$, so S_1 is axial plane cleavage.

3. Cleavage (S_1). Usually the orientations of cleavages do not differ between the fold limbs. In profile CC', however, the cleavage shows significant (convergent) fanning in the fold profile, to be seen in the divergence of the $\vec{\tau}_2$ ellipses of confidence. In profiles AA' and EE' there is a slight difference in strike of S_1 between the limbs (the reason of

which is not understood), again shown by differences in $\vec{r}_2$ ellipses of confidence.

4. Cleavage/intersection lineations (S_1/L_1). In all cases the $\vec{r}_3$ confidence ellipse of S_1 overlaps with the $\vec{r}_1$ confidence ellipse of L_1, i.e. intersection lineations lie within the cleavage planes, as they should.

5. Intersection lineations and small-scale foldaxes (L_1 and B_1). Ellipses of confidence for long and short limbs overlap, indicating that there is no significant difference in orientation between them.

The spreading along great circles of L_1 and B_1 directions is much larger than to be expected in view of the (sometimes approximate) point maximum distributions of poles to cleavage, under the assumption that sedimentary bedding was co-planar before mainphase folding occurred. As only data from areas devoid of post-mainphase folding have been collected (as proven by the poles to cleavage distributions), this may be taken to indicate that pre-mainphase folding of the sedimentary bedding has taken place.

In conclusion, the analysis of directional data shows that mainphase folds in the northern part of the Orri dome are non-cylindrical folds, cut by an axial plane cleavage, while foldlimbs often show pseudo co-axiality. This observation, combined with the anomalously large spreading in the great circle distribution of lineations, indicates that sedimentary bedding had probably already been folded before mainphase deformation took place.

CHAPTER IV

THE STRUCTURAL DEVELOPMENT OF THE ORRI-DOME, SOUTHERN VARISCAN PYRENEES, SPAIN

(Submitted to Eclogae Geologicae Helvetiae)

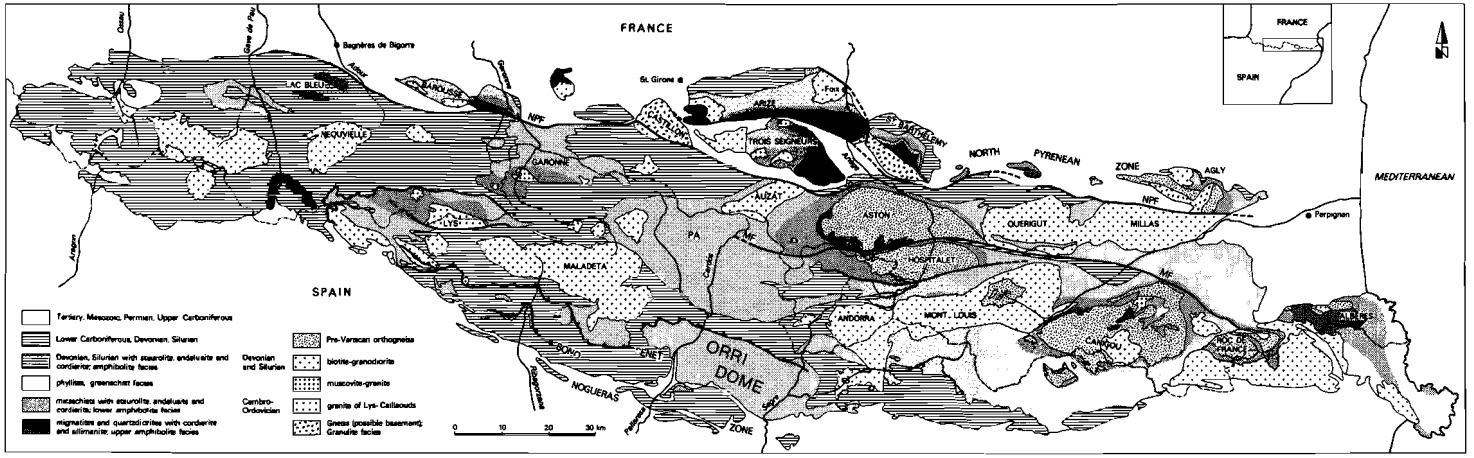
FRANCE
SPAIN
MEDITERRANEAN
NORTH PYRENEAN ZONE
Bagnères de Bigorre
St. Girons
Perpignan
LAC BLEU
MENDIBELLE
BARROUSSE
ARIZE
TROIS SEIGNEURS
ST BARTHELEMY
AUZAT
ASTON
QUERIGUT
MILLAS
AGLY
MALADETA
PA
MF
PORTALET
ANDORRA
MONT LOUIS
CANIGOU
ROC DE FRANCE
NOGUERAS
ORRI DOME
ZONE
NPF
Tertiary, Mesozoic, Permian, Upper Carboniferous
Lower Carboniferous, Devonian, Silurian
Devonian, Silurian with staurolite, andalusite and cordierite amphibolite facies
phyllites, greenschist facies
micaschists with staurolite, andalusite and cordierite; lower amphibolites facies
migmatites and quartzdiorites with cordierite and sillimanite; upper amphibolite facies
Devonian and Silurian
Cambro-Ordovician
Pre-Varscan orthogneiss
biotite-granodiorite
muscovite-granite
granite of Lys- Caillaouds
Gneiss (possible basement); Granulite facies
0 10 20 30 km

INTRODUCTION

Within the Alpine mountain belt of the Pyrenees a large mass of Variscan rocks is exposed, which is commonly referred to as the Axial Zone (Fig. IV.1). The Axial Zone consists of deformed sedimentary, metamorphic and intrusive rocks of pre-Stephanian age (Zwart, 1979), intruded by undeformed late Variscan batholiths, and unconformably overlain by post-Westphalian rocks. The large-scale Variscan structure of the Axial Zone comprises a number of east-west trending anticlines and synclines, like the Orri "dome" (Schmidt, 1931; Hartevelt, 1970) in the south-central part of the Variscan outcrop. This complicated structure can be traced some 45 km along strike (Figs. IV.1 and IV.2), and has an exposed width of about 12 km. Its true width is not known, as the southern flank of the Orri dome is unconformably covered by Stephanian, Permian and Lower Triassic rocks. Towards the north, the Orri dome is bordered by the narrow Llavorsi syncline (Fig. IV.2).

The Orri dome is almost entirely built of very thick, unfossiliferous, non-metamorphic to very low-grade Cambro-Ordovician sediments of the Seo Formation (Hartevelt, 1970), probably deposited in a shallow marine environment. They are characterised by a monotonous alternation of thin slates, silts and sand layers (up to a few cm thickness), although locally shales and silts may be much thicker. In some cases, individual sandstone and quartzite layers reach thicknesses of some meters to some tens of meters. Marker horizons are completely lacking within the Cambro-Ordovician rocks. The distribution of lithotypes in the Seo Formation seems to be determined by variations in sedimentary facies, rather than by structural organisation (Fig. IV.2).

Fig. IV.1. Map of the Variscan Pyrenees, after Zwart (1979). The Orri dome is situated in the south-central part of the Axial Zone.

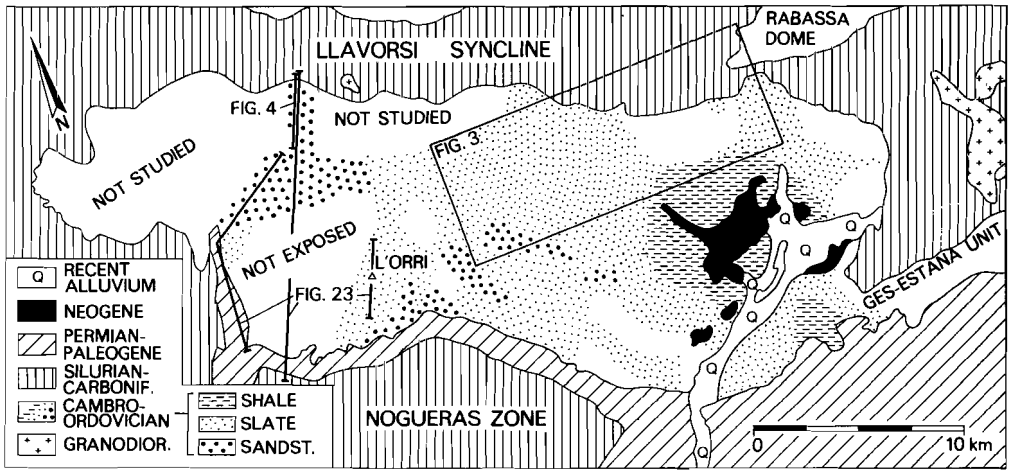

Fig. IV.2. Simplified geological map of the Orri dome and surroundings. The following lithologies are indicated in the Seo Formation: "sandstone" (and quartzite, Fig. IV.5b), "slate" (usually a regular monotonous interlayering of clay and sand on cm scale, Fig. IV.5a), and "shales" (silt- and clay size, often a "pencil-shale"due to strong cleavage development). The profile lines of Figs. IV.4 and IV.23 and the map area of Fig. IV.3 are shown. Upper Ordovician rocks crop out in the northeastern part of the dome and in the Ges-Estana unit (Hartevelt, 1969).
Note: this is not a palinspastically restored map as it shows ultimate lithology distribution after deformation.

On the northern flank of the Orri structure, at the transition to the Llavorsi syncline, some higher stratigraphic units crop out (from bottom to top, data mainly after Hartevelt, 1970):

The Rabassa Conglomerate Formation of Caradoc age, which in spite of its very coarse-grained nature overlies the Cambro-Ordovician conformably; the Cava Formation, mainly built of sandstones, which may be up to 850 m thick east of the Orri dome but gradually wedges out along its northwestern border; the Estana Formation is a marl and limestone unit; the Ansobell Formation, developed over the whole Pyrenees, consists of black shales which replace the sandstones of the Cava Formation towards the north; the Bar Quartzite is a thin sandsheet, which only occurs in the south-central part of the Axial Zone; and finally the black carbonaceous shales of the

Silurian. In the synclinal units of the Axial Zone, the Silurian is conformably overlain by predominantly calcareous and marly rocks of Devonian and Early Carboniferous age.

The conformable superposition of sediments from Cambro-Ordovician to Carboniferous age, without any significant hiatus, excludes the occurrence of major Caledonian deformation in the Pyrenees. The main phase of Variscan deformation took place in the Westphalian (Zwart, 1979). In the post-orogenic stage, Stephanian slope breccias, tuffs, andesitic basalts and alluvial sediments were deposited in fault-bounded sedimentary basins (Aguiro, Erill Castell and Malpas Formations of Mey et al., 1968). During the Permian, elongated strike-slip basins developed locally, which were rapidly filled with often coarse-grained redbeds (Nagtegaal, 1969; Speksnijder, 1985; chapter II). The importance of post-Variscan strike-slip movements to the Orri dome will be one of the main subjects of this article.

Finally, after a period of erosion, a Lower Triassic conglomerate (part of the Buntsandstein) was laid down unconformably on one of the previously mentioned post-Variscan formations, or directly on the Variscan basement, as is the case along part of the southern boundary of the Orri dome. The Buntsandstein and its younger cover suffered from subsequent Alpine deformation, which left its mark in the essentially Variscan Orri dome as well. The marls of the Keuper, which overlie the Buntsandstein, acted as a decollement horizon for an extensive thrust system of Alpine (Eocene) age, which includes Variscan rocks in the so-called Nogueras Zone (Séguret, 1970), directly south of the Orri dome (Figs. IV.1 and IV.2).

East and south of the dome, rocks of Tertiary (up to Miocene) age are offset by faults on different scales, indicating post-Alpine brittle deformation which influenced the Orri dome as well.

Structural interpretation in the Orri dome is seriously hampered by the lack of marker horizons in the Cambro-Ordovician rocks of the Seo Formation. Hence, emphasis had to be laid on the analysis of directional data of the various structural elements; in total over 20,000 measurements were collected on the orientations of planar surfaces and lineations.

In the following chapters the characteristics of successive deformation generations in the Orri dome will be discussed in detail. Distinction is made, in chronological order, between deformation of Variscan, post-Variscan, Alpine and post-Alpine age.

VARISCAN DEFORMATION

Pre-mainphase deformation (D_{V1} & D_{V2})

The most important Variscan deformational event in the Pyrenees, the mainphase folding, has for a long time been considered the oldest in the Variscan orogenic evolution. The occurrence of still older folds which are transected by the mainphase cleavage, was nevertheless recognised by various authors in the sixties (e.g. Boschma, 1963; Mey, 1967b, 1968). Pre-mainphase folds, also called pre-cleavage folds, can in many cases easily be detected if marker horizons are available to show interference patterns between mainphase folds and earlier structures. Such a technique, however, can not be applied to the monotonous slates and sandstones of the Orri dome. For this reason, a directional analysis of mainphase structural elements was carried out by Speksnijder (1986a; chapter III), who shows that two generations of pre-mainphase folding must have occurred in the northern part of the dome (Fig. IV.3).

In both cases the folds appear to be very open (interlimb angles at least 115°) and to have subvertical axial planes and subhorizontal foldaxes. There is, however, an important difference in strike direction of the axial planes: approximately north-south for the oldest generation of pre-mainphase folds, and approximately east-west for the younger. The folds of both systems appear to be symmetrical in profile.

The structural significance of the occurrence of pre-mainphase folds in the Pyrenean Variscan evolution is discussed by Speksnijder (1986a; chapter III). They have been generated at the transition from a divergent to a

Fig. IV.3. Pre-mainphase structures in the northern part of the Orri dome; location shown in Fig. IV.2. This schematic structural map shows N-S trending (D_{V1}) and E-W trending (D_{V2}) pre-mainphase foldaxes. The locations of foldaxes within the Seo Formation are defined by sudden changes in orientation of intersection lineations of sedimentary bedding and mainphase cleavage. The four sections indicated on this map are shown in Speksnijder (1986a; Fig. III.4); for related stereographic projections see Fig. IV.6.

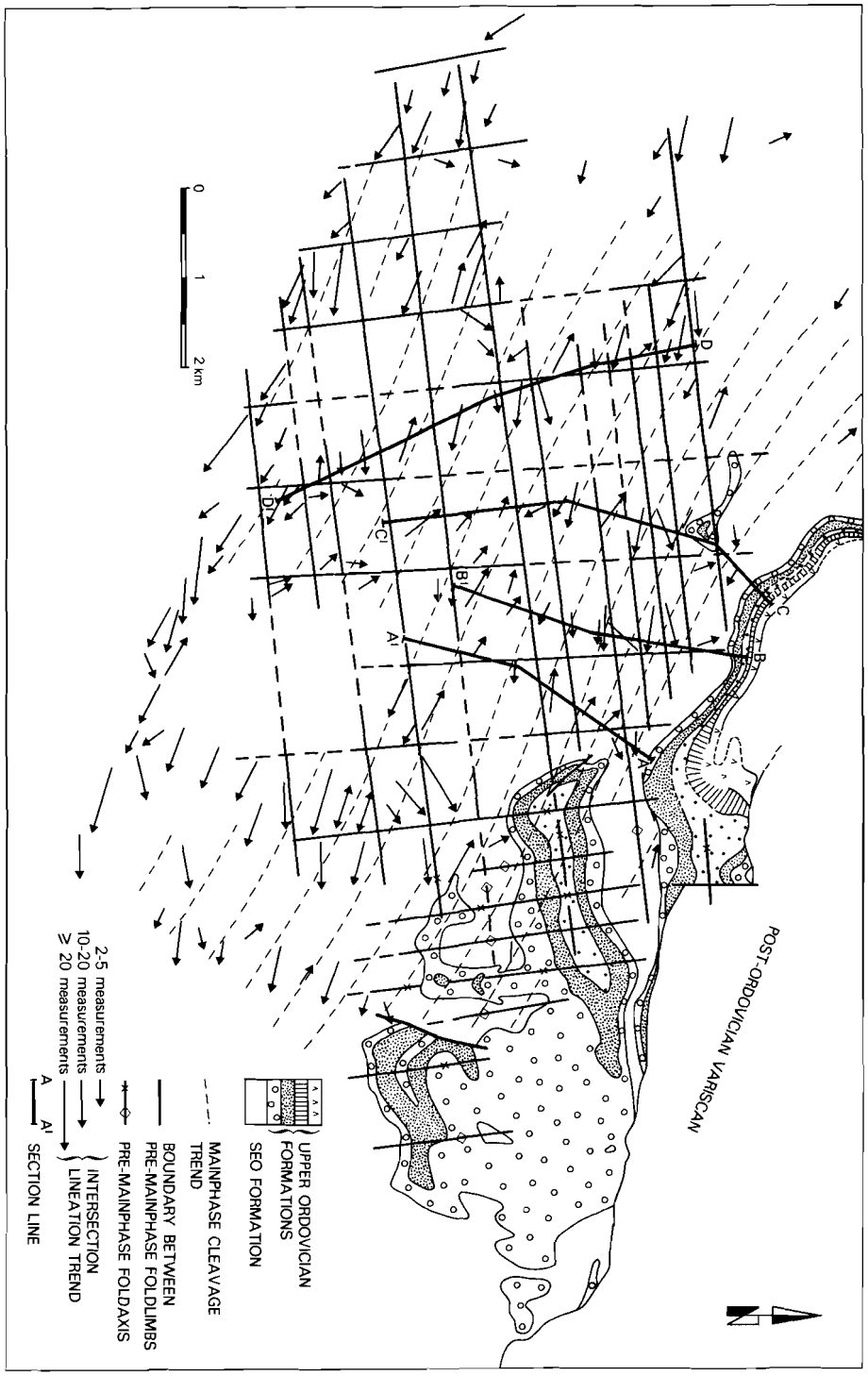
0
1
2 km
POST-ORDOVICIAN VARISCAN
UPPER ORDOVICIAN FORMATIONS
SEO FORMATION
MAINPHASE CLEAVAGE TREND
BOUNDARY BETWEEN PRE-MAINPHASE FOLDLIMBS
PRE-MAINPHASE FOLDAXIS
2-5 measurements
10-20 measurements
≥ 20 measurements
INTERSECTION LINEATION TREND
A A'
SECTION LINE

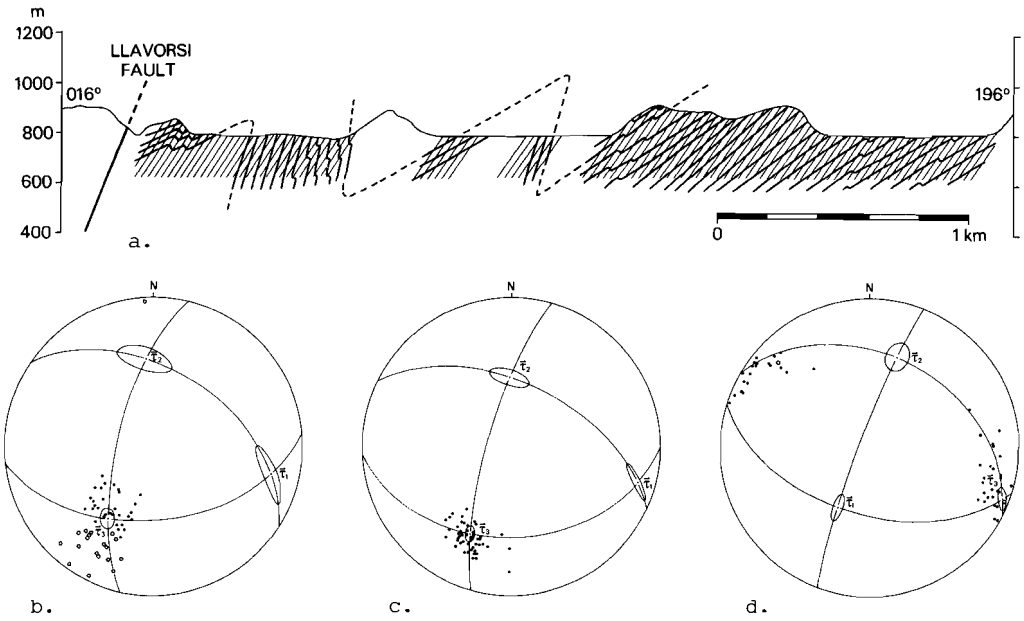

Fig. IV.4. Representative structural profile and associated stereographic projections of mainphase folds.
(a) North-south structural profile along the Rio Noguera Pallaresa showing the orientations of mainphase cleavage (thin lines) and sedimentary bedding (thick lines) within Cambro-Ordovician rocks. Devonian sediments crop out north of the Llavorsi fault. The position of this profile is indicated on Figs. IV.2 & IV.7. (b) Equal area projection of poles to sedimentary bedding. Discrimination is made between data from long foldlimbs (dots) and short limbs (open circles). $\vec{\tau}_1$ - $\vec{\tau}_3$ represent eigenvector directions of the total distribution; confidence ellipses are drawn around these eigenvectors (see Speksnijder, 1986a; chapter III). Number of measurements: N=50. (c) Poles to mainphase cleavage. Note the strong coplanarity of the cleavage planes as indicated by the small size of the $\vec{\tau}_3$ confidence ellipse. Number of measurements: N=52. (d) Intersection lineations of sedimentary bedding and mainphase cleavage (dots), and small-scale mainphase foldaxes (open circles). Number of measurements: N=48.

convergent oblique-slip setting of the Variscan mountain chain (D_{V1}), and to an early stage of deformation resulting from collision (D_{V2}).

Mainphase deformation (D_{V3})

Mainphase structures can be traced all over the Variscan Pyrenees (which does not necessarily imply they are everywhere of the same age), and

mainphase cleavage is the major foliation in the Axial Zone. Mainphase folds in the Orri dome can be studied best in its northern part, where the effects of later Variscan and Alpine overprinting are negligible. It turns out that mainphase deformation (F_1 of Zwart, 1979; F_2 of Hartevelt, 1970) is characterised by north-vergent asymmetrical folds, developed on any scale between some mm and one or more kilometers (Figs. IV.4 and IV.5a). Generally, long foldlimbs exhibit shallow dips towards the north (Figs. IV.4a,b; IV.5b; IV.6a), whereas short limbs are usually overturned, thus dipping (steeply) north as well (Fig. IV.4a,b; IV.5c; IV.6a). Very often a penetrative axial plane cleavage is associated with mainphase folds (Figs. IV.4a,c; IV.5b,c; IV.6b), which may show convergent fanning in the foldprofile. Generally the cleavage is a slaty cleavage in fine-grained sediments (Fig. IV.5c), or a spaced cleavage in sandstones (Fig. IV.5b). In some cases a crenulation cleavage does occur, folding sedimentary lamination on a micro-scale. In areas of large strain, e.g. in foldhinges, differentiated layering has sometimes developed parallel to the mainphase foliation. Intersection lineations between sedimentary bedding and mainphase cleavage are well developed throughout the Orri dome (Figs. IV.4d; IV.6c), although on some long flanks of mainphase folds, especially in sandstones, cleavages (and, for that matter, intersection lineations) may be absent.

Mainphase structures are non-cylindrical and show unusual large spreading of intersection lineation directions in the cleavage plane (Fig. IV.6c), which is attributed to the occurrence of pre-mainphase folds (Speksnijder, 1986a; chapter III). Large-scale mainphase foldaxes are subhorizontal and are directed WNW-ESE.

In the northwestern part of the Orri dome, the orientation of the mainphase cleavage is very constant (Figs. IV.4 and IV.7), which indicates that the cleavage has not been affected by major later deformation. In the rest of the dome, however, strong reorientation of the mainphase cleavage has taken place. In the western and southwestern part, the mainphase cleavage dip-angle gradually decreases towards the south, until it eventually occupies a subhorizontal position. The cleavage then abruptly changes dip direction and may dip as much as 30° to 35° towards the south along the southwestern rim of the Orri structure (Fig. IV.7). This change in orientation is not an original feature of the mainphase cleavage development: it will be shown later that Alpine thrusting may be held

a.

b.

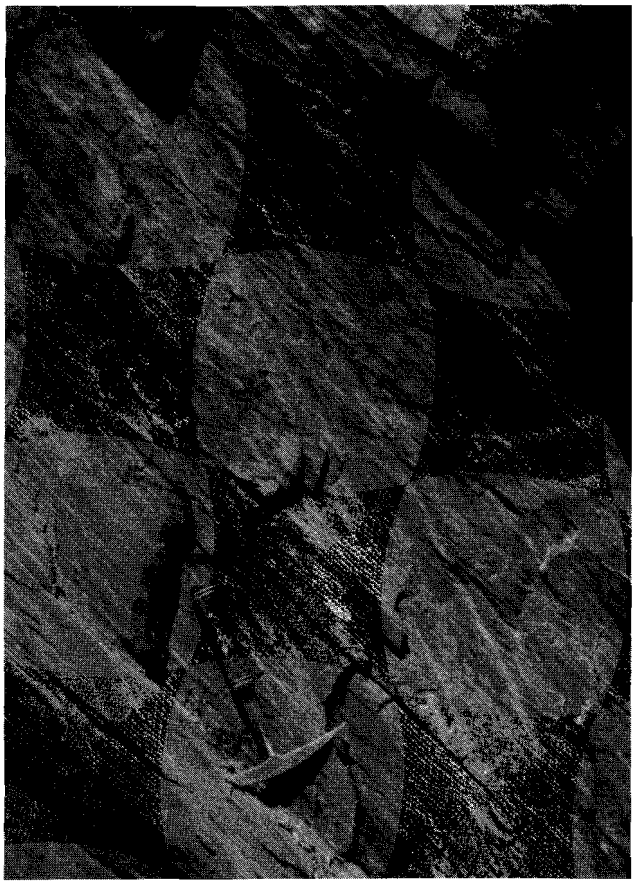

c.

Fig. IV.5. Photographs of D_{V3} structures. For locations see Fig. IV.7. (a) Small-scale mainphase fold in the southwestern part of the Orri dome. Penetrative axial plane cleavage has not developed in this case. The axial plane of the fold is only gently dipping north (towards the right). (b) Spaced mainphase cleavage in flatlying sandstones on the long limb of a macroscopic mainphase fold. Located in the central-northern part of the dome, where no significant overprinting of mainphase structures does occur. North towards the left. (c) Steep overturned bedding (parallel to the hammer shaft), and relatively steeply north dipping slaty cleavage, developed in very fine-grained sediments in the northern part of the dome. North towards the right.

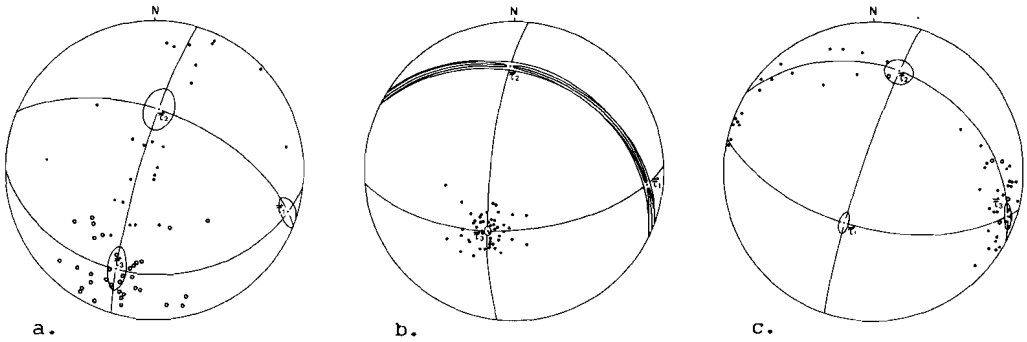

Fig. IV.6. Equal area stereographic projections of structural elements in profile C - C' of Fig. IV.3. In all three cases the eigenvector directions and their confidence ellipses for the orientation tensors of the distributions are indicated (from Speksnijder, 1986a; chapter III). (a) Poles to sedimentary bedding. Dots indicate normal polarity of the beds, open circles represent reverse polarity (on overturned short foldlimbs). Number of measurements: N=57. (b) Poles to mainphase cleavage. N=51. (c) Intersection lineations of sedimentary bedding and mainphase cleavage (dots), and small-scale mainphase foldaxes (open circles). N=54.

responsible for the larger part of the rotation of Variscan structures and cleavages in the vertical plane.

In the central, southern and eastern parts of the Orri structure, the cleavage has been gently to strongly folded during later Variscan deformation, as will be discussed in the following sections.

Fig. IV.7. Cleavage trend map of the Orri dome; the outline of the structure is defined by the outcrop area of the Seo Formation. This map is based on almost 3,000 cleavage measurements. Shown are traces of mainphase cleavage (full drawn lines), traces of D_{V4} cleavage (stippled, E-W trending), and traces of D_{V5} cleavage (stippled, N-S trending). Heavy lines indicate the positions of postulated faults: an Alpine thrust in the north and post-Alpine faults in the south (for discussion see text). Numbers in the western part of the dome refer to mainphase cleavage dips. Boxes outline areas covered by other figures; dots show positions of photographs.

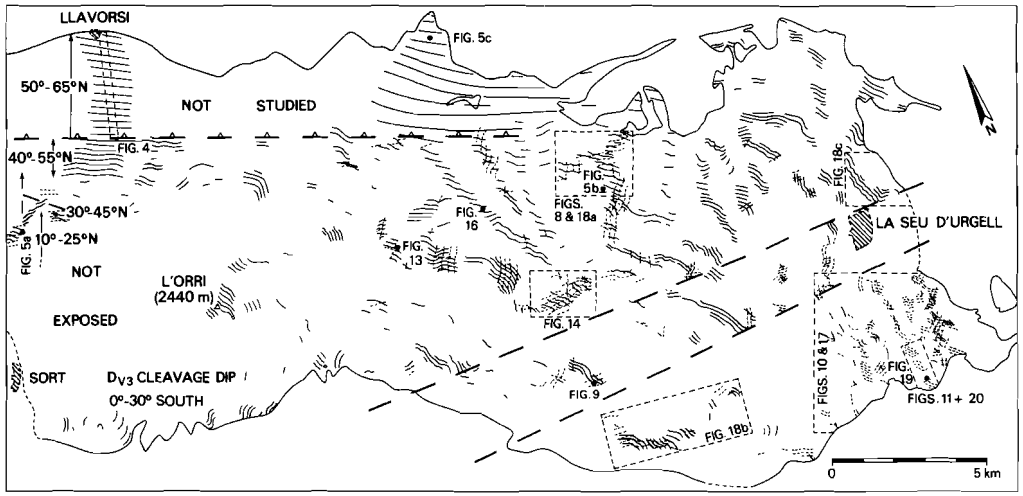
LLAVORSI
FIG. 5c
50°-65°N
NOT STUDIED
40°-55°N
FIG. 4
30°-45°N
10°-25°N
FIG. 5a
NOT EXPOSED
L'ORRI (2440 m)
FIG. 5b
FIGS. 8 & 18a
FIG. 16
FIG. 13
FIG. 14
FIG. 18c
LA SEU D'URGELL
FIGS. 10 & 17
FIG. 19
FIGS. 11 + 20
FIG. 9
FIG. 18b
SORT
D_{V3} CLEAVAGE DIP 0°-30° SOUTH
N
0
5 km

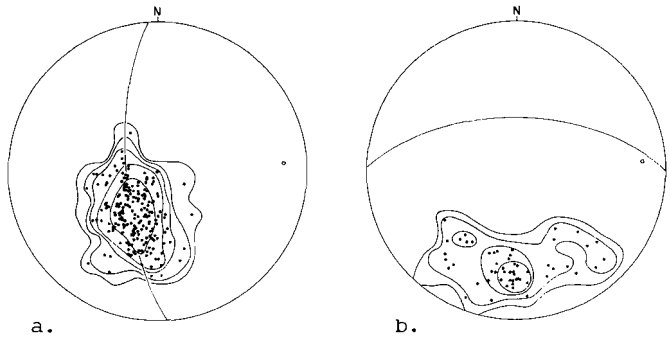

Fig. IV.8. The impact of D_{V4} deformation on the orientations of older structures in the central Orri dome. For location see Fig. IV.7. (a) Poles to D_{V3} cleavage; equal area projection. The open circle indicates the (apparent) foldaxis, see Fig. IV.18. Number of measurements: N=195. Contours: 1, 2, 5, 10, and 25 poles per 1% area (0.5, 1.0, 2.6, 5.1, and 12.8% per 1% area). (b) Poles to D_{V4} cleavage. This projection shows that this cleavage has been folded (by D_{V5} and D_{PV1} deformation), but no major reorientation has occurred in this case. The great circle shows the averaged D_{V4} orientation; the foldaxis of Fig. IV.8a lies approximately within the cleavage plane. Number of measurements: N=57. Contours represent 1, 2, 5, and 10 poles per 1% area (1.7, 3.5, 8.1, and 17.5% per 1% area).

First Variscan refolding (D_{V4})

In the central part of the Orri dome, mainphase structures are often overprinted by tight macroscopic folds (dm to m scale), that do not seem to affect the enveloping surface of the earlier folds significantly. The folds of the first Variscan refolding generation in this area (corresponding to the F_4 phase of Hartevelt, 1970 and Zwart, 1979) have subvertical axial planes and gently plunging foldaxes (Fig. IV.8). Axial planes strike approximately E-W and the D_{V4} folds are asymmetrical showing a Z-shape when looking east (Fig. IV.9). They are cut by a well-developed axial-plane cleavage.

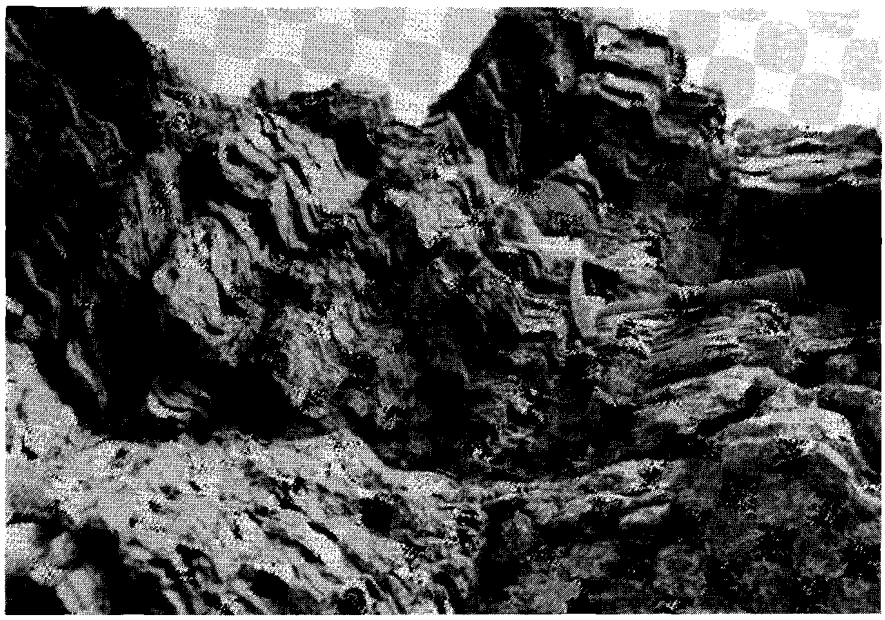

Fig. IV.9. D_{V4} folds in the southern part of the Orri dome (Fig. IV.7). The hammer rests on - and its shaft is parallel to - a long D_{V4} fold limb. The overall asymmetry of the folds is Z-shaped. View towards the east.

Inspection of the cleavage-trend map of the Orri dome (Fig. IV.7) and stereographic projections (Fig. IV.8) shows that the influence of D_{V4} folding on mainphase structures is much more widespread and occurs on a larger scale than outcrop study does suggest. In plan view, the mainphase cleavage can be traced across km scale, seemingly very open folds showing a Z-shape asymmetry. This very open aspect of the folds in the horizontal plane is caused by the gentle overall plunge of the D_{V4} structures towards the east. In profile they appear to be rather tight. The folds are often, but not always, cut by a steep (usually north dipping) D_{V4} axial plane cleavage. The northern boundary of the extent of D_{V4} deformation

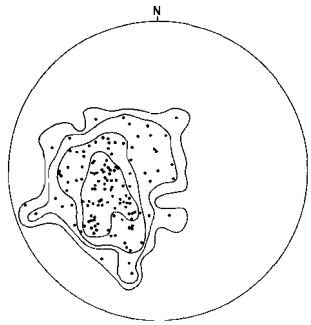

Fig. IV.10. Stereographic projection of poles to D_{V3} cleavage in the south-eastern Orri dome (Fig. IV.7), showing the accumulated effects of post-mainphase deformation. The spreading in N-S direction must be mainly attributed to D_{V4} folding. The orientation of D_{V4} cleavages in the same area is shown in Fig. IV.17. Number of measurements: N=129; contours represent 1, 2, 5, and 10 poles per 1% area (0.8, 1.6, 3.9, and 7.8% per 1% area).

approximates a straight line, running E-W (i.e. parallel to the D_{V4} strike) along the northern border of the central part of the Orri dome (Fig. IV.7).

Quite a different situation occurs in the southeastern part of the dome (Fig. IV.7). Here mainphase axial planes dip towards the east instead of towards NNE like in the central area, so that the E-W strike of the D_{V4}

Fig. IV.11. Very tight D_{V4} folds in the southeastern part of the Orri structure. For location see Fig. IV.7.
(a) Form surface map of sedimentary bedding (thick lines) and D_{V4} cleavage in a river valley outcrop. The D_{V4} structures have been deformed by later D_{V5} and D_{PV1} deformation. Arrows indicate the facing direction of the beds. The Variscan folds are unconformably covered by Upper Carboniferous rocks in the southern part of the map. (b) Downward view on a sub-horizontal weathered surface in the river bed; east is towards the left. The D_{V4} cleavage planes and foldaxes are very steep.

a.

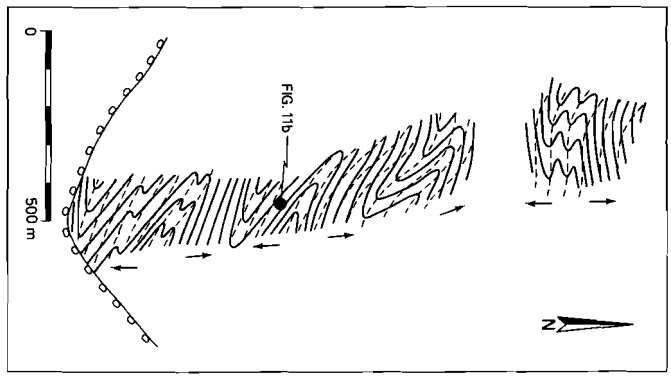

b.

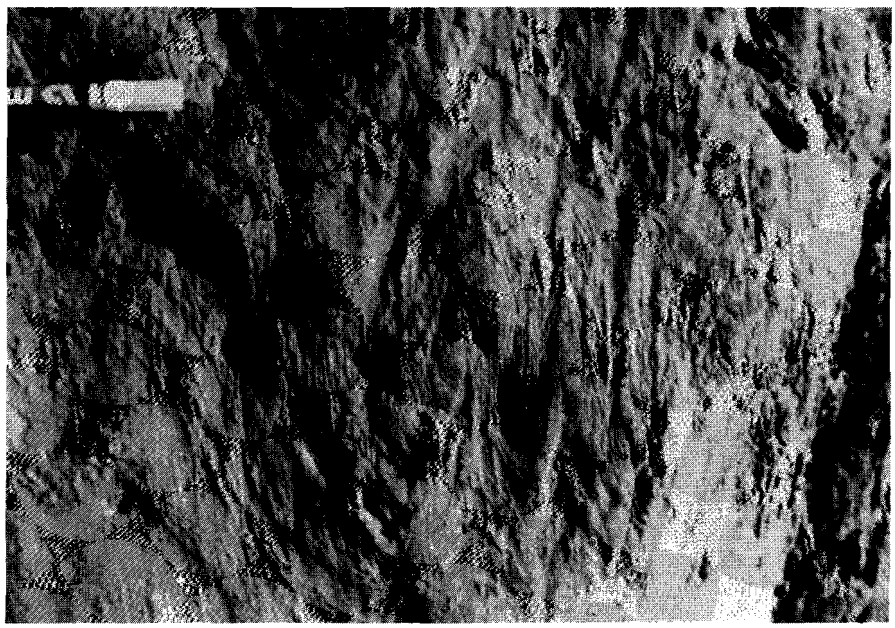

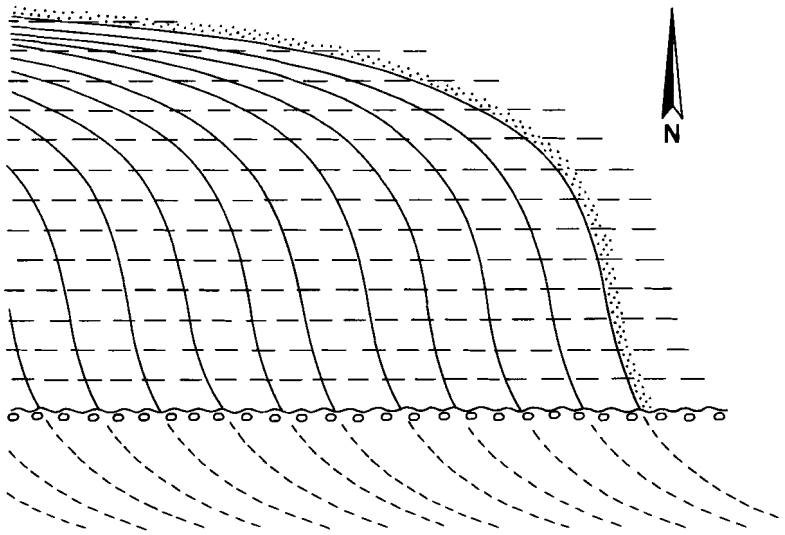

Fig. IV.12. Schematic map of the eastern part of the Orri dome showing folded D_{V3} cleavage, east-west striking D_{V4} cleavage, and the Variscan unconformity. The orientation of the D_{V3} cleavage changes from north dipping in the north to east dipping in the east (and probably north again below the unconformity). Compare with Fig. IV.7.

axial planes is at large angles to sedimentary bedding and mainphase cleavage. As a result, the axes of the D_{V4} folds plunge relatively steeply to the east (Fig. IV.10). The strain related to D_{V4} folding has locally been relatively large, as witnessed by the occurrence of very tight to isoclinal folds. The nature of these folds can easily be demonstrated by the frequently changing polarity of sedimentary bedding, see Fig. IV.11.

The configuration of deformed mainphase cleavage traces (Fig. IV.7) and the distribution of structural elements in stereographic projection (Figs. IV.8 and IV.10), suggest that the mainphase and older folds in the presently exposed part of the Orri dome have been refolded into one large asymmetrical

Fig. IV.13. Asymmetrical D_{V5} folds east of the Orri mountain (Fig. IV.7). This exposure shows the unique occurrence of D_{V5} folds on an overturned mainphase foldlimb; for this reason their asymmetry differs from what is normally encountered. View towards the north. Note that intersection lineations of sedimentary bedding and mainphase cleavage can be traced across the folds.

structure. The northern part of the dome represents, together with the southern limb of the Llavorsi syncline, the relatively undeformed long D_{V4} flank, whereas the central, southern and eastern parts are occupied by a composite D_{V4} short limb and fold-hinge area. In analogy with smaller-scale folds, the gentle eastward axial plunge of the large D_{V4} structure gives the impression that the foldsystem is much more open than it is in reality. The postulated southern long limb of the refolding structure is presently covered by post-Variscan rocks, which determines the minimum width of the fold-hinge area to be in the order of 12 km (Fig. IV.12).

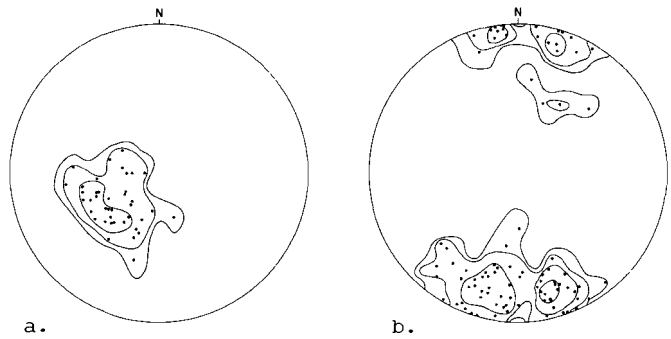

Fig. IV.14. Reorientation of cleavages as a result of D_{V5} deformation in the central part of the Orri dome (for location see Fig. IV.7). (a) Equal area projection of poles to D_{V3} cleavage. Shows the effects of reorientation by D_{V4}, D_{V5} and possibly D_{PV1} deformation. Number of measurements: N=40; contours represent 1, 2, and 5 poles per 1% area (2.5, 5.0, and 12.5% per 1% area). (b) Poles to D_{V4} cleavage. The D_{V5} foldaxis is subvertical in this case. Number of measurements: N=90; contours represent 1, 2, 5, and 10 poles per 1% area (1.1, 2.2, 5.6, and 11.1% per 1% area).

Second Variscan refolding (D_{V5})

Except for the long D_{V4} foldlimb along its northern edge, most parts of the Orri dome experienced a second Variscan refolding. D_{V5} folds do not occur very frequently in outcrop, where they usually exhibit small amplitudes and wavelenghts (cm-m scale). Cleavage development is restricted to small-scale folds. Generally, the structures show a marked S-shaped asymmetry when looking north along the subvertical, N-S striking axial planes (Fig. IV.13). In some areas of the Orri dome, D_{V5} deformation has affected older structural elements (e.g. D_{V3} and D_{V4} cleavages, Fig. IV.14) on a larger scale. In such cases the D_{V5} cleavage is usually poorly developed.

The existence of still larger D_{V5} folds (up to km scale) can only be detected from deviations in trends of older cleavages (Fig. IV.7). In the southern half of the dome, large D_{V5} folds seem to occur rather frequently, but no foliation has developed, and folds are less tight than further north.

In many cases, D_{V5} folds are chevron-shaped, in particular the D_{V5} structures observed on outcrop scale. In addition, the folds may be very asymmetrical, giving them a kinkband-like appearance. For this reason, it is often impossible to distinguish in the field between kink-like D_{V5} folds and true kinkbands (see next section).

Kinkbands of probable Variscan age (D_{V6})

Kinkbands are not unfrequent in the central part of the dome, where they are developed uniquely on (very) flat-lying long flanks of macroscopic mainphase folds. Their occurrence seems to be further restricted to finely laminated rocks in areas where no significant Variscan refolding has taken place and mainphase cleavage is poorly developed. Obviously, the distribution of the kinkbands has not only been governed by the direction and magnitude of the stress field in which they formed, but also by the presence of a strong anisotropy in the rock and its orientation with respect to the principal stresses.

The kinkbands are usually steep and most frequently strike NE-SW, or otherwise NW-SE (Fig. IV.15). The NE-SW kinks can be subdivided into two groups on the basis of their asymmetry: firstly a large group showing S-shaped asymmetry when looking NE (Fig. IV.15a), and, secondly, a group of kinks showing Z-asymmetry looking NE (Fig. IV.15b). As the kinkbands from these two groups predominantly dip towards SE and NW respectively, there is an obvious relationship between kink orientation and kink asymmetry, induced by the flattish attitude of the anisotropy (=bedding) plane. A similar, but less pronounced tendency can be observed regarding the dip angle of NW-SE striking kinkbands. Figs. IV.15c & d demonstrate that most of the SW dipping kinks have Z-asymmetry, whereas the larger part of the NE dipping kinks have S-asymmetry when looking north.

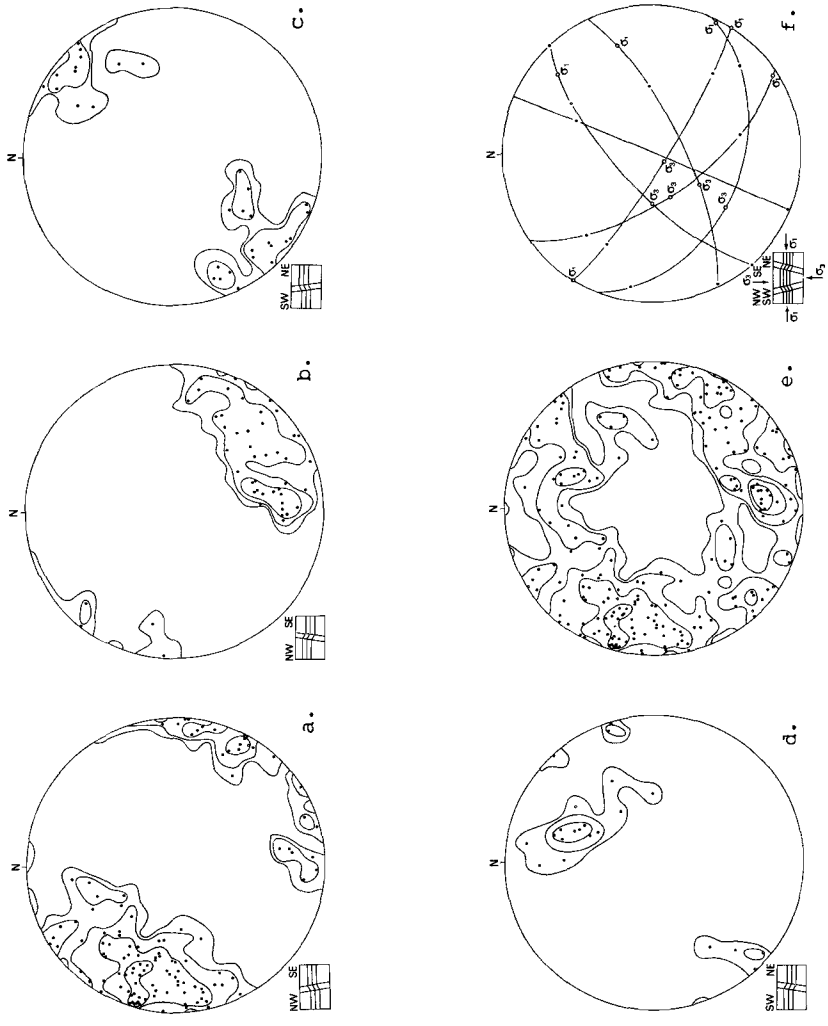
a.
b.
c.
d.
e.
f.
N
NW
SE
SW
NE
σ1
σ2
σ3

The (very limited) occurrence of conjugate pairs of kinkbands (Fig. IV.16) further substantiates our ideas on the relation between dip direction and asymmetry of the kinkbands. From the orientation of the conjugate kinks, the direction of the largest principal stress σ_1 can be easily reconstructed (Ramsay, 1962b; Powell et al., 1985; Fig. IV.15f), indicating NW-SE and NE-SW subhorizontal compression (orthogonal to the strikes of the kinkbands). It is evident that σ_1 (and also σ_2) is at a low angle with the anisotropy plane (Fig. IV.15f). This appears to be a pre-requisite for kinkband development (Donath, 1969; Weiss, 1969).

The relationship between the kinkbands described above and other structures in the Orri dome needs some further discussion.

Fig. IV.15. Equal area stereographic projections related to D_{V6} kinkbands in the central Orri dome. In the schematic profiles a horizontal anisotropy (bedding) plane has been chosen for convenience.
(a) Poles to NE-SW striking kinkband boundaries showing S-shaped asymmetry when looking NE. N=112; contours represent 1, 2, 5, and 10 poles per 1% area (0.9, 1.8, 4.5, and 8.9% per 1% area.). (b) Poles to NE-SW striking kinkband boundaries showing Z-shaped asymmetry when looking NE. N=45; contours represent 1, 2, and 5 poles per 1% area (2.3, 4.4, and 11.1% per 1% area). (c) Poles to NW-SE striking kinkband boundaries showing S-shaped asymmetry when looking NW. N=32; contours represent 1 and 2 poles per 1% area (3.1 and 6.3% per 1% area). (d) Poles to NW-SE striking kinkband boundaries showing Z-shaped asymmetry when looking NW. N=21; contours represent 1, 2, and 5 poles per 1% area (4.8, 9.5, and 23.8% per 1% area). (e) Poles to all observed D_{V6} kinkband boundaries in the central part of the Orri dome. Note that part of the steep, east dipping planes may be D_{V5} chevron-type folds, as explained in the text. This diagram contains the combined data of Figs. IV.15a-d. Number of measurements: N=210; contours represent 1, 2, 5, and 10 poles per 1% area (0.5, 1.0, 2.4, and 4.8% per 1% area). (f) Conjugate kinkband sets in the central Orri dome. Plotted are poles to kinkband boundaries (dots), planes containing poles to kinks (great circles), and the constructed orientations of the maximum (σ_1) and the minimum (σ_3) principal stress components related to kink formation. Note that σ_1 is horizontal in the case of NW-SE shortening (i.e. roughly parallel to the strike of mainphase structures), while it plunges 20°- 30° along the gradient of long mainphase foldlimbs in the case of NE-SW shortening.

Fig. IV.16. Conjugate kinkbands, central Orri dome. View towards northeast. The kinks deform flat-lying sedimentary bedding on a long mainphase flank. Location given in Fig. IV.7.

The kinkbands overprint Variscan mainphase folds, but have never been found to overprint younger Variscan structures. Nevertheless, the fact that kinks only developed on flat, non-refolded mainphase foldlimbs may be used as negative evidence that the kinks are younger than D_{V4} and D_{V5}, as bedding was no longer flattish in areas affected by refolding, thus hampering kinkband development.

Deformation of the kinks themselves has not been observed in the Orri dome, so their minimum age can not be established. We must therefore conclude that they may be of late Variscan or Alpine age. There are two reasons to assume that the former alternative applies:

Firstly, the kinkbands were formed by compression in the horizontal plane, in contrast to the extensional kinks of probable Alpine age

encountered in the south-eastern part of the dome; to be discussed later. (Note: the terms compressional and extensional as used in this section on kinkbands refer to compression or extension in the horizontal plane only). This fundamental difference between the two types suggests different ages of deformation. A Variscan age for the compressional kinkbands ties in nicely with the overall compressional late Variscan evolution.

Secondly, there seems to be a genetic relationship between compressional kinkbands and Variscan D_{V5} structures in the Orri dome. In the field it is often hard to distinguish between kink-like D_{V5} folds and kinks. Still, D_{V5} axial planes tend to be very steep and strike N-S, whereas most D_{V6} kinks dip towards NE, SE, SW, or NW. It is very well possible, therefore, that most of the steep N-S planes shown in Fig. IV.15 do not represent "true" D_{V6} kinks but instead "kink-like" D_{V5} chevron-type folds. The work of Patterson & Weiss (1966) suggests that the genesis of kinks, conjugate folds and chevron-type similar folds can be closely related: whereas (conjugate) kinking is associated with a total shortening up to 10-25% (Ramsay, 1967), chevron folds can develop in the same anisotropic material when it is further shortened to roughly 50%.

This might explain the difficulty to separate D_{V5} and D_{V6} structures from each other in the field. Possibly there has been a gradual evolution from the development of "true" D_{V5} structures (macro- meso structures, the latter with axial plane foliations), via chevron-type folding, to D_{V6} kinking, thus reflecting an overall decrease of shortening in the horizontal plane with time. This in turn probably reflects a drop in stress-level at the end of the Variscan orogeny. The magnitudes and directions of minor stresses will be relatively sensitive to local rock inhomogeneities. Therefore kinkbands may show a larger variation in orientation than D_{V5} folds (Figs. IV.14 and IV.15). Nevertheless, like second refolding structures, all observed kinkbands have a E-W component of shortening.

Kinkbands of similar nature as the D_{V6} kinks, encountered in other parts of the Axial Zone of the Pyrenees, appear to be overprinting D_{V5} structures (called F_4 by Zwart, 1979), confirming their late Variscan age.

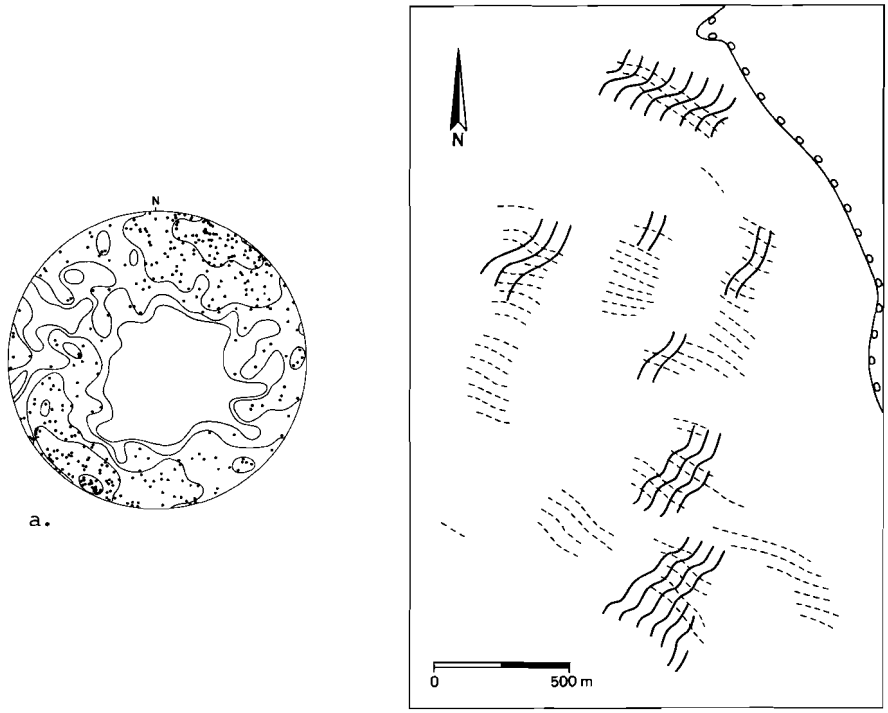

Fig. IV.17. Redistribution of D_{V4} and D_{V5} cleavages in the southeastern Orri dome (Fig. IV.7) caused by post-Variscan shear. Poles to D_{V3} cleavages from the same area are shown in Fig. IV.10.
(a) Equal area stereographic projection of poles to D_{V4} cleavage (NNW-SSE to ENE-WSW strike), and poles to D_{V5} cleavage (N-S to NE-SW strike). In this projection no attempt has been made to strictly distinguish between the two cleavages, as discrimination between the two on the basis of their orientation is also difficult to make in the field. Number of measurements: N=366; contours represent 1, 2, 5, 10, and 20 poles per 1% area (0.3, 0.5, 1.4, 2.7, and 5.5% per 1% area). (b) Simplified structural trend map showing deformed D_{V5} (full drawn lines) and D_{V4} (stippled) cleavages. Upper Ordovician formations crop out in the upper right part of the map. Note the relatively strong reorientation of D_{V5} cleavage caused by right-lateral shear.

POST-VARISCAN DEFORMATION

The expression "post-Variscan deformation" is used here to refer to the Late Paleozoic (Stephanian and Permian) strike-slip and extensional deformation which took place directly after the Variscan orogeny had come to an end (Speksnijder, 1986a; chapter III). It is hard or even impossible to completely distinguish post-Variscan deformation from Alpine deformation, just like it is difficult to assess the chronological order, if any, of post-Variscan events themselves. For this reason, the subdivisions used in this chapter are mainly of systematical nature and do not necesserarily represent successive steps in the tectonic evolution of the Pyrenees.

Post-Variscan shearing (D_{PV1})

Figures IV.7 & IV.17 show that D_{V5} axial plane cleavages do not have constant orientations, but have consistently been bend towards the east (going from south to north) along approximately E-W to ESE-WNW trending zones. The deformation generation which caused this reorientation must be post-Variscan (probably Stephano-Permian) in age, and is referred to as D_{PV1} deformation.

In the following the effects of D_{PV1} deformation on older Variscan structures will be discussed. Figure IV.17a shows the orientations of D_{V4} and D_{V5} cleavages in the southeastern part of the Orri dome. It is evident that both cleavages have been reoriented by post-Variscan shearing. The structural trend map of Fig. IV.17b shows that the D_{V4} cleavage has been relatively little reoriented compared to the D_{V5} cleavage, although D_{V4} cleavage has been folded around steep N-S axial planes during D_{V5} deformation. This observation is taken to indicate that the younger cleavage was more susceptible to shearing, as a function of its orientation, than the older cleavage. The fact that D_{V4} cleavage traces have seemingly been little affected by D_{PV1} deformation, suggests that post-Variscan shearing has taken

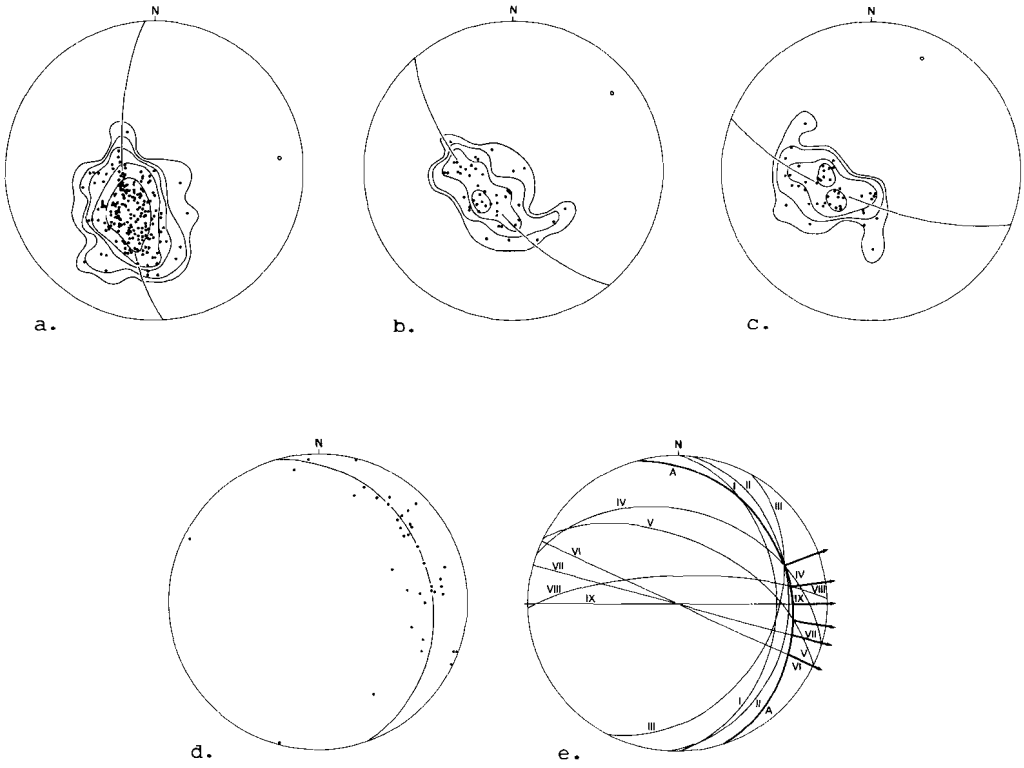

Fig. IV.18. Reorientation of D_{V3} cleavage as a result of D_{PV1} deformation. Locations shown in Fig. IV.7.
(a) Poles to mainphase cleavage in the north-central part of the dome. The position of the (apparent) foldaxis is indicated. This diagram is identical to Fig. IV.8a. Number of measurements: N=195; contours: 1, 2, 5, 10, and 25 poles per 1% area (0.5, 1.0, 2.6, 5.1, and 12.8% per 1% area). (b) Poles to mainphase cleavage, and foldaxis; central-east Orri dome. N=45, contours: 1, 2, 5, and 10 poles per 1% area (2.2, 4.4, 11.1, and 22.2% per 1% area). (c) Poles to mainphase cleavage, and foldaxis; northeastern Orri dome. N=46; contours 1, 2, 5, and 10 poles per 1% area (2.2, 4.3, 10.9, and 21.7% per 1% area). (d) Apparent foldaxes of mainphase cleavages from 38 subareas in the Orri dome, including the axes shown in Figs. IV.18a-c. The great circle represents the redistribution plane of the foldaxes. (e) D_{PV1} shear directions (indicated by heavy arrows) are found as intersection lines between possible shear (anisotropy) planes and the redistribution great circle shown in Fig. IV.18d. Great circles represent the following planes: (A) Foldaxes redistribution plane; (I) Thrustplanes in the eastern part of the Orri dome (Hartevelt, 1970); (II) Average mainphase cleavage orientation northeastern part dome, N=107; (III) Average mainphase cleavage orientation

(continued on opposite page)

Fig. IV.18. (continued)
in a subarea in the southwest, N=11; (IV) Average mainphase cleavage orientation area Fig. IV.3, N=141; (V) Average mainphase cleavage orientation area Fig. IV.4, N=52; (VI) Average D_{V4} cleavage orientation Fig. IV.20b, N=62; (VII) Reorientation direction D_{V5} cleavages (see text); (VIII) Average orientation D_{V4} cleavages area Fig. IV.14, N=90; (IX) Strike Alt Segre fault (Sole Sugrañes, 1978) and faults La Seu Basin (Speksnijder, 1985; chapter II). Possible shear planes turn out to be either parallel to the redistribution plane (I-III), or indicate a shallow east plunging shear direction (IV-IX).

place more or less parallel to the D_{V4} cleavage planes; i.e. in E-W to ENE-WSW direction with right-lateral sense.

The interpretation of mainphase (D_{V3}) cleavage diagrams is more complicated, as it has been affected by D_{V4}, D_{V5} and D_{PV1} deformations (the effect of D_{V6} deformation on mainphase cleavage is negligible). Figures IV.18a-c show the distributions of D_{V3} cleavage for a number of subareas in the Orri dome. The distributions define great circles and therefore apparent foldaxes for the combined effects of post-mainphase deformation. If the apparent foldaxes of these and other areas are subsequently plotted in one stereographic projection (Fig. IV.18d), it turns out that they define a great circle as well and thus lie in one plane. Redistribution of lineations, such as foldaxes, in a plane suggests that the (latest) deformation has been of the simple shear type (Ramsay, 1967; chapter 8). The slip direction will be defined by the intersection line between the lineation distribution plane and the shear plane (Hobbs et al., 1976; p.192). Figure IV.14 demonstrates that reorientation of D_{V5} cleavages takes place along E-W to ESE-WNW striking planes. In addition, the fact that D_{V5} axial planes do not significantly change in dip-angle in Figs. IV.14a and IV.17a, suggests that the D_{PV1} apparent foldaxes must be subvertical.

Combination of the observations allows us to postulate steep E-W to ESE-WNW striking planes as possible shear planes for the D_{PV1} simple shear deformation. The slip vector can then be established to be slightly E to ESE plunging for the central and eastern parts of the Orri dome (Fig. IV.18e).

The sense of shear movement has been right-lateral, as can be read off Figs. IV.12 and IV.17b.

All rocks in the Orri dome are mechanically strongly anisotropic due to the fine sedimentary lamination and the presence of several penetrative foliation planes. When favourably oriented with respect to the slip direction, existing anisotropy planes can have taken up much or all of the simple shear movement. This might apply to the ESE-WNW striking mainphase cleavage (except when it is folded), and in particular to the steep E-W striking D_{V4} cleavage. Cleavage-parallel movement on these planes might explain why D_{V4} cleavages sometimes appear to be undeformed on a large scale. Structural elements that make large angles with the shearing direction, such as D_{V5} cleavage, could not take up any cleavage-parallel movement, but became folded instead. The slip direction of simple shear is parallel to gently east dipping thrusts along the eastern border of the Orri dome (Hartevelt, 1970), which suggests that these structures are of post-Variscan age as well.

There are further independent observations which indicate that important E-W directed shearing or faulting may have taken place in the Orri dome. Although it is not always possible to determine the age of this shearing or faulting, it can be shown without any ambiguity that east-west post-Variscan Late Paleozoic movements took place just south of the Orri dome. Speksnijder (1985; chapter II) describes large-scale synsedimentary strike-slip faulting in Stephanian and Permian rocks which unconformably overlie the dome. Post-Variscan divergent strike-slip movements (Speksnijder, 1986a; chapter III) resulted in the formation of an elongated, narrow sedimentary basin with a complex internal organisation. The maximum sediment thickness (approximately 1500m), the length and width of the basin (more than 50 km and 5 km respectively), and the occurrence of thick sequences of tuffs and andesitic basalts indicate that the basin developed above a major fault zone which must reach deep into the crust. It can be shown that the strike-slip movement along the fault zone must have been right-lateral; the minimum horizontal displacement appears to have been in the order of 10-20 kms (Speksnijder, 1985; chapter II).

Upper Carboniferous and Permian rocks which were affected by this strike-slip faulting have been tilted, together with the Variscan unconformity plane and the underlying Variscan rocks, to a dip of

approximately 45° to the south during Tertiary uplift (to be discussed later). It follows that the rocks of the Orri dome, which now crop out to the north of the Upper Paleozoic sedimentary basins, must have been more or less underlying these basins before Alpine tilting took place.

Thus a relationship can be established between superficial E-W post-Variscan synsedimentary (strike-slip) brittle failure, and semi-brittle right-lateral simple shear in the Variscan basement. East-west right-lateral movements along the Pyrenean Variscan mobile belt probably played an important role throughout the Paleozoic (Speksnijder, 1986a; chapter III). Post-Variscan dextral strike-slip movements in the Pyrenees and the rest of southern Europe have been attributed to shear between the Urals and the Appalachians by Arthaud & Matte (1977).

Post-Variscan cleavage fanning (D_{PV2})

The gradual decrease of mainphase cleavage dip towards the south (Fig. IV.7) reflects part of the so-called cleavage fanning in the Axial Zone of the Pyrenees (Zwart, 1979). Whereas mainphase cleavages are subvertical in the northern part of the axial zone, they dip north and flatten in a southern direction (Zandvliet, 1960; Muller & Roger, 1977). The significance and timing of the cleavage fan formation has been a matter of dispute: some authors attribute the fanning to late-Variscan horizontal N-S dilatation (Zwart, 1979, 1981), others to both late-Variscan and Alpine wharping of an originally steep cleavage (Muller & Roger, 1977). Mey (1968) and many French authors (see Zwart, 1981) claim that the foliations of the Axial Zone were originally formed in a horizontal position. The present writer agrees with Zwart (1981), that the latter hypothesis seems unlikely.

As will be shown later, most of the wharping of the Variscan cleavage, in particular along the southern rim of the Orri dome, can be attributed to Alpine deformation. Nevertheless, part of the fanning can result from post-Variscan extension (Speksnijder, 1986a; chapter III), rather than from late Variscan dilatation as envisaged by Zwart (1979), as no further indications for extension of that age can be found. The strain related to extension could have been taken up on cleavage parallel normal faults leading to outward rotation of the cleavage planes. Such a rotation in the vertical plane as a result of post-orogenic relaxation has already been proposed by

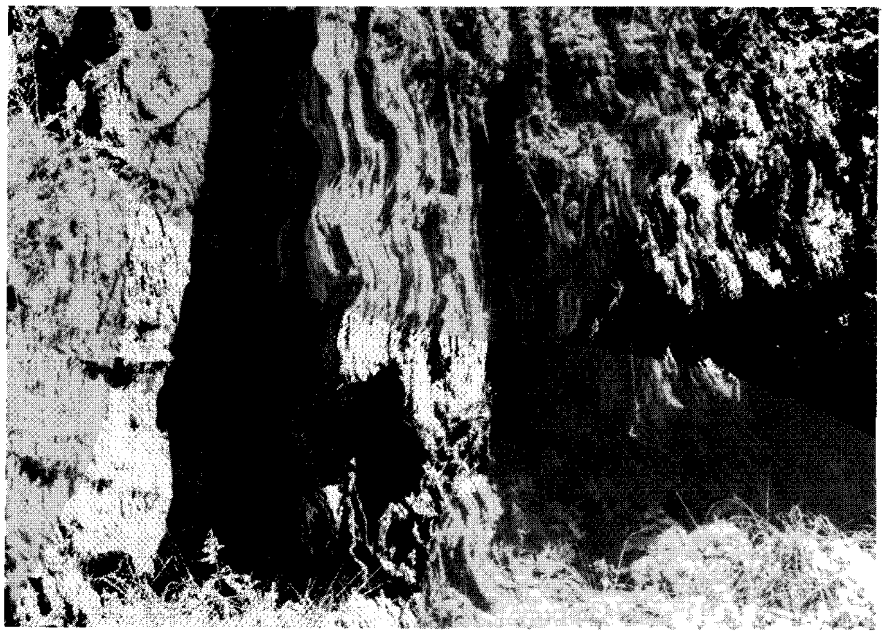

Fig. IV.19. Conjugate kinkbands deforming steep D_{V4} cleavage in the southeastern Orri dome. North is towards the left. Position in Fig. IV.7.

Hoeppener (1955) for the Rhenic slate belt. Correlation problems across the mainphase folds of the northern Orri dome led Speksnijder (1986a; Fig. IV.4) to postulate cleavage-parallel normal faults, similar to those envisaged by Zandvliet (1960). As cleavage parallel movement will not allow the cleavage planes to rotate through the horizontal, the south dipping attitude of the mainphase cleavage in the southernmost part of the Orri dome must be attributed to another mechanism, i.e. Alpine thrusting.

Kinkbands of probable post-Variscan age (D_{PV3})

Kinkbands encountered in the southeastern part of the dome are of different nature than the previously described D_{V6} kinks. They overprint a very steep penetrative D_{V4} axial plane cleavage, which only occurs as a dominant cleavage in this part of the dome. D_{PV3} kinks were generated as a result of N-S extension in the horizontal plane, as witnessed by the often occurring conjugate sets of kinkbands (Figs. IV.19 and IV.20a). This in contrast to the D_{V6} kinks, which were formed by horizontal east-west directed compression. Also in this case, the largest principal stress component is roughly parallel to the anisotropy (cleavage) plane (Figs. IV.20b & c).

The age of the extensional kinks can not be established with any certainty. As they overprint D_{V4} cleavage, they are possibly of post-Variscan age in view of their dilatational nature. They could, on the other hand, also be related to Alpine uplift. The fact that D_{PV3} kinks have not developed in the Stephanian tuffs directly overlying the Variscan rocks does not necessarily indicate a pre-Stephanian age of formation, but instead must be attributed to the lack of a penetrative fabric within the massive tuffs. Figure IV.20c shows orientation data of kinkbands, maximum principal stress directions related to conjugate kinks, and D_{V5} cleavages, projected on a vertical NNE-SSW plane which runs parallel to the measured structural profile. One can read directly read off the diagram that kinks are only present in an area where the strongest change in dip angle of the kinks takes place. This may suggest that kinkband development and change in cleavage attitude are closely related, but on the other hand the diagram reveals that the kinks experienced exactly the same rotation in the vertical plane as the cleavages. In other words, the kinks must have developed in an extensional regime which did not affect cleavage dips significantly, to become rotated together with the cleavage planes during a later deformation phase. For this reason, kinkband development and rotation are tentatively attributed to post-Variscan and Alpine deformation, respectively.

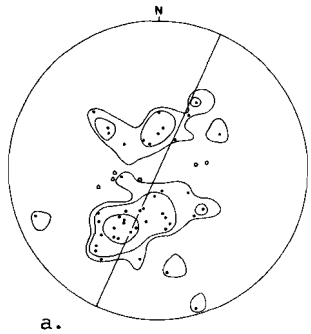
N

a.

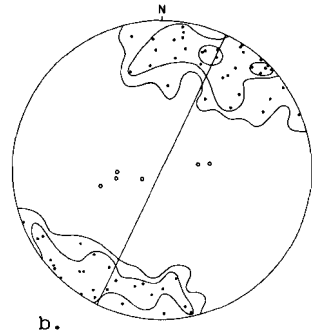
N

b.

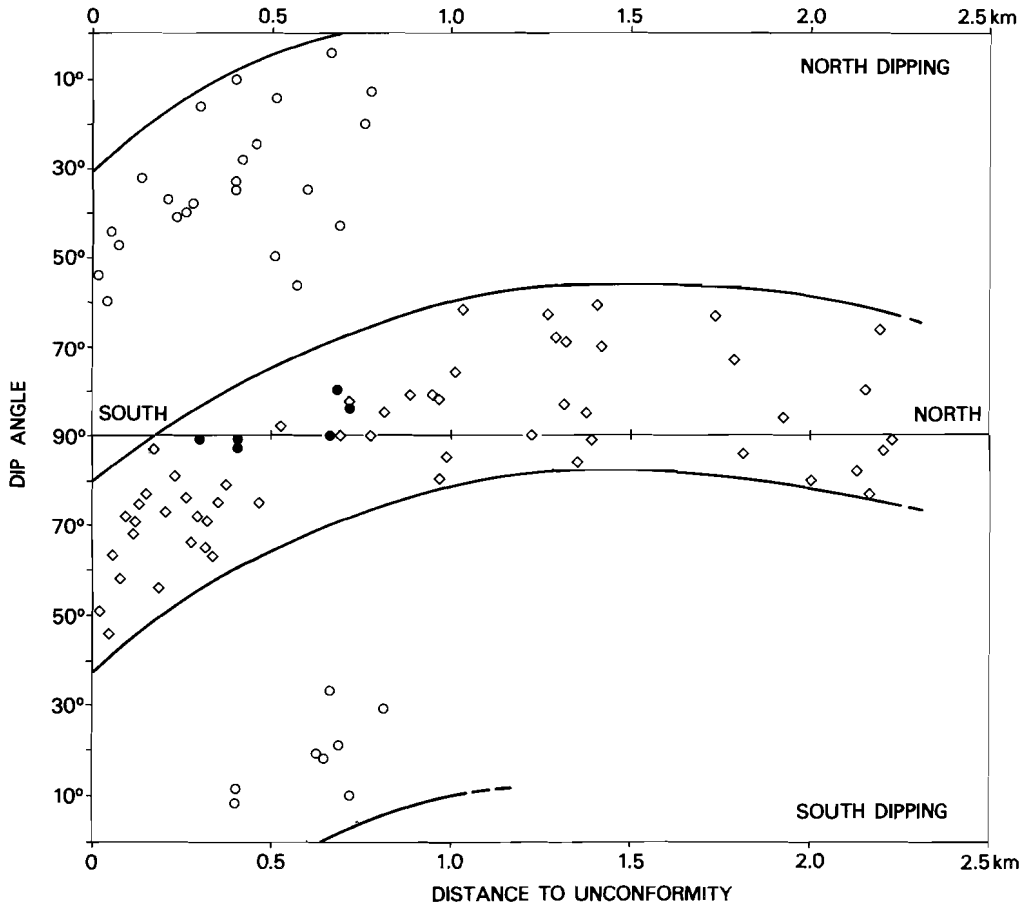
0
0.5
1.0
1.5
2.0
2.5 km
NORTH DIPPING
10°
30°
50°
70°
SOUTH
90°
NORTH
70°
50°
30°
10°
SOUTH DIPPING
DIP ANGLE
DISTANCE TO UNCONFORMITY

c.

ALPINE DEFORMATION

There has been much debate in the literature concerning the influence of deformation of Alpine age in the Axial Zone. While the impact of Alpine deformation was originally thought to be restricted to the Tertiary uplift of the Axial Zone as a whole (c.f. Zwart, 1968), it was already known that Alpine thrusts may cut deep into the Variscan (de Sitter, 1965). Séguret (1970) demonstrated the existence of major Alpine nappe systems south of the Axial Zone (involving pre-Stephanian rocks in the Nogueras Zone). More recently Williams and Fischer (1984) and Williams (1985) presented their reconstructions of balanced sections across the Pyrenean belt, based on the assumption of thin-skinned thrusting affecting the whole of the Axial Zone, as well as the southern foreland.

The development of mylonitic shear zones of Alpine age in the Variscan has been discussed, amongst others, by Lamouroux et al. (1981).

In the Orri dome, no reliable overprinting relationships are available to establish the sequence of Alpine and post-Alpine deformational events, especially because they have been of brittle nature. Comparison with

Fig. IV.20. Orientation and geometry of extensional kinkbands in a NNE-SSW profile; southeastern part of the Orri dome. See Fig. IV.7.
(a) Poles to kinkband boundaries (dots). Open circles represent constructed σ_1 directions related to the development of six conjugate kink sets (c.f. Fig. 15f). The great circle indicates the vertical NNE-SSW plane on which data have been projected in Fig. IV.20c. Number of measurements: N=45; contours: 1, 2, and 5 poles per 1% area (2.2, 4.4, and 11.1% per 1% area). (b) Poles to D_{V5} cleavages in the same profile. The great circle represents the projection plane of Fig. IV.20c. Note that reconstructed σ_1 directions (open circles) approximately lie within the cleavage planes. Contours: 1, 2, and 5 poles per 1% area (1.6, 3.2, and 7.7% per 1% area). (c) The data of Figs. IV.20a & b projected upon a 25° - 205° striking vertical plane, parallel to the measured section. In this diagram (two-dimensional) orientation data are plotted as a function of their distance to the Variscan unconformity plane towards the south. Diamonds: dip of D_{V5} cleavages; heavy dots: σ_1 orientations of conjugate kinks; open circles: dips of kinkbands. For discussion see text.

surrounding areas suggests that thrusting is of Eocene age (Séguret, 1970), while normal and oblique-slip faulting on various scales occurred during the post-Alpine period, offsetting rocks up to Pliocene age.

Alpine thrusting (D_{A1})

The Orri dome is surrounded by thrusts of proven or probable Alpine age. In the south, a complicated allochtonous unit called the Nogueras Zone (Séguret, 1970), has been emplaced on Keuper evaporites which almost directly overlie the Orri dome unconformably (Fig. IV.2). Towards the north, the dome is cut-off by the Llavorsi fault, which might be of Alpine age (Zwart, 1979), whereas a number of thrusts to the west of the Orri dome are definitely of Alpine age (Mey, 1967b, 1968).

Along the southwestern edge of the Orri structure, a major river cuts deeply into Cambro-Ordovician rocks (topographic relief more than 1700 m). At the bottom of the rivervalley, flat-lying Keuper evaporites are exposed, which seemingly underlie Variscan rocks (Fig. IV.2). This observation suggests that (this part of) the dome is allochtonous as well, emplaced on a décollement level within the Triassic evaporites.

The details of nappe tectonics in and around the Orri dome appear to be complicated and largely fall beyond the scope of this paper. Nevertheless, a short resume will be given of the published literature on the subject, and a conceptual cross-section will be presented which might explain the important change in cleavage attitude from north to south in the Variscan.

Palinspastic reconstruction of balanced sections west of the Orri dome (Williams and Fischer, 1984; Williams, 1985) indicates that thrusting can not have been restricted to movements concentrated within the Keuper evaporites alone, but that instead a number of duplexes must have developed in the southern Axial Zone (Fig. IV.21). All thrusts are supposed to join downward in a sole thrust within the Variscan basement. The strong southward dip of the Variscan unconformity and thrust planes along the Nogueras Zone can be elegantly explained by antiformal stacking below the southern part of the present day Variscan outcrop.

The variation in mainphase cleavage dip can be attributed to three effects. Firstly, post-Variscan cleavage fanning (D_{PV2}) may have caused an

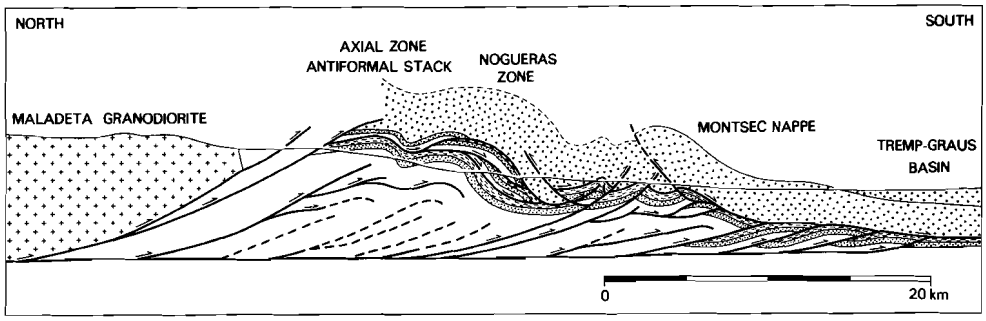

Fig. IV.21. Structural cross section through the south-central Pyrenees, west of the Orri dome (modified after Williams, 1985). Ornamentation represents intrusive Variscan rocks (crosses), Permo-Triassic redbeds (stippled), Keuper evaporites (parallel lines) and undifferentiated Mesozoic and Tertiairy sedimentary rocks (dots). Non-intrusive Variscan rocks have been left unornamented. The main decollement plane is located within the Keuper evaporites (N.B.: The thickness of the strongly deformed Keuper evaporites is somewhat exaggerated in this section).

initial decrease of cleavage dip towards the south before Alpine thrusting took place, or, alternatively, Variscan cleavage may not have developed with uniform orientation during orogenesis. Secondly, cleavage attitude will be affected by the flat-ramp geometry of thrust units as shown in Fig. IV.22. Thirdly, a foreland (southward) directed tilt of the thrust system due to anticlinal stacking will equally impose a southward tilt on Variscan structures as conceptually shown in Fig. IV.23. Note that this section is only intended as an illustration of the possible thrust geometry and can not be palinspastically reconstructed.

The position of the postulated roof-thrust is related to cleavage attitude: steep co-planar in the north, and decreasing in dip towards the south. If this interpretation is correct, the thrust should also have developed towards the east over at least some distance in the Orri dome. The monotonous nature of the Cambro-Ordovician rocks does not allow to locate any structural contact, but it is striking that the northern limit of Variscan refolding (D_{V4} and D_{V5}) seems to be more or less coinciding with

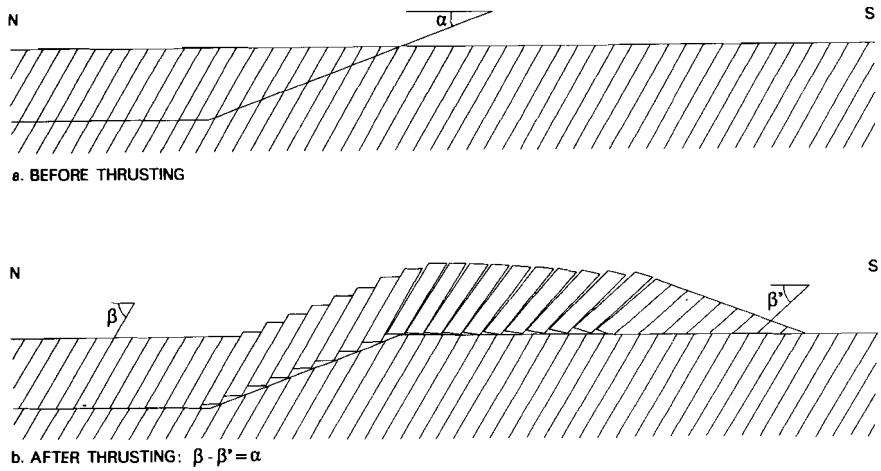

Fig. IV.22. Schematic diagram showing the variation of cleavage attitude as a result of thrusting within strongly anisotropic rock. The orientation of cleavage planes above the ramp may remain approximately parallel to their original orientation due to cleavage-parallel slip. A strong decrease of cleavage dip will occur above the flat; the maximum rotation angle (β - β') is equal to the dip α of the ramp. If a ramp would develop parallel to the anisotropy plane, the cleavage in the southern part of the thrusted unit would be subhorizontal. Cleavage dips towards the south, however, could never occur in the configuration shown here, even not if post-Variscan cleavage fanning (D_{PV2}) had taken place. A strong foreland dip of the thrustplane is therefore required to rotate cleavage planes through the horizontal, as shown in Fig. IV.23.

the boundary between tilted and co-planar cleavage planes (Fig. IV.7). Obviously, the occurrence of Variscan refolding and mainphase cleavage reorientation can be closely related, but alternatively the postulated Alpine thrust now juxtaposes two different Variscan structural units (with and without refolding) which were previously separated from each other. Based on this reasoning, the tentative trace of the thrust under discussion is shown stippled in Fig. IV.7.

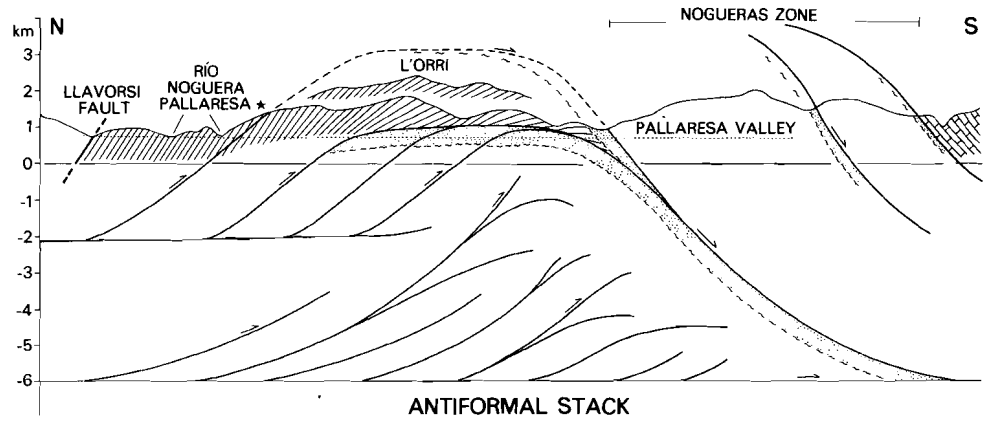

Fig. IV.23. Conceptual cross-section through the western part of the Orri dome (profiles over the top of the Orri mountain and along the valley of the Rio Noguera Pallaresa have been projected), and the northern part of the Nogueras Zone. Location shown in Fig. IV.2. The point at the surface which marks the southern limit of coplanar mainphase cleavage (shown by an asterisk), is taken to indicate the position of a roofthrust to an emplaced unit which is mainly composed of Cambro-ordovician rocks. In this interpretation the roofthrust joins with the southwards dipping thrustplane that forms the northern boundary of the allochtonous Nogueras Zone. The foreland dip of this plane is attributed to antiformal stacking as suggested by Williams (1985); see Fig. IV.21. The large outcrop of the Keuper evaporite in the Noguera Pallaresa valley (4.5 km in north-south direction), combined with its restricted undisturbed maximum thickness (some hundreds of meters), suggests duplex development below the Orri thrust unit. As the details of thrust configuration in the Nogueras Zone are not known, and as the nature and age of the latest movement on the Llavorsi fault is unclear, the section is not balanced and no attempt has been made to reconstruct it. Ornamentation represents cleaved Cambro-Ordovician; undifferentiated Paleozoic rocks (white); (Permo-) Triassic including Keuper evaporites (stippled); and Mesozoic limestone (southernmost part of the profile). Horizontal and vertical scales are equal.

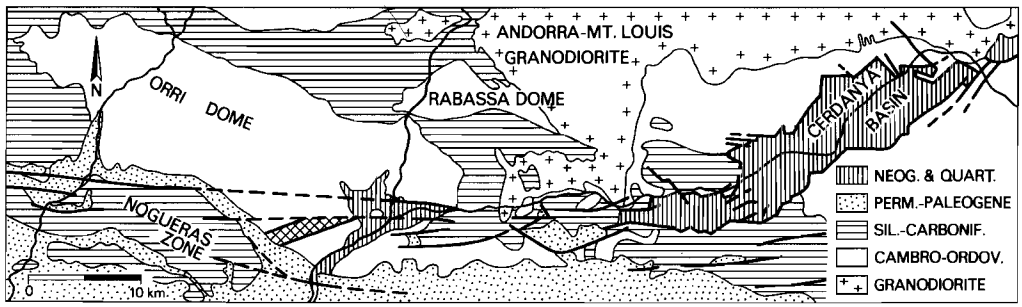

Fig. IV.24. Faults of proven or probable post-Alpine age, together forming a complicated E-W striking oblique-slip system along the southern boundary of the Axial Zone of the Pyrenees. The part east of the Orri dome has been named Alt Segre fault by Sole-Sugrañes (1978). The cross-hatched area in the southern Orri dome represents a major overturned mainphase (D_{V3}) foldlimb which is cut-off in the north. "Permian-Paleogene" in the legend to the figure includes Westphalian D and Stephanian rocks. Fault traces mainly after Zwart & Roberti (1976), Hartevelt (1970) and Brouwer (1968); structural outline of the Cerdanya Basin after Gourinard (1971).

POST-ALPINE DEFORMATION

Post-Alpine deformation is defined to incorporate all (brittle) deformation which took place after the main Alpine (or Pyrenean) compressional event. Its occurrence is therefore restricted to the Neogene and the Quarternary.

Post-Alpine faulting (D_{PA1})

South of the Orri dome, numerous east-west steep normal faults with throws up to some meters were recorded in Permian and Triassic redbeds, usually involving a downthrown northern block.

The same sense of movement has been recorded on an east-west striking fault which offsets Miocene and younger rocks in the eastern part of the

dome. Along strike towards the east, a complicated fault system, named the Alt Segre fault by Sole-Sugrañes (1978), affects Eocene and older rocks including Variscan basement (Fig. IV.24). The dip-slip offset on the Alt Segre fault (northern block downthrown) may be in the order of a kilometer or more (Hartevelt, 1969). The existence of a possible strike-slip component of movement can be inferred from the geometry of the Neogene Cerdanya basin (Fig. IV.24). It has been shown by Gourinard (1971) that this basin is an asymmetric structure bordered by major E-W and NE-SW striking faults on its southern and eastern sides. The thickness of the basinfill sediments rapidly decreases towards the north, where only minor adjustment structures have been detected. The Cerdanya basin can therefore be considered to be an asymmetrical pull-apart type structure (Crowell, 1974), generated by a sinistral component of horizontal movement on the Alt Segre fault. As rocks of Miocene and Pliocene age have been deposited in the basin, the fault must have been active during that timespan. The occurrence of a very large earthquake (epicentral intensity XI) in the Cerdanya Basin on 2-2-1428 (Fourniguet et al., 1981), shows that the faults are, geologically speaking, still active today.

There are a some indications that the Alt Segre fault extends westward into the Orri dome. Firstly, the abrupt termination of a major overturned Variscan mainphase foldlimb (Fig. IV.24) suggests the existence of an anomalous contact. Secondly, differences in style, size and orientation of folds do occur across the postulated continuation of the Alt Segre fault zone, such as the geometry of D_{V4} folds (isoclinal in the south, open to tight in the north). Further westward, the Alt Segre fault most likely joins up with the northern boundary fault of the Nogueras Zone, which explains the sudden change in strike of post-Variscan deposits that overlie the Orri dome unconformably (Fig. IV.24).

In conclusion, post-Alpine faulting is of oblique-slip nature, involving a sinistral horizontal component of movement of unknown, but probably small magnitude. In spite of the frequent occurrence of dip-slip movement on east-west faults, including the large offset on the Alt Segre fault, the north-south extension related to normal faulting must have been limited because of the steep attitude of the fault planes.

LINEAMENT ANALYSIS

A photogeological study of the Orri dome and surroundings reveals the presence of numerous well-defined lineaments. Without exception, they run perfectly straight across accidented terrane so that it may be assumed that the lineaments represent subvertical planes. In some areas of good outcrop and monotonous lithology (e.g. in Permian redbeds), lineament traces can be easily correlated with (cemented) fractures in the field. The occurrence of lineaments is therefore attributed to brittle deformation affecting the rocks. By consequence, a directional analysis of lineament directions may throw light on the possible relations between fractures seen on aerial photographs and structures observed in outcrop.

For this purpose, the exposure area of Cambro-Ordovician rocks in the Orri dome has been subdivided into 69 subareas (cf. Fig. IV.25a), in which length and orientation of each lineament were determined. In total some 11,000 lineaments were measured, representing a total length of over 6,500 km. In all subareas, east-west lineaments are abundant, while NNW-SSE directions occur frequently. When plotted in rose diagrams, the

Fig. IV.25. Lineament analysis in the Orri dome.
(a) Outline of the Orri dome, indicated by the outcrop area of Cambro-Ordovician rocks, and location of two subareas (of a total 69) referred to in Figs. IV.25b & c. The area covered by Fig. IV.26 is also shown. (b) Lineaments observed in the southern part of the dome (Fig. IV.25a). The left-hand part of the diagram shows length distribution of the lineaments per 10° interval (scale in meters). The right-hand part shows the frequency distribution and the calculated orientation of the resultant vector (Θ=90.1°). The magnitude of the normalised resultant vector amounts to α=0.428; a Rayleigh test for direction vectors confirms the unimodal character of the distribution at 99% confidence level. Total number of lineaments N=276, accumulated lineament length ΣL=144,150 m. (c) Lineaments from a subarea in the western Orri dome (Fig. IV.25a). Length distribution is shown on the left (scale in meters) and frequency distribution to the right. The direction of the resultant vector: Θ=93.2°, its normalised magnitude α=0.278 (unimodal at 99% confidence level). Total number of measurements N=254, accumulated length ΣL=114,222 m.

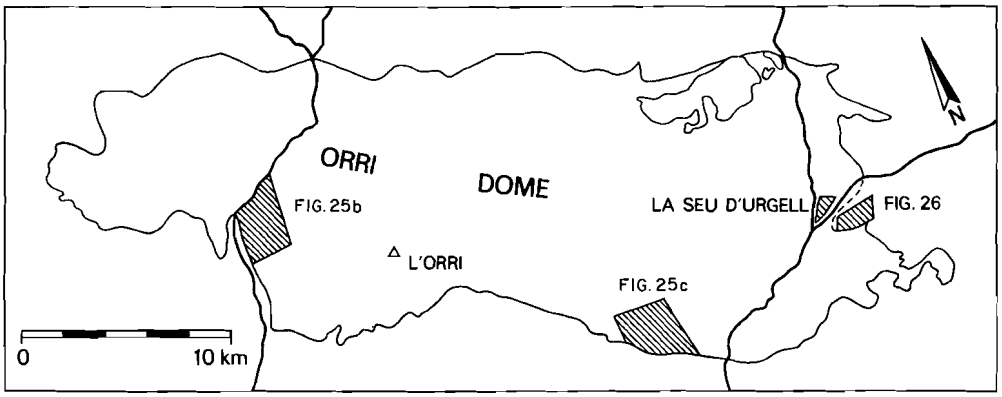
ORRI
DOME
FIG. 25b
L'ORRI
FIG. 25c
LA SEU D'URGELL
FIG. 26
N
0
10 km

a.

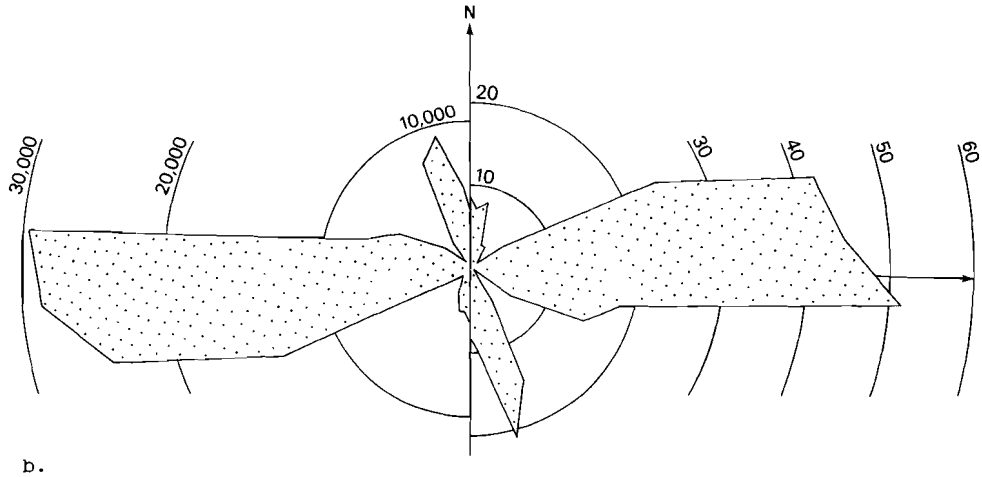
N
10,000
20
10
30,000
20,000
30
40
50
60

b.

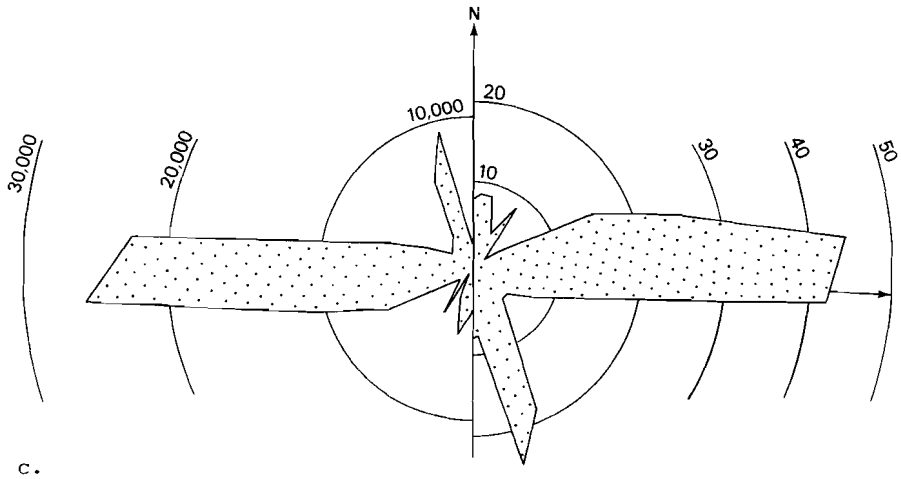
N
10,000
20
10
30,000
20,000
30
40
50

c.

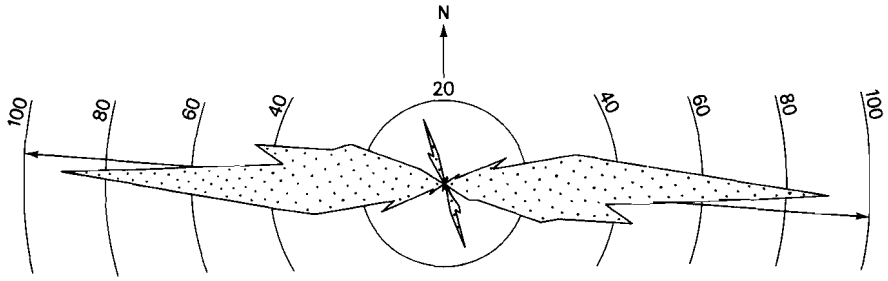

Fig. IV.26. Frequency distribution of lineaments in Pliocene rocks just east of the Orri dome (see Fig. IV.25a). Total number of readings N=460, direction of resultant vector (indicated by the arrow): Θ=95.1°, magnitude of normalised resultant vector α=0.716 (unimodal at 99% confidence level).

distributions appear to have a unimodal character (Figs. IV.25b & c). Indeed, a simple Rayleigh significance test for the calculated resultant vector magnitudes of the distributions confirms unimodality in each subarea at 95% confidence level. Furthermore, the directions of resultant vectors per subarea turn out to be very constant over the dome, as they only vary between 87.7° - 267.7° and 95.3° - 275.3°. (For an outline of calculation methods and significance tests see Curray, 1956).

Similar (but less detailed) results were obtained from photogeological studies of surrounding areas of the Orri dome in which younger rocks are exposed. Figure IV.26 shows, as an example, the lineament direction distribution within unconsolidated Pliocene rocks just east of the dome. East-west lineaments are also frequently developed in the Quarternary alluvial deposits around La Seu d'Urgell (Fig. IV.2).

We may conclude that lineament (fracture) directions are more or less constant over the entire investigated area, irrespective of the age of the rocks in which they have developed.

The steep fractures observed in the field are some mm to some cm in width, and are either extensional fractures or dilatational shear fractures.

Their nature therefore suggests that they may be of post-Variscan or post-Alpine age, also because they transsect Variscan structures. The fact that the fractures have not only been observed in Paleozoic to Tertiary rocks but even in recent alluvial sediments, would rather indicate that they all developed, geologically speaking, extremely recently.

It seems more realistic to assume that fracturation in the Orri dome has been a more or less continuous process, involving generation of new fractures and reactivation of existing fractures whenever conditions were favourable to this effect (in terms of magnitude and direction of stress fields, material properties, strain rates, etc.). Extensional fractures and dilatational shear fractures may thus have formed on any moment in essentially extensional structural regimes which existed during Paleozoic basin development (Speksnijder, 1986a; chapter III), in the post-Variscan stage, or in the post-Alpine stage.

SUMMARY

As this study is constrained by the dimensions of the Orri dome and the age of the investigated rocks, no comprehensive correlation exercise of our data with other areas has been undertaken. As far as Variscan deformation is concerned, correlation within the Axial Zone turns out to be difficult anyway (Zwart, 1981). For regional overviews regarding the structure of the Pyrenees the reader is referred to Zwart (1979), Muller & Roger (1977), Arthaud & Matte (1977), Souquet et al. (1977), Séguret (1970), Williams (1985), Speksnijder (1986a; chapter III), and many others.

In the area of the present-day Orri dome, minor basin development occurred during the Early Paleozoic. There are no indications for major Caledonian deformation. Strong subsidence and basin differentiation took place in the Devonian and Early Carboniferous in a divergent oblique-slip setting (Speksnijder, 1986a; chapter III). When conditions changed from divergent to convergent wrenching, early N-S folds were generated (D_{V1}). Progressive convergence of the Iberian and European plates subsequently resulted in the development of open E-W folds (D_{V2}), tight ESE-WNW mainphase

folds (D_{V3}) characterised by a penetrative foliation, and D_{V4} folds which are coaxial to mainphase folds, but of smaller dimensions.

The latest stage of the Variscan orogeny is characterised by minor folds (D_{V5}) and compressional kinkbands (D_{V6}) which might be of only local significance. In the post-Variscan stage important lateral movements took place (D_{PV1}), accompanied by extensional features referred to as D_{PV2} (cleavage fanning) and D_{PV3} (dilatational kinkbands). One of the main results of this study is that the occurrence of relatively deep-seated D_{PV1} shearing can be directly correlated with superficial faulting and sedimentation in the Upper Carboniferous - Permian (Speksnijder, 1985; chapter II).

No record of Mesozoic deformation has been preserved in the Orri dome or its direct vicinity.

Important compression took place in the Eocene and Oligocene (Pyrenean phase of Alpine deformation). As a result, large nappes, including Paleozoic rocks of the Orri dome, were emplaced towards the southern foreland. The last stage of deformation in the southern Pyrenees has been extensional, resulting in the generation of minor fractures, as well as large-scale fault systems which transsect all older structures.

The shape of the Orri dome as it outcrops today results mainly from interference between Variscan pre-mainphase (D_{V1} and D_{V2}), mainphase (D_{V3}), and first refolding (D_{V4}) structures, modified by post-Variscan faulting and shearing, Alpine thrusting and post-Alpine faulting.

ACKNOWLEDGEMENTS

Eppo van Straten and Wim Bosman assisted during fieldwork. Many others, in particular Ineke Smeets, offered help in many ways.

REFERENCES

Arthaud, F. & Matte, P. (1977). Late Paleozoic strike-slip faulting in southern Europe and northern Africa: Result of right-lateral shear zone between the Appalachians and the Urals.
Geol.Soc.Am.Bull., 88, pp. 1305-1320.

Boschma, D. (1963). Successive Hercynian structures in some areas of the Central Pyrenees.
Leidse Geol.Meded., 41, pp. 153-220.

Brouwer, Th.N. (1968). Verslag van een geologische kartering in de omgeving van de Cerdaña vallei, oostelijke Pyreneeën, Spanje.
Internal report Leiden University, 34 pp.

Crowell, J.C. (1974). Sedimentation along the San Andreas Fault, California. In: R.H. Dott, Jr. and R.H. Shaver (Editors), Modern and ancient Geosynclinal Sedimentation.
Spec.Publ.Soc.Econ.Paleont.Miner., 19, pp. 292-303.

Curray, J.R. (1956). The analysis of two-dimensional orientation data.
Journ.Geol., 64, pp. 117-131.

Donath, F.A. (1969). Experimental study of kink-band development in strongly anisotropic rock. In: A.J. Baer & D.K. Norris (Eds.), Proceedings, conference on research in tectonics (Kinkbands and brittle deformation), Ottawa, March 1968. Geological Survey of Canada, paper 68-52, pp. 255-287.

Fourniguet, J., Vogt, J. & Weber, C. (1981). Seismicity and recent crustal movements in France.
Tectonophysics, 71, pp. 195-216.

Gourinard, Y., (1971). Détermination cartographique et géophysique de la position des failles bordières du fosse néogene de Cerdagne (Pyrénées orientales franco-espagnoles).
96^{e} Congr.nat.Soc.Sav.Toulouse, II, pp. 245-263.

Hartevelt, J.J.A. (1970). Geology of the Upper Segre and Valira valleys, Central Pyrenees, Andorra/Spain.
Leidse Geol.Meded., 45, pp. 167-236.

Hobbs, B.E., Means, W.D. & Williams, P.F. (1976). An outline of structural geology.
John Wiley & Sons, Inc., New York, 571 pp.

Hoeppener, R. (1955). Tektonik im Schiefergebirge.
Geol.Rundschau, 44, pp. 26-58.

Lamouroux, C., Soula, J.-C. & Roddaz, B. (1981). Les zones mylonitiques des massifs du Bessiès et de l'Aston (Haute Ariège).
Bull.B.R.G.M., I, 2, pp. 103-111.

Mey, P.H.W. (1967b). The geology of the Upper Ribagorzana and Baliera valleys, Central Pyrenees, Spain.
Leidse Geol.Meded., 41, pp. 153-220.

Mey, P.H.W. (1968). Geology of the Upper Ribagorzana and Tor valleys, Central Pyrenees, Spain.
Leidse Geol.Meded., 41, pp. 229-292.

Mey, P.H.W., Nagtegaal, P.J.C., Roberti, K.J. & Hartevelt, J.J.A. (1968). Lithostratigraphic subdivision of post-Hercynian deposits in the South-Central Pyrenees, Spain.
Leidse Geol.Meded., 41, pp. 221-228.

Muller, J. & Roger, Ph. (1977). L'évolution structurale des Pyrénées (domaine central et occidental). Le segment hercynien, la chaîne de fond alpine.
Géologie alpine, 3, pp. 149-191.

Nagtegaal, P.J.C. (1969). Sedimentology, paleoclimatology, and diagenesis of post-Hercynian continental deposits in the south-central Pyrenees, Spain.
Leidse Geol.Meded., 42, pp. 143-238.

Patterson, M.S. & Weiss, L.E. (1966). Experimental deformation and folding in phyllite.
Geol.Soc.Am.Bull., 77, pp. 343-374.

Powell, C.McA., Cole, J.P. & Cudahy.T.J. (1985). Megakinking in the Lachlan Fold Belt, Australia.
Journ.Struct.Geol., 7, pp. 281-300.

Ramsay, J.G. (1962b). The geometry of conjugate fold systems.
Geol.Mag., 99, pp. 516-526.

Ramsay, J.G. (1967). Folding and fracturing of rocks.
McGraw-Hill, New York, 568 pp.

Schmidt, H. (1931). Das Paläozoikum der spanischen Pyrenäen.
Abh.Ges.Wiss.Gottingen math.-phys. Kl.3, Folge H.5, 8, pp. 1-85.

Séguret, M. (1970). Etude tectonique des nappes et séries décollées de la partie centrale du versant sud des Pyrénées.
Ph.D. thesis, Montpellier, 155 pp.

Sitter, L.U de (1965). Hercynian and Alpine orogenies in northern Spain.
Geol.Mijnbouw, 44, pp. 373-383.

Sole Sugrañes, L. (1978). Alineaciones y fracturas en el sistema Catalan a segun las imagenes Landsat-1.
Tecniterrae, 22, pp. 1-11.

Souquet, P., Peybèrnes, B., Bilotte, M. & Debroas, E.-J. (1977). La chaîne alpine des Pyrénées.
Géologie Alpine, 53, pp. 193-216.

Speksnijder, A. (1985). Anatomy of a strike-slip fault controlled sedimentary basin, Permian of the southern Pyrenees, Spain.
Sediment.Geol., 29, pp. 31-66 (Chapter II of this thesis).

Speksnijder, A. (1986a). The detection and significance of early deformation in the southern Variscan Pyrenees, Spain; implications for regional Paleozoic structural evolution.
Geol.Rundschau (Chapter III of this thesis).

Weiss, L.E. (1969). Flexural slip folding of foliated model materials.
In: A.J. Baer & D.K. Norris (Editors), Proceedings, conference on research in tectonics (Kink bands and brittle deformation), Ottawa, March 1968.
Geological Survey of Canada, paper 68-52, pp. 294-357.

Williams, G.D. (1985). Thrust tectonics in the south central Pyrenees.
Journ.Struct.Geol., 7, pp. 11-17.

Williams, G.D. & Fischer, M.W. (1984). A balanced section across the Pyrenean orogenic belt.
Tectonics, 3, pp. 773-780.

Zandvliet, J. (1960). The geology of the Upper Salat and Pallaresa valleys, Central Pyrenees, France/Spain.
Leidse Geol.Meded., 25, pp. 1-127.

Zwart, H.J. (1968). The paleozoic crystalline rocks of the Pyrenees in their structural setting.
Krystalinikum, 6, pp. 125-140.

Zwart, H.J. (1979). The geology of the central Pyrenees.
Leidse Geol.Meded., 50, pp. 1-74.

Zwart, H.J. (1981). Three profiles through the Central Pyrenees.
Geol.Mijnbouw, 60, pp. 97-106.

Zwart, H.J. & Roberti, K.F. (1976). Geological map of the Central Pyrenees. Sheet 9: Flamisell- Pallaresa.
Geological Institute Leiden.

CHAPTER V

POST-VARISCAN SUPERFICIAL FAULTING AND CONTEMPORANEOUS BASEMENT SHEARING IN THE SOUTH-CENTRAL PYRENEES, SPAIN

INTRODUCTION

Major fault systems are characterised by a transition from brittle failure in the upper part of the crust to ductile deformation at lower levels. The mechanisms controlling continental faulting and resulting fault properties have been described by Sibson (1977, 1983). A profile through a fault zone will typically show the following fault-related rocktypes, from top to bottom: faultgouges and breccias, cataclasites, pseudotachylytes, and (different types of) mylonites (Grocott, 1979, 1981; Macaudière & Brown, 1982; Obee & White, 1985). Whereas the last type of fault rock represents a quasi-plastic mode of deformation, all other types are related to elastic-frictional behaviour. The transition zone between the two types of deformational mechanisms is commonly referred to as the brittle-ductile transition (Gibson & Gray, 1985), which is usually situated at a depth of 8 to 15 km in the case of active continental faulting (Sibson, 1977, 1983). Below this zone, deformation is of the aseismic ductile shear type, whereas both brittle and ductile shearing may operate within the brittle-ductile transition zone (Ramsay, 1980). Descriptions of exposed transition zone rocks have been given by White & White (1983), Simpson (1985), and Gibson & Gray (1985). In the upper crust brittle shearing or faulting prevails (Ramsay, 1980; Sibson, 1983), which is often of discontinuous nature (Gamond, 1983; Tchalenko, 1970).

The present article describes the properties of superficial post-Variscan oblique-slip faulting and contemporaneous basement shear in the south-central Pyrenees. It will be shown that shearing in the basement took place not far above the brittle-ductile transition zone along pre-existing anisotropy planes (Variscan cleavages). Distribution of movement on individual cleavage planes gives the macroscopic effect of simple shear in the studied region, comparable to smaller-scale ductile shear zones found elsewhere in the Pyrenees.

GEOLOGICAL SETTING

The studied area is situated along the southern border of the Axial Zone of the Pyrenees (Zwart, 1979), a large outcrop of Paleozoic rocks in the Alpine Pyrenean orogenic belt. Its pre-Stephanian sedimentary and crystalline rocks have been strongly affected by several Variscan deformations. The structure of the Axial Zone is characterised by a series of elongated, WNW-ESE striking macroscopic folds, including the Orri "dome" (Hartevelt, 1969), shown in Fig. V.1. The southern part of the Axial Zone is unconformably overlain by Upper Paleozoic and Triassic sedimentary rocks. The Variscan unconformity plane and the overlying post-Variscan sediments presently dip 45° towards the south due to strong Alpine uplift of the Axial Zone (Speksnijder, 1986b; chapter IV).

The schematic representation of the stratigraphy of post-Variscan deposits in the southern Pyrenees, given in Fig. V.2, is based on earlier work by Mey (1968), Mey et al. (1968), Nagtegaal (1969), and Hartevelt (1970). Each of the units of Fig. V.2 may directly overlay the Variscan basement, as shown in Fig. V.1.

The deposition of the Malpas and Peranera Formations has been strongly influenced by synsedimentary faulting, as will be discussed below. At a deeper level, this faulting also had an impact on the structure of the Orri dome, which will be the subject of a next chapter.

SYNSEDIMENTARY FAULTING IN STEPHANO-PERMIAN SEDIMENTS

The Stephanian Malpas Formation and the conformably overlying Permian Peranera Formation (Figs. V.1 and V.2) are entirely composed of alluvial sediments (Nagtegaal, 1969), or, more specifically, continental redbeds in the case of the Permian. South of the Orri dome, the Peranera Formation crops out in the elongated La Seu basin and the associated Rubio-Vilamu basins further west (Fig. V.1; Speksnijder, 1985; chapter II). The Malpas Formation is only preserved in the La Seu basin. There is an important

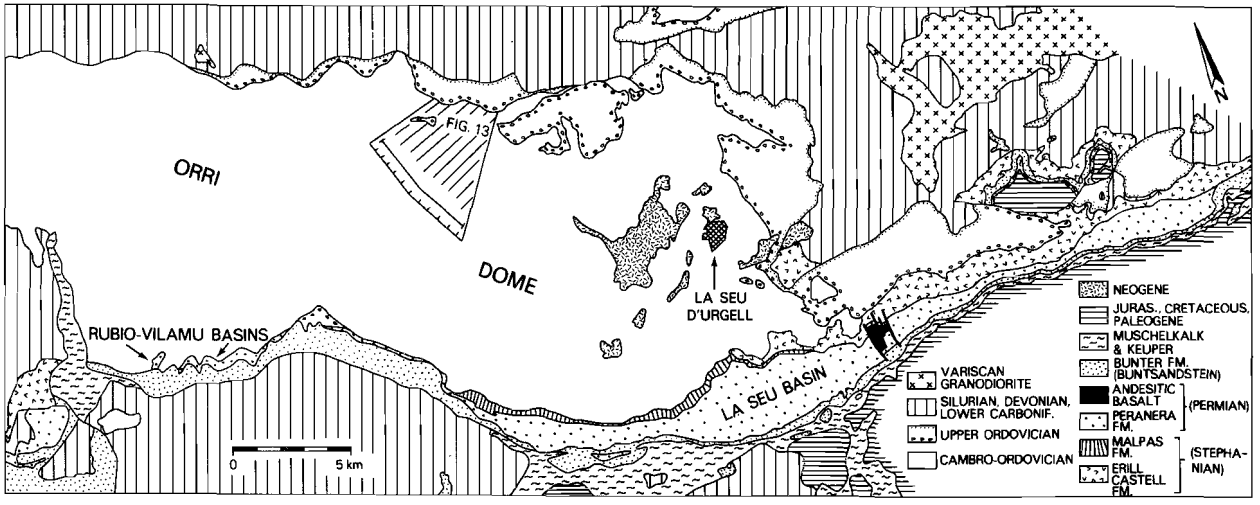
FIG. 13
ORRI
DOME
LA SEU D'URGELL
RUBIO-VILAMU BASINS
LA SEU BASIN
0
5 km
N
NEOGENE
JURAS., CRETACEOUS, PALEOGENE
MUSCHELKALK & KEUPER
BUNTER FM. (BUNTSANDSTEIN)
ANDESITIC BASALT
PERANERA FM.
(PERMIAN)
MALPAS FM.
ERILL CASTELL FM.
(STEPHANIAN)
VARISCAN GRANODIORITE
SILURIAN, DEVONIAN, LOWER CARBONIF.
UPPER ORDOVICIAN
CAMBRO-ORDOVICIAN

variation in thickness of the Permian redbeds: from a few hundred meters in the Rubio-Vilamu basins, up to 1500 m in the centre of the La Seu basin.

Three sedimentary facies associations can be distinguished in the Peranera Formation (Speksnijder, 1985; chapter II):

(1) The grabenfill facies association, ideally comprising from bottom to top: fossil scree deposits, debris-flow deposits (breccia and conglomerate), alluvial fan and ephemeral stream deposits (mainly sandstones), and a top of thick silts, which may comprise as much as half of the thickness of the grabenfill (Fig. V.3). The badly sorted cobbles and pebbles of the breccia facies are derived from the underlying basement and have been transported over only short distances. Breccia units are wedge-shaped and are situated at the downthrown sides of steep fault planes. Alluvial fan and ephemeral stream sediments classified with this facies association are only of limited extent.

The development of the grabenfill facies association is directly related to dip-slip movements on the border faults of the sedimentary basins. Its occurrence is restricted to the Rubio-Vilamu basins and parts of the La Seu basin adjacent to its boundary faults.

(2) The alluvial fan and ephemeral stream facies association mainly comprises water-laid conglomerates and (sometimes pebbly) sandstones and silt, organised in FU sequences. Conglomerate beds combine a large lateral extent along the basin strike (km scale) with a restricted thickness (not more than a few meters). Although the 45° dip of the beds does not allow for observations in directions at large angles to the basin-axis, indirect evidence shows that conglomerate beds are wedge-shaped. A strong correlation has been established between conglomerate bed thickness and maximum pebble diameter (Fig. V.4). As pebble-size decreases in directions away from the source in alluvial systems (Heward, 1978), it follows that conglomerate bed thickness must decrease away from the source, too. The same conclusion can

Fig. V.1. Geological map showing the Orri dome and post-Variscan sedimentary basins (modified after Hartevelt, 1970; and Zwart & Roberti, 1976). The position of the profile of Fig. V.13a, and the area covered by Figs. V.13b-d are indicated.

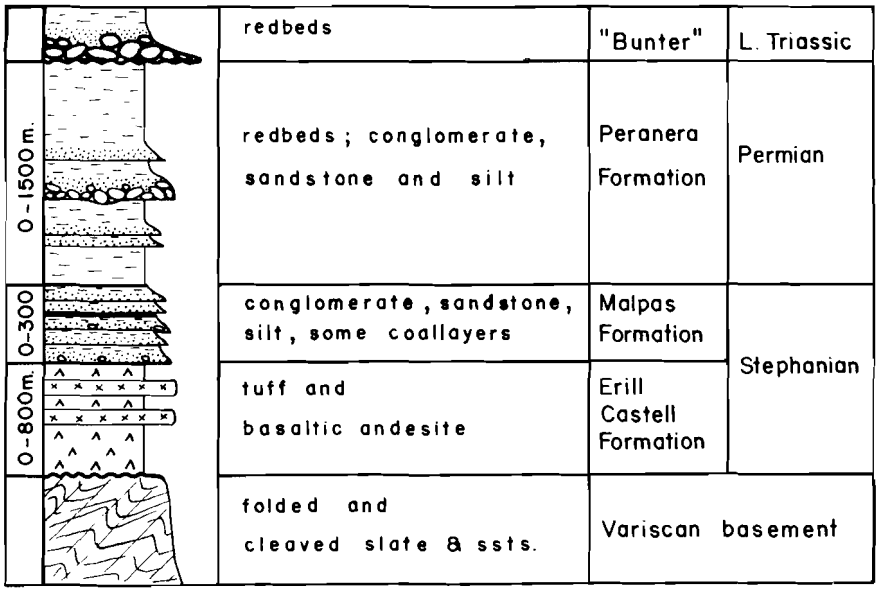

Fig. V.2. Generalised stratigraphical section of post-Variscan rocks in the south-central Pyrenees. No scale implied; thicknesses refer to the studied area.

be drawn from Fig. V.5, in which the dips of individual sandstone- and conglomerate beds within a coarsening-upward/fining-upward (CU-FU) alluvial fan unit have been plotted. Conglomerate beds (and combined conglomerate-sandstone sequences) thus form thin, strongly elongated wedge-shaped bodies that dip away from faultscarps along the basin edges. Sedimentary analysis

Fig. V.3. Sedimentary log from the centre of the Rubio-Vilamu basins as a typical example of grabenfill facies association deposits. Note the occurrence of pebbly mudstone interbedded with breccias in the lower 30 m of the section. The interval between 90 and 160 m consists entirely of silt.

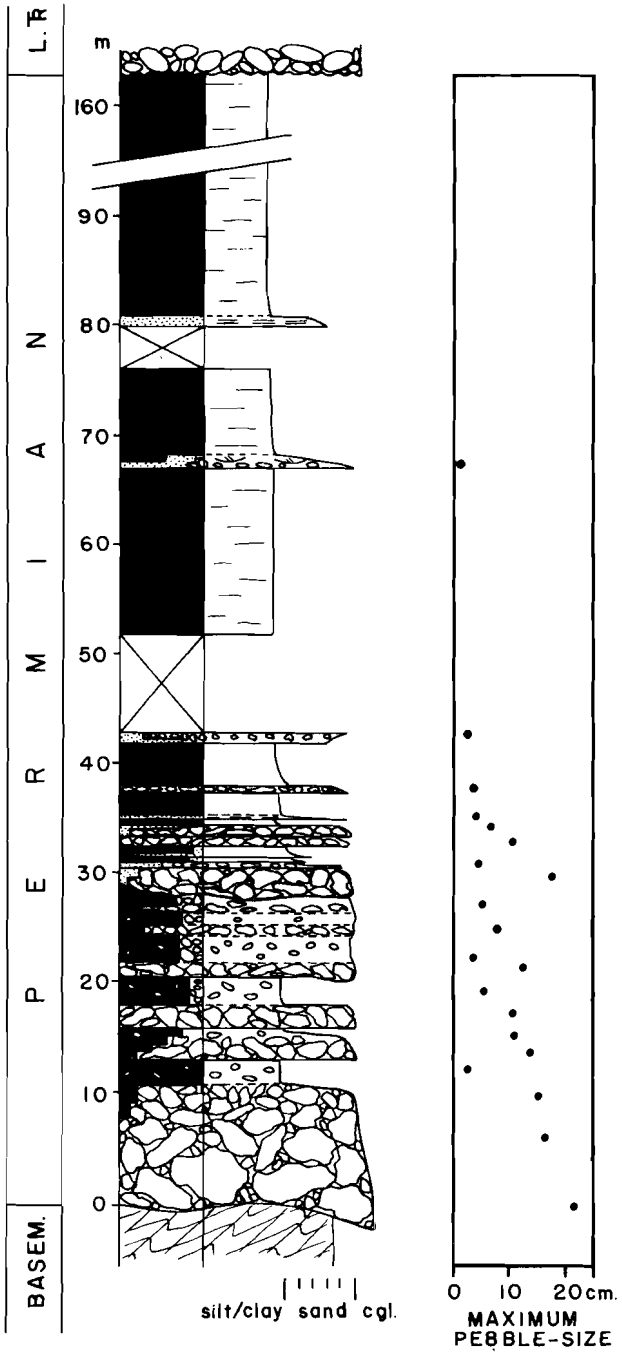
L.R.
PERMIAN
BASEM.
m
160
90
80
70
60
50
40
30
20
10
0
silt/clay sand cgl.
0 10 20cm.
MAXIMUM
PEBBLE-SIZE

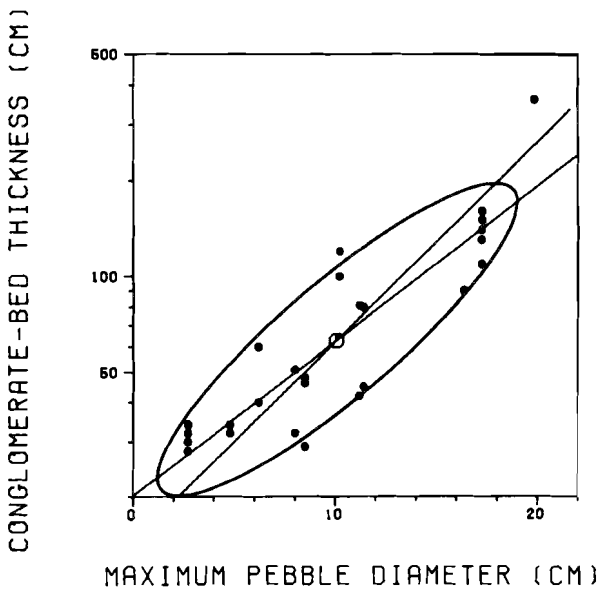

Fig. V.4. Relation between conglomerate bed thickness and maximum pebble diameter from a section in the centre of the La Seu basin. Number of readings: 26; correlation coefficient: 0.88. Regression lines x-on-y and y-on-x, and 75% confidence ellipse are shown.

indicates that most of the conglomerates are proximal alluvial fan sediments, dominated by debris flows in the upper fan reaches and ephemeral stream deposits lower down on the fans. Mineralogical composition and texture of the pebbles suggests that reworking of the sediments took place as a result of fault-scarp retreat and lowering of relief.

Pebbly sandstones, coarse cross-bedded sandstones and fine-grained sandstones were laid down as lateral and downstream equivalents of the conglomerates. The genesis of silts will be discussed in the next paragraph.

Towards the basin edges the deposits of this facies association may grade into coarser-grained rocks of the grabenfill association, while towards the basin interior they grade into the basinfloor facies association.

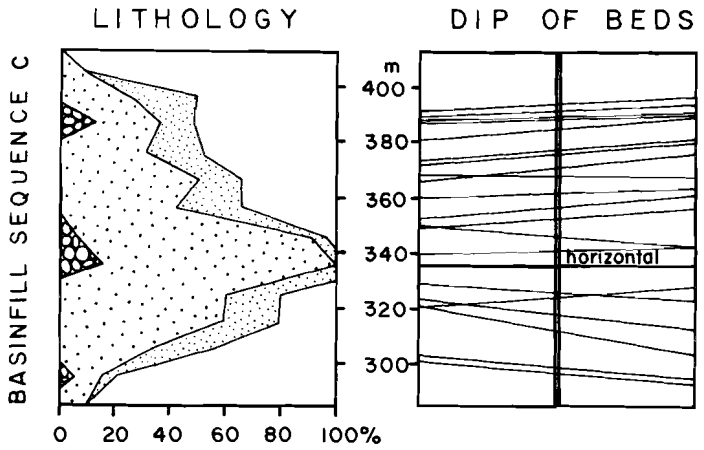

Fig. V.5. Wedge-shaped arrangement of conglomerate and sandstone beds in a major CU-FU megasequence of the La Seu basin. Vertical scale represents height above the base of the section. The left-hand part of the diagram shows lithotype distribution (conglomerate, coarse sandstone, fine sandstone, and silt). The right-hand part depicts dips of individual beds; the thickest conglomerate bed of the section (at 336 m) has been rotated to a horizontal position.

(3) The basinfloor facies association includes some (fine-grained) sandstones, but is mainly built of silt which comprises more than half of the total sediment volume of the La Seu basin. The larger part of the silts probably has an aeolian genesis, but intercalated thin limestone layers are interpreted as fossil sabkha deposits, developed from evaporation of ephemeral lakes that occupied shallow topographical depressions in the centre of the basin. This, and several other paleoclimatological indications, point to an environment of deposition comparable to the present-day savannahs and steppes (Nagtegaal, 1969; Gisbert, 1982). The lack of a permanent vegetational cover induced a direct response of sedimentary processes and products to structural events; therefore, interpretation of sedimentary facies and their distribution provides direct information about the structural setting of the basins.

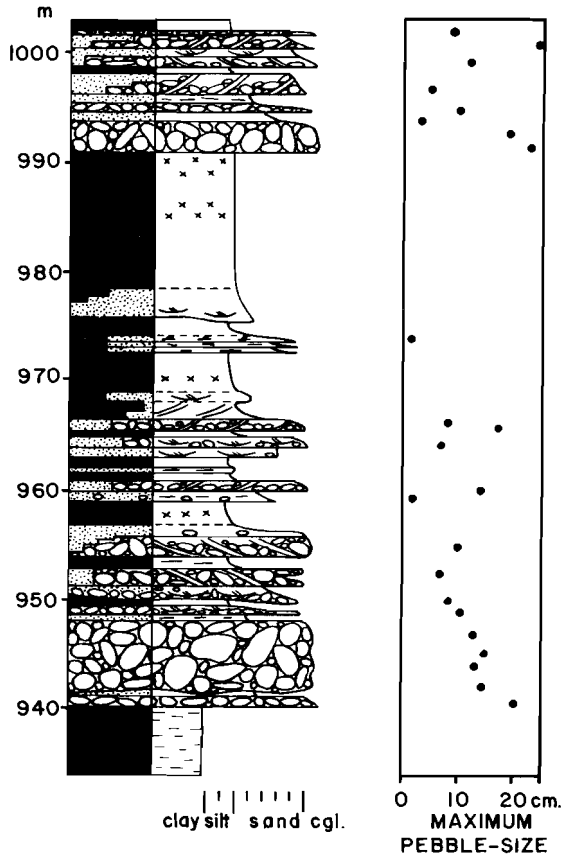

Fig. V.6. Fining-upward megasequence (between 940 and 990 m) in the central part of the La Seu basin. The base of an overlying FU unit is exposed above 990 m. Small crosses in silt intervals indicate calcite concretions (caliches).

A second approach to understanding the tectonic framework of the La Seu and Rubio-Vilamu basins is to study the sequential arrangement of their sediments. Three types of sequences have been distinguished (Heward, 1978; Speksnijder, 1985; chapter II):

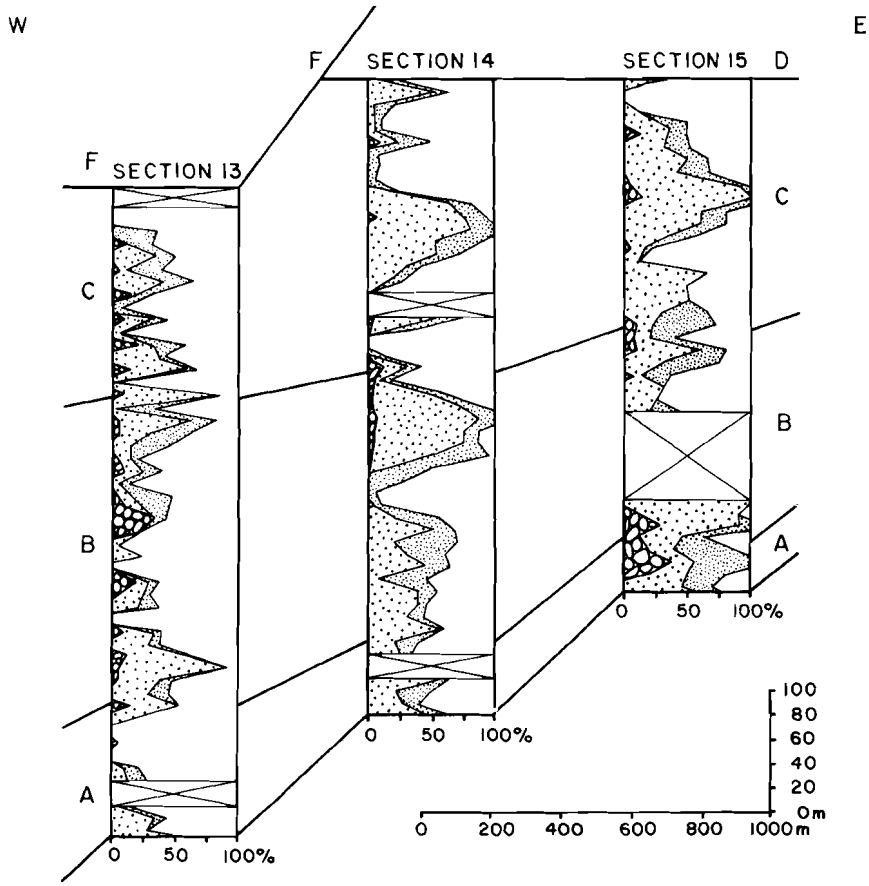

Fig. V.7. Symmetrical CU-FU megasequences in three sections measured in the central La Seu basin. Ornamentation as in Fig. V.5. Capitals refer to basinfill sequences (compare Figs. V.8 and V.10).

(1) "sequences", 1 - 10's m thick, consisting of a series of related beds. These are always organised in FU units, as confirmed by a Markov transition probability analysis. Sequences were laid down during single depositional events, directly or indirectly triggered by slip on the basin border faults. Their FU properties reflect waning current conditions during sedimentation.

(2) "megasequences", 10's - 100's of m thick, consisting of arrangements of related sequences. In some cases megasequences show stacking of several identical FU sequences, or alternatively show an overall FU tendency (Fig. V.6). In the central part of the La Seu basin, however, megasequences are usually of combined CU-FU nature (Fig. V.7). Symmetrical CU-FU megasequences must result from a gradual but increasing subsidence of the basinfloor up to a certain maximum rate, followed by a decrease of the vertical fault movement which eventually drops to zero.

(3) "basinfill sequences", consisting of a number of megasequences, are indicated in the strike section of Fig. V.8. The six basinfill sequences (A-F) are separated from each other by angular unconformities at the edges of the basin, but in the basin centre the succession is seemingly (para-?) conformable. The lower basinfill sequences are internally dominated by CU-FU megasequences, whereas the upper basinfill sequence is characterised by well-developed FU megasequences (mainly consisting of silt in their top parts).

The following kinematic history of the La Seu and Rubio-Vilamu basins can be deduced from the above observations: A phase of gentle, but increasing subsidence was followed by several phases of initially strongly accelerating but subsequently decelerating subsidence; these phases are generally separated by unconformities, suggesting that deformation and uplift of previously deposited strata has taken place. The last stage of basin development is characterised by a sudden major downward movement of the basinfloor, followed by decreasing subsidence and eventually very gentle regional downwarp of the whole basin.

Fig. V.8. True scale (above) and 10x vertical exaggerated (below) strike profile through the Rubio-Vilamu and La Seu basins along the southern border of the Axial Zone (see Fig. V.1). The base of the unconformably overlying Triassic rocks is supposed to be flat. Ornamentation shows (compare Fig. V.2): Erill Castell Formation (crosses), Malpas Formation (gray), basinfill sequences A-E of the Peranera Formation (unornamented), andesite (black), and basinfill sequence F of the Peranera Formation (stippled). Note that the basinfill sequences A-E are only fully developed west of the Ges Fault Zone in the La Seu Basin, whereas basinfill sequences C and D form the bases of the Peranera Formation east of the Ges Fault Zone and in the Rubio-Vilamu Basins.

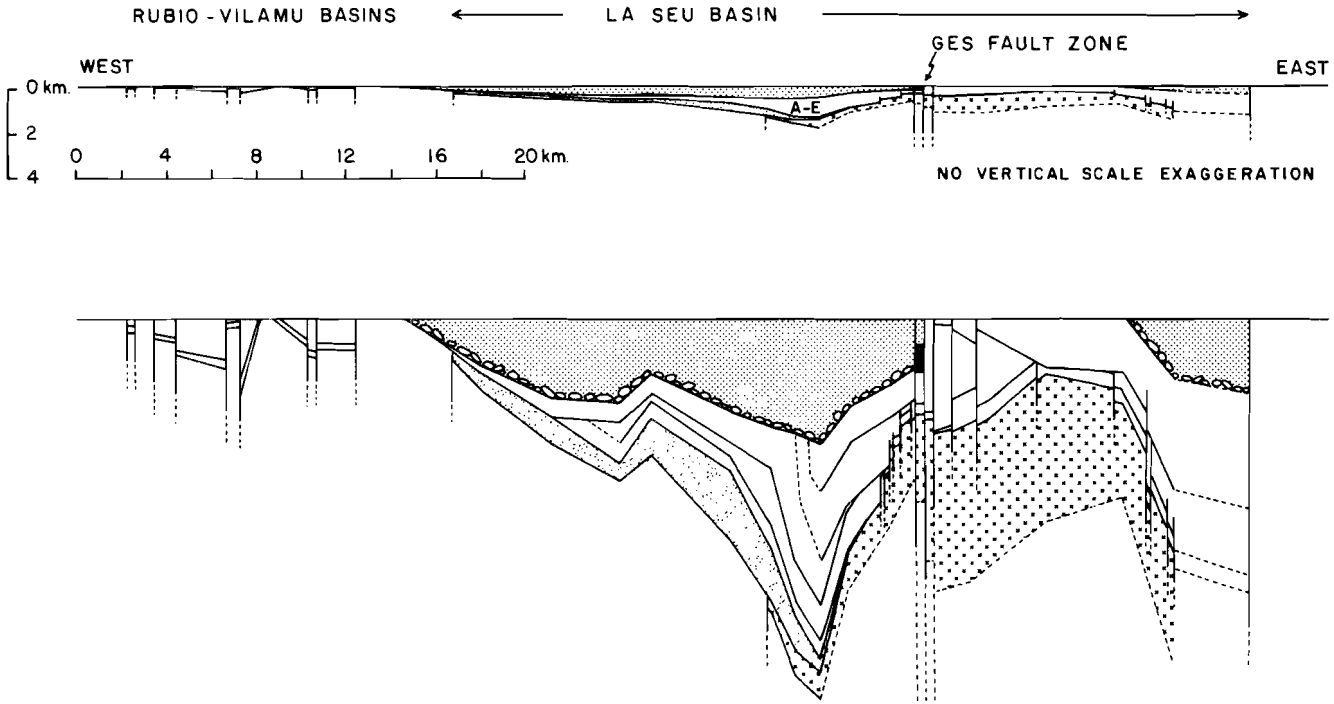
RUBIO - VILAMU BASINS
LA SEU BASIN
GES FAULT ZONE
WEST
EAST
0 km.
2
4
0
4
8
12
16
20 km.
A-E
NO VERTICAL SCALE EXAGGERATION

GEOMETRY AND STRUCTURAL ORGANISATION OF THE POST-VARISCAN BASINS

A study of paleocurrent directions (Fig. V.9) significantly contributes to our understanding of the geometry of the basins. Sediment transport in the Rubio-Vilamu basins is unidirectional and confined to narrow N-S running grabens that are perpendicular to the main La Seu basin. Paleocurrent directions within the La Seu basin itself show that sediment transport was mainly lateral, at right angles to the strike of the basin. The lack of dispersion of transport directions close to the border faults, and the very elongated wedge-shape of coarse-grained sedimentary units, both show that coalescing fans must have built out into the basin, together forming a bajada (Collinson, 1978). This suggests the existence of straight, continuous fault traces at the surface. In the basin centre, current directions often swing round (in relatively fine-grained fluviatile deposits), eventually to become parallel to the basin axis. Sediment transport was consistently towards the east.

The trace of the northern basin fault can be easily delineated, as the Permian north of the fault is either very thin or not present at all, while towards the south the sediment thickness amounts to an average 1000 m. The approximate position of the southern boundary fault is indicated by the outcrop of fault-related breccia deposits and a large flapfold, generated by vertical movement along the fault and subsequent decoupling of part of the sedimentary sequence (Fig. V.10). Also in this case the boundary fault appears to have a straight east-west trace.

Thus a picture emerges of an elongated sedimentary basin (length/width ratio =10, or more), bordered by straight E-W running faults, along which major dip-slip movement took place. The sudden deflection of lateral current directions into axial directions reveals the presence of secondary N-S

Fig. V.9. Semi-quantitative representation of paleocurrent directions in the Rubio-Vilamu and La Seu basins. Length and density of arrows are a measure for the number of readings; the whole diagram is based on 417 paleocurrent measurements. The positions of normal faults, the sense of movement upon them, and possible outline of alluvial fans are based on interpretation. Capitals refer to basinfill sequences in the Peranera Formation.

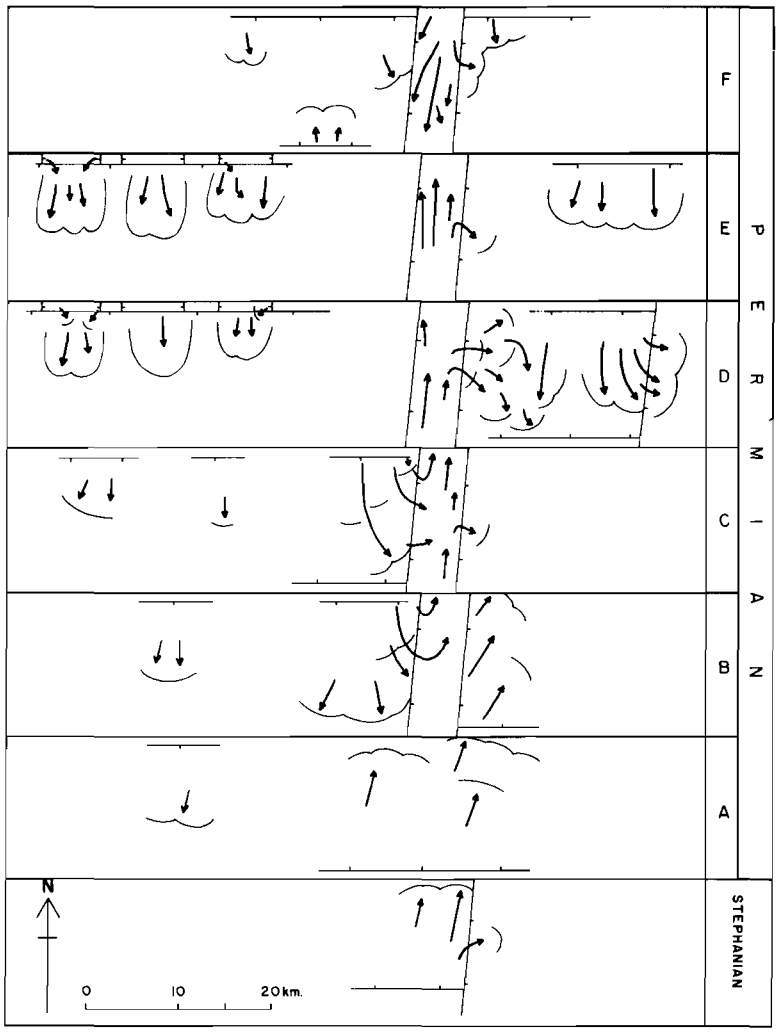
F
E
D
C
B
A
PERMIAN
STEPHANIAN
N
0
10
20km.

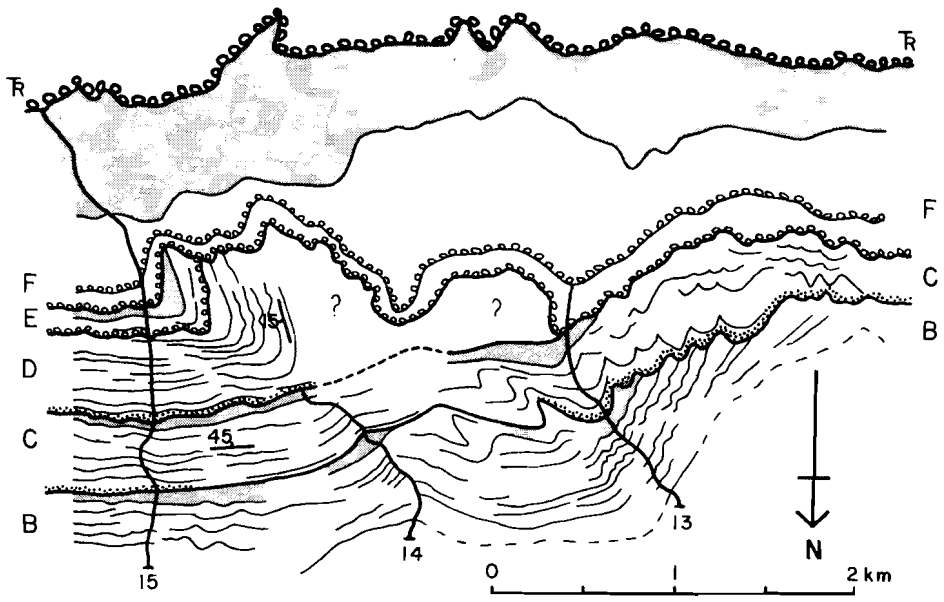

Fig. V.10. Map (drawn from aerial photographs) of flapfold in the central part of the La Seu basin. This gravitational structure developed as a result of detachment on the upper silt layer of Basinfill Sequence C (shown in gray), along the southern boundary fault of the basin (now hidden below younger deposits). The axis of the fold trended 100°-280° before Alpine rotation. The fold and surrounding sediments have been deeply eroded and the basal conglomerates of Basinfill Sequence F unconformably overlie older Permian rocks. The irregular bed traces in Basinfill Sequences B and C do not result from folding but from badland erosion. The three sections shown on this map are (partially) reproduced in Fig. V.7.

intrabasinal faults. The equally N-S trending Rubio-Vilamu grabens acted as lateral feeder channels to the La Seu basin.

Apart from indications for dip-slip offset along the straight boundary faults, there is also good evidence for lateral movements in the La Seu basin. As can be read from Fig. V.11, the basin depocentre migrated eastward over a considerable distance with time. Such a depocentre shift is considered to be indicative of the overall oblique-slip nature of the basin faults. Analysis of the available data (Speksnijder, 1985; chapter II),

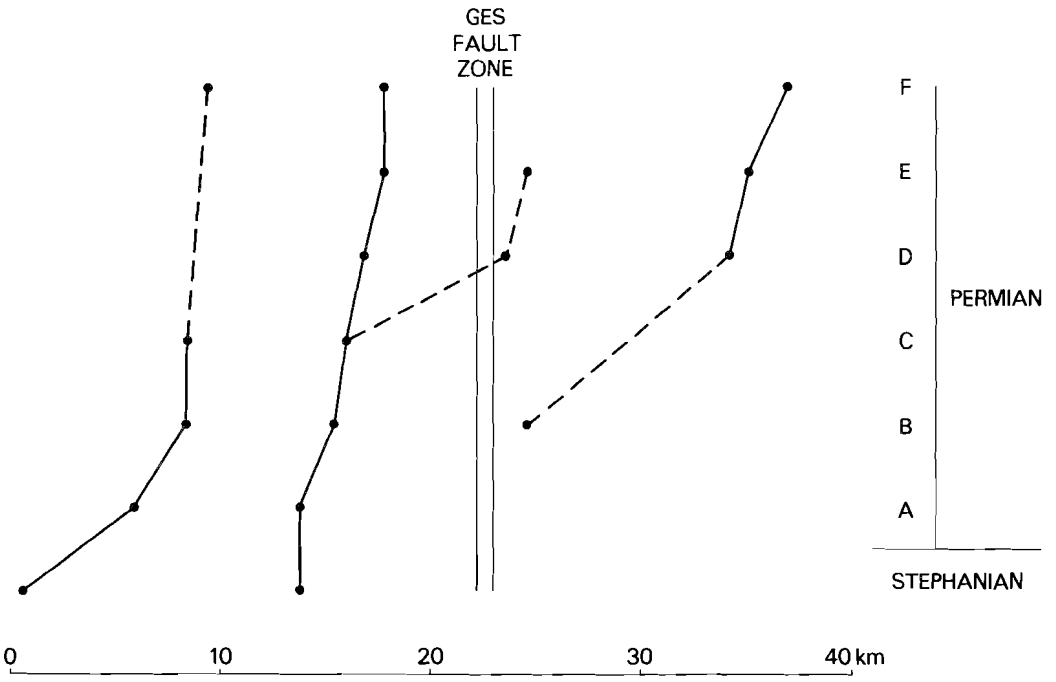

Fig. V.11. Migration of the depocentre of the La Seu basin with time. Capitals refer to basinfill sequences.

shows that the total horizontal displacement along the basin faults must have been in the order of 10 km (or more), compared to the maximum thickness of 1.5 km of the Permian sediments.

The La Seu basin is cut by a number of roughly N-S running faults (Fig. V.9), amongst them the Ges Fault zone depicted in Fig. V.8. This fault zone must reach deep into the crust, as andesitic basalts have extruded along its trace at the surface. The net dip-slip offset on the Ges Fault has nevertheless been very small during the Permian. The Ges Fault system, the Rubio-Vilamu boundary faults, and similar N-S faults of lesser magnitude are considered to be pre-existing zones of weakness or anisotropy planes that

influenced the evolution of the La Seu basin in detail, without, however, masking its overall oblique-slip character.

In conclusion, the post-Variscan sedimentary basins south of the Orri dome were generated in a major, E-W trending oblique-slip zone. The good correlation of megasequences and basinfill sequences emphasises the structural control on facies distribution and sequential arrangement of the deposits. This direct control was enhanced by semi-arid climatic conditions during the Permian.

The occurrence of angular unconformities between basinfill sequences points to alternating conditions of divergent and convergent oblique-slip faulting. Divergence resulted in strong subsidence of the basin floor and subsequent deposition, drape folding and outpouring of lava. Convergent phases are represented by the occurrence of erosional levels, angular unconformities and reverse faulting along N-S faults (such as the Ges Fault zone). Alternations of convergent and divergent wrenching are attributed to local changes in the regional stressfield caused by continuous movement on slightly curved strike-slip faults at depth (Reading, 1980). Still, the E-W basin boundary faults at the surface appear to have been rather straight and no convincing evidence has been found for en-echelon arrangement of secondary Riedel structures, which are considered typical for strike-slip zones (Tchalenko, 1970). One of the consequences of the absence of these secondary structures is that the sense of horizontal movement of the oblique-slip fault zone can not be directly established. Independent observations (to be discussed in the next chapter) indicate that the horizontal movement must have been right-lateral.

A conceptual block diagram of the La Seu and Rubio-Vilamu basins is shown in Fig. V.12.

Fig. V.12. Block diagram of the Rubio-Vilamu (left) and La Seu basins. Arrows indicate the sense of lateral movement on the basin boudary faults.

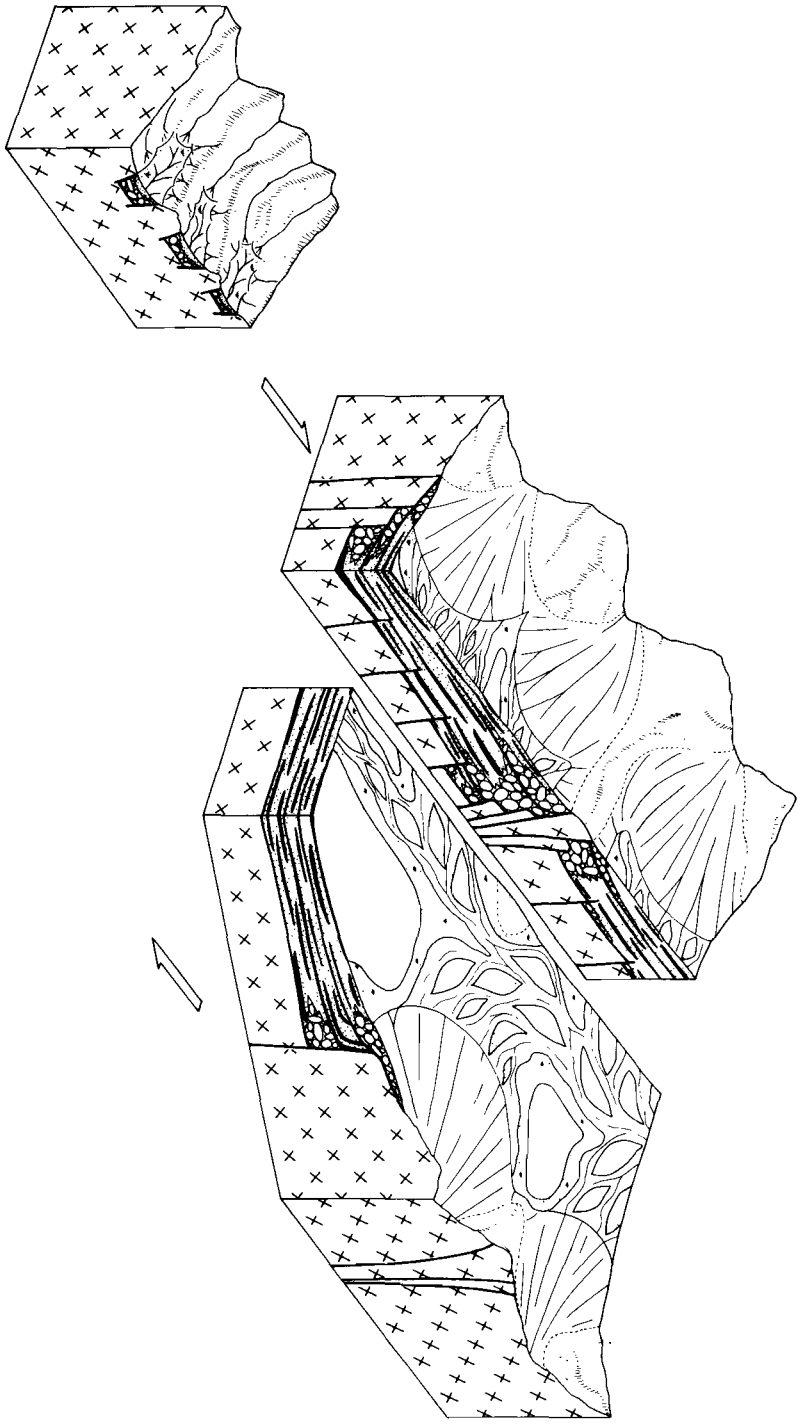

THE STRUCTURE OF THE BASEMENT IN THE ORRI DOME

The present-day outcrop of the Orri dome, which forms part of the structural basement of the La Seu and Rubio-Vilamu basins, has been shaped by interference of several Variscan, post-Variscan, Alpine and post-Alpine deformational events (Speksnijder, 1986b; chapter IV). The impact of Late Paleozoic shearing on the basement can only be appreciated after a detailed structural analysis of the Orri dome and direct surroundings, the results of which have been reported elsewhere (Speksnijder, 1986a, 1986b; chapters III and IV). In the following a concise description of the structural evolution of the dome will be presented.

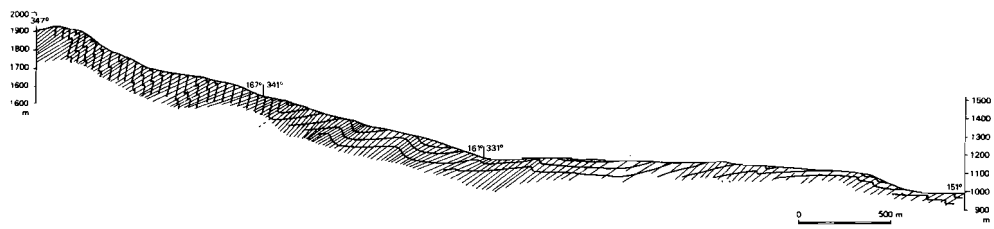

Fig. V.13. (a) (above) Structural profile through the north-central Orri dome, showing mainphase cleavage and sedimentary bedding (thick lines). This profile is in part conceptual as no marker horizons can be traced in the monotonous Cambro-Ordovician rocks. The broad undulations on the flat-lying mainphase foldlimb are caused by pre-mainphase folding. Location in Fig. V.1.
(b-d) (right) Stereographic projections of directional data related to mainphase structures from the area indicated in Fig. V.1. (b) Poles to sedimentary bedding. Number of measurements: N=1140; contours represent 0.09, 0.18, 0.44, 0.88, 2.19, 4.39, and 6.58% per 1% area. (c) Poles to mainphase cleavage. N=763; contours represent 0.1, 0.3, 0.7, 1.3, 3.2, 6.6, and 13.1% per 1% area. (d) Intersection lineations of sedimentary bedding and mainphase cleavage; and small-scale mainphase foldaxes. N=928; contours represent 0.1, 0.2, 0.5, 1.1, 2.7, 5.4, 8.1, and 10.8% per 1% area.

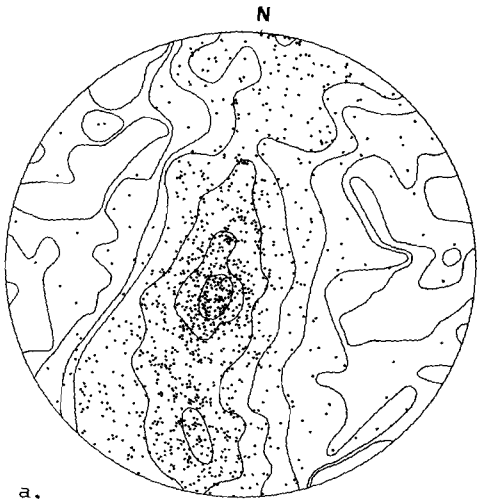

a.

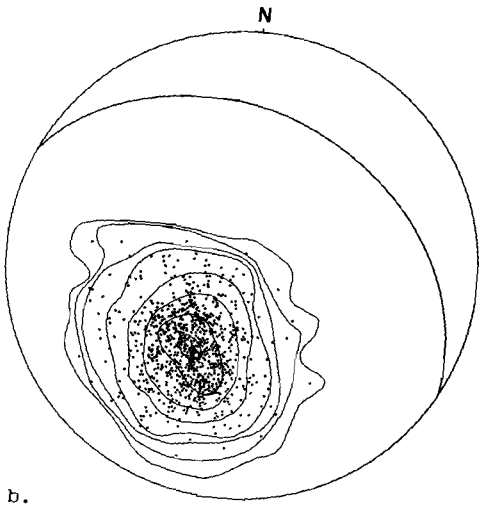

b.

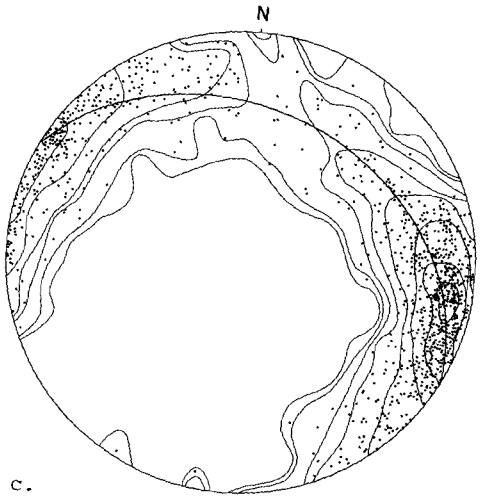

c.

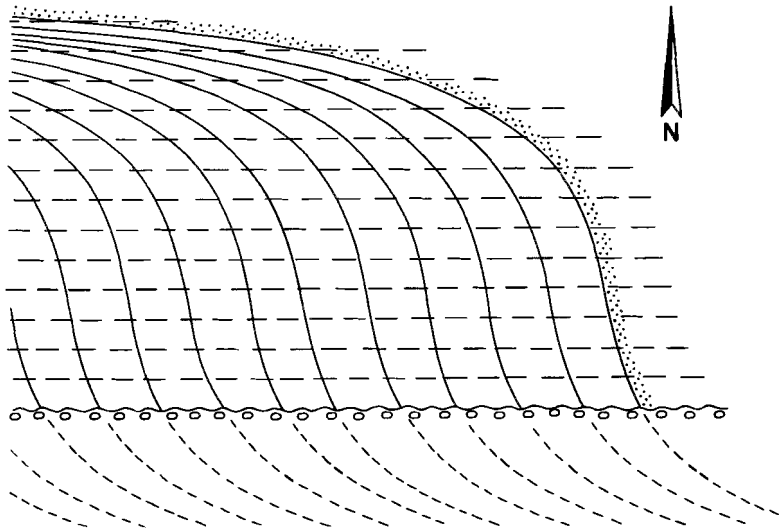

Fig. V.14. Schematic cleavage trend map of the eastern Orri dome. As a result of macroscopic D_{V4} and D_{PV1} deformation, the orientation of the D_{V3} cleavage changes from north-dipping in the north to east-dipping in the eastern part of the dome (and probably north again below the Variscan unconformity). Note the right-lateral sense of D_{PV1} movement.

After deposition of thick shallow marine sediments of Cambro-Ordovician age, the first important deformation in the south-central Pyrenees took place during the Devonian and the Early Carboniferous, when basin differentiation was induced by right-lateral oblique-slip. The onset of the Variscan orogeny in the Late Carboniferous resulted in the generation of early, very open macroscopic folds with N-S and E-W axes and subvertical axial planes. These folds can not be observed in outcrop in the Orri dome; their presence can only be traced by means of statistical analysis of orientation data (Speksnijder, 1986a; chapter III). The early Variscan deformation generations are referred to as D_{V1} and D_{V2}. In contrast, so-called mainphase (D_{V3}) folds of the Variscan deformation can be traced

throughout the Axial Zone. They usually are asymmetrical south-vergent structures with gently north dipping long limbs and overturned, steeply north dipping short limbs. The folds, which occur an any scale between a few mm and some km, are cut by a well-developed 40° - 60° north dipping axial plane cleavage (Fig. V.13). In the central part of the Orri dome mainphase folds strike WNW-ESE, but in the eastern part they have been strongly reoriented to a N-S strike due to a first Variscan refolding (D_{V4}) and post-Variscan shearing (Fig. V.14). Like mainphase structures, D_{V4} folds occur an any scale from a few mm to some km. They have steep E-W striking axial planes and the folds are asymmetrical, their long limbs normally dipping north (Fig. V.15). Refolding was most intense in the eastern and southeastern part of the Orri dome and as a consequence penetrative steep D_{V4} cleavages are well developed in that area.

The Variscan structures described above have been affected by later D_{V5} folds and minor D_{V6} kinkbands. D_{V5} folds are either mesoscopic chevron-type structures, with very steep N-S axial planes and sometimes a penetrative axial plane foliation, or they are gentle macroscopic folds lacking an axial plane cleavage. The D_{V6} kinkbands have only developed on long mainphase foldlimbs, where they deform the subhorizontal bedding plane, sometimes in conjugate sets. The kinkbands, which strike NW-SE or NE-SW, were generated by subhorizontal shortening with an E-W component, in analogy to D_{V5} folds. The occurrence of kinkbands at a large angle to the general strike of the Pyrenees marks the end of the Variscan orogenic cycle.

Post-Variscan deformation in the southern Pyrenees is characterised by N-S extension and lateral E-W movements (Speksnijder, 1986b; chapter IV). Extension resulted in a general, south directed fanning of Variscan cleavages (D_{PV2}), and development of extensional kinkbands (D_{PV3}) in the southeastern part of the dome. Lateral movements are expressed by right-lateral shearing (D_{PV1}) along pre-existing E-W and ESE-WNW anisotropy planes such as D_{V3} and D_{V4} cleavages. Cleavage planes which were not favourably oriented with respect to the stressfield related to the lateral movements (Gibson, 1985) were deformed by the D_{PV1} shearing.

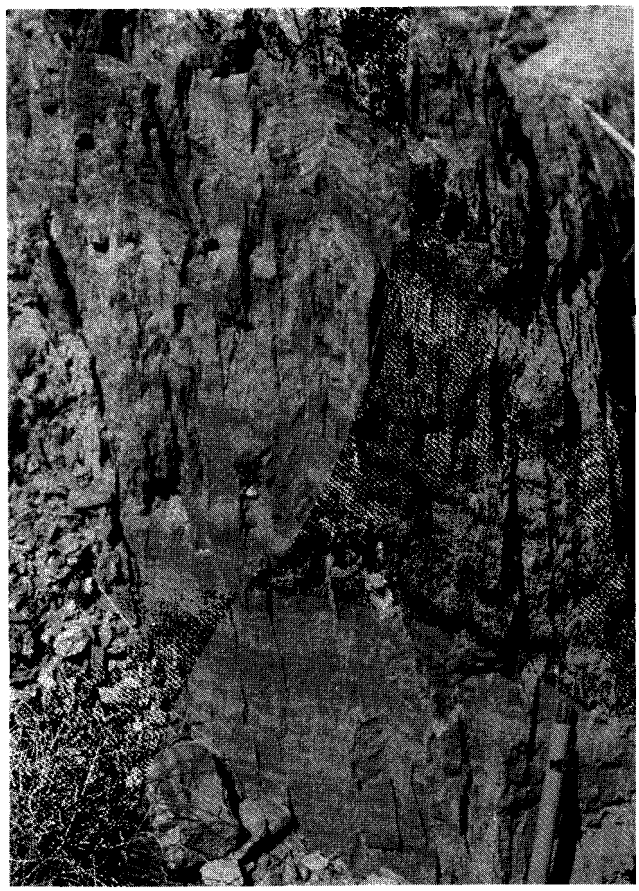

Fig. V.15. Mesoscopic D_{V4} foldhinge, showing steep axial plane cleavage developed on a long, subhorizontal D_{V3} foldlimb. North is towards the right.

The stereographic projections of Fig. V.16a-c show the reorientation of D_{V3} cleavage induced by post-D_{V3} deformation in three areas of the Orri dome. In all three cases apparent foldaxes are defined, which, together with a large number of apparent foldaxes from other areas, plot on a great circle (Fig. V.16d). This lineation redistribution pattern suggests a simple-shear type of deformation (Ramsay, 1967). Slip directions of simple shear can be

found as the intersection lines between the lineation distribution plane and possible shear planes (Fig. V.16e). It turns out that the average shear direction plunges slightly towards the east. Shallow east dipping thrust planes with N-S strike, more or less parallel to the foldaxes redistribution plane, have been mapped directly east of the Orri dome by Hartevelt (1970).

The sense of lateral movement along E-W and ESE-WNW striking planes can be determined from Figs. V.14 and V.17. The redistribution of D_{V4} and D_{V5} cleavages is shown in the stereographic projection of Fig. V.17a, while Fig. V.17b is a simplified structural trend map revealing the consistent eastward bending of N-S striking D_{V5} cleavages (going from south to north), thus indicating dextral displacement of simple-shear type on a macroscopic scale. Note that the D_{V4} cleavage is relatively little reoriented compared to the D_{V5} cleavage, in spite of the fact that it was deformed during D_{V5} folding. This observation emphasises the D_{V4} cleavage-parallel direction of basement shearing in the southeastern part of the Orri dome. As stated before, shear may have taken place along D_{V3} cleavage in other parts of the dome, but in this case the mainphase cleavage was folded instead.

Post-Variscan movements ceased in the Triassic (Soula et al., 1979), and no record of Mesozoic or Early Tertiary deformation is left in the Orri dome (compare Souquet et al., 1977). Alpine orogenic shortening in the Eocene resulted in foreland directed emplacement of large nappe systems in the southern Pyrenees. Movement mainly concentrated on a décollement level within Triassic evaporites south of the Axial Zone (Séguret, 1970), whereas deep-seated thrusts affected the Variscan rocks further north (Williams, 1985). Thrusting within the Orri dome, and antiformal stacking of thrusted units below it, both induced a strong rotation of Variscan structures in the vertical plane. The D_{V3} cleavage now locally dips 30° south in the plunging noses of thrusted units along the southern rim of the Orri dome, compared to the 60° N dip in its northern part (Speksnijder, 1986b; chapter IV).

Post-Alpine deformation (of Neogene age) has been of similar nature as post-Variscan deformation: N-S extension combined with a lateral component of movement which was sinistral in this instance. The occurrence of a very large earthquake east of the Orri dome, some 500 years ago, indicates that faulting is still actively going on (Fourniguet et al., 1981).

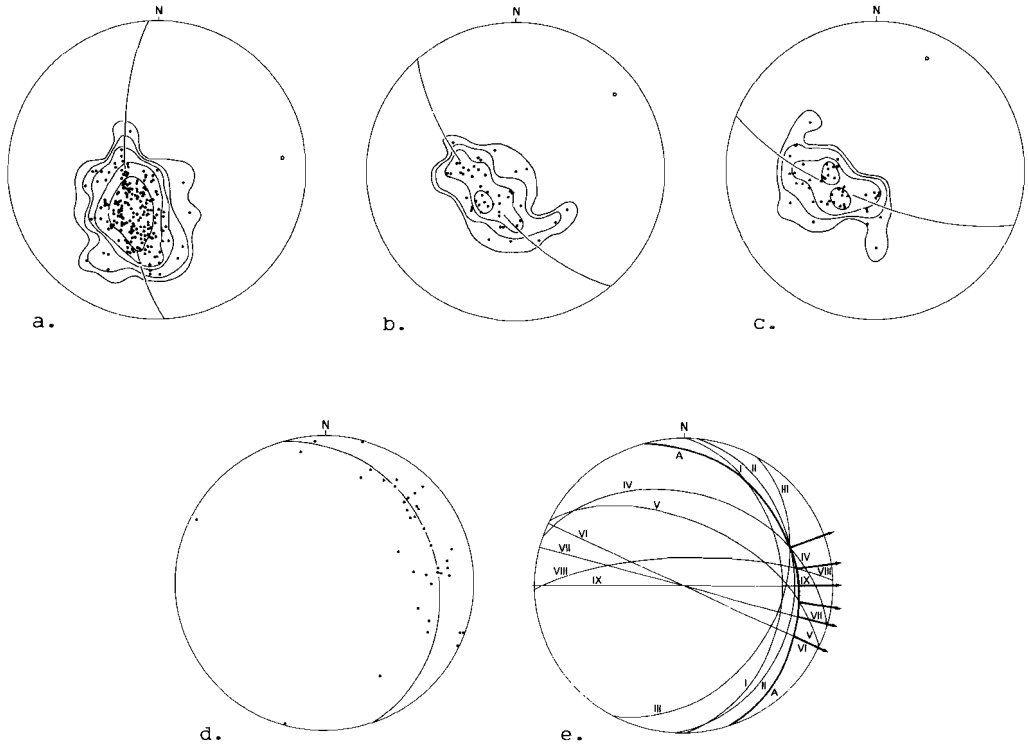

Fig. V.16. Reorientation of D_{V3} cleavages by D_{PV1} deformation. For details see Speksnijder (1986b; chapter IV).
(a-c) Poles to mainphase cleavage in three subareas of the Orri dome, with orientation of apparent foldaxes. Number of measurements: a. N=195; b. N=45; c. N=46. (d) Apparent foldaxes of mainphase cleavages from 38 subareas in the Orri dome, including the axes shown in Figs. V.16a-c. The great circle represents the redistribution plane of the foldaxes. (e) D_{PV1} shear directions (heavy arrows) as intersection lines between possible shear (anisotropy) planes, labelled I-IX, and the redistribution great circle (A) of Fig. V.16d. Possible shear planes are either parallel to the redistribution plane (I-III), or a shallow east plunging shear direction is indicated (IV-IX).

a.

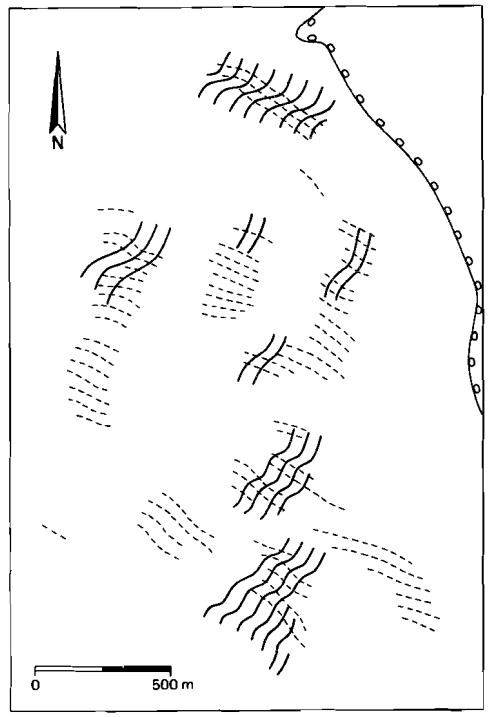

b.

Fig. V.17. Redistribution of D_{V4} and D_{V5} cleavage caused by post-Variscan shear in the southeastern Orri dome.
(a) Equal area projection of poles to D_{V4} cleavage (NNW-SSE to ENE-WSW strike), and poles to D_{V5} cleavage (N-S to NE-SW strike). As discrimination between these cleavages is often difficult to make in the field, no attempt has been made to distinguish them in this projection. N=366, contours represent 0.3, 0.5, 1.4, 2.7, and 5.5% per 1% area. (b) Simplified structural trend map showing deformed D_{V5} (full drawn lines) and D_{V4} (stippled) cleavages. Upper Ordovician formations crop out in the upper right corner of the map. For explanation see text.

PALEO-DEPTH OF BASEMENT SHEARING

As a result of strong Tertiary uplift of the Axial Zone, mainly attributed to Eocene thrusting, the Variscan unconformity now dips 45° south. Basement and cover rocks experienced a similar tilt, so that parts of the basement once directly underlying the La Seu basin now crop out to the north of the post-Variscan basins. If we assume a broad monoclinal shape for the deformed Variscan unconformity plane (Hartevelt, 1970), the maximum "paleo-depth" of the presently exposed basement can be calculated to be in the order of 4 km below the Permian sedimentary surface. The effects of erosion in post-Variscan times, which may have removed large volumes of rock, have not been taken into account in this approximation; therefore it is estimated that most of the Variscan basement outcropping in the Orri today was at a depth of 4 - 5 km during the Permian.

The monotonous Cambro-Ordovician slates and sandstones of the Orri dome are non- to low-grade metamorphic; some pumpellyite crystals encountered in these rocks (Kaars Sijpesteyn, pers.com., 1986) suggest a depth of 8 - 13 km during metamorphosis, assuming "normal" P-T gradients. It is well known, however, that an anomalously high heat flow characterises the Variscan orogeny in the Pyrenees (Zwart, 1979), so that the minimum depth of the upper boundary of the prehnite-pumpellyite facies may have been considerably less than 8 km.

As a conservative guess it is estimated that the post-Variscan shearing observed in the Orri dome today occurred at a depth of 4 - 5 km, not very far above the brittle-ductile transition zone which spans the prehnite-pumpellyite facies and the lower greenschist facies (Sibson, 1983).

Some large domes that crop out in the central part of the Axial Zone (Fig. V.1) are similar to the Orri dome as far as their macroscopic structure is concerned. At the present level of erosion, however, they differ from the Orri dome in that a metamorphic core is exposed in their centre, distincted by the occurrence of a flat lying foliation. Based on this observation, Zwart (1962) made a distinction between a low-grade suprastructure, dominated by steep axial plane cleavages and a relatively simple structures, and a metamorphic infrastructure (upper greenschist to amphibolite facies) with subhorizontal foliations and a complex

deformational history. The Orri dome typically belongs to the suprastructure, while the Aston massif, described by Soula (1982) and Verhoef et al. (1984), forms a representative part of the infrastructure. Verhoef et al. (1984) demonstrate that the flattish attitude of the foliation results from thermally induced vertical shortening, leading to partial transposition of older steep foliations.

The strong difference in structural development and metamorphic grade between infra- and suprastructure in the Pyrenees is interpreted to mark the brittle-ductile transition (compare Gibson & Gray, 1985). The Aston metamorphic evolution suggests a depth of 7 km or more for the upper boundary of the transition zone (Verhoef et al., 1984), in correspondance with our indirect conclusions regarding its depth in the Orri dome.

SUMMARY AND DISCUSSION

The E-W to ESE-WNW directed anisotropies in the Variscan basement determined the orientation of the post-Variscan La Seu basin. The basin was generated in an overall divergent oblique-slip setting, involving N-S extension and dextral lateral movement.

In a dynamic sense, the lateral movement along the basin boundary faults requires σ_1' and σ_3', the maximum and minimum components of (effective) stress, to have been horizontal during faulting. The extension at right angles to the basin indicates that the regional σ_3' direction was at a large angle to the boundary faults, at least larger than predicted by the Mohr-Coulomb criterion for brittle faulting. The normal stress acting upon the faults must have been of small magnitude and as a consequence the fault traces are rather straight. If Riedel shears developed at all, they made very small angles to the strike of the basin (Sanderson & Marchini, 1984). In addition, they would have soon joined up into one, more or less straight through-going fault at the surface in view of the large total lateral offset in the basin. Similarly, the relatively small normal stresses upon E-W to ESE-WNW Variscan cleavage planes facilitated shear movement upon them (Fig.

I. SHEAR PLANE STRIKES 90° - 270°

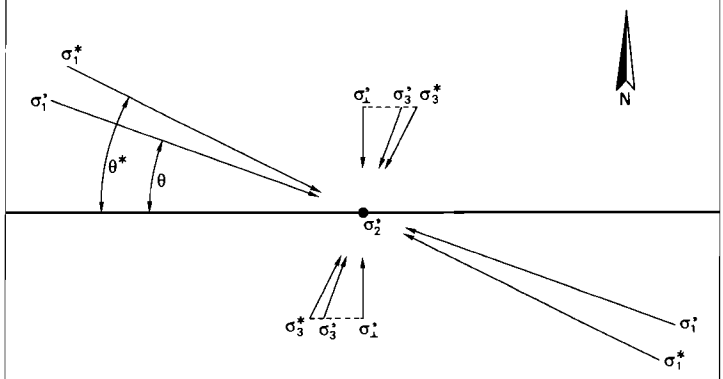

$\sigma_1^* = 1.000$ $\sigma_1' = 1.000$

$\sigma_3^* = 0.250$ $\sigma_3' = 0.238$ $\theta^* = 26.5°$

$\sigma_\perp^* = 0.224$ $\sigma_\perp' = 0.224$ $\theta = 20.0°$

II. SHEAR PLANE STRIKES 100° - 280°

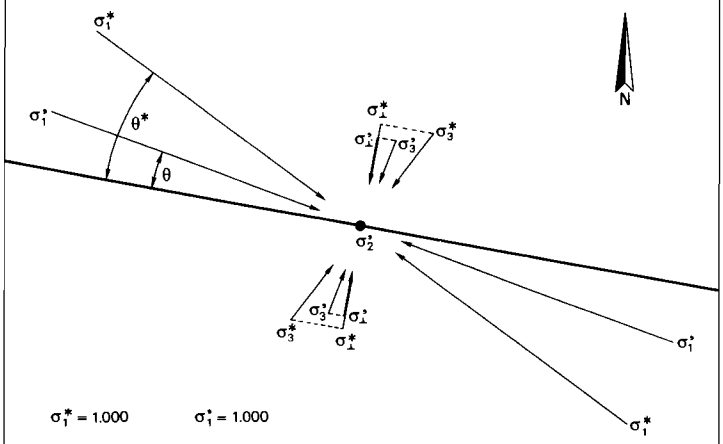

$\sigma_1^* = 1.000$ $\sigma_1' = 1.000$

$\sigma_3^* = 0.250$ $\sigma_3' = 0.165$ $\theta^* = 26.5°$

$\sigma_\perp^* = 0.224$ $\sigma_\perp' = 0.162$ $\theta = 10.0°$

V.18). The occurrence of post-Variscan cleavage fanning and extensional kinkbands further add to our interpretation of the paleo-stressfield.

Shear on individual anisotropy planes above the brittle-ductile transition in the basement distributed the total strain over a relatively large area, thereby resembling a simple-shear mechanism of deformation which typically occurs below the transition zone (Sibson, 1983). Genuine ductile deformation in E-W trending Variscan mylonites north of the Orri dome has been described by Lamouroux et al. (1981). The large width of the basement shear zone compared to the width of the La Seu basin at the surface may reflect a broadening downward of entire fault system (Sibson, 1983).

The magnitudes of throw and lateral offset of the post-Variscan fault system, the distance over which it extends in depth and along strike, its parallelism to the general Variscan orogenic trend, the outpouring of andesitic basalt, its reactivation as left-lateral fault system during the Neogene, and many other indications, all confirm that it must be considered a fundamental fault system which reaches down into the crust far below the brittle-ductile transition and has remained intermittently active for a long period of geological time.

Fig. V.18. Schematic representation of stress conditions required for dextral frictional shear on pre-existing cleavage planes (heavy lines). Two cases are considered: (I) shear plane strikes 90°-270° (e.g. D_{V4} cleavage), and (II) shear plane strikes 100°-280° (e.g. D_{V3} cleavage). For both cases the optimum reactivation direction of the maximum principal stress component is indicated (σ_1^*), which is determined by the optimum reactivation angle Θ^* required for renewed shear on existing planes of weakness (see Gibson, 1985). The magnitude of σ_1^* is arbritrarily chosen unity, and it follows that σ_3^*=0.250 and the normal stress $\sigma_\perp^*$=0.224. If the regional maximum component of effective stress (σ_1') makes a relatively small angle with the cleavage planes, and is for example directed 110°-290°, then $\sigma_3' < \sigma_3^*$. In the examples discussed here normal stresses are related as $\sigma_\perp' \leqslant \sigma_\perp^*$.

It is evident that the normal stress on the anisotropy plane is of small magnitude compared to the maximum principal stress, thereby facilating frictional shear on the existing cleavage planes.

REFERENCES

Collinson, J.D. (1978). Alluvial sediments. In: H.G. Reading (Editor), Sedimentary Environments and Facies. Blackwell, Oxford, pp. 15-60.

Fourniguet, J., Vogt, J. & Weber, C. (1981). Seismicity and recent crustal movements in France.
Tectonophysics, 71, pp. 195-216.

Gamond, J.F. (1983). Displacement features associated with fault zones: a comparison between observed examples and experimental models.
J.Struct.Geol., 5, pp. 33-45.

Gibson, R.G. & Gray, D.R. (1985). Ductile-to-brittle transition in shear during thrust sheet emplacement, Southern Appalachian thrust belt.
J.Struct.Geol., 7, pp. 513-525.

Gisbert, J. (1981). Estudio geológico-petrológico del Estefaniense-Pérmico de la Sierra del Cadí (Pirineo de Lérida).
Tesis doctoral, Departemento de Petrología, Universidad de Zaragoza, 313 pp.

Grocott, J. (1977). The relationship between Precambrian shear belts and modern fault systems.
Jl.geol.Soc.London, 133, pp. 257-262.

Grocott, J. (1981). Fracture geometry of pseudotachylyte generation zones: a study of shear fractures formed during seismic events.
J.Struct.Geol., 3, pp. 169-178.

Hartevelt, J.J.A. (1970). Geology of the Upper Segre and Valira Valleys, Central Pyrenees, Andorra/Spain.
Leidse Geol.Meded., 45, pp. 167-236.

Heward, A.P. (1978). Alluvial fan sequence and megasequence models: with examples from Westphalian D- Stephanian B coalfields, northern Spain.
In: A.D. Miall (Editor), Fluvial Sedimentology. Mem.Can.Soc.Pet.Geol., 5, pp. 669-702.

Lamouroux, C., Soula, J.C. & Roddaz, B. (1981). Les zones mylonitiques des massifs de Bassiès et de l'Aston (Haute Ariège).
Bull.Bur.Rech.géol.min.Fr., 2, pp. 103-111.

Macaudière, J. & Brown, W.L. (1982). Transcrystalline shear fracturing and pseudotachylyte generation in a meta-anorthosite (Harris, Scotland).
J.Struct.Geol., 4, pp. 395-406.

Mey, P.H.W. (1968). Geology of the Upper Ribagorzana and Tor Valleys, Central Pyrenees, Spain.
Leidse Geol.Meded., 41, pp. 229-292.

Mey, P.H.W., Nagtegaal, P.J.C., Roberti, K.J. and Hartevelt, J.J.A. (1968). Lithostratigraphic subdivision of post-Hercynian deposits in the South-Central Pyrenees, Spain.
Leidse Geol.Meded., 41, pp. 221-228.

Nagtegaal, P.J.C. (1969). Sedimentology, paleoclimatology, and diagenesis of post-Hercynian continental deposits in the south-central Pyrenees, Spain.
Leidse Geol.Meded., 42, pp. 143-238.

Obee, H.K. & White, S.H. (1985). Faults and associated fault rocks of the Southern Arunta block, Alice Springs, Central Australia.
J.Struct.Geol., 7, pp. 701-712.

Ramsay, J.G. (1967). Folding and fracturing of rocks.
McGraw-Hill, New York, 568 pp.

Ramsay, J.G. (1980). Shear zone geometry: a review.
J.Struct.Geol., 2, 1/2, pp. 83-100.

Reading, H.G. (1980) Characteristics and recognition of strike-slip fault systems. In: P.F. Ballance and H.G. Reading (Editors), Sedimentation in Oblique-Slip Mobile Zones. Spec.Publ.Int.Assoc.Sedimentol., 4, pp. 7-26.

Sanderson, D.J. & Marchini, W.R.D. (1984). Transpression.
J.Struct.Geol., 6, pp. 449-458.

Séguret, M. (1970). Etude tectonique des nappes et séries décollées de la partie centrale du versant sud des Pyrénées.
Ph.D. thesis, Montpellier, 155pp.

Sibson, R.H. (1977). Fault rocks and fault mechanisms.
Jl.geol.Soc.London, 133, pp. 191-214.

Sibson, R.H. (1983). Continental fault structure and the shallow eartquake source.
Jl.geol.Soc.London, 140, pp. 741-767.

Sibson, R.H. (1985). A note on fault reactivation.
J.Struct.Geol., 7, pp. 751-754.

Simpson, C. (1985). Deformation of granitic rocks across the brittle-ductile transition.
J.Struct.Geol., 7, pp. 503-511.

Soula, J.-C. (1982). Characteristics and mode of emplacement of gneiss domes and plutonic domes in the central-eastern Pyrenees.
J.Struct.Geol., 3, pp. 313-342.

Soula, J.-C., Lucas, C. & Bessière, G. (1979). Genesis and evolution of Permian and Triassic basins in the Pyrenees by regional simple shear acting on older Variscan structures: field evidence and experimental models.
Tectonophysics, 58, pp. T1-T9.

Souquet, P., Peybèrnes, B., Bilotte, M. & Debroas, E.-J. (1977). La chaîne alpine des Pyrénées.
Géologie alpine, 53, pp. 193-216.

Speksnijder, A. (1985). Anatomy of a strike-slip fault controlled sedimentary basin, Permian of the southern Pyrenees, Spain.
Sediment.Geol., 44, pp. 179-223 (Chapter II of this thesis).

Speksnijder, A. (1986a). The detection and significance of early deformation in the southern Variscan Pyrenees, Spain; implications for regional Paleozoic structural evolution.
Geol.Rundschau (Chapter III of this thesis).

Speksnijder, A. (1986b). The structural development of the Orri dome, southern Variscan Pyrenees, Spain.
Eclogae geol.Helv. (Chapter IV of this thesis).

Tchalenko, J.S. (1970). Similarities between shear zones of different magnitudes.
Bull.geol.Soc.Am., 81, pp. 1625-1640.

Verhoef, P.H.W, Vissers, R.L.M. & Zwart, H.J. (1984). A new interpretation of the structural and metamorphic history of the western Aston Massif (Central Pyrenees, France).
Geol.Mijnbouw, 63, pp. 399-410.

White, J.C. and White, S.H. (1983). Semi-brittle deformation within the Alpine fault zone, New Zealand.
J.Struct.Geol., 5, pp. 579-589.

Williams, G.D. (1985). Thrust tectonics in the south central Pyrenees. J.Struct.Geol., 7, pp. 11-17.

Zwart, H.J. (1962). On the determination of polymetamorphic mineral associations, and its applications to the Bosost area (Central Pyrenees). Geol.Rundsch., 53, pp. 38-65.

Zwart, H.J. (1979). The geology of the central Pyrenees. Leidse Geol.Meded., 50, pp. 1-74.

Zwart, H.J. & Roberti, K.F. (1976). Geological map of the central Pyrenees. Sheet 9: Flamisell-Pallaresa. Geol.Inst., Leiden.

CURRICULUM VITAE

Arie Speksnijder werd op 15 februari 1951 geboren in Gouda. Na zijn eindexamen HBS-B (1969) studeerde hij geologie aan de Rijksuniversiteit te Utrecht. Het kandidaatsexamen G3 werd afgelegd op 2 juli 1973, waarna de studie werd voortgezet aan de Rijksuniversiteit te Leiden. Op 28 februari 1978 behaalde hij het doktoraalexamen met als hoofdrichting geologie en als bijvakken sedimentologie en strukturele geologie. Gedurende zijn gehele doktoraal opleiding vervulde hij kandidaats-assistentschappen. Van 1978 tot 1982 is hij als doktoraal-assistent verbonden geweest aan de Subfakulteit Geologie en Geophysica, aanvankelijk aan de Rijksuniversiteit te Leiden en vervolgens aan de Rijksuniversiteit te Utrecht. Sinds 1982 is hij als onderzoeker werkzaam bij het Koninklijke/Shell Exploratie en Produktie Laboratorium te Rijswijk.